Year : 2017

ANTI-CANCER PROPERTIES OF TAT-RasGAP317-326 AND MOLECULAR MECHANISMS OF RESISTANCE TO SORAFENIB

Chevalier Nadja

Chevalier Nadja, 2017, ANTI-CANCER PROPERTIES OF TAT-RasGAP317-326 AND MOLECULAR MECHANISMS OF RESISTANCE TO SORAFENIB

Originally published at : Thesis, University of Lausanne

Posted at the University of Lausanne Open Archive http://serval.unil.ch
Document URN : urn:nbn:ch:serval-BIB_02F0A2758C821

UNIL | Université de Lausanne
Faculté de biologie et de médecine

Département de Physiologie

ANTI-CANCER PROPERTIES OF TAT-RasGAP317-326 AND MOLECULAR MECHANISMS OF RESISTANCE TO SORAFENIB

Thèse de doctorat

MD - PhD

présentée à la

Faculté de biologie et de médecine
de l'Université de Lausanne

par

Nadja CHEVALIER

Médecin diplômée de la Confédération Helvétique

Jury

Prof. Ivan Stamenkovic, Président
Prof. Christian Widmann, Directeur de thèse
Dr. Nicole Gross, Co-directrice de thèse
Dr. Isabelle Janoueix-Lerosey, Experte
Prof. Fabio Martinon, Expert
Prof. Jean Gruenberg, Expert

Lausanne 2017

UNIL | Université de Lausanne
Faculté de biologie et de médecine

Ecole Doctorale
Doctorat MD-PhD

Imprimatur

Vu le rapport présenté par le jury d'examen, composé de

Président·e	Monsieur Prof. Ivan **Stamenkovic**
Directeur·trice de thèse	Monsieur Prof. Christian **Widmann**
Co-Directeur·trice de thèse	Madame Dre Nicole **Gross-Fötisch**
Répondant·e	Monsieur Prof. Ivan **Stamenkovic**
Expert·es	Monsieur Prof. Jean **Grünberg**
	Monsieur Prof. Fabio **Martinon**
	Madame Dre Isabelle **Janoueix-Lerosey**

le Conseil de Faculté autorise l'impression de la thèse de

Madame Nadja CHEVALIER

Médecin diplômée de la Confédération Helvétique

intitulée

ANTI-CANCER PROPERTIES OF TAT-RasGAP $_{317-326}$ AND MOLECULAR MECHANISMS OF RESISTANCE TO SORAFENIB

Lausanne, le 28 avril 2017

pour Le Doyen
de la Faculté de Biologie et de Médecine

Prof. Ivan Stamenkovic

La science efface l'ignorance d'hier et révèle l'ignorance de demain.
David Gross

TABLE OF CONTENTS

SUMMARY

Although some types of tumours are now considered curable, cancer remains one of the deadliest diseases in the world. While various therapeutic strategies exist to treat malignant disease, too many tumours are refractory to current treatments. To improve cancer outcome several approaches can be undertaken, including the amelioration of the current anti-cancer therapies, the development of novel and more efficient drugs, or the reduction of treatment associated long-term side effects.

Our laboratory previously developed an anti-cancer peptide called TAT-RasGAP$_{317-326}$. This ten amino acid peptide, derived from the RasGAP protein and coupled to the TAT cell-penetrating peptide, sensitizes adult cancer cells to various chemotherapies and radiotherapy. In addition, it possesses the ability to prevent metastasis formation by hampering cell migration and invasion.
In the present study, we report the identification of two new features of TAT-RasGAP$_{317-326}$: its capacity to sensitize pediatric tumours to several chemotherapeutic agents and its ability to directly kill some cancer cells. The former property may be of considerable benefit to children by increasing the efficacy of anti-cancer therapies, which could allow to lower their dosage and associated side-effects. The second feature gave us the opportunity to investigate the mechanism of action of the peptide, which remained to be precisely determined, through the characterization of the mode of cell death triggered by it. Using pharmacological and genetic strategies, we demonstrated that cell death was not fully prevented when regulated forms of death including apoptosis, necroptosis, autophagy, parthanatos, and pyroptosis were inhibited. In addition, we performed CRISPR/Cas9 screens to identify genes that were required for the peptide to kill. The top candidates highlighted by the screens were mostly regulators of potassium flux including three potassium channels (KCNQ5, KCNN4, and KCNK5) as well as a subunit of the Na^+/K^+-ATPase pump (ATP1B3). However, instead of being required in the death induction process *per se*, we demonstrated that they were involved in the cytosolic access of TAT-RasGAP$_{317-326}$. Although the mode of action of the peptide is still not fully understood, the RasGAP-derived peptide could be used to fight cancer on several fronts as a sensitizer or a direct cancer cell killer.

At present, a major concern in anti-cancer therapies is treatment resistance leading to the relapse of the tumour. Despite the use of a multi-kinase inhibitor named sorafenib, advanced hepatocellular carcinoma has a poor prognosis, mainly due to intrinsic and acquired resistances. As the exact mechanisms of resistance to sorafenib are still incompletely understood, we performed exome sequencing analyses and CRISPR/Cas9 screening to identify novel pathways that lead to sorafenib resistance. Although we are still analysing and validating the data, preliminary results highlighted already known genetic alterations, such as p53 Y220C structural mutation and EGFR amplification. A better knowledge of sorafenib resistance could ultimately lead to the development of alternative therapies.

RESUME

Bien qu'il soit aujourd'hui possible de guérir certaines tumeurs, le cancer demeure une des maladies les plus meurtrières dans le monde. Si différentes stratégies thérapeutiques ont été développées, un grand nombre de tumeurs restent encore réfractaires aux traitements. Le développement de nouveaux médicaments plus efficaces, la potentialisation des thérapies anti-cancéreuses existantes, ainsi que la réduction des effets secondaires inhérents à la toxicité des traitements offrent l'espoir d'améliorer considérablement le pronostique du cancer.

Notre laboratoire a développé un peptide anti-cancéreux nommé TAT-RasGAP$_{317-326}$. Ce dernier est capable de pénétrer dans les cellules cancéreuses et de les sensibiliser à différentes chimiothérapies, ainsi qu'à la radiothérapie. Il possède également la capacité d'empêcher la formation de métastases en inhibant la migration et l'invasion des cellules tumorales.
La présente étude identifie deux nouvelles propriétés de TAT-RasGAP$_{317-326}$: celle de sensibiliser les tumeurs pédiatriques à plusieurs chimiothérapies, afin d'en augmenter l'efficacité, et celle de tuer directement certaines lignées cancéreuses. Cette dernière propriété a permis l'investigation du mécanisme d'action de ce peptide anti-cancéreux par la caractérisation du type de mort qu'il engendrait. L'utilisation d'antagonistes pharmacologiques et l'inhibition génétique des différentes modalités de mort cellulaire ont montré que TAT-RasGAP$_{317-326}$ déclenche une nouvelle forme de mort ne correspondant à aucune de celles que nous avions testées. Une seconde approche a été utilisée, qui est capable de cribler le génome entier afin d'identifier les gènes nécessaires à la toxicité du peptide. Les meilleurs candidats générés par cette méthode sont principalement des régulateurs du flux potassique, comprenant trois canaux potassiques (KCNN4, KCNQ5 et KCNK5) et une sous-unité de la pompe Na^+/K^+-ATPase (ATP1B3). Cependant, nous avons démontré que ces gènes n'étaient pas impliqués dans l'induction de la mort cellulaire, mais dans l'accès cytoplasmique de TAT-RasGAP$_{317-326}$. Bien que le mode d'action de ce peptide n'ait été que partiellement élucidé, il possède la qualité de pouvoir combattre le cancer de deux manières : en l'éradiquant directement ou en le sensibilisant à d'autres traitements anti-cancéreux.

Une des causes majeures d'échec des thérapies anti-cancéreuses est le développement de résistances par les cellules néoplasiques, induisant la rechute de la maladie. Le carcinome hépatocellulaire illustre idéalement ce phénomène. En effet, le pronostique désastreux de ce cancer est principalement dû aux résistances intrinsèques et acquises contre le sorafenib, seule molécule actuellement disponible pour traiter cette pathologie à un stade avancé. Les mécanismes de résistance étant incomplètement élucidés, le second volet de cette thèse repose sur l'identification de nouvelles voies moléculaires utilisées par les cellules hépatiques malignes pour contrer la toxicité du sorafenib. Le séquençage des exomes de lignées cellulaires résistantes à ce traitement a révélé des altérations génétiques déjà décrites dans la littérature, telles que la mutation Y220C de p53 et l'amplification d'EGFR. Nous sommes actuellement toujours en cours d'analyse des données générées par le séquençage, afin de mettre en évidence d'autres mutations impliquées dans la

résistance au sorafenib. En effet, une meilleure connaissance de ces altérations pourrait conduire au développement de thérapies alternatives.

ABBREVIATIONS

7-AAD	7-AminoActinomycin D
ACD	Accidental cell death
ACT	Adoptive cellular therapy
AFP	Alpha-fetoprotein
AIF	Apoptosis-inducing factor
AP2	Adaptor protein 2
APAF1	Apoptotic protease activating factor 1
APG-2	Asante Potassium Green 2
ATG	Autophagy-related
ATP	Adenosine triphosphate
Bcl-2	B-cell lymphoma-2
BCLC	Barcelona Clinic Liver Cancer
bFGF	Basic fibroblast growth factor
BID	BH3-Interacting domain Death
CAF	Cancer-associated fibroblast
CavME	Caveolae-mediated endocytosis
CCV	Clathrin-coated vesicle
CDH1	E-cadherin
CHX	Cycloheximide
CME	Clathrin-mediated endocytosis
CNV	Copy number variation
CO_2	Carbon dioxide
CPP	Cell-penetrating peptide
CRISPR/Cas9	Clustered regularly interspaced short palindromic repeats-Cas9
CT	Computerized tomography
CTL	Cytotoxic T lymphocyte
DAMPs	Damage-associated molecular patterns
DC	Dendritic cells
DG	α-Dystroglycan
DISC	Death-inducing signalling complex
DMEM	Dulbecco's modified Eagle Medium
ECM	Extracellular matrix
EGF	Epidermal growth factor
EGFR	Epidermal growth factor receptor
EMT	Epithelial-mesenchymal transition
EndoG	Endonuclease G
FADD	Fas-Associated protein with Death Domain

FBS	Fetal bovine serum
FDA	Food and Drug Administration
GATK	Genome Analysis Toolkit
GP	Glycoprotein
GPX4	Glutathione peroxidase 4
HBV	Hepatitis B virus
HCC	Hepatocellular carcinoma
HCV	Hepatitis C virus
HIV	Human immunodeficiency virus
HSC70	Heat shock cognate 70
hTfR1	Human transferrin receptor-1
IL-1β	Interleukin 1β
KO	Knockout
LC3	Light chain 3
LCMV	Lymphocytic choriomeningitis virus
LDL	Low-density lipoprotein
LDLR	Low-density lipoprotein receptor
LigIII	Ligase III
mAb	Monoclonal antibody
MAGeCK	Model-based Analysis of Genome-wide CRISPR-Cas9 Knockout
MOI	Multiplicity of infection
MLKL	Mixed lineage kinase domain-like
MOMP	Mitochondrial outer membrane permeabilization
MRI	Magnetic resonance imaging
MTS	(3-[4,5 dimethylthiazol-2-yl]-5-(3-carboxymethoxyphenyl)-2-(4-sulfophenyl)-2H-tetrazolium)
MVB	Multivesicular body
NAD	Nicotinamide adenine dinucleotide
NASH	Nonalcoholic steatohepatitis
Nec-1	Necrostatin-1
NK	Natural killer
NRF2	Nuclear factor erythroid 2-related factor 2
NSA	Necrosulfonamide
OA	Okadaic acid
P53	Tumour protein 53
PAMPs	Pathogen-associated molecular patterns
PAR	Poly(ADP-ribose)
PARP-1	Poly(ADP-ribose) polymerase protein-1
PB	Pyrenbutyrate
PBS	Phosphate-buffered saline

PDGFR	Platelet-derived growth factor receptor
PDT	Population doubling time
PI	Propidium iodide
PI(4,5)P2	Phosphatidylinositol 4,5-biphosphate
PI4P	Phosphatidylinositol 4-phosphate
PMS	Phenazine methosulfate
PNA	Peptide nucleic acid
polβ	Polymerase beta
PTEN	Phosphatase and tensin homolog
RasGAP	Ras GTPase-activating protein
RB	Retinoblastoma-associated
RCD	Regulated cell death
RIPK1	Receptor-interacting protein kinase-1
RIPK3	Receptor-interacting protein kinase-3
ROS	Reactive oxygen species
RTK	Receptor tyrosine kinase
sgRNA	Single-guide RNA
SMAC	Second mitochondria-derived activator of caspases
SNP	Single nucleotide polymorphism
SR	Sorafenib resistant
TACE	Transarterial chemoembolization
TAT	Trans-Activator of Transcription
Th	T helper
TNF	Tumour necrosis factor
TRAIL	TNF-related apoptosis-inducing ligand
TSP-1	Thrombospondin-1
TWEAK	TNF-related weak inducer of apoptosis
UPR	Unfolded protein response
US	Ultrasonography
UV	Ultraviolet
VAF	Variant allele frequency
VEGF-A	Vascular endothelial growth factor-A
VEGFR	Vascular endothelial growth factor receptor
VHF	Viral hemorrhagic fever
V_m	Membrane potential
VSV	Vesicular stomatitis virus
WT	Wild-type

INTRODUCTION

Cancer

In 2012, 8.2 million people died from cancer worldwide and the global burden was grown to 14 million newly diagnosed cases [1]. By 2030, 13 million cancer-related deaths and 22 million new cancer cases are predicted to occur all over the world [2]. Cancer is the first leading cause of death in developed countries and the second one in developing countries. On a global scale, one in seven deaths is due to cancer [3].

ORIGIN OF CANCER

The oldest description of cancer comes from Egypt and dates back to about 3000 B.C. An ancient manuscript, the Edwin Smith Papyrus, describes that some cases of breast and bone tumours were found in human mummies in ancient Egypt [4]. Though, it is Hippocrates (460-370 B.C.), the "Father of Medicine", who first established the word *cancer* (karkinos in ancient Greek). It means crab, referring most likely to the morphology of tumours with an irregular shape and some finger-like spreading projections [5]. At that time, the pathogenesis and the causes of cancer were not yet established. We had to wait until the 20th century to understand that cancer is a generic name for a heterogeneous group of diseases, which are caused by somatic mutations mainly in tumour-suppressor genes, oncogenes, and microRNA genes. These acquired alterations confer competitive advantages over the non-mutated cells, characterized by an uncontrolled growth and spread of abnormal cells. The transformation from a normal into a cancer cell is rarely a single genetic change, but most often a multistage process of sequential alterations in several genes that regulate cell homeostasis [6]. Only a few genomic mutations have the ability to induce tumorigenicity. There are driver mutations that directly or indirectly induce the oncogenic transformation, and the so-called passenger mutations that, for instance, lie in non-exonic regions or in regions that are not crucial for the protein function [7]. The latter do not contribute to cancer progression. Some mutations confer high genomic instability to cancer cells which in turn results in the accumulation of several other mutations. This genomic instability leads to the formation of cytogenetically different clones that arise from multiple secondary or tertiary mutations. This high heterogeneity is responsible for variations in clinical behaviour and responses to treatment of tumours originating from the same diagnostic type. In addition to genetic modifications, the state of a cell can be affected by epigenetic processes. Almost all human cancers bear epigenetic dysregulation including DNA methylation, histone modifications, and signalling by non-coding RNAs. Epigenetic transformation is a major contributing factor for tumour heterogeneity [8].

Our knowledge of the exact mutational processes, that induce somatic mutations, remains limited. However, some tumour types were found to be characterized by specific mutational signatures that could be the consequence of viral, chemical, or physical carcinogen exposures, such as hepatitis B or C virus (HBV/HCV) infections in hepatocellular carcinoma, tobacco smoking in lung tumours, or ultraviolet light in skin cancers, respectively. Moreover, around 15% of malignancies are due to inherited mutations. Finally, aging increases the probability to develop cancers, most likely because cellular repair mechanisms tend to be less effective and due to a build-up of risks for specific tumours [9].

HALLMARKS OF CANCER

Despite the remarkable biological heterogeneity of cancers in human, these diseases share common biological traits acquired during their multistage development. These distinctive and complementary hallmarks enable the driving of a population of normal cells to become a tumour. In 2011, Doug Hanahan and Robert Weinberg published “Hallmarks of cancer: the next generation”, a report of principles that points out eight hallmarks of cancer, which are sustaining proliferative signalling, evading growth suppressors, resisting cell death, enabling replicative immortality, inducing angiogenesis, activating invasion and metastasis, reprogramming of energy metabolism, and evading immune destruction (Figure 1) [10]. The acquisition of these functions comes out at different times and via diverse mechanisms during malignant progression.

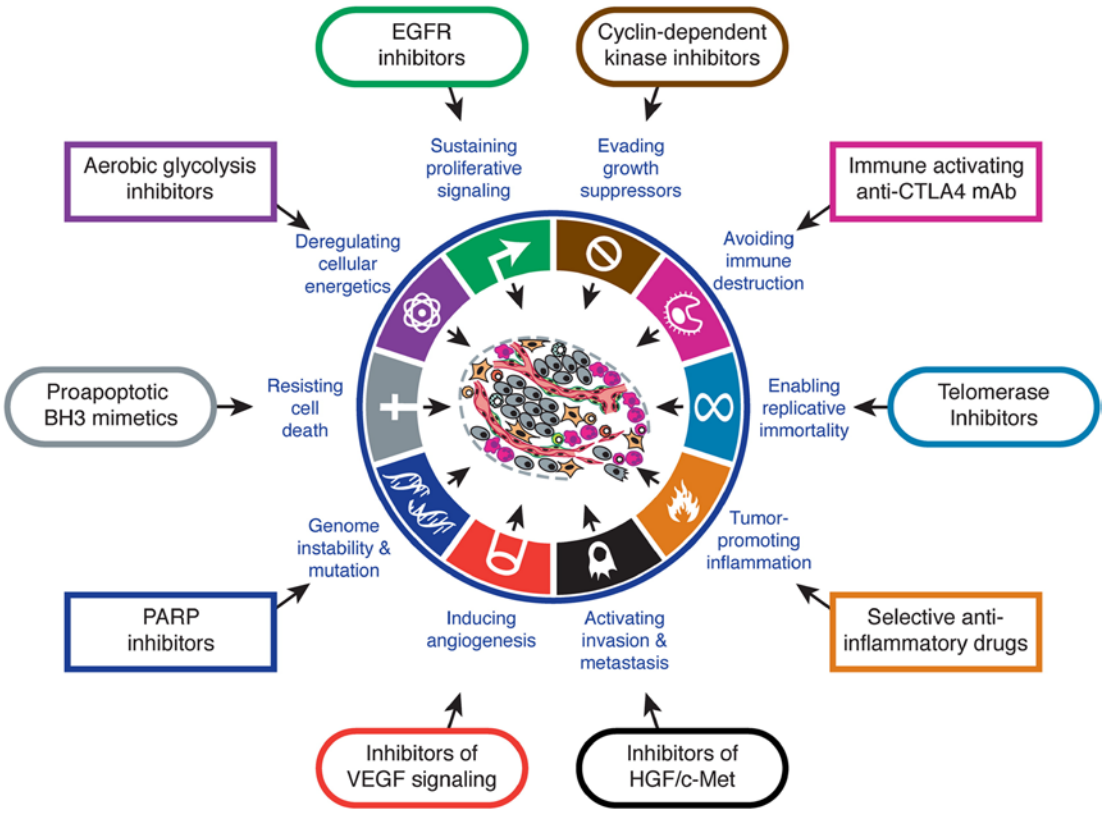

Figure 1. The hallmarks of cancer and their therapeutic targeting. The hallmarks of cancer are required for tumor progression and expansion. Targeted therapies against these abilities are promising strategies to fight cancer. Some of the illustrative examples of drugs depicted in this figure are in clinical trials or currently used in the clinic. From Hanahan and Weinberg, Cell, 2011 [10].

Sustaining proliferative signalling and evading growth suppressors

Normal cell proliferation is regulated both by proliferative signals and by growth arrest signals to maintain homeostasis and tissue architecture. Cell growth and proliferative signals are mainly conveyed by growth factors that bind cell-surface receptors, such as epidermal growth factor receptor (EGFR), platelet-derived growth factor receptor (PDGFR), or vascular endothelial growth factor receptor (VEGFR) [11]. Cancer cells can modulate their paracrine and autocrine proliferative stimulation to maintain constant proliferation. They can reprogram normal cells within the tumour microenvironment to release growth factors or they can be autonomous by producing their own growth factors. Finally, tumor cells can acquire growth factor independence, either by structural alterations in the growth factor receptor that can render it constitutively active independently of the ligand binding, or by generating persistent activation of constituents downstream of the receptor signalling pathways [12].

In addition, cancer cells can evade the growth arrest signals through genetic changes in tumour suppressor genes. These genes are responsible for slowing down cell division, controlling apoptosis, and repairing DNA damage. This is exemplified by some genes like tumour protein 53 (p53), phosphatase and tensin homolog (PTEN), and retinoblastoma-associated (RB) that are three tumour suppressors that are often down-regulated in cancers [13].

Resisting cell death

One natural barrier to cancer progression is programmed cell death. When the cell is subjected to high level of stress, such as DNA damage due to hyperproliferation or elevated levels of oncogene signalling, a normal cell can commit suicide through a process called apoptosis. The physiologic regulation of apoptosis is driven by an equilibrated balance between anti- and pro-apoptotic proteins. To circumvent cell death, tumour cells upregulate anti-apoptotic factors (Bcl-2, Bcl-x_L) or repress pro-apoptotic regulators (Bax, Bim, Puma) [14]. There is a diversity of mechanisms that tumour cells use to counteract cell death, illustrating the complexity and multiplicity of ways for a cell to die.

Enabling replicative immortality

Normal cells pass through a limited number of replication cycles before dying or entering into a quiescent but viable state called senescence. This process is regulated by progressive telomere shortening at each cell division, which induces the loss of their protective effect on chromosomal ends and eventually cell death or senescence [15]. These definite growth-and-division cycles represent another barrier to tumour development. Indeed, cancer cells have to become immortalized in order to generate macroscopic tumours. To counteract this obstacle, almost all malignant cells (but not normal cells) express the telomerase enzyme, which is a DNA polymerase that circumvents telomere erosion by adding DNA segments to the end of the telomeres [16].

Inducing angiogenesis

Angiogenesis, the sprouting of new vasculature, is a physiological process that takes place during embryogenesis, but also transiently during adulthood as part of wound healing process and female reproductive cycling. In the context of tumour progression, the fast growing and expansion of cancer cell requires an important and continuous supply of oxygen and nutrients. Consequently, in malignant diseases, the angiogenic program is constitutively on to sustain neoplastic development. This angiogenic switch is orchestrated by countervailing factors, such as thrombospondin-1 (TSP-1) and vascular endothelial growth factor-A (VEGF-A) that inhibit and induce angiogenesis, respectively [17]. Unsurprisingly, VEGF and its associated tyrosine kinase receptors (VEGFR1-3) are often found upregulated in cancers [18].

Activating invasion and metastasis

Ninety percent of deaths from cancer are due to the metastatic spread of the disease [19]. The invasion-metastasis cascade includes several steps beginning with the local invasion of cancer cells into the extracellular matrix (ECM). Although currently debated, this initial event driving metastasis is probably directed by the so-called “epithelial-mesenchymal transition” (EMT). EMT is a developmental regulatory program, which takes place at various stages of embryonic morphogenesis and during wound healing. It is characterized by the loss of cell polarity and cell-to-cell adhesion, and the gain of mesenchymal phenotype, such as enhanced migratory capacity, increased resistance to apoptosis, and invasiveness [20]. Tumour cells can activate transcriptional regulators of EMT during the course of the metastatic process. After having evaded the ECM, cancer cells intravasate through the basal membrane into a blood or lymphatic vessel. Tumour cells can then transit through the haematogenous or lymphatic systems, evade from the vessel through a process called extravasation, to eventually colonize a new site and form a metastasis [21].

Reprogramming of energy metabolism

To fuel the growing need of energy due to their high proliferation rate, cancer cells have to adapt their energy metabolism. Among the heterogeneity of metabolic alterations characterizing tumor cells, increased glucose uptake and glycolysis have been described. In normal situation, healthy cells metabolize a glucose molecule in the presence of oxygen via glycolysis, which results in the production of two pyruvates, two adenosine triphosphates (ATP) and two reduced nicotinamide adenine dinucleotide (NADH) molecules. Pyruvate is then oxidized to carbon dioxide (CO_2) in the mitochondria, producing approximately 36 molecules of ATP. Under anaerobic conditions, pyruvate is mostly reduced to lactate away from the mitochondria. However, cancer cells metabolize glucose to lactate even in aerobic conditions, despite the poor efficiency regarding ATP production (~18 fold less efficient). This paradigm is known as the aerobic glycolysis or Warburg effect [22]. This glycolytic switch acidifies the tumour microenvironment resulting in several selective advantages for the cancer cells, including the acquisition of resistance to chemical drugs or an increased invasiveness [23, 24].

Evading immune destruction

Immune surveillance operates as a barrier towards cancer progression by recognizing and eradicating the emerging cancer cells. To escape elimination by the immune system, cancer cells undergo immunoediting process, characterized by changes in the immunogenicity profile of tumours to produce immune-resistant clones. However, the immune system plays a dual role in the tumorigenic process, by being implicated in the tumour-associated inflammatory response. Indeed, inflammation can contribute to cancer growth and survival [25].

The knowledge of these hallmarks of cancers allowed scientists to design new strategies to fight cancer (Figure 1). Targeted therapies against these capabilities required for tumour progression are promising strategies to fight cancer. Some of them are in clinical trials or currently used in the clinic.

ANTI-CANCER THERAPEUTICS

Early in the 20th century, surgery was the unique way to cure cancer. Only small and localized tumours were completely removable. Later, the discovery of radiations as an anti-cancer therapy allowed to better control cancers that were not or only partially removed. Finally, the discovery of chemotherapy allowed to destroy the remaining small tumour growths that had spread beyond the reach of surgery or radiations. Since the discovery of the first chemotherapies, such as nitrogen mustard during World War II or aminopterin that was demonstrated by Sidney Farber to induce remissions in children with acute leukemia in 1947 [26], great advances have been made in the field of anti-cancer therapeutics.
Nowadays, surgery remains the primary therapeutic approach and the most effective single modality to cure cancer. The goal of cancer surgery is to excise the tumour with a clear margin of healthy tissue, while preserving the form and function of the organ, thereby improving the quality of life. Surgical mortality and morbidity rates have declined thanks to technological advances, minimally invasive techniques such as laparoscopy, and the use of neoadjuvant and adjuvant therapies [27]. Neoadjuvant therapy aims to reduce the extent of the tumour using radiation-, chemo-, immune-, or hormonal therapy prior to cancer resection. Whereas, adjuvant therapy is any treatment given after surgical resection to decrease the need for more radical surgery and maximized its effectiveness.
The majority of the existing nonsurgical anti-cancer strategies are designed to induce cancer cell death mostly via apoptosis. Radiation therapy is prescribed to treat cancer in about 50% of all cancer patients [28]. Its purpose is to deliver the maximal ionizing radiation dose to the tumour whilst sparing healthy tissue. Radiations deposit energy in cells inducing DNA damage and cell death. Accurate delivery of radiation can be achieved through two different ways; external beam radiation (the most common approach) or brachytherapy. The latter is internal radiations delivered from a sealed radiation source placed inside or close to the tumour [29].

Chemotherapy, as surgery and radiotherapy, is a mainstay of cancer treatment. More than 100 chemotherapeutical agents exist. Although their chemical composition, their mechanism of action,

their route of administration, and their secondary effects vary widely from one to another, their principal goal is to eradicate cells with high division capacities. The rationale being that the proliferative rate of cancer cells is higher than the proliferative rate of normal cells. Accordingly, malignant cells acquired stronger dependency on DNA replication than healthy cells.

Cytotoxic drugs can be classified according to their mode of action into five main groups: alkylating agents, antimetabolites, cytotoxic antibiotics, topoisomerase inhibitors and anti-microtubule agents.

Alkylating agents: They induce DNA damage by covalent binding of their alkyl group to DNA. The resulting intra- or inter-strand crosslink interferes with DNA replication, which prevents the cell division and leads to apoptosis (e.g. cyclophosphamide) [30]. As alkylating agents target DNA, they can also induce long-term damage to the bone marrow. This can increase the risk of acute leukemia, as a secondary effect, about 5 to 10 years post-chemotherapy.

Antimetabolites: They are structurally similar to nucleosides. They compete for binding sites of natural substrates that are essential for biosynthetic processes or they directly incorporate into DNA or RNA. This prevents mitosis or induces DNA damage, eventually triggering apoptosis (e.g. methotrexate) [31].

Cytotoxic antibiotics: They affect the function and the synthesis of nucleic acids by multiple mechanisms, such as intercalation with DNA, inhibition of DNA transcription, DNA fragmentation, or inhibition of DNA synthesis (e.g. doxorubicin). A major concern with some of these drugs is cardiotoxicity, which can be irreversible [32].

Topoisomerase inhibitors: They affect topoisomerase I or II activity, resulting in the inhibition of DNA replication (e.g. etoposide) [33]. They can cause secondary cancer (mostly acute myelogenous leukemia) as early as 2 to 3 years after the treatment.

Anti-microtubule agents: They work by binding to tubulin, the building block of microtubules. This prevents mitosis by inhibiting assembly of the spindle during metaphase (e.g. vincristine) [34].

As chemotherapeutic agents do not specifically target cancer cells, one of the major limitations is the safety profile with a high incidence of adverse effects. Though, a better understanding of molecular cancer cell biology in the late 1990s has allowed the development of novel agents, called molecular targeted therapies.

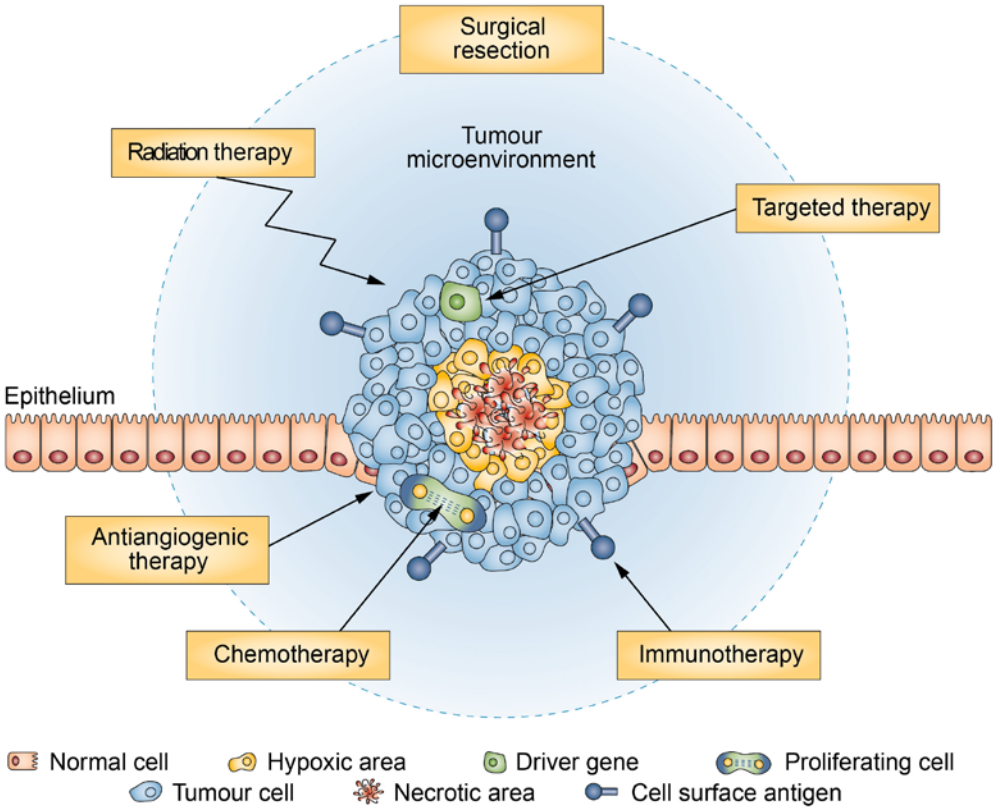

Figure 2. Anti-cancer therapeutic strategies. Whereas surgery, chemotherapy, and radiotherapy are the mainstays of cancer treatment, other strategies have been designed to eradicate malignant diseases, such as immunotherapy, targeted therapy, or antiangiogenic therapy (which is also classified as targeted therapy). Modified from Walther et al., Nat Rev Clin Oncol., 2015 [35].

Targeted therapeutics include the use of monoclonal antibodies or small molecule inhibitors aiming at the inhibition of a well-defined target or hallmark of cancer essential for the biology of the tumour [36]. As targeted cancer therapies affect tumour cells but not normal cells, they are less prone to serious side effects. Some of the targets in cancer therapy are depicted in Figure 1. Most of targeted agents act on angiogenesis or on signalling pathways directing cell survival, proliferation and growth [10]. While monoclonal antibodies interfere with extracellular components of these pathways (i.e. ligands and receptor-binding domain due to their large molecular weight of approximately 150,000 Da), small molecule inhibitors (molecular weight of around 500 Da) are able to act within the cancer cell by blocking receptor signalling and by inhibiting downstream intracellular molecules. Most commonly they interfere with tyrosine kinases (e.g. EGFR, VEGFR) because of their central role in tumorigenesis, as cell growth, proliferation, migration and angiogenesis signalling initiators [36]. Since these targeted drugs may be effective only in patients whose cancers bear a specific molecular target, such therapies raised the new concept of personalized cancer medicine. Nowadays, the therapeutic management of patients with cancer is dictated by a specific molecular and genetic signature of the tumour, and not only by the type, histology, and localization of the disease.

More recently, new insights about the crucial role of the immune system in the tumorigenic process led to the development of immunotherapeutic agents that modulate anti-tumour immune response. The immune system can sustain an anti-cancer response through the activation of immune cells (e.g. natural killer cells (NK), cytotoxic T lymphocyte (CTL), dendritic cells (DC) or T helper cells (Th cells)) that are able to detect the foreign neo-antigens presented by the tumour cells and consequently target them for destruction. The two most effective strategies are immune-cell-targeted monoclonal antibody (mAb) and adoptive cellular therapy (ACT). Immunomodulatory mAb can activate T-cells by blocking their inhibitory receptors (checkpoint blockade) or by targeting their stimulatory receptors (T-cell co-stimulation). ACT relies on the *ex vivo* selection and manipulation of T cells for their ability to attack tumour cells. The best killers are then amplified and infused back into the vein of the patients [37].

Thanks to all the various therapeutic strategies summarized in Figure 2, cancer outcome still improves, while minimizing the impact of cancer management on quality of life. However, primary and acquired resistances to these treatments remain considerable challenges. Whereas primary resistance means that resistance-conferring factors pre-exist in the bulk of cancer cells prior to initial therapy, acquired resistance ensues from the genetic instability, heterogeneity and high mutational rate of tumour cells that induce high risk of selection for drug-resistant cell clones [38]. The acquired mechanisms of resistance are vast and illustrate the ability of cancer cells for eluding death. This aptitude to evade apoptosis, which is the main cell death pathway activated by most anti-tumour therapies, leads to cancer cell survival and the relapse of the disease. Therefore, the development of novel, low-toxicity, better targeted and efficient therapeutic strategies is a priority to improve cancer prognosis. Strategies to circumvent such obstacles include triggering alternate forms of death, combining the different anticancer modalities, but also improving the sensitivity of treatments currently used in clinical practice.

However, prevention is better than cure. One of the strategies to reduce the burden of cancer is to decrease the risk and incidence of the disease. Avoiding exposure to key risk factors, including tobacco use, alcohol abuse, unhealthy diet, lack of physical activity, or ionizing and non-ionizing radiations, could prevent more than 30% of cancer deaths.

HEPATOCELLULAR CARCINOMA

EPIDEMIOLOGY

Worldwide, liver cancer is the second most common cause of cancer mortality and the fifth most common cancer type [39]. Liver cancer is a general term including various kinds of primary tumours according to their cellular origin, such as intrahepatic cholangiocarcinoma, angiosarcoma, hepatoblastoma, and hepatocellular carcinoma (HCC). The latter is the most frequent form of liver cancer (80% of total liver cancer cases) and one of the deadliest cancers, with a five-year survival rate averaging 10% [40]. The global mortality rate is proportional to the global incidence, highlighting the

poor efficacy of current therapies and the aggressiveness of the tumour. While HCC incidence has decreased in developing countries thanks to national HBV vaccination programs, it remains the most common type of cancer in many countries in Sub-Saharan Africa and Southeast Asia. Furthermore, in western countries, the rate of occurrence is increasing steadily over the last 30 years because of an augmented emergence of obesity, type II diabetes, alcohol and drug abuse [41]. Consequently, HCC is a major and universal health problem which emphasizes the need for better understanding of its biology and improved therapeutic management.

PATHOGENESIS

Chronic infections with HBV or HCV contribute to the greatest number of HCC all over the world. Metabolic syndrome with nonalcoholic steatohepatitis (NASH), chronic alcohol consumption, iron overload (hemochromatosis) and aflatoxin-B1-contaminated food exposition are additional risk factors. All of them are known to induce an inflammatory microenvironment that facilitates hepatocarcinogenesis. Sustained inflammation predisposes the liver to fibrogenesis and subsequently cirrhosis, which often progresses to dysplasia and finally malignant transformation [42]. This complex multistep process generates a large landscape of genetic and epigenetic alterations. The various causes, the multistage pathogenesis, and the multistep sequence of molecular modifications of HCC explain the highly heterogeneous phenotype of this disease. The most frequent genetic modifications induce telomere maintenance (TERT), cell cycle dysregulation (e.g. TP53, RB1), aberrant activation of the WNT/β-Catenin signalling pathway (e.g. CTNNB1; AXIN1/2; APC), mutations of epigenetic regulators (e.g. ARID1A, ARID2, MLL) and oxidative stress alterations (e.g. NRF2, KEAP1). Less often, receptor tyrosine kinases (RTKs) are upregulated (e.g. EGFR, VEGFR, MET) or the activation of their downstream elements (e.g. PTEN) is modified (Figure 3) [43-46]. All these somatic alterations enable tumour cells to acquire the phenotypic hallmark of cancer. Moreover, the tissue microenvironment is critical in HCC pathogenesis. Cancer-associated fibroblasts (CAFs), endothelial cells, pericytes, hepatic stellate cells and invading inflammatory cells interact with each other to produce factors contributing to liver fibrosis and malignancy growth [47].

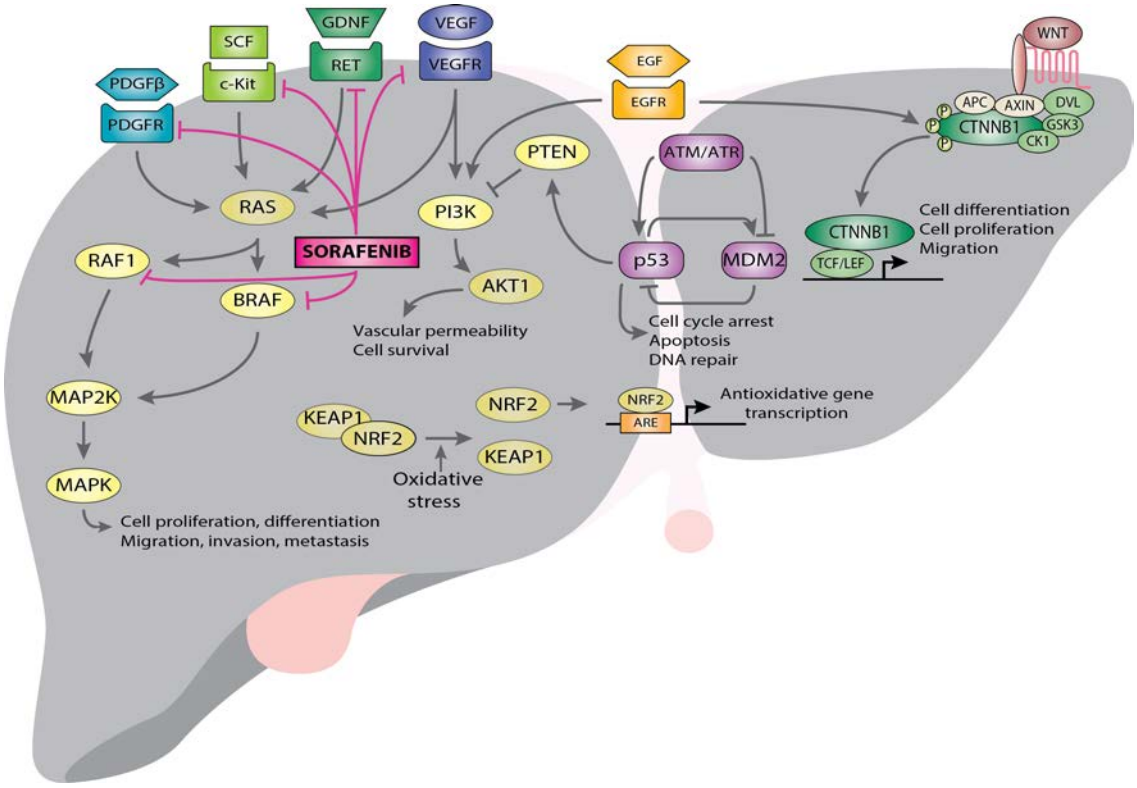

Figure 3. Pathogenesis of HCC. Several risk factors, such as HCV, HBV, alcohol, or aflatoxin-B1 can trigger hepatocarcinogenesis through various mechanisms depicted in this figure. The core oncogenic pathways in HCC are genomic instability (p53, ATM), growth factor signalling (PDGFR, c-Kit, RET, VEGFR, EGFR), oxidative stress (NRF2, KEAP1), and WNT signalling (CTNNB1, AXIN1, APC). However, other pathways can be involved in the disease, including cell cycle regulation (RB1, MYC, CCND1), immortalization (TERT), or chromatin regulation (ARID1A). HCV, hepatitis C virus; HBV, hepatitis B virus; HCC, hepatocellular carcinoma.

DIAGNOSIS

Clinically, patients suffering from HCC usually have only the symptoms related to their chronic liver disease, such as loss of appetite, weight loss, hepatosplenomegaly, and itching. This absence of pathognomonic symptoms delays the diagnosis of HCC. As a result, when the tumour is detected, its size is often bigger than 2 cm rendering the tumour incurable. However, cirrhotic decompensation, including ascites, encephalopathy, variceal bleeding, and upper abdominal pain, should induce suspicion for HCC. Laboratory examination lacks reliable biomarkers. A rising serum alpha-fetoprotein (AFP) level is usually present, although it has poor sensitivity and specificity values. HCC diagnosis can be made purely by radiology on the basis of the presence of a classic vascular pattern on computerized tomography (CT) scans (early arterial enhancement and delayed washout) or in dynamic contrast-enhanced magnetic resonance imaging (MRI). If there is a diagnostic doubt, an image-guided biopsy should be considered [41]. Nevertheless, the best way to diagnose HCC efficiently and in a timely fashion is to screen, using ultrasonography (US) at 6 monthly intervals, individuals who are at high risk for development of HCC, such as patients with established liver cirrhosis [39].

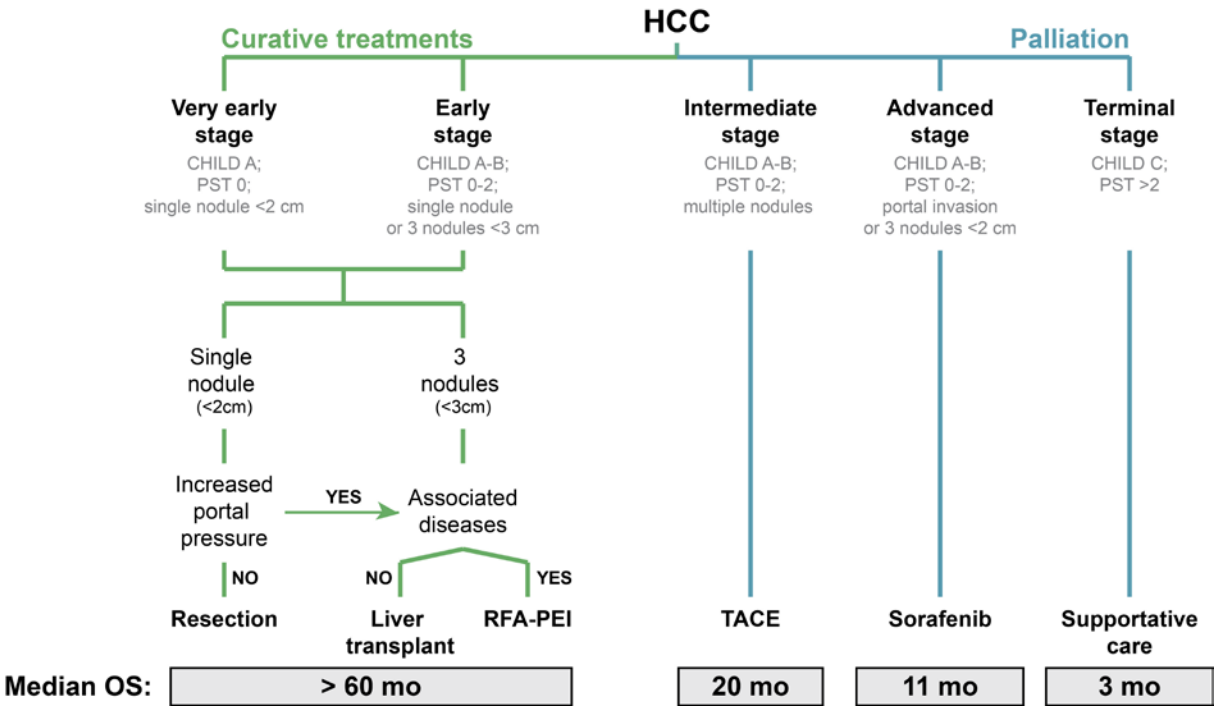

Figure 4. BCLC staging and therapeutic. BCLC staging classifies HCC in five stages according to the extent of the disease, the Child-Pugh score, and the performance status. It suggests the first line treatment strategy for each stage and enables prognostication. BCLC, Barcelona Clinic Liver Cancer; HCC, hepatocellular carcinoma; PST, performance status; RFA, radiofrequency ablation; PEI, percutaneous ethanol injection; TACE, transarterial chemoembolization; OS, overall survival. Modified from Forner et al., The Lancet, 2012 [48].

TREATMENT

Once the diagnosis is made, the treatment procedure is driven by the cancer stage as shown in Figure 4. Barcelona Clinic Liver Cancer (BCLC) staging is a useful classification tool that takes into account data on the patient's performance status, number and size of nodules, cancer symptoms, and liver function, as determined by the Child-Pugh scoring system [49]. The latter rates the severity of the liver disease according to five clinical measures (ascites, bilirubin, albumin, prothrombin time and encephalopathy). Each measure is scored 1 to 3 points, with 3 points indicating the most serious derangement. Liver disease is then classified into three Child-Pugh classes (A, B, and C), employing the added score from the five measures [50]. According to BCLC system, HCC is divided into five stages: very early, early, intermediate, advanced and terminal (Figure 4). Patients presenting with very-early-stage HCC are rare because of late diagnosis of HCC due to the paucity of symptoms at earlier stages. They can benefit from surgical resection which is associated with an overall survival rate of 90%. Liver transplantation is the most appropriate therapy for early-stage HCC patients, who are not suitable to undergo liver resection or who present underlying cirrhosis. If transplantation is not suitable, percutaneous ablation using radiofrequency ablation is the next best therapeutic strategy. For patients with an intermediate-stage disease, transarterial chemoembolization (TACE) is the recommended palliative treatment. Finally, sorafenib (Nexavar®), an oral multi-kinase inhibitor (VEGFR, PDGFR, RET, c-KIT, C-Raf, B-Raf), is the sole Food and Drug Administration (FDA)-

approved drug for patients with advanced-stage HCC [51]. However, in spite of clinical trials showing that the median overall survival time with sorafenib is higher than with placebo (10.7 mo vs 7.9 mo), the outcomes are far from satisfactory [52]. Genetic heterogeneity of HCC and primary and acquired resistance to sorafenib are part of the explanations for the poor prognosis. Patients with terminal-stage disease do not benefit from the therapies mentioned above. The 1-year survival rate is less than 10% with supportive care alone.

SORAFENIB RESISTANCE

Usual genotoxic agents are not frequently used in HCC therapeutic strategy because of several reasons. First, tolerance to systemic chemotherapy is limited due to the significant underlying hepatic dysfunction. Then, HCCs are highly genotoxic refractory tumours, mostly because of the high expression of drug resistance genes. Finally, the immunosuppressive state induces by these compounds may reactivate chronic HBV or HCV infections [53]. In this context, data from two different clinical trials, showing that sorafenib monotherapy prolonged life expectancy by nearly three months in advanced-stage HCC patients, were of great interest and enthusiasm [54, 55].

As mentioned above, dysregulation of several signalling pathways is implicated in hepatocarcinogenesis (Figure 3). Consequently, there is no dominating pathway or no prototypical oncogene addiction that could be targeted by one specific agent. Indeed, in HCC, a potent targeted molecular therapy should inhibit more than one signalling pathway and ideally more than one step in the targeted pathways. Sorafenib possesses these required characteristics. It simultaneously blocks several cell surface and downstream kinases, which are often deregulated during hepatocarcinogenesis, such as components of the mitogen-activated protein kinase/extracellular-signal-regulated kinase (RAF/MEK/ERK). In parallel, this drug can abrogate angiogenesis through the inhibition of VEGFR and PDGFR. VEGFR plays a dual role in HCC tumorigenesis, which is one of the most vascularized tumours. Indeed, in addition to its involvement in angiogenesis, VEGFR signalling may also favor metastasis by increasing vascular permeability. The effectiveness of sorafenib can be attributed to its capacity to target tumour microenvironment in addition to cancer cells [56]. Furthermore, as a targeted therapy, the safety profile of sorafenib is favourable with a limiting widespread systemic toxicity and a good tolerance. Most common side effects include diarrhea, fatigue, hand-foot skin reaction and loss of appetite.

Despite all these abilities, sorafenib only improves moderately the overall survival of patients, suggesting the existence of primary and acquired resistance mechanisms. HCC molecular heterogeneity and genetic instability are both responsible for resistance to this antiangiogenic and anti-proliferative agent. To date, many mechanisms have been implicated in the failure to respond to sorafenib [57]. One of them is activation of the escape pathway of canonical RAF/MERK/ERK cascade. In addition, EGFR aberrant activation and the subsequent stimulation of PI3K/AKT pathway are such examples [58]. In this context, other mechanisms, such as JNK, Mcl-1, Mapk14, SDF-1α, Galectin-1, and Sirtuin 1 activations, have been reported as well [59-64]. Sorafenib resistance can also be acquired through its antiangiogenic activity as sustained sorafenib treatment induces an increased intratumour hypoxia, which leads to cell survival in a HIF-1α-dependent manner [65].

Despite the fact that several signalling pathways have been described to be implicated in sorafenib primary and acquired resistance, the exact mechanisms are still incompletely understood. A better knowledge and overcoming chemoresistance to this drug are primordial to improve the outcome of advanced-stage HCC patients.

PEDIATRIC CANCERS

The biologic nature of pediatric cancers is clinically, histopathologically and biologically distinct from adult cancers. Childhood malignancies have shorter latency periods, are often rapidly growing and aggressively invasive. Moreover, they are rarely associated with exposure to carcinogens, have fewer somatic mutations per tumour, and are generally more responsive to standard modalities of treatments than adulthood cancers [9]. Finally, epigenetic alterations play a critical role in the pathogenesis of pediatric tumours. Prenatal period is very important for epigenetic mechanisms because they are reset during early *in utero* development [66]. It is also during this period that the initiation of many pediatric malignancies occurs [67]. Indeed, disruptions to normal development have been suggested to be involved in the genesis of most of the childhood cancers [68].

Although children are affected by cancer at a lower frequency compared to adults, this disease represents the second cause of death after accidents in Europe [69]. Globally, more than 160,000 new pediatric cancer cases occur per year among patients before 15 years of age and almost 100,000 children die from their disease every year [70]. The causes of the majority of childhood malignancies are unknown. In a small percentage, some cases are attributable to inherited genetic conditions (e.g. RB1, FWT1/2, APC mutations are risk factors for retinoblastoma, Wilm's tumour, and hepatoblastoma respectively) [71-73]. Moreover, known environmental exposures or exogenous factors, such as ionizing radiations or viral infections, have been identified as risk factors for some types of cancers, including leukemias (ionizing radiations), liver carcinoma (HBV), Kaposi sarcoma (HHV8), Burkitt lymphoma, Hodgkin lymphoma, and nasopharyngeal carcinoma (all associated with EBV)[73].

Childhood cancers have clearly benefited from advances in research in the last 30 years. Chemotherapy and radiotherapy have revolutionized cancer treatment and more than 80% of leukemias and lymphomas can now be cured, yet approximately 30% of solid and embryonic tumours are refractory to known treatments [74]. Additionally, the treatment-associated long-term side effects induced by damage to non-tumour cells remain a challenging problem. Currently, beyond 5-year survival, the mortality rate from recurrence decreases. However, the risk of death from second primary cancers and non-neoplastic conditions, such as circulatory or respiratory diseases, due to high dose administration of chemo- or radiotherapy, continues to be elevated compared with the general population (Figure 5) [75]. As children are by definition long-term survivors, there is a strong need for the development of low-toxicity, better targeted and efficient new therapeutic strategies for all types of childhood cancers.

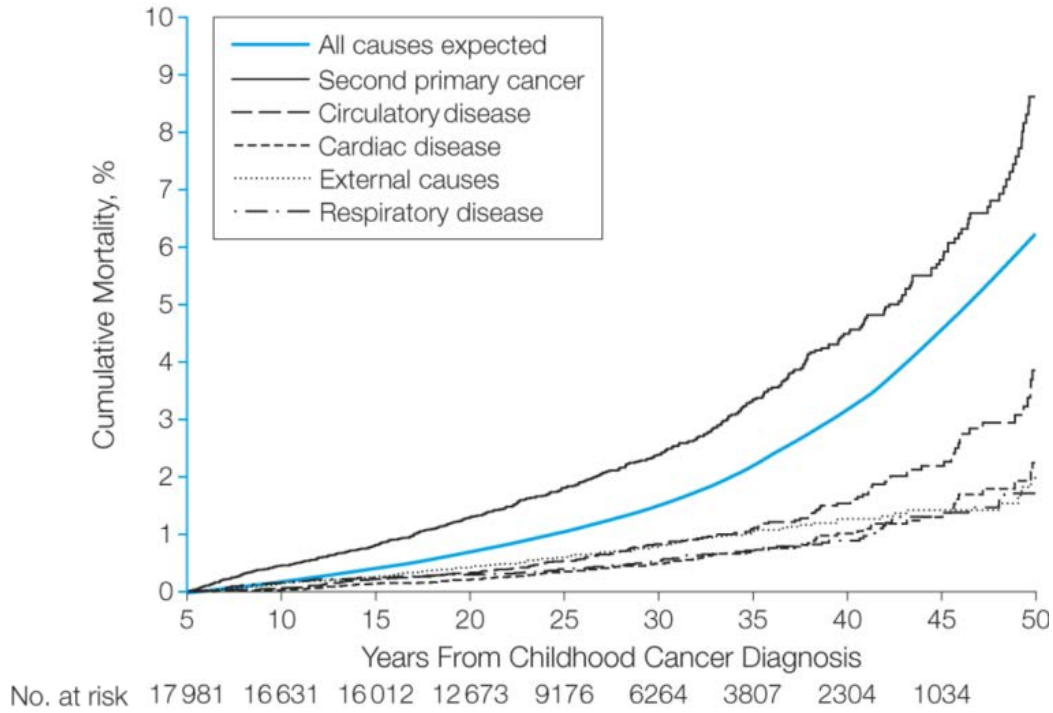

Figure 5. Cumulative mortality of causes of death among survivors of childhood cancer. Observed cumulative mortality of causes of death other than recurrence was 19.0% at 50 years from initial diagnosis, whereas 6.3% was expected based on rates from the general population. For example, in the case of second primary cancer, cumulative mortality increased gradually with time to 2.4% by 30 years but then expanded rapidly to 8.6% by 50 years. From Reulen et al., JAMA, 2010 [75].

Cell death

Ironically, life depends on death. Mammalian development and tissue homeostasis require the controlled death of cells, mostly through apoptosis. The stability of the body is maintained by the balance between stimuli that regulate the proliferation and the death of cells [76]. However, cell death plays also a key role in pathogenesis [77]. Too much or too little activation of death can induce diseases, such as autoimmunity or neurodegeneration [78, 79]. Moreover, defects in the apoptotic machinery occur in the majority of cancers, allowing them to escape cell death and thus survive. As most chemotherapeutic compounds trigger apoptosis in malignant cells, tumour resistance to this cell death pathway remains a major clinical problem, leading to cancer cell survival and finally the relapse of the disease. Henceforth, triggering non-apoptotic cell death pathways could be a route for effective targeted therapy in cancers resistant to apoptosis.

Classification of mammalian cell death is divided into two main categories: accidental cell death (ACD) and regulated cell death (RCD) [80]. ACD, such as necrosis, is mainly promoted by exposure to intense mechanical or chemical insults, but does not require the signalling machinery of cells. On the contrary, cell death is regulated if there is a genetically encoded molecular signalling pathway. Consequently, pharmacologic agents and genetic modulations can initiate or inhibit RCD. Apoptosis and necroptosis are the fundamental forms of RCD, but there are also less known modalities of death, such as parthanatos, pyroptosis, or ferroptosis [80].

Distinctions between the various types of death entail differences in the morphological, biochemical and molecular attributes [81]. The different mode of cell death and their associated molecular cascades are reviewed here below.

APOPTOSIS

Apoptosis aims at the destruction of damage and harmful cells. The principal morphologic features of apoptosis are cell shrinkage, nuclear and DNA fragmentation, chromatin condensation and blebbing into membrane-bound apoptotic bodies [82]. The plasma membrane integrity is maintained until late stage of cellular disintegration [83]. Apoptosis can be triggered by intracellular or extracellular ligands, resulting in the activation of one of the two distinct but convergent pathways called intrinsic (or mitochondrial pathway) or extrinsic (or death receptor pathway) apoptosis (Figures 6B and 6C).

External stimulation of the extrinsic pathway happens through activation of death receptor family members exposed on the cell surface, including tumour necrosis factor (TNF) receptor, TNF-related apoptosis-inducing ligand (TRAIL) receptor, or FAS receptor. Once the ligand has bound to the death receptor, this elicits the clustering of activated receptors and the recruitment of intracellular adapter proteins, such as Fas-Associated protein with Death Domain (FADD) and caspase-8, to form the death-inducing signalling complex (DISC)[84]. Caspase-8 belongs to the family of cysteine-aspartic proteases, called caspases that are expressed ubiquitously as zymogens. Apoptosis is mainly

orchestrated by the sequential activation of caspases. Caspase-8 and -9 are initiator caspases that cleave inactive forms of executioner caspases (caspase-3, -6, and -7). The latter trigger proteolytic events inducing cell death [85]. Caspase-8 specifically activates caspase-3 and -7, provoking substrate proteolysis and the elimination of the cell (Figure 6C). Caspase-8 can also indirectly induce apoptosis through the cleavage of the pro-apoptotic protein BH3-Interacting domain Death agonist (BID) (Figures 6B and 6C) [86].

In the intrinsic apoptotic program, cellular stress signals, such as DNA damage, increased reactive oxygen species (ROS), the withdrawal of growth factors, or the unfolded protein response (UPR), induced by radiation, toxins, or viral infections for instance, disturb the physiological equilibrium of B-cell lymphoma-2 (Bcl-2) family proteins [87]. This family plays a crucial role in the regulation of the mitochondrial membrane integrity. The Bcl-2 family is divided into pro-apoptotic members, including BAX, BAK, BOK, and BH3-only protein family (BID, BAD, BIM, BMF, NOXA, PUMA, and HRK) and anti-apoptotic members (BCL-X_L, MCL1, BCL2A1, BCL-W, and BCL-B) [85]. The interplay between players of these two sub-groups determines whether apoptosis is elicited or not. In the presence of apoptotic stimuli, the activation of BH3-only proteins promotes the mitochondrial outer membrane permeabilization (MOMP) via the oligomerization of BAX and BAK in the outer mitochondrial membrane. This creates channels that mediate the release of proteins, such as cytochrome *c* or second mitochondria-derived activator of caspases (SMAC), into the cytoplasm [88]. Cytochrome *c* can then interact with apoptotic protease activating factor 1 (APAF1), promoting apoptosome assembly, which activates the caspase cascade through the executioner caspase-9, leading to apoptosis (Figure 6B) [89]. Among the other mitochondrial proteins that are discharged into the cytoplasm secondary to MOMP, apoptosis-inducing factor (AIF) and endonuclease G (EndoG) can trigger caspase-independent cell death [90].

NECROPTOSIS

Unlike apoptosis, early loss of integrity of the plasma membrane happens during necroptosis (also named regulated necrosis). This causes the release of cellular contents into the extracellular space but also the influx of extracellular ions and fluid, inducing an increase of cell volume with cell rounding and organelle swelling [91]. Necroptosis occurs when the caspase activity is suppressed and in the presence of tumour necrosis factor alpha (TNF-α) stimulation [92]. However, many other triggers of necroptosis have been identified, including TRAIL, FASL, or TNF-related weak inducer of apoptosis (TWEAK) among others [93]. Regulated necrosis is involved in several clinical disorders, such as myocardial infarction, inflammatory bowel diseases, or viral infection [94]. For instance, in the context of viral aggression, TNF-α secretion induces its receptor TNFR1 activation and the formation of a protein complex called necrosome. The latter, composed of receptor-interacting protein kinase-1 (RIPK1), -3 (RIPK3), FADD, and inactive caspase-8, activates mixed lineage kinase domain-like (MLKL) protein. MLKL phosphorylation drives its own oligomerization and translocation from the cytosol to the plasma membrane, leading to the formation of membrane-disrupting pores [95-97].

Necroptosis can be pharmacologically repressed using necrostatin-1 (Nec-1), an inhibitor of RIPK1, and the MLKL blocker necrosulfonamide (NSA) (Figure 6D) [96, 98].

PARTHANATOS

Parthanatos is a form of regulated cell death characterized by an overactivation of poly(ADP-ribose) polymerase protein-1 (PARP-1), due to a wide array of stress signals, such as ultraviolet (UV), ROS, or alkylating agents. PARP-1, one of the PARP family proteins, is implicated in DNA repair, chromosome stability, and the inflammatory response [99]. To maintain genomic homeostasis, PARP-1 detects single strand DNA breaks, binds to DNA, and uses nicotinamide adenine dinucleotide (NAD^+) to synthesize poly(ADP-ribose) (PAR). The latter triggers the recruitment of other DNA-repairing enzymes, such as DNA ligase III (LigIII) or DNA polymerase beta (polβ) [100]. Once the repair is made, the PAR chains are degraded. However, in some pathological conditions, hyperactivation of PARP-1 contributes to NAD^+ and ATP depletion, and to the translocation of AIF from the mitochondria to the nucleus [101, 102]. PARP-1-induced AIF release elicits cell demise (Figure 6A). Parthanatos is a regulated necrotic-like cell death. It means that its regulation occurs independently of RIPK1 or RIPK3, but it has similar morphologic features of regulated necrosis (cell swelling and loss of plasma membrane integrity) [93]. However, nuclear translocation of AIF leads to large-scale DNA fragmentation and chromatin condensation, which are morphological features of apoptotic death [103].

PYROPTOSIS

Execution of pyroptosis requires caspase-1 activation. Like parthanatos, pyroptosis is a necrotic-like cell death morphologically characterized by cell swelling and rapid plasma membrane disruption [104]. Caspase-1 is a pro-inflammatory molecule that processes interleukin 1β (IL-1β) and IL-18 precursors into active inflammatory cytokines. Various pathological stimuli, including stroke, cancer, or microbial infection, can stimulate caspase-1 [105]. Its activation generates the formation of plasma membrane pores, inducing the release of inflammatory cytoplasmic contents and water influx into the cell (Figure 6E). Nevertheless, the exact mechanism of how caspase-1 induces death remains incompletely understood. Although pyroptosis requires the activation of a caspase, it differs from apoptosis in several ways. Indeed, mitochondrial membrane permeabilization does not occur during pyroptosis, and the substrates of caspase-1 differ from those of pro-apoptotic caspases [104].

AUTOPHAGY

Autophagy is a process of self-degradation induced in response to starvation. In most cases, autophagy protects cells from death by recycling organelles and cytoplasmic constituents to fulfill its need of energy. Autophagy is characterized by the formation of double-membrane bound vesicles, named autophagosomes that sequester cytoplasmic components. These vesicles are then trafficked to lysosomes, where the engulfed cargos are degraded. The autophagosome formation requires autophagy regulators called autophagy-related (ATG) proteins, including ATG5 and ATG6, as well as the lipidation of the microtubule-associated protein light chain 3 (LC3). However, under specific conditions, it has been suggested that autophagy can mediate cell death (Figure 6G) [106].

FERROPTOSIS

Ferroptosis was recently described as a new form of cell death mediated by the inhibition of the system x_c^- antiporter [107]. The system x_c^- is a glutamate/cystine antiporter, allowing the import of cystine into the cell. Depletion of the intracellular cysteine pool, due to the decrease of cystine uptake, induces a reduction of glutathione. Subsequently, inhibition of glutathione-dependent enzymes, such as the repair lipid enzyme glutathione peroxidase 4 (GPX4), as well as the loss of cellular antioxidant ability result in the accumulation of lipid-based ROS [108-110]. Ferroptosis requires abundant cellular iron, as demonstrated by inhibition of ferroptosis-induced cell death in the presence of iron chelators [111]. Erastin and sorafenib are compounds able to induce ferroptosis, by inhibiting the system x_c^- antiporter (Figure 6F) [112, 113].

A cell has other multiple and distinct ways to die than the ones described above, such as anoikis, cornification, entosis, mitotic catastrophe, and netosis. Various cell death pathways can be interconnected. This interplay needs to be taken into account to improve pharmacological strategies to fight cancer cells and to reduce anti-cancer treatment resistance (Figure 6).

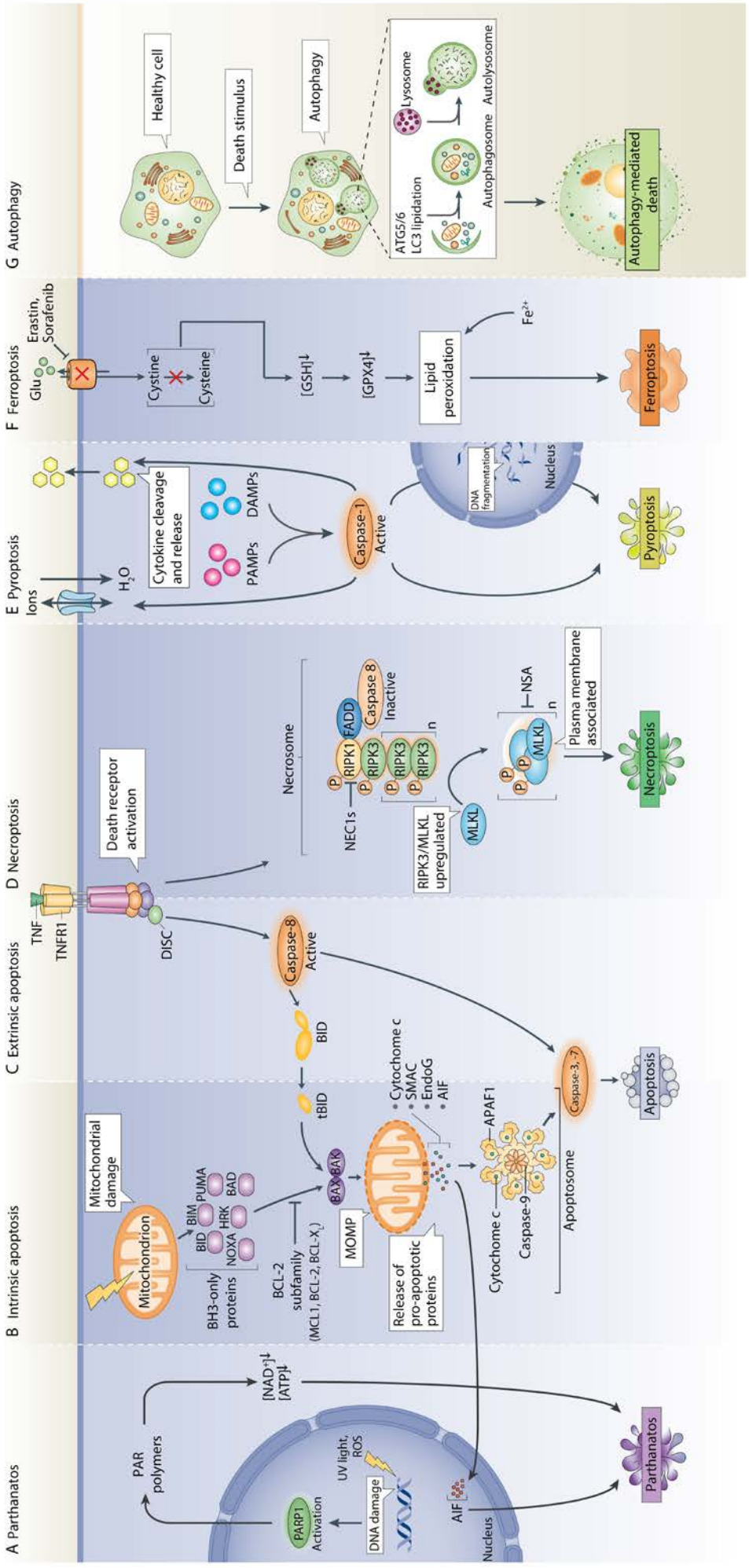

Figure 6. The interplay of cell death modalities. (see next page for the legend)

Figure 6. The interplay of cell death modalities. There are many ways for a cell to die that can, sometimes, be interconnected. **A.** PARP1 hyperactivation, mostly due to DNA damage, causes the accumulation of PAR polymers into the cytosol. The latter PARylate several proteins, leading to the depletion of NAD^+ and, consequently, ATP. In addition, PAR polymers induce the translocation of AIF from the mitochondria to the nucleus and the cytoplasm, eliciting cell demise. **B.** Mitochondrial damage, induced by various cellular stress signals, disturb the physiological equilibrium of Bcl-2 family proteins, leading to MOMP and, consequently, the release of pro-apoptotic proteins, such as cytochrome *c*. The latter promotes the apoptosome assembly and the subsequent activation of the caspase cascade, provoking cell death via the intrinsic apoptotic program. **C.** Extrinsic apoptosis is triggered by the activation of death receptor family members, such as TNFR1. Activation of caspase-8 is the key event of this pathway. It can lead to the stimulation of caspase-3 and -7 as well as to the cleavage of BID, eliciting cell death. **D.** The activation of TNFR1 can also trigger necroptosis, through the formation of the necrosome composed of RIPK1, RIPK3, FADD, and inactive caspase-8. This complex recruits and phosphorylates MLKL, driving the oligomerization and translocation to the plasma membrane of this activated protein. This leads to the creation of membrane-disrupting pores and cell demise. **E.** Caspase-1 is the key element of pyroptosis execution. Caspase-1 activation, elicited by pathogen-associated molecular patterns (PAMPs) and damage-associated molecular patterns (DAMPs), provokes the rapid formation of plasma membrane pores, inducing the release of inflammatory cytoplasmic contents and water influx into the cell. **F.** Inhibition of the glutamate/cystine antiporter reduces the level of GSH and subsequently GPX4 as well as the cellular antioxidant capacity. In presence of abundant cellular iron, this results in the accumulation of lipid-based ROS and cell death through ferroptosis. **G.** In cell death with autophagy, the pro-death stimulus induces the formation of autophagosome, which requires ATG5, ATG6, and the lipidation of LC3 protein. PARP1, poly(ADP-ribose) polymerase protein-1; PAR, poly(ADP-ribose); NAD^+, nicotinamide adenine dinucleotide; ATP, adenosine triphosphate; AIF, apoptosis-inducing factor; UV, ultraviolet; ROS, reactive oxygen species; Bcl-2, B-cell lymphoma-2; MOMP, mitochondrial outer membrane permeabilization; SMAC, second mitochondria-derived activator of caspases; TNFR1, tumour necrosis factor receptor 1; TNF, tumour necrosis factor; DISC, death-inducing signalling complex; NEC1, necrostatin-1; RIPK1/3, receptor-interacting protein kinase-1/3; FADD, Fas-Associated protein with Death Domain; MLKL, mixed lineage kinase domain-like; NSA, necrosulfonamide; PAMPs, pathogen-associated molecular patterns ; DAMPs, damage-associated molecular patterns; Glu, glutamate; GSH, glutathione; GPX4, glutathione peroxidase 4; ATG5/6, autophagy-related protein-5/6; LC3, microtubule-associated protein light chain 3.Modified from Marino et al., Nat Rev Mol Cell Biol., 2014 [88], Vanden Berghe et al., Nat Rev Mol Cell Biol., 2014 [114], Taylor et al., Nat Rev Mol Cell Biol., 2008 [115], and Kroemer et al., Nat Rev Mol Cell Biol., 2008 [116].

The TAT-RasGAP$_{317-326}$ peptide

ORIGIN OF TAT-RASGAP$_{317-326}$

TAT-RasGAP$_{317-326}$ is a cell-permeable peptide derived from the p120 Ras GTPase-activating protein (RasGAP). The p120 RasGAP protein is an ubiquitously expressed multi-domain protein that acts as a regulator of Ras and Rho GTP-binding proteins. It contains two conserved caspase-3 cleavage sites [117]. When a cell faces a stress, RasGAP is cleaved at position 455, generating a N-terminal fragment that bears potent anti-apoptotic activities. This process allows the cell to survive in mild stress situations through the stimulation of Ras/PI3K/Akt pathway (Figure 7A) [118, 119]. In the presence of apoptotic stimuli, when caspase-3 activity levels are high, the N-terminal fragment is further cleaved. The smaller fragments resulting from this second cleavage (in particular fragment N2 [RasGAP 158-455]) regulate tumour cell death by sensitizing them to stress-induced apoptosis which is thought to be a natural mechanism to make a cell die when facing high stress situations [120, 121].
The sensitizing activity of fragment N2 was also shown to occur for anti-cancer agents like chemotherapies and this biological activity lies in a 10 amino acid sequence (WMNVTNLRTD) that corresponds to amino acid 317-326 of the human p120 RasGAP protein sequence (Figure 7B) [122]. This sequence, when fused to a cell-penetrating peptide derived from the human immunodeficiency virus (HIV), HIV-TAT$_{48-57}$ (the so-called TAT-RasGAP$_{317-326}$ peptide), efficiently sensitizes adulthood tumour cell lines of various origins to chemotherapies. This effect seems to be specific for cancer cells as non-transformed human endothelial cells and human keratinocytes had their sensitivity to anti-cancer agents unaffected by TAT-RasGAP$_{317-326}$ [122].
The stability of the RasGAP-derived peptide could then be increased by using D-amino acids for its synthesis. When used *in vivo*, this stable form of TAT-RasGAP$_{317-326}$ potentiates the anti-tumoral growth efficacy of cisplatin, doxorubicin, and radiotherapy [123]. Once injected intraperitoneally in mice, TAT-RasGAP$_{317-326}$ is delivered to various organs and can thereby reach tumours. Importantly, doses that are >100 fold below the lethal doses (the LD$_{50}$ is between 2.5 and 5.0 mg/kg) still exert sensitization activity and no toxicity has been observed. However, one weakness of this peptide is its non-optimal bioavaibility with a high excretion rate via renal and hepatic routes [123].

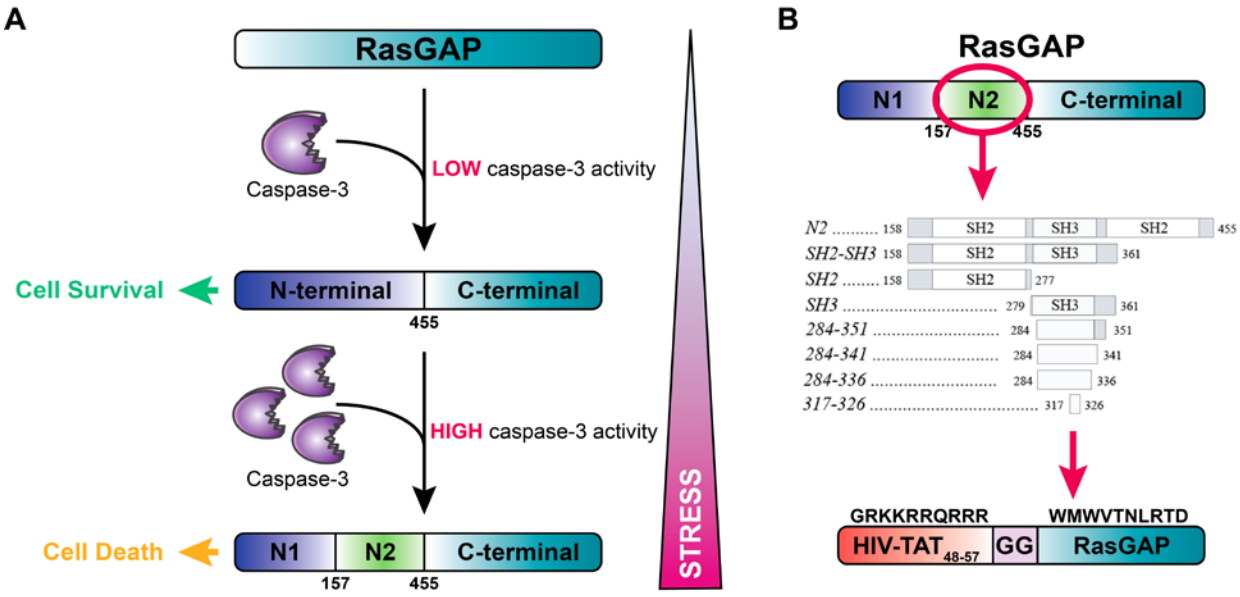

Figure 7. p120 RasGAP cleavage upon stress (A) and the TAT-RasGAP$_{317-326}$ sequence (B). **A.** RasGAP bears two cleavage sites with different sensitivities towards caspase-3 activity. In situations of mild stress, low caspase-3 activity cleaves RasGAP into fragment C and fragment N. The latter promotes cell survival. In the presence of a strong stress, caspase-3 is more activated, resulting in further cleavage of fragment N into fragment N1 and fragment N2. This favours cell death. **B.** Fragment N2 was narrowed down to a 10 amino acid sequence (WMWVTNLRTD). This sequence was then fused to the cell permeable peptide HIV-TAT (GRKKRRQRRR) to generate the TAT-RasGAP$_{317-326}$ peptide.

Moreover, it was discovered that, besides its sensitizing activity in tumours, TAT-RasGAP$_{317-326}$ inhibits cell migration and invasion through extra-cellular matrices, which indicates that it has the potential to prevent the dissemination of primary tumours and thus to function as an antimetastatic compound [124].

Recently, it has been shown that the anti-cancer properties of TAT-RasGAP$_{317-326}$ rely on two tryptophan residues at positions 317 and 319 (see Annex I [125]). However, the mechanism of action of TAT-RasGAP$_{317-326}$ is not fully characterized yet. It has been previously shown that this peptide does not favour the death of tumour cells by modulating MAPK signalling pathways, NF-κB transcriptional activity, or Akt protein levels and phosphorylation status [120, 126]. As genotoxins are DNA-damaging substances that exert their anti-tumour activity by causing apoptosis in cancer cells mainly through the mitochondrial pathway, the involvement of Bcl-2 family members in TAT-RasGAP$_{317-326}$ –induced sensitization activity was investigated [127-129]. All the Bcl-2 family members that were tested were shown to be individually dispensable for the sensitizing activity of the peptide [130]. Consequently, the mode of action of TAT-RasGAP$_{317-326}$ remains to be determined.

PEPTIDE-BASED DRUGS

Peptides are short chains of amino acid monomers linked by covalent amide bonds [131]. They are distinguished from proteins on the basis of their size. An arbitrary cutoff of 50 amino acids is set up to describe peptides, although this limit can vary according to some authors [131, 132]. Peptides include hormones, growth factors, neurotransmitters, or ion channel ligands supporting key roles in human physiology. These extremely potent signal transduction molecules raised interest by the pharmaceutical companies. Their main advantages are their high selectivity, efficiency, and, at the same time, their relative safety and good tolerance. As a result, more than 60 FDA-approved peptide therapeutics are commonly used in the clinic, such as insulin, cyclosporine, and desmopressin. Besides, around 140 peptide-based drugs are currently in clinical trials and more than 500 are in preclinical development [133]. However, the use of natural peptides is also highly criticized for the following reasons: a short circulating plasma half-life, a low biodelivery, and a weak bioavailability. Nevertheless, these limitations can be circumvented by designing more stable synthetic peptides that are less prone to enzymatic degradation, using for instance unnatural amino acids (D-configuration instead of L-configuration), peptide cyclization, or binding peptide to the circulating protein albumin [134, 135]. In addition, to allow peptides to reach intracellular targets, they can be coupled to cell-penetrating peptides (CPPs), or conjugated with antibodies or small molecules that take the role of the targeting unit, whereas the peptide is the effector entity.

Peptides are commonly used in a diversity of therapeutic areas, including endocrinology, urology, ophthalmology, infectious disease, metabolic disease, and oncology [136]. In oncology, peptides are utilized as direct cytotoxic compounds (e.g. goserelin (Zoladex®), for prostate cancer) or as carriers of cytotoxic compounds and radioisotopes by targeting cancer cells (e.g. radiolabeled somatostatin analogs (Octreoscan®) to find carcinoid and other types of tumours) [137]. Besides peptides already available for cancer patients, other peptide-based treatments such as cancer vaccines or anti-angiogenic peptides are currently in clinical trials [138, 139].

CELL-PENETRATING PEPTIDES

Due to the selective permeability of the cell membrane, improving drug delivery into cells remains a challenge. For cellular internalization, a drug must be either lipophilic or very small. In order to increase the restricted repertoire of possible therapeutic molecules, CPPs can be conjugated to cargoes of interest to achieve their intracellular delivery. CPPs are short peptides (usually less than 30 amino acids) able to spontaneously and ubiquitously transport various biochemically active molecules, such as proteins, peptides, DNA, or RNA inside living cells [140].

In 1988, it was reported that the full-length Trans-Activator of Transcription (TAT) protein of HIV could efficiently enter cells in a non-toxic and receptor-independent manner [141]. Some years later, it was found that only a short sequence of the full-length TAT, TAT_{48-57} that bears arginine-rich motif (Table

1), was sufficient to deliver cargoes into cells [142]. Since this discovery, multiple other peptides with cell-penetrating abilities have been described including Penetratin, Transportan, or Polyarginine peptides (Table 1) [143-145]. They can be divided into three main categories: cationic CPPs, hydrophobic CPPs, and amphipathic CPPs. The former ones are the most common CPPs (e.g. TAT, Polyarginine) and are positively charged sequences of amino acids, such as lysine or arginine, whereas the latter contain both hydrophobic and hydrophilic residues (e.g. Penetratin) [146]. Finally, hydrophobic CPPs are characterized by either only non-polar residues, a low net charge, or a hydrophobic motif that is crucial for their uptake (e.g. Transportan) [140].

Name	Amino acid sequences	Origin	Biochemical category
TAT	GRKKRRQRRR	TAT protein of HIV-1 virus	Cationic
Penetratin	RQIKIWFQNRRMKWKK	Homeoproteins	Amphipathic
Transportan	GWTLNSAGYLLGKINLKALAALAKKIL	Chimeric peptide of galanin and mastoparan	Hydrophobic
Polyarginine	$(R)_n$; 6<n<12	Artificial peptide	Cationic

Table 1. The representative cell-penetrating peptides. Amino acid sequences, origin, and the biochemical category of four representative CPPs are denoted in this table.

Mechanisms of entry, trafficking routes, and degradation pathways of CPPs remain poorly characterized and greatly debated, rendering their clinical use limited. Indeed, there is inconsistency in the literature regarding uptake mechanisms that can be attributed to the fact that a CPP according to its sequence, structure, or amphipathicity enters cell via a singular mechanism. Moreover, cellular uptake of a single CPP is dependent on several factors such as peptide concentration, time of incubation, local lipid composition, or cargo characteristics [147]. According to these features, CPP internalization can be passive (cell energy-independent, such as direct translocation), active (cell energy-dependent, such as endocytosis) or both simultaneously [148].

The first step of CPP entry is its interaction with the plasma membrane. The efficacy of this process varies according to amino acids constituting the CPP. For instance, the positive charges of cationic CPPs cluster which creates strong electrostatic interactions with the negatively charged membrane composed of proteoglycans and phospholipids. More precisely, it has been demonstrated that arginine residues are more efficient than lysines to undergo internalization into cells [145]. This is due to the guanidinium headgroup of the arginine side chain that binds to the cell surface in a more effective manner than ammonium cations in lysines [149]. Another key amino acid for CPP internalization is the hydrophobic and aromatic tryptophan residue. Tryptophan plays a crucial role in CPP interaction with the plasma membrane, due to its tendency to insert into biological membranes. Indeed, tryptophan can induce membrane destabilization processes and translocation mechanisms [150, 151]. Additionally, it was also reported that adding tryptophan residues to a CPP sequence improves its endocytosis [152-154]. These observations demonstrate that one amino acid can modify the uptake of a CPP.

Once the peptide binds to the membrane, it may either directly penetrate into the cell or it undergo endocytosis. In some conditions, both processes can be achieved at the same time.

Unlike endocytosis, direct translocation can occur at 4°C and in ATP depletion conditions. It requires

the destabilization of the plasma membrane through different ways detailed below and illustrated in Figure 8 [155-157].

- *Transient toroidal pore formation*: This translocation process occurs secondary to the accumulation of the positively charged peptides in the outer leaflet of the bilayer membrane. This causes the thinning of the membrane and formation of pores by some of the CPPs, allowing the other CPPs to diffuse [155].
- *Barrel stave model*: This is a model of pore formation by amphipathic α-helices CPPs. The latter bind to the bilayer surface in α-helical structures. Helices attach into the hydrophobic core of the membrane and recruit additional monomers to progressively increase the pore size [158].
- *Inverted micelle formation*: CPP interaction with the plasma membrane leads to invagination of the membrane followed by the reorganization of neighbouring lipids. This induces the encapsulation of the CPP in the bilayer membrane. Ultimately, its release into the cytoplasm is due to subsequent membrane disruption [156].
- *Carpet-like model*: This is characterized by the binding of CPPs onto the bilayer surface covering it in a carpet-like manner. Above a critical threshold of local surface density, it leads to membrane disruption in a detergent-like manner [157].

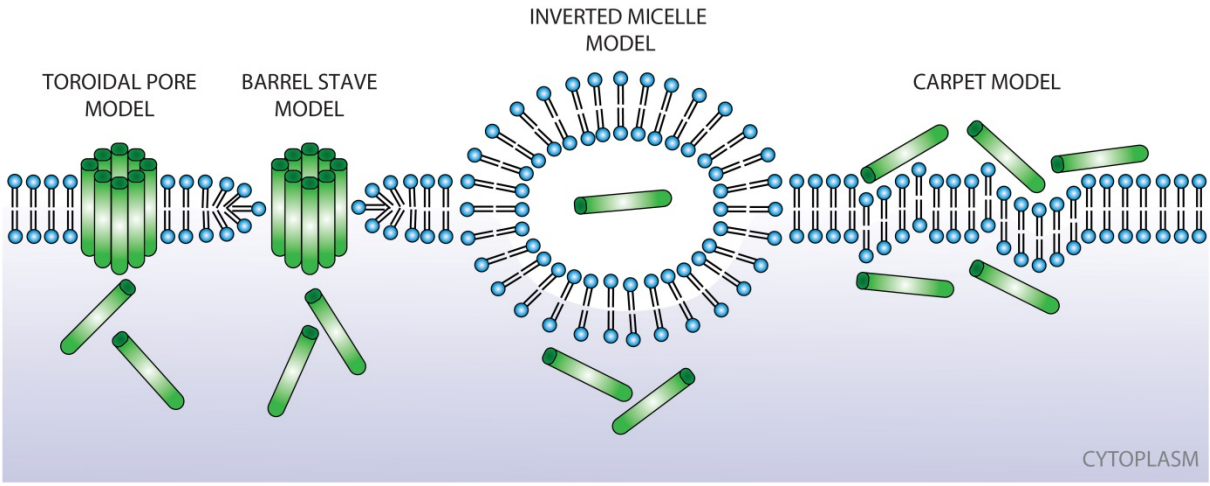

Figure 8. Mechanisms of direct translocation of CPPs through the plasma membrane. Several mechanisms, including the toroidal pore model, the barrel stave model, the inverted micelle model, or the carpet model, are proposed to explain the direct translocation of CPPs through the bilayer surface. Modified from Ruczynski, Folia Histochem Cytiobiol., 2014 [159].

In contrast to direct translocation, endocytosis is a generic name describing different processes that allow cells to absorb material via an ATP-depend manner [160]. CPPs can trigger endocytosis by the direct contact with the cell membrane, its binding to a receptor, or by their electrostatic interactions with the proteoglycans. There are several endocytic routes to reach the cytoplasm that are briefly described below and depicted in Figure 9 [161].

- *Macropinocytosis*: It is initiated from membrane ruffling driven by dynamic remodeling of the actin cytoskeleton. It induces the extension of the bilayer surface to ingest large amounts of extracellular fluid and plasma membrane once the ruffles close off [162]. This gives rise to large (from 0.2 to 5 μm in diameter) and irregularly shaped vesicles named macropinosomes [160]. Macropinocytosis is in part regulated by Rac1 and Cdc42, two proteins that mediate actin cytoskeleton remodelling [163].
- *Clathrin-mediated endocytosis (CME)*: This is the most studied and well-characterized endocytic route. It occurs through the construction of clathrin-coated vesicles (CCVs) composed of the heavy and light chains of clathrin that form upon interaction with each other a polyhedral lattice. Those CCVs are also composed of the adaptor protein 2 (AP2) complex that binds to the cargo but also to the clathrin coats [164]. In addition, other cargo-specific adaptor proteins can constitute the CCVs to increase the repertoire of cargo that can be recognized. For instance, the cellular uptake of low-density lipoprotein (LDL) and transferrin occur through CME after binding to their respective receptors [165, 166]. Once the CCV is mature, the GTP hydrolysis of the GTPase dynamin is required to pinch off the vesicles from the plasma membrane by constricting their neck [167]. Finally, the vesicle is uncoated by the heat shock cognate 70 (HSC70) protein that disassembles the clathrin coat and allows its travel and fusion with endosomes [168].
- *Caveolae-mediated endocytosis (CavME)*: Some regions in the plasma membrane, called caveolae, are highly hydrophobic, enriched in cholesterol and sphingolipids, and show an omega-shaped or flask invagination. Although present in most eukaryotic plasma membranes, some cells (e.g. various lymphoid cell lines) do not carry caveolae regions [169, 170]. Caveolae are composed of the caveolin protein family, whose the main member is caveolin-1. This protein is necessary for the internalization process. It is inserted into the inner leaflet of the plasma membrane, binding to cholesterol and to other important signalling molecules. To form carriers to transport cargoes, caveolins cluster with cytosolic coated proteins named cavins [171]. The latter process is regulated by kinases and phosphatases [172]. Finally, dynamin enables the detachment of the vesicles from the bilayer membrane [173].
- *Clathrin- and caveolae-independent endocytosis*: CLICs/GEEC pathway, IL-2, flotillin-, and Arf6-dependent endocytosis represent more recently described processes. They are all cholesterol-dependent mechanisms. Whereas IL-2 endocytosis requires dynamin for scission of the endocytic pit, Arf6 and CLICs/GEEC pathways undergo endocytosis via a dynamin-independent mechanism [174-176]. Flotillin-mediated endocytosis supposedly functions as CavME, although flotillin proteins localize to membrane invagination other than caveolae [177].

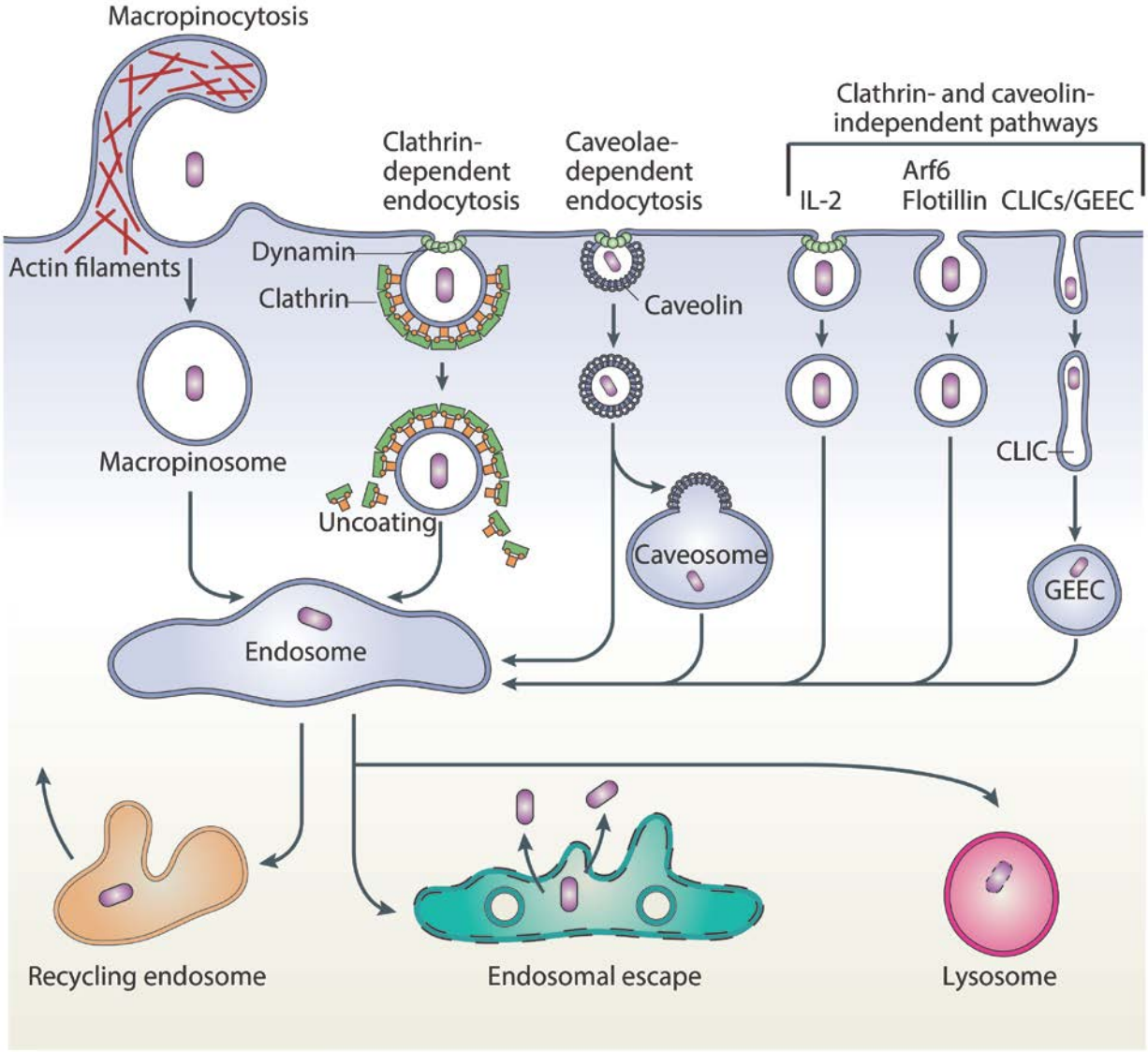

Figure 9. Diverse routes of endocytosis. CPPs can be endocytosed by numerous mechanisms, whose the main ones are depicted in this figure. Clathrin-, caveolin-, and IL-2-dependent endocytosis are dynamin-mediated, whereas Arf6, Flotillin, and CLICs/GEEC pathways are dynamin-independent. Macropinocytosis, for which involvement of dynamin is debated, requires actin remodeling to form large vesicles called macropinosomes. Some endocytic routes may first traffic to intermediate compartments, such as caveosome, macropinosome, or GEEC, before reaching an endosome. Once the cargo has been trapped into an endosome, it can either be recycled back to the cytoplasmic membrane, escape the endosome to gain access to the cytoplasm, or be degraded by a lysosome. CPP, cell-penetrating peptide; CLICs/GEEC, clathrin-independent carriers and glycophosphatidylinositol-anchored protein-enriched endosomal compartments. Modified from Mayor et al., Nat Rev Mol Cell Biol., 2007, [178] and Soldati et al., Rev Mol Cell Biol., 2006, [179].

Once the cargo is sequestered into a vesicle, it is then internalized and sorted into a series of tubulovesicular compartments named endosomes. The latter are subjected to maturation from early to late endosomes. The maturation step is characterized by the fall of the luminal pH, the recruitment and activation of sequential proteins such as the Rab family GTPases, and the alteration of phosphatidylinositol lipids by lipid kinases and phosphatases [180]. After being trapped to endosomes, cargoes can have various fates, e.g. recycled back to the cytoplasmic membrane, delivered and

degraded to lysosomes, or escaped to the cytosol (Figure 9) [180]. Endosomal escape is necessary for most of cargoes to reach their target and exert their function. Indeed, by escaping the final maturation steps of the endosomes, the cargo hampers its lysosomal destruction. Although, the exact mechanisms by which a cargo is released from endosomes are still not well-understood, there are evidences suggesting the involvement of endosomal acidification and lipid composition modifications in this process [181, 182].

Although the clinical application of CPPs is currently limited because their entry and endosomal escape mechanisms remain to be elucidated in details, some of them conjugated to therapeutic cargoes are under clinical trials to treat cancers among other diseases [183, 184]. In addition, a large number of preclinical studies have shown that proteins or nucleic acids such as siRNA, which are promising strategies to treat cancers, infectious diseases, and genetic disorders, have successful application when attached to a CPP [185]. Finally, coupling currently used small chemotherapeutic drugs, such as doxorubicin or methotrexate, improves the efficacy of the compound [186, 187].
However, no FDA approval has yet been delivered for the clinical application of the TAT CPP, although it was and is still studied in preclinical and clinical trials. This is explained by its lack of specificity for a defined cell type, the intrinsic weaknesses of peptide compounds (described above, in the part dedicated to peptide-based drugs), and its debated mechanism of entry into cells. Whereas some authors describe macropinocytosis as the primary mechanism of TAT entry, clathrin- and caveolae-mediated endocytosis are likely to be also involved [188-191]. Moreover, direct translocation of TAT has been shown at threshold concentration or when it is conjugated to a hydrophobic cargo [140, 192, 193]. The discrepancies between the studies highlight the complexity and variability of the mode of entry according to multiple experimental factors. Nevertheless, CPPs emerge as interesting tools to better understand the prime mechanisms of cellular entry and endosomal escape.
Interestingly, many pathogens, such as viruses and bacteria, hijack the endocytic routes to mediate their internalization into the cytoplasmic compartment [194, 195]. Like CPPs, these microorganisms have to reach the cytoplasm for their survival and activity. Thus, they develop various mechanisms to escape endosomes once trapped into these vesicles [158]. Knowing that they use existing cellular pathways, a better understanding and knowledge of cellular uptake and endosomal escape mechanisms could allow a prophylactic inhibition of microorganisms infection.

AIMS OF THE PROJECTS

This thesis work is articulated around two distinct projects. The first and major one aims at the investigation of the sensitization potential of TAT-RasGAP$_{317-326}$ in pediatric tumours and its mechanism of action. This RasGAP-derived peptide, that bears anti-malignant properties, was developed in our laboratory. One of its anti-cancer capabilities is to inhibit cellular migration and invasion, indicating that it has the ability to function as an anti-metastatic compound. In addition, this peptide does not by itself affect non-tumoral cells, but it potently sensitizes adult cancer cells *in vitro* and *in vivo* to various anti-cancer therapies, including genotoxins and gamma radiations.

The specific aims of the first project are:

I. **To assess the chemosensitizing activity of TAT-RasGAP$_{317-326}$ in childhood cancers.** Knowing that this peptide has the potential to increase the potency of anti-cancer therapies in adult tumour cells without affecting the sensitivity of healthy tissues to these treatments, it may, therefore, be of considerable benefit to children cancer patients. This could allow decreasing the efficacious dosage administration so that deleterious side effects can be reduced. If side-effects are not too problematic, the peptide would anyway exert a beneficial effect by increasing the killing efficiency of the treatment.

II. **To characterize which type of cell death is triggered by TAT-RasGAP$_{317-326}$.** While screening several cell lines for the chemosensitizing activity of the peptide (Aim I), I found out that some of them were directly killed by it. Indeed, previously to this work, TAT-RasGAP$_{317-326}$ was not found to affect cell viability alone. This gave us the opportunity to investigate the mode of death triggered by the peptide. As the mode of action of TAT-RasGAP$_{317-326}$ remains to be determined, this approach could help us to better understand how this peptide works.

III. **To identify proteins involved in TAT-RasGAP$_{317-326}$-induced cell death.** The other approach used to elucidate the mechanism of action of the peptide was to screen for genes that mediate the pro-death activity of the peptide alone. A CRISPR/Cas9 (clustered regularly interspaced short palindromic repeats-Cas9) screening was performed and the top candidate genes were validated, followed by the study of the role of their proteins in the activity of TAT-RasGAP$_{317-326}$.

We took advantage of the well-implemented CRISPR/Cas9 technology in the lab to apply it to a new project about hepatocellular carcinoma (HCC) resistance to sorafenib. The latter, a multi-kinase inhibitor, is the sole approved drug for patients with advanced HCC. Despite this treatment, the outcome is far from satisfactory, in part due to primary and acquired resistance to sorafenib.

The specific aim of the second project is:

IV. **To identify novel sorafenib resistance pathways that could be targeted to treat HCC.** Whereas some pathways have already been described to be implicated in intrinsic and acquired resistance, the exact resistance mechanisms are still incompletely understood. To this purpose, we performed exome sequencing analysis and CRISPR/Cas9 screening on HCC cell lines that were previously rendered resistant to sorafenib.

RESULTS

PART I

ASSESSMENT OF THE CHEMOSENSITIZING ACTIVITY OF TAT-RASGAP$_{317-326}$ IN CHILDHOOD CANCERS.

Although current anti-cancer protocols are reasonably effective, treatment-associated long-term side effects induced by lack of specificity of the anti-cancer procedures remain a challenging problem in pediatric oncology. The TAT-RasGAP$_{317-326}$ peptide may, therefore, be of considerable benefit to children cancer patients because it has the potential to increase the potency of anti-cancer therapies in tumour cells without affecting the sensitivity of healthy tissues to these treatments. This peptide could have a valuable effect by allowing the decrease of the efficacious dosage of chemotherapeutic agents so that side effects could be reduced. In addition, if the secondary deleterious effects of treatment are not too problematic, the peptide would anyway increase the killing efficiency of the therapeutic agents. However, it was previously unknown if the peptide can sensitize pediatric tumours as it does to adult cancers.

The evaluation of the sensitizing property of the peptide in pediatric tumours led to a first author paper published in Plos One in March 2015: “Assessment of the chemosensitizing activity of TAT-RasGAP$_{317-326}$ in childhood cancers”. This work, entirely carried out by me, is attached in the following section. As discussed in this study, the effect of TAT-RasGAP$_{317-326}$ was analyzed in several childhood cancer cell lines. All the tested pediatric tumours were sensitized by TAT-RasGAP$_{317-326}$ in response to at least one genotoxin. Moreover, the RasGAP-derived peptide did not increase cell death of normal lymphocytes, alone or in combination with the majority of the tested chemotherapies. Consequently, TAT-RasGAP$_{317-326}$ may benefit children with tumours by increasing the efficacy of anti-cancer therapies notably by allowing reductions in anti-cancer drug dosage and the associated drug-induced side effects.

Interestingly, by screening several cell lines for the chemosensitizing activity of the peptide, we found that a neuroblastoma cell line was directly killed by the peptide alone. The mechanism of action of the RasGAP-derived peptide remains to be determined and the characterization of the cell death induced by this peptide will be very helpful to understand its mode of action. Consequently, the second part of the results of this thesis report is dedicated to the study of the type of cell death induced by TAT-RasGAP$_{317-326}$.

PLOS | ONE

RESEARCH ARTICLE

Assessment of the Chemosensitizing Activity of TAT-RasGAP$_{317-326}$ in Childhood Cancers

Nadja Chevalier[1], Nicole Gross[2], Christian Widmann[1]*

1 Department of Physiology, University of Lausanne, Lausanne, Switzerland, **2** Paediatric Oncology Research Unit, University Hospital Center (CHUV), Lausanne, Switzerland

* Christian.Widmann@unil.ch

Citation: Chevalier N, Gross N, Widmann C (2015) Assessment of the Chemosensitizing Activity of TAT-RasGAP$_{317-326}$ in Childhood Cancers. PLoS ONE 10(3): e0120487. doi:10.1371/journal.pone.0120487

Academic Editor: Salvatore Papa, Institute of Hepatology - Birkbeck, University of London, UNITED KINGDOM

Received: October 3, 2014

Accepted: January 23, 2015

Published: March 31, 2015

Data Availability Statement: The data concerning the CGH array profiles of the NB1 neuroblastoma derived-cell lines were obtained from a third party: Dr. Aurélie Coulon (aurelie.coulon@gmail.com) from the Paediatric Oncology Research Unit, University Hospital Center (CHUV), Lausanne, Switzerland) where readers can send requests for data.

Funding: Funding provided by FORCE foundation - http://www.force-fondation.ch/ (NC NG); MD-PhD fellowship from the Swiss National Science Foundation (n°158116) (NC). The funders had no role in study design, data collection and analysis, decision to publish, or preparation of the manuscript.

Abstract

Although current anti-cancer protocols are reasonably effective, treatment-associated long-term side effects, induced by lack of specificity of the anti-cancer procedures, remain a challenging problem in pediatric oncology. TAT-RasGAP$_{317-326}$ is a RasGAP-derived cell-permeable peptide that acts as a sensitizer to various anti-cancer treatments in adult tumor cells. In the present study, we assessed the effect of TAT-RasGAP$_{317-326}$ in several childhood cancer cell lines. The RasGAP-derived peptide-induced cell death was analyzed in several neuroblastoma, Ewing sarcoma and leukemia cell lines (as well as in normal lymphocytes). Cell death was evaluated using flow cytometry methods in the absence or in the presence of the peptide in combination with various genotoxins used in the clinics (4-hydroperoxycyclophosphamide, etoposide, vincristine and doxorubicin). All tested pediatric tumors, in response to at least one genotoxin, were sensitized by TAT-RasGAP$_{317-326}$. The RasGAP-derived peptide did not increase cell death of normal lymphocytes, alone or in combination with the majority of the tested chemotherapies. Consequently, TAT-RasGAP$_{317-326}$ may benefit children with tumors by increasing the efficacy of anti-cancer therapies notably by allowing reductions in anti-cancer drug dosage and the associated drug-induced side effects.

Introduction

Cancer represents the second cause of death in children after accidents in industrialized countries [1, 2]. Our understanding of childhood cancers has benefited from significant advances over the four last decades. Standard treatments to cure pediatric tumor include surgery, radiation therapy and intensive multi-agent chemotherapy such as etoposide, vincristine, doxorubicin, and cyclophosphamide [3].

In developed countries, eighty percent of children who are diagnosed with cancer are expected to survive within 5 years following the treatment. However, most of them will suffer from chronic diseases by 40 years of age [4]. Extended surveillance of pediatric cancer survivors shows a high risk for life-threatening late effects from second malignancies, cardiac conditions and pulmonary diseases [5, 6]. The risk of early mortality is mostly determined by treatment-specific factors such as the cumulative dose of chemotherapy [7]. Therefore, treatment-associated long-term side effects induced by damage to non-tumor cells are a challenging

Competing Interests: The authors have declared that no competing interests exist.

problem and remain largely unresolved. As children are by definition long-term survivors, there is a strong need to develop low-toxicity, better targeted and efficient new therapeutic strategies for all types of childhood cancers [8]. Strategies to circumvent such obstacles include the improvement of anti-cancer drug sensitivity and specificity toward cancer cells [9–11].

In this context, we previously reported that a cell-permeable peptide derived from the p120 RasGAP protein, called TAT-RasGAP$_{317-326}$, is a tumor-sensitizer to various anti-cancer drugs. Indeed, although it does not show any toxicity toward cells on its own, it efficiently and specifically sensitizes adult tumor cells *in vitro* and *in vivo* to various anti-cancer therapies, including chemotherapy [12,13], and photodynamic therapy [14]. Importantly, it displays specificity to cancer cells as it does not sensitize non-tumor cells to genotoxin-induced apoptosis [12, 14]. TAT-RasGAP$_{317-326}$ appears to have additional anti-cancer activities than tumor cell sensitization as it has been recently demonstrated that this peptide can hamper cell migration and invasion *in vitro* [15, 16] and that this activity can inhibit the metastatization process *in vivo* [17]. This indicates that the RasGAP-derived peptide has the ability to act as an anti-metastatic compound on top of its tumor sensitization effects. Recently, it has been shown that the anti-cancer properties of TAT-RasGAP$_{317-326}$ are dependent on two tryptophan residues at position 317 and 319 [16]. However, the mode of action of TAT-RasGAP$_{317-326}$ is not fully characterized. It has been previously shown that this peptide does not favor the death of tumor cells by modulating Ras activity, MAPK signaling pathways, NF-κB transcriptional activity, Akt protein levels and phosphorylation status [18, 19]. Moreover, the Bcl-2 family members, which regulate mitochondrial-dependent cell death, were shown to be individually dispensable for the sensitizing activity of the peptide [20].

The effect of this peptide in childhood cancer is however not known. The molecular biology of pediatric tumors is distinct from cancers in adults in many ways. As the genesis of most childhood cancers seems to come from disruptions of normal early development, they accumulate fewer mutations than adult tumors. On the other hand, it appears that development of pediatric tumors rely heavily on epigenetic modifications [21–23]. In the present study, we have therefore investigated whether TAT-RasGAP$_{317-326}$ was able to render childhood tumors more sensitive to clinically relevant anti-tumor drugs.

Methods

Cell lines and culture cells

The CCRF-CEM [24], THP-1 [25] and A673 [26] cell lines were obtained from the American Type Culture Collection (ATCC) (references CRL-8436, TIB-202, CRL-1598 respectively). The LAN-1 [27] and M-07e [28] cell lines were obtained from the Leibniz Institute DSMZ-German Collection of Microorganisms and Cell Cultures (references ACC655, ACC104 respectively). The EW-11 [29], TC252 [30] and NB1-derived [31] cell lines were described earlier. All cell lines were cultured in 5% CO_2 at 37°C. The neuroblastoma cell lines (LAN-1, NB1-FBS, NB1-FBS-Re) and the EW-11 Ewing sarcoma cell line were grown in Dulbecco's modified Eagle Medium (DMEM) (Gibco, Paisley, UK) containing 10% fetal bovine serum (FBS) (Gibco). The NB1-NBM neuroblastoma primary tumor cells were maintained in neural basic medium made of DMEM/F12 (Gibco) supplemented with 2% B27 serum-free supplement (Invitrogen, Carlsbad, CA), 20 ng/ml human recombinant basic fibroblast growth factor (bFGF) (Peprotech), and 20 ng/ml human recombinant epidermal growth factor (EGF) (Peprotech). The CCRF-CEM and THP-1 acute leukemia cell lines, and the A673 and TC252 Ewing sarcoma cells, were cultured in RPMI 1640 (Gibco) containing 10% FBS. M07e, an acute myeloid leukemia cell line, was maintained in Minimum Essential Medium alpha (MEMα) (Gibco) supplemented with 10% FBS and 5 ng/ml recombinant human granulocyte

macrophage colony-stimulating factor (GM-CSF) (Peprotech). Human peripheral blood lymphocytes (PBLs) were isolated by density centrifugation over a Ficoll-Paque gradient (Lymphoprep; Stemcell Technologies) from buffy coats of healthy human donors, obtained from the state of Vaud blood transfusion service. The donors gave written consent for potential use of their blood for medical research. PBLs were cultured in RPMI 1640 (Gibco) supplemented with 8% of pooled human serum and supplemented with 100 U/ml recombinant human interleukin-2 (Proleukin, Roche Pharma AG).

Chemicals

The drugs used were vincristine (Sigma-Aldrich, St Louis, USA), etoposide (Sigma-Aldrich), 4-hydroperoxycyclophosphamide (4-HC) (Niomech, Bielefeld, Germany) and doxorubicin (Pfizer AG, Zurich, Switzerland). The staining used to perform flow cytometry were 7-aminoactinomycin D (7-AAD) and Annexin V-FITC (Annexin V-FITC/7-AAD kit, Beckman Coulter, Miami, USA).

Peptide synthesis

TAT-RasGAP$_{317-326}$ (GRKKRRQRRRGGWMWVTNLRTD), TAT$_{48-57}$ (from now on referred to as TAT) (GRKKRRQRRR), TAT-Scrambled (GRKKRRQRRRGGWLDMTTVNRW) and TAT-Mutated (GRKKRRQRRRGGAMWVTNLRTD) were synthesized at the Department of Biochemistry, University of Lausanne, Switzerland as described previously [12].

Cytotoxic assay

For cells growing in suspension (THP-1, M07e, CCRF-CEM, and lymphocytes), three hundred thousand cells were seeded in 6-well plates and directly treated with the indicated doses of 4-HC, etoposide, vincristine, or doxorubicin in the presence or in the absence of 10 μM TAT-RasGAP$_{317-326}$, TAT, TAT-Scrambled or TAT-Mutated. For adherent cell lines (NB1-NBM, NB1-FBS, NB1-FBS-Re, LAN-1, EW-11, TC252, and A673), two hundred thousand cells were allowed to adhere for 48 hours in 6-well plates and were then treated like cells growing in suspension. Twenty-four hours after drug incubation, cells were subjected to flow cytometry to evaluate cell death. Briefly, adherent cell lines were detached by trypsin-EDTA (Gibco) and single-cell suspensions were processed and stained with 1 μg/ml 7-AAD and 50 ng/ml Annexin V-FITC in 500 μl binding buffer. A minimum of ten thousand cells were analyzed. The 7-AAD dye-derived signal could not be used when cells were treated with doxorubicin because 7-AAD and doxorubicin have similar fluorescent properties (7-AAD emission wavelength: 525 nm; doxorubicin emission wavelength: 530 nm [32]).

Statistical analysis

Unless otherwise mentioned, all experiments were derived from three or more independent experiments. The results were expressed as mean ± 95% confidence intervals. Significance was assessed using t-tests performed with Microsoft Excel 2010 followed by Bonferroni corrections (i.e. differences were considered significant when p values $< 0.05/n$, where n is the number of comparisons made). Asterisks represent statistically significant differences. In the last figure, significance was assessed by one-way ANOVAs followed by Bonferroni (Dunn) t post-hoc tests using the SAS 9.2 software (SAS Institute Inc., Cary, NC, USA).

Table 1. Mechanism of action and clinical use of cyclophosphamide, doxorubicin, etoposide and vincristine.

Drugs	Class	Mechanism of action	Clinical use
Cyclophosphamide	Alkylating agent	Interstrand DNA crosslinker	NB, ES, ALL, AML
Doxorubicin	Antracycline	DNA intercalation and inhibition of the progression of topoisomerase II enzymes	NB, ES, ALL, AML
Etoposide	Topoisomerase inhibitor	Single or double strand breaks by trapping topoisomerase II enzymes on DNA	NB, ES, AML
Vincristine	Mitotic inhibitor	Inhibition of assembly of microtubule structures	NB, ES, ALL, AML

Only the tumor types that were analyzed in this study are mentioned here. The listing was based on the protocols of the Children's Oncology Group and the International Society of the Pediatric Oncology (EURO-E.W.I.N.G. 99; AALL0232; HR-NBL-1.5/SIOPEN). NB, neuroblastoma; ES, Ewing sarcoma; ALL, acute lymphoblastic leukemia; AML: acute myeloid leukemia.

doi:10.1371/journal.pone.0120487.t001

Results

In this study, three types of childhood cancers were analyzed: neuroblastoma, leukemia, and Ewing sarcoma. Among childhood malignancies, neuroblastoma is the most frequent extracranial solid cancer. Deaths resulting from neuroblastoma account for 15% of all tumor related death in children [33]. Multidrug resistance, acquired during exposure to chemotherapies, plays a major role in this poor outcome [34, 35]. Leukemia is the most common childhood cancer type and represents one third of all pediatric tumors [36]. Although less prevalent than leukemia, Ewing sarcoma is an aggressive cancer with a poor prognosis and a high rate of relapse with metastatic disease [37]. The drugs employed here are all used in the clinics. Their properties are presented in Table 1.

TAT-RasGAP$_{317-326}$ sensitizes acute lymphoblastic and myeloid leukemia cells to various chemotherapeutic agents without showing any effect toward tumor cells by itself

To investigate the sensitization effect of TAT-RasGAP$_{317-326}$ in leukemia cells, three different cell lines were subjected to increasing concentrations of cytostatic agents in the absence or in the presence of 10 μM TAT-RasGAP$_{317-326}$. Etoposide, vincristine, doxorubicin, and 4-hydroperoxycyclophosphamide (4-HC), the active form of cyclophosphamide, were the drugs used here and are each currently employed in the clinic. Cell death was assessed using 7-AAD that labels dead cells that have permeabilized plasma membrane and with Annexin V that binds to phosphatidylserine exposed on dead cells. Some of the anti-cancer drugs used here induced a concomitant appearance of the 7-AAD and Annexin V signals (Fig 1A shows the representative case of 4-HC). In other words, as soon as a cell became Annexin V-positive it also picked up the 7-AAD dye. Hence, in our hands, anti-cancer drugs such as 4-HC induced a necrosis-like type of death. In the next figures, the 7-AAD data are reported as we found them to be associated with a lower variance than those obtained with Annexin V staining (Fig 1B). The only exception was when doxorubicin was used. Indeed, this dye fluoresces at similar wavelengths as 7-ADD. In this case therefore, the Annexin V data are presented. These experiments revealed that TAT-RasGAP$_{317-326}$ significantly sensitizes leukemia cells to almost all tested drugs (Fig 2A). However, in some conditions (for example when THP-1 cells are treated with vincristine) tumor cells did not respond well to TAT-RasGAP$_{317-326}$. A limited sensitization effect of the RasGAP-derived peptide is not necessarily a consequence of intrinsic resistance to a drug as the CCRF-CEM cell line, which is vincristine-resistant, was efficiently sensitized by TAT-RasGAP$_{317-326}$. This point is of particular clinical relevance as it indicates that TAT-RasGAP$_{317-326}$ can exert a sensitization effect in chemo-resistant cells.

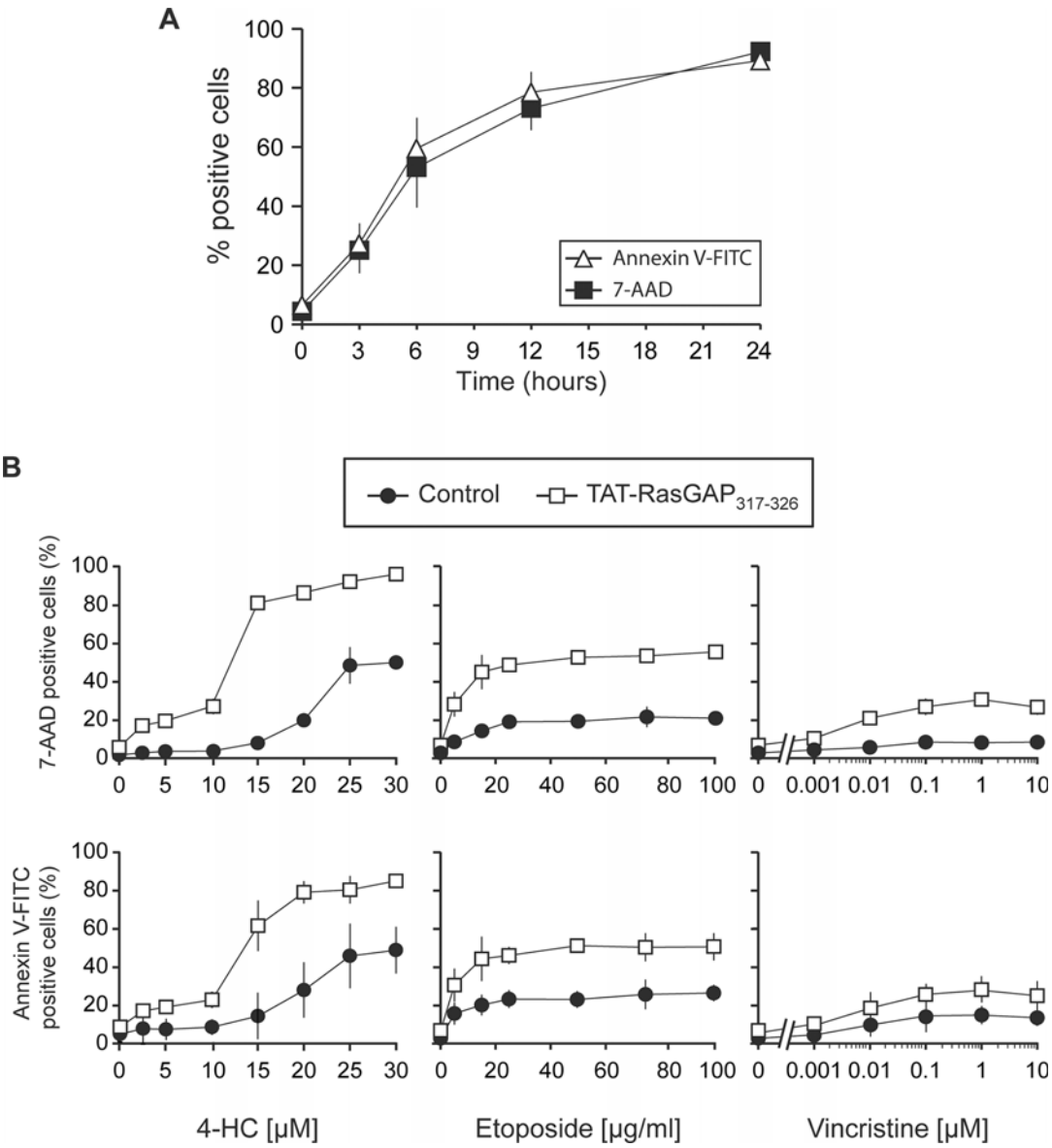

Fig 1. Necrosis-like death induced by 4-HC in CCRF-CEM cells. A. Three hundred thousand CCRF-CEM cells were seeded in 6-well plates and directly treated with 50 μM 4-HC. Cell death was evaluated after several time points (0, 3, 6, 12 and 24 hours) using 7-AAD and Annexin V-FITC staining. **B.** CCRF-CEM cells were seeded in 6-well plates and directly treated with the indicated doses of 4-HC, etoposide or vincristine in the presence or in the absence of 10 μM TAT-RasGAP$_{317-326}$. After 24 hours of drug incubation, 7-AAD and Annexin V-FITC staining was performed to evaluate cell death. 4-HC, 4-hydroperoxycyclophosphamide.

doi:10.1371/journal.pone.0120487.g001

TAT-RasGAP$_{317-326}$ by itself did not induce cell death in the tested leukemia cell lines, even at a two-fold higher concentration (20 μM) than the one used to induce a sensitization effect (10 μM) (Fig 2A).

TAT-RasGAP$_{317-326}$ does not display toxicity toward non-tumor lymphocytes from healthy subjects.

It was shown previously using non-tumor immortalized human keratinocytes (HaCaT) and umbilical vascular endothelium (HUV-EC-C) cells that TAT-RasGAP$_{317-326}$, in combination

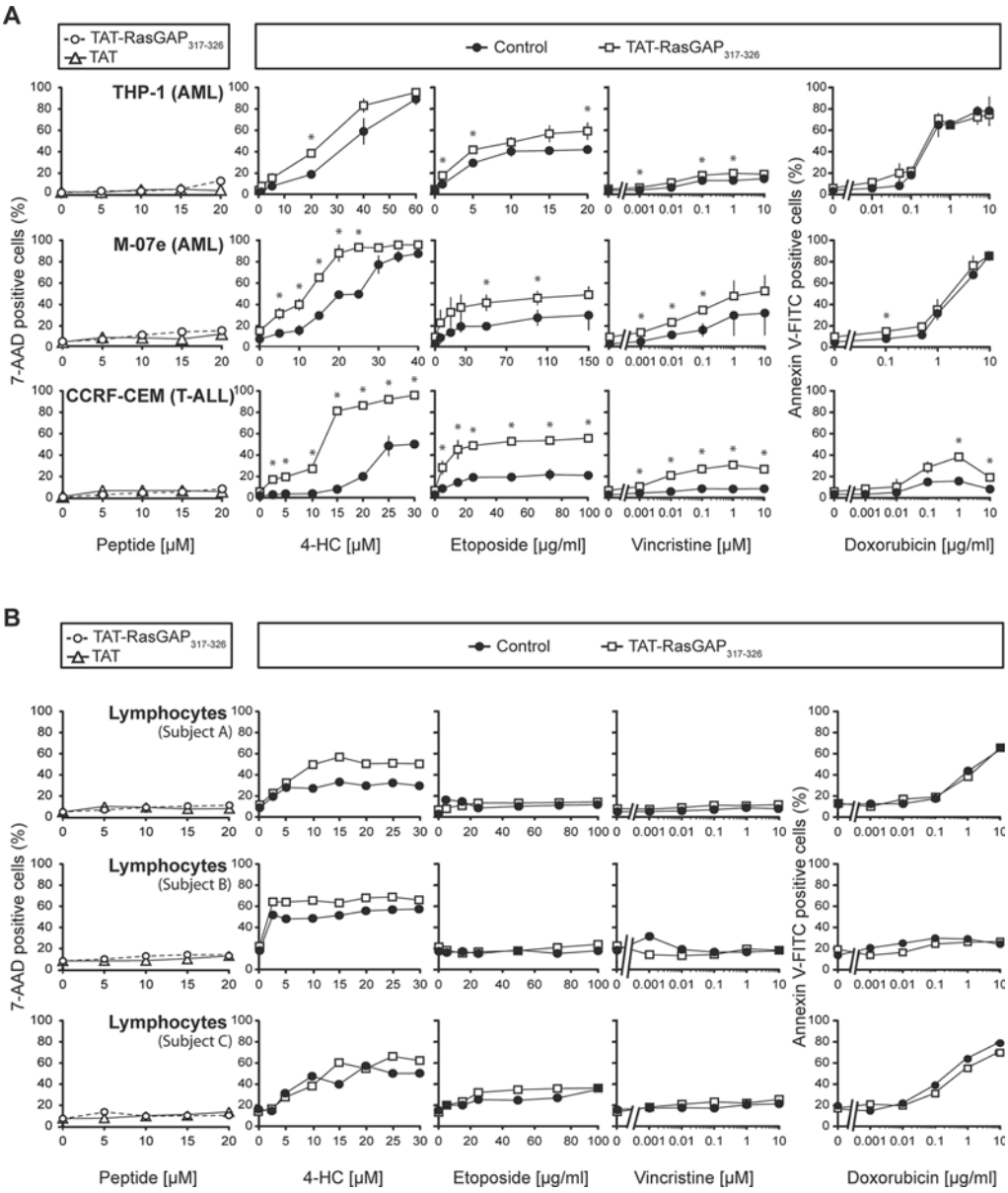

Fig 2. The effect of TAT-RasGAP$_{317-326}$ as a chemosensitizer of leukemia cells and non-tumor lymphocytes. A. Two acute myeloid leukemia cell lines (THP-1 and M-07e) and one T acute lymphoblastic leukemia cell line (CCRF-CEM) were seeded in 6-well plates and directly treated with 4-HC, etoposide, vincristine or doxorubicin at the indicated concentrations in the presence or in the absence of 10 µM TAT-RasGAP$_{317-326}$. After 24 hours of drug incubation, 7-AAD or Annexin V-FITC staining was performed to evaluate cell death (last four columns). Alternatively (first column), the cells were treated with increasing concentrations of TAT or TAT-RasGAP$_{317-326}$ alone. After 24 hours, the evaluation of cell death was carried out using 7-AAD staining. **B.** Isolated lymphocytes from three distinct healthy subjects were treated as described in Fig. 2A. The dosages of chemotherapeutic agents used to treat the healthy lymphocytes from the three subjects are similar to those used to treat the T-ALL CCRF-CEM cells. Note that the graphs are derived from single experiments where lymphocytes are immediately used after their isolation (if cultured *in vitro*, they would experience high levels of spontaneous apoptosis that would prevent accurate measurement of anti-cancer drug- and peptide-induced death). T-ALL, T-acute lymphoblastic leukemia; AML, acute myeloid leukemia; 4-HC, 4-hydroperoxycyclophosphamide. * $p<0.05$ t-test after Bonferroni correction.

doi:10.1371/journal.pone.0120487.g002

with various genotoxins, did not sensitize non-tumor cells [12]. In the present study, we used isolated lymphocytes from whole blood of healthy patients to investigate the selectivity of the RasGAP-derived peptide toward cancer cells. We used the same dosages of chemotherapeutic agents to treat healthy lymphocytes as those used to treat the CCRF-CEM T-acute

lymphoblastic leukemia (T-ALL) cell line (Fig 2A). Fig 2B shows the response of peripheral blood lymphocytes (PBLs) derived from three different healthy subjects (subjects A-C) to the RasGAP-derived peptide in combination or not with the genotoxins used in Fig 2A. The RasGAP-derived peptide by itself did not display any toxicity toward the PBLs. The sensitivity of the non-tumor lymphocytes for the tested chemotherapies alone was similar to the sensitivity of the CCRF-CEM cell line (even slightly increased in the case of doxorubicin for the healthy subjects A and C). The observation that cancer and normal lymphocytes were similarly sensitive to genotoxins was somehow surprising because the rationale to use a given chemotherapy is that it will target preferentially the malignant cells. Nevertheless, the important information drawn from Fig 2B is that TAT-RasGAP$_{317-326}$ does not sensitize PBLs to etoposide-, vincristine- and doxorubicin-mediated death. The peptide however did sometimes sensitize PBLs to 4-HC (Fig 2B), suggesting that TAT-RasGAP$_{317-326}$ can affect the viability of normal cells in some treatment combinations.

TAT-RasGAP$_{317-326}$ can potentiate genotoxin-induced cell death in Ewing sarcoma

To extend the investigation on TAT-RasGAP$_{317-326}$ in non-leukemia childhood cancer, the efficacy of TAT-RasGAP$_{317-326}$ was also tested in Ewing sarcoma cells. The results show that the RasGAP-derived peptide is also able to sensitize these cells to various genotoxins, although to a lower extent than in leukemias (Fig 3). In some cases, no sensitization was observed (e.g. when vincristine was used in the A673 and TC252 cell lines). Here again, TAT-RasGAP$_{317-326}$ alone did not display any toxicity toward the Ewing sarcoma cells (Fig 3).

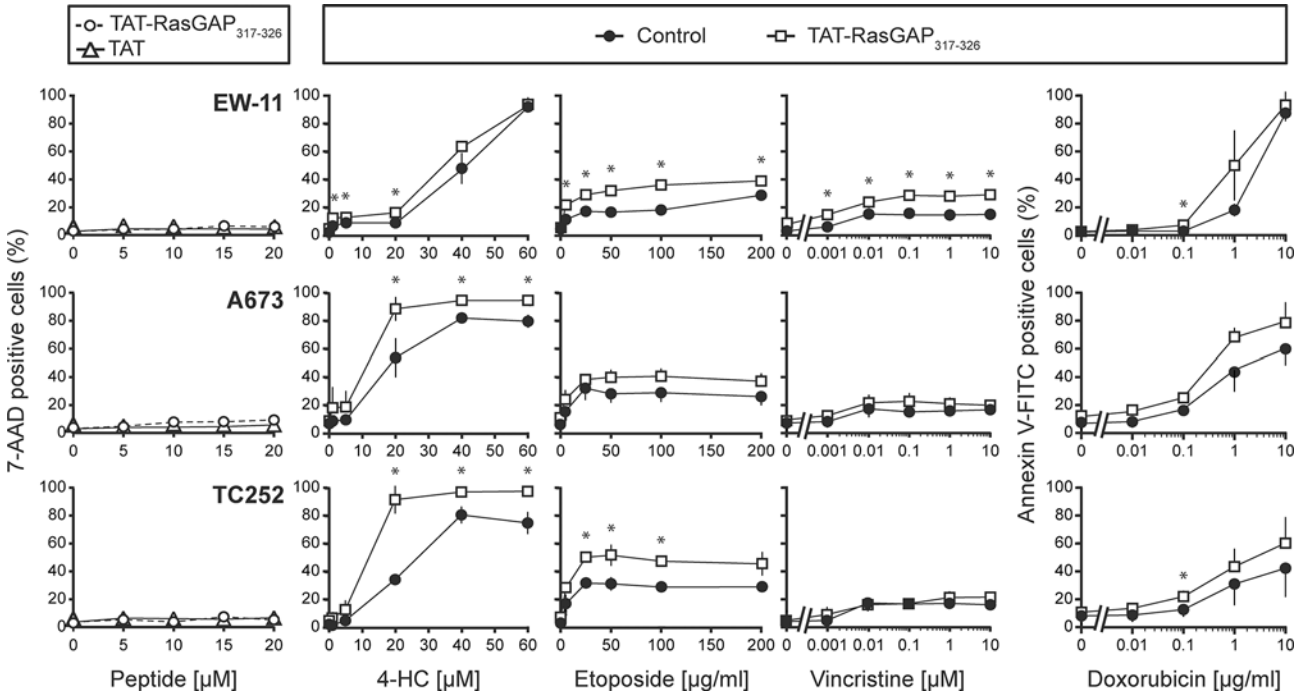

Fig 3. TAT-RasGAP$_{317-326}$ potentiates genotoxin-induced cell death in Ewing sarcoma. Three Ewing sarcoma cell lines (EW-11, A673 and TC252) were seeded in 6-well plates and after 24 hours were treated with 4-HC, etoposide, vincristine, or doxorubicin at the indicated concentrations in the presence or in the absence of 10 μM TAT-RasGAP$_{317-326}$. One day later, cell death was evaluated. 4-HC, 4-hydroperoxycyclophosphamide. * $p<0.05$ t-test after Bonferroni correction.

doi:10.1371/journal.pone.0120487.g003

The NB1 neuroblastoma derived-cell lines are directly killed by TAT-RasGAP$_{317-326}$

Acquired chemoresistance is an important cause of failure of treatment of neuroblastoma. To assess the effect of TAT-RasGAP$_{317-326}$ in cells that were exposed to high doses of chemotherapies and therefore that potentially have acquired resistance to these cytotoxic agents, we selected primary tumor cells of a single patient at different stages of the disease. The NB1 cells are high risk stage 4 primary neuroblastoma cells derived from bone marrow samples that were established at initial diagnosis (NB1-NBM and NB1-FBS) and at subsequent relapse after multi-agent chemotherapy (NB1-FBS-Re) (Fig 4A). NB1-FBS and NB1-FBS-Re cell lines were cultured in 10% fetal bovine serum (FBS)-containing DMEM medium, while NB1-NBM cells were established in neural basic medium (NBM). NBM is a stem cell permissive serum-free, bFGF-, EGF- and B27-supplemented medium to support the growth of neural crest cells, the tissue of origin of neuroblastoma [38, 39].

Fig 4A shows that the NB1-NBM and NB1-FBS cell lines do not display the same sensitivity toward the tested chemotherapies. Moreover, the efficacy of TAT-RasGAP$_{317-326}$ to improve the killing efficiency of 4-HC varies between these two cell lines: the NB1-FBS cells were found to be very sensitive to the sensitization effect of the peptide, while the NB1-NBM cells were not affected by the presence of TAT-RasGAP$_{317-326}$. As the only difference between the NB1-NBM and NB1-FBS cell lines is the medium in which they are cultured, one could hypothesize that the metabolism of the NB1 cells varies from one culture condition to the other and that this differentially modulates the sensitivity of the tumor cells to TAT-RasGAP$_{317-326}$.

To investigate whether the sensitization effect of TAT-RasGAP$_{317-326}$ was still efficient on relapsed neuroblastoma cells, we compared its efficacy between the NB1-FBS cells and the NB1-FBS-Re cells. Both cell lines are cultured in the same culture medium. The treatment regimen that was used to treat the patient is illustrated in Fig 4A. The patient, the relapsed cells of which were derived, was exposed to the four drugs (4-HC, etoposide, vincristine and doxorubicin) tested in this study. However, except for the 4-HC-treated conditions where we can observe a slight resistance to this drug in the NB1-FBS-Re cells, the relapsed cells are not more resistant to etoposide, vincristine and doxorubicin than the cells derived from initial diagnosis (Fig 4A). On the contrary, NB1-FBS-Re cells show an increased sensitivity to doxorubicin compared to the NB1-FBS cells. Nevertheless, TAT-RasGAP$_{317-326}$ sensitizes the three primary NB1-derived cell lines, although to a different level of efficacy according to the cell line and the tested chemotherapy (Fig 4A).

In most cases, TAT-RasGAP$_{317-326}$ does not induce tumor cell death by itself. However, we found out that the three NB1 derived-cell lines can be directly killed by the RasGAP-derived peptide (Fig 4A). The dose needed to induce cell death (20 μM) is nevertheless higher than the dose used to sensitize the cells to genotoxins (10 μM).

To complete the investigation of the effect of TAT-RasGAP$_{317-326}$ in neuroblastoma tumor type, we also tested the peptide on LAN-1, another neuroblastoma cell line derived from an aggressive stage 4 neuroblastoma. Fig 4B shows that the RasGAP-derived peptide displays a slight sensitization effect toward this cell line. Unlike the NB1 derived-cell lines, TAT-RasGAP$_{317-326}$ alone was not able to kill LAN-1 cells (Fig 4B), meaning that TAT-RasGAP$_{317-326}$-induced cell death is not a specificity shared by all neuroblastomas.

The sensitizing activity of TAT-RasGAP$_{317-326}$ is carried by the RasGAP-derived sequence

To assess the specificity of the chemo-sensitizing activity of TAT-RasGAP$_{317-326}$, three different control peptides were tested: a peptide composed of the TAT sequence only (TAT), a

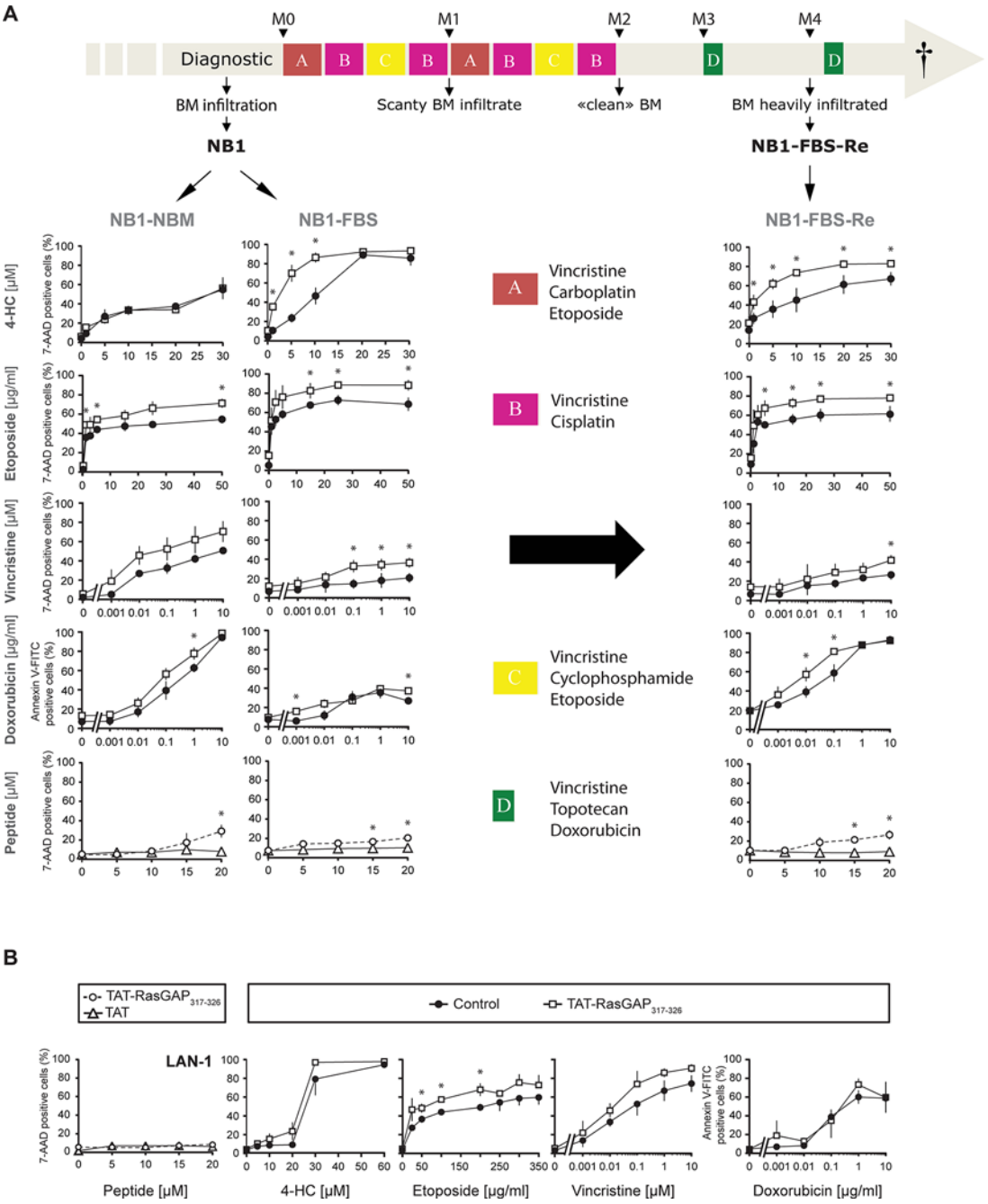

Fig 4. TAT-RasGAP$_{317-326}$ sensitizes neuroblastoma cells to chemotherapy and displays a direct killing effect on NB1-derived cell lines. A. The light grey thick arrow on top of the figure represents the treatment regimen administrated to the patient from whom the three NB1-derived cell lines were established. The NB1 cells are derived from primary high risk neuroblastoma bone marrow samples. NB1-NBM and NB1-FBS were established at initial diagnosis and cultured in NBM and DMEM media, respectively. NB1-NBM-Re was established at a subsequent relapse and cultured in DMEM. The three NB1-derived cell lines were treated as described in Fig 3. **B.** The LAN-1 cell line is derived from a high risk neuroblastoma. LAN-1 cells were treated as described in Fig 3. M, month; BM, bone marrow; 4-HC, 4-hydroperoxycyclophosphamide. * $p<0.05$ t-test after Bonferroni correction.

doi:10.1371/journal.pone.0120487.g004

peptide in which the RasGAP sequence was scrambled (TAT-Scrambled), and a peptide in which the first tryptophan of the RasGAP sequence was substituted into an alanine residue (TAT-Mutated). This tryptophan was recently shown to be essential for the sensitizing activity of TAT-RasGAP$_{317-326}$ in adult tumors [16]. The effect of TAT-RasGAP$_{317-326}$ and the three control peptides was tested in CCRF-CEM cells in combination with various anti-cancer drugs at doses that allowed the greatest sensitization activity to be detected. CCRF-CEM cells were used because this leukemia cell line was the one most efficiently sensitized by the RasGAP-derived peptide. Fig 5A shows that all three control peptides had a tendency to slightly favor the death of CCRF-CEM cells when combined with the different anti-cancer drugs but in most cases this did not reach statistical significance. In contrast, TAT-RasGAP$_{317-326}$ markedly, and always significantly, sensitized these cells to the drugs. The slight sensitization effect of the control peptides is most likely due to the cell penetrating activity of the TAT moiety, which has the potential to negatively affect cellular homeostasis [40]. Similar results were obtained when the TC252 Ewing sarcoma cell line and the NB1-FBS neuroblastoma cell line were used: TAT-RasGAP$_{317-326}$ significantly increased their sensitivity to 4-HC, while the three control peptides did not, or only minimally (Fig 5B and 5C). These data indicate that the tumor sensitizing activity of TAT-RasGAP$_{317-326}$ only marginally relies on its ability to penetrate cells via the TAT cell-permeable sequence. Therefore, it can be concluded that the sensitizing activity of TAT-RasGAP$_{317-326}$ is mainly carried by the RasGAP-derived sequence.

Discussion

The currently applied therapies to treat childhood solid cancers, such as neuroblastoma and Ewing sarcoma, need to be more efficient and specific to improve clinical outcome. Leukemia has usually a better 5-year survival rate than pediatric solid tumors, but long-term effects of the therapy remain an important cause of morbidity and mortality. Furthermore, acquired resistance to the conventional treatments is responsible for relapses and poor outcome. Accordingly, finding less toxic and more efficient therapeutic agents to treat pediatric cancers is a necessity to decrease drug-induced deleterious side effects and the associated mortality [3].

In the present study, we assessed the effect of TAT-RasGAP$_{317-326}$ in several childhood cancer cell lines. This RasGAP-derived peptide was already known to sensitize adult tumor cells *in vitro* and *in vivo* to various anti-cancer therapies [12]. Our results show that TAT-RasGAP$_{317-326}$ significantly sensitizes childhood cancer cells in the majority of the tested conditions. However, in some cases, tumor cells did not, or minimally, respond to the peptide. The pediatric tumor-sensitizing effect illustrated in this study was reached using half of the peptide concentration used previously to sensitize adult cancer cells (10 μM TAT-RasGAP$_{317-326}$ in this study instead of 20 μM in the paper of Michod et al. [12]). Possibly, the dose of TAT-RasGAP$_{317-326}$ could be doubled to increase the sensitizing efficacy of the peptide in the conditions where it was less efficient. Since primary tumor cells represent a more clinically relevant condition, we also tested the peptide in primary neuroblastoma cells derived from bone marrow samples from a single patient (the three NB1-derived cell lines showed in Fig 4). The results show that the RasGAP-derived peptide sensitizes primary tumor cells, suggesting that it could exert its anti-cancer activity on tumors in an *in vivo* context.

The mechanism of action of TAT-RasGAP$_{317-326}$ remains to be precisely determined [18–20]. We initially assumed that working with a large panel of cell lines and cytotoxic agents would allow us to draw a pattern that could be used to predict which type of childhood tumors display sensitivity to TAT-RasGAP$_{317-326}$ in response to a given drug. Such information would be helpful to decipher the mode of action of TAT-RasGAP$_{317-326}$. For this purpose, we analyzed how the half maximal inhibitory concentration (IC_{50}) for each chemotherapeutic agent was

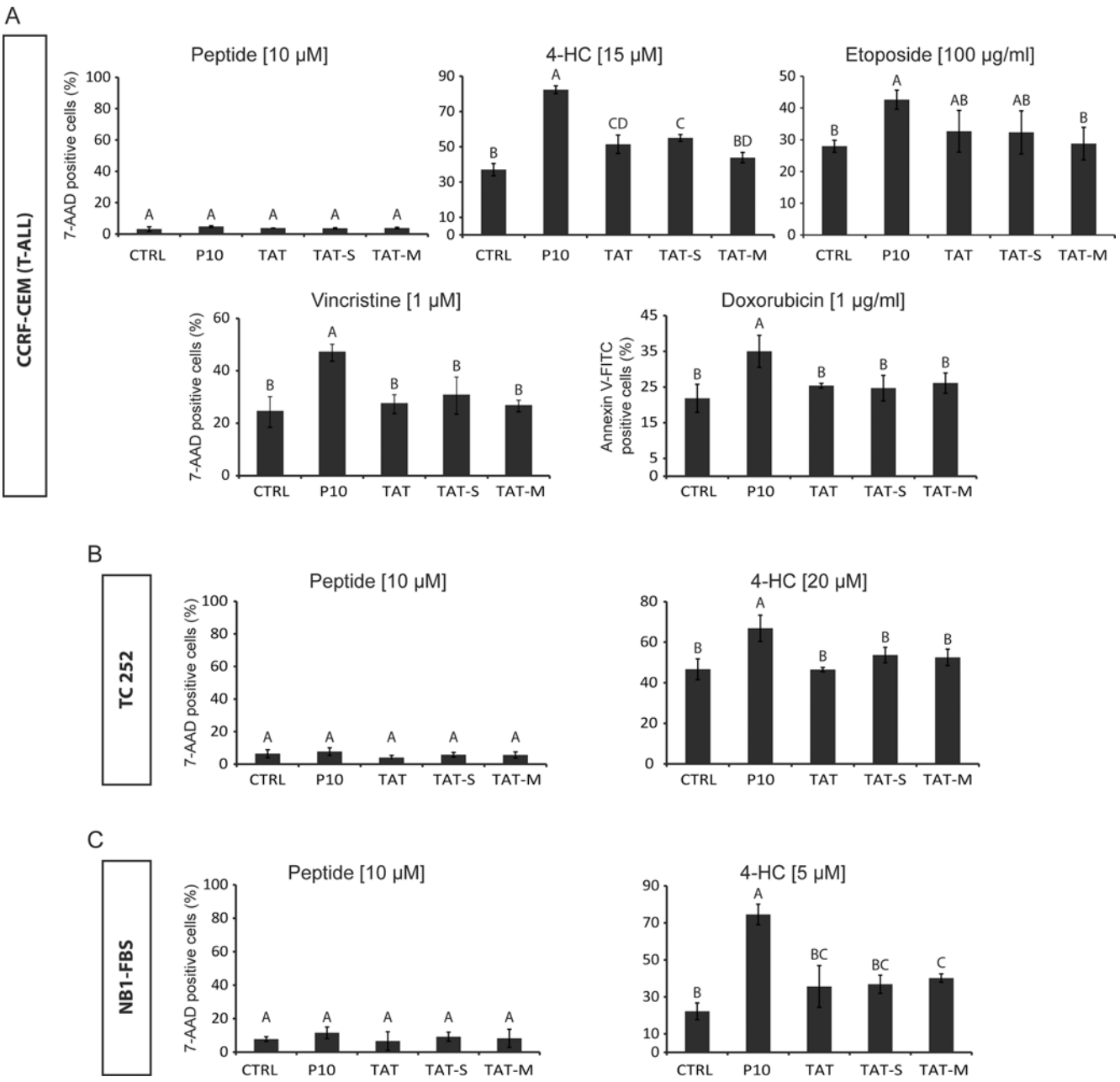

Fig 5. The RasGAP moiety carries the tumor sensitizing activity of TAT-RasGAP$_{317-326}$. A. CCRF-CEM cells were seeded in 6-well plates and directly treated with 10 µM TAT-RasGAP$_{317-326}$, TAT, TAT-Scrambled or TAT-Mutated in the absence or in the presence of 4-HC, etoposide, vincristine or doxorubicin at the indicated concentrations. After 24 hours of drug incubation, 7-AAD or Annexin V-FITC staining was performed to evaluate cell death. **B-C.** The TC252 (B) and NB1-FBS (C) cell lines were treated similarly but in combination with 4-HC only. P10, TAT-RasGAP$_{317-326}$; TAT-S, TAT-Scrambled; TAT-M, TAT-Mutated; 4-HC, 4-hydroperoxycyclophosphamide. Means with the same letter are not significantly different.

doi:10.1371/journal.pone.0120487.g005

modified by the presence of TAT-RasGAP$_{317-326}$ for a given cell line (Table 2). The RasGAP-derived peptide decreased the IC_{50} for most genotoxins in most cell lines. However, no specific pattern based on tumor origin or drug type could be deduced from the data presented in Table 2. We also looked whether there were some common specific mutations in well-known oncogenes or tumor suppressor genes (e.g. HRAS, KRAS, NRAS, HDM2, N-MYC, C-MYC, TAL1, FLI-1, MLL, p53 and Rb1) in the analyzed cell lines. Again, no association could be

Table 2. Sensitizing effect of the TAT-RasGAP$_{317-326}$ toward childhood tumors.

Cell line	Tumor type	Chemotherapy	IC_{50} (without peptide)	IC_{50} (with 10 μM TAT-RasGAP$_{317-326}$)	Effect of TAT-RasGAP$_{317-326}$ on IC_{50}
THP-1	AML	4-HC [μM]	38	25	Decrease
		Etoposide [μg/ml]	>20	10	Decrease
		Vincristine [μM]	>10	>10	-
		Doxorubicin [μg/ml]	0.3	0.3	No change
M-07e	AML	4-HC [μM]	20	11	Decrease
		Etoposide [μg/ml]	>150	150	Decrease
		Vincristine [μM]	>10	1	Decrease
		Doxorubicin [μg/ml]	2	2	No change
CEM	T-ALL	4-HC [μM]	25	12.5	Decrease
		Etoposide [μg/ml]	>100	25	Decrease
		Vincristine [μM]	>10	>10	-
		Doxorubicin [μg/ml]	>10	>10	-
EW-11	Ewing sarcoma	4-HC [μM]	40	35	Decrease
		Etoposide [μg/ml]	>200	>200	-
		Vincristine [μM]	>10	>10	-
		Doxorubicin [μg/ml]	3	1	Decrease
A673	Ewing sarcoma	4-HC [μM]	20	10	Decrease
		Etoposide [μg/ml]	>200	>200	-
		Vincristine [μM]	>10	>10	-
		Doxorubicin [μg/ml]	2	0.4	Decrease
TC252	Ewing sarcoma	4-HC [μM]	27	10	Decrease
		Etoposide [μg/ml]	>200	25	Decrease
		Vincristine [μM]	>10	>10	-
		Doxorubicin [μg/ml]	>10	3	Decrease
NB1-NBM	Neuroblastoma	4-HC [μM]	27	27	No change
		Etoposide [μg/ml]	25	1	Decrease
		Vincristine [μM]	10	0.04	Decrease
		Doxorubicin [μg/ml]	0.3	0.07	Decrease
NB1-FBS	Neuroblastoma	4-HC [μM]	10	3	Decrease
		Etoposide [μg/ml]	2.5	1	Decrease
		Vincristine [μM]	>10	>10	-
		Doxorubicin [μg/ml]	>10	>10	-
NB1-FBS-Re	Neuroblastoma	4-HC [μM]	15	2.5	Decrease
		Etoposide [μg/ml]	2.5	1	Decrease
		Vincristine [μM]	>10	>10	-
		Doxorubicin [μg/ml]	0.05	0.004	Decrease
LAN-1	Neuroblastoma	4-HC [μM]	26	24	Decrease
		Etoposide [μg/ml]	200	50	Decrease
		Vincristine [μM]	0.1	0.02	Decrease
		Doxorubicin [μg/ml]	0.3	0.3	No change

This table summarizes the effect of TAT-RasGAP$_{317-326}$ in combination with 4-HC, etoposide, vincristine or doxorubicin on the IC_{50} of the cell lines studied in this paper. IC_{50} were calculated for each chemotherapeutic agent in the absence or in the presence of 10 μM TAT-RasGAP$_{317-326}$. AML, acute myeloid leukemia; T-ALL, T-acute lymphoblastic leukemia; 4-HC, 4-hydroperoxycyclophophamide.

doi:10.1371/journal.pone.0120487.t002

found between the presence of specific mutations in a cancer cell line and its ability to be sensitized by the RasGAP-derived peptide.

An interesting aspect of this research is that the sensitization effect of TAT-RasGAP$_{317-326}$ can be differentially modulated by the cell culture conditions. This feature is illustrated by the fact that the NB1-FBS cells, but not the NB1-NBM cells, are sensitive to the effect of the peptide. These two cell lines are derived from the same neuroblastoma tumor at initial diagnosis (see Fig 4) but they were cultured in different media. These two cell lines appear to have the same genomic alterations. Indeed, they possess identical array-CGH profiles with the same typical neuroblastoma-associated segmental chromosomic alterations (unpublished data). So if these two cell lines have identical array-CGH profiles, what could explain their different sensitivity to TAT-RasGAP$_{317-326}$? One possibility is that the medium in which they are grown modulate their metabolism differentially. This might in turn affect their sensitivity to anti-cancer treatments. There are indeed accumulating evidence that the metabolic state of cancer cells play an important role in the way they respond to anti-cancer drugs [41]. Another hypothesis is that different cell populations are selected upon passages in different medium. Unlike the FBS-containing DMEM medium, the NBM medium blocks cell differentiation. Consequently, the NB1-FBS cells are potentially more differentiated than the NB1-NBM cells. The state of differentiation of the cells could explain their different behavior in response to TAT-RasGAP$_{317-326}$. Alternatively, passage in different medium may induce differential epigenetic modifications or mutations that impact on the sensitivities of the NB1-FBS and NB1-NBM cell lines toward the RasGAP-derived peptide.

We have previously shown that the genotoxin sensitivity of non-tumor cells is not affected by TAT-RasGAP$_{317-326}$ [12]. Moreover, doses that induce tumor sensitization *in vivo* do not exert any detectable toxic side effects [13]. In the present study, we tested the effect of the peptide in isolated lymphocytes from blood of healthy patients. We confirmed the non-toxic effect of the RasGAP-derived peptide in these cells. The peptide was also unable to sensitize the isolated lymphocytes to etoposide, vincristine or doxorubicin. However, TAT-RasGAP$_{317-326}$ was found sometimes to sensitize non-malignant lymphocytes to 4-HC-induced death. This finding is clinically relevant because one of the most frequent dose-limiting side effect of chemotherapy is hematological toxicity [42]. Consequently, if TAT-RasGAP$_{317-326}$ increases genotoxin-induced side effects toward non-tumor cells, it would lose its attractivity as an anti-cancer candidate to treat childhood tumors. However, cyclophosphamide (and consequently its active form 4-HC) possesses hematologic toxic effects. This toxicity depends of the cellular expression level of aldehyde dehydrogenase (ALDH), an enzyme responsible for cyclophosphamide detoxification. The expression level of ALDH is very low in mature hematopoietic cells such as lymphocytes, while in hematopoietic stem cells, ALDH is expressed at high levels. Thus, the later are relatively resistant to cyclophosphamide, whereas this alkylating agent is toxic toward mature lymphocytes [43]. This feature explains why white blood cell counts drop in patients treated with cyclophosphamide [44]. However this drop is transient and a rapid hematologic recovery invariably occurs after cyclophosphamide therapy. Consequently, the observed sensitizing effect of TAT-RasGAP$_{317-326}$ in combination with 4-HC in healthy lymphocytes may not be clinically incompatible, provided that the negative effect of the peptide is limited to mature hematopoietic cells and does not affect hematopoietic stem cells.

Although in most cases TAT-RasGAP$_{317-326}$ by itself does not kill tumor cells, we found out that it induced the cell death of the three NB1-derived cell lines tested here. This newly discovered feature has two consequences. First, it will give us the opportunity to study the pro-death activity of the peptide alone. This possibly may facilitate deciphering its mode of action by, for example, using genome-scale knockout screenings [45, 46]. Second, it indicates that the RasGAP-derived peptide, in its own right, corresponds to a new cytotoxic agent in certain tumors.

In conclusion, our work shows that in most cases TAT-RasGAP$_{317-326}$ sensitizes childhood cancer cells to genotoxins. However, it was not possible to predict the efficacy of this sensitization based on the tumor type and the drug used. Additional investigation is therefore required to increase our understanding on how TAT-RasGAP$_{317-326}$ works and to determine the indications for which it might be useful in the clinic.

Acknowledgments

The authors thank Dr. Camilla Jandus and Pr. Pedro Romero (Ludwig Center for Cancer Research of the University of Lausanne, Lausanne, Switzerland) for the gift of the isolated lymphocytes from the blood of healthy subjects and Sandrine Cornaz (Experimental Pathology, University Hospital Center (CHUV), Lausanne, Switzerland) for the gift of the A673 and TC252 cell lines. The authors also thank Pr. Ivan Stamenkovic (Experimental Pathology, University Hospital Center (CHUV), Lausanne, Switzerland) and Dr. Jean-Marc Joseph (Pediatric Department, University Hospital Center (CHUV), Lausanne, Switzerland) for their fruitful discussions. The authors thank Dr. David Barras (Department of Physiology, University of Lausanne, Switzerland) for valuable comments on this report.

Author Contributions

Conceived and designed the experiments: NC NG CW. Performed the experiments: NC. Analyzed the data: NC CW. Contributed reagents/materials/analysis tools: NG. Wrote the paper: NC CW.

References

1. Stiller CA, Marcos-Gragera R, Ardanaz E, Pannelli F, Almar Marqués E, Cañada Martinez A, et al. Geographical patterns of childhood cancer incidence in Europe, 1988–1997. Report from the Automated Childhood Cancer Information System project. European Journal of Cancer. 2006 9//; 42(13):1952–60. PMID: 16919763
2. Ward E, Desantis C, Robbins A, Kohler B, Jemal A. Childhood and adolescent cancer statistics, 2014. CA: a cancer journal for clinicians. 2014. Epub 2014 Jan 31.
3. Vassal G, Zwaan CM, Ashley D, Le Deley MC, Hargrave D, Blanc P, et al. New drugs for children and adolescents with cancer: the need for novel development pathways. The Lancet Oncology. 2013 3//; 14 (3):e117-e24. doi: 10.1016/S1470-2045(13)70013-5 PMID: 23434337
4. Robison LL, Hudson MM. Survivors of childhood and adolescent cancer: life-long risks and responsibilities. Nat Rev Cancer. 2014 01//print; 14(1):61–70. doi: 10.1038/nrc3634 PMID: 24304873
5. Reulen RC, Winter DL, Frobisher C, et al. LOng-term cause-specific mortality among survivors of childhood cancer. JAMA. 2010; 304(2):172–9. doi: 10.1001/jama.2010.923 PMID: 20628130
6. Mertens AC, Liu Q, Neglia JP, Wasilewski K, Leisenring W, Armstrong GT, et al. Cause-specific late mortality among 5-year survivors of childhood cancer: the Childhood Cancer Survivor Study. Journal of the National Cancer Institute. 2008 Oct 1; 100(19):1368–79. PMID: 18812549. Pubmed Central PMCID: 2556702. doi: 10.1093/jnci/djn310
7. Fulbright J, Raman S, McClellan W. Late effects of childhood leukemia therapy. Current Hematologic Malignancy Reports. 2011; 6(3):195–205. doi: 10.1007/s11899-011-0094-x PMID: 21695425
8. Armenian SH, Robison LL. Childhood cancer survivorship: an update on evolving paradigms for understanding pathogenesis and screening for therapy-related late effects. Current opinion in pediatrics. 2013 Feb; 25(1):16–22. PMID: 23295717. Pubmed Central PMCID: 3771864. doi: 10.1097/MOP.0b013e32835b0b6a
9. Barras D, Widmann C. Promises of apoptosis-inducing peptides in cancer therapeutics. [review]2011.
10. Sawyers C. Targeted cancer therapy. Nature. 2004 11/18/print; 432(7015):294–7. PMID: 15549090
11. Michod D, Widmann C. DNA-damage sensitizers: Potential new therapeutical tools to improve chemotherapy. Critical Reviews in Oncology/Hematology. 2007 8//; 63(2):160–71. PMID: 17544289
12. Michod D, Yang J-Y, Chen J, Bonny C, Widmann C. A RasGAP-derived cell permeable peptide potently enhances genotoxin-induced cytotoxicity in tumor cells. Oncogene. 2004 09/27/online; 23(55):8971–8. PMID: 15467750

13. Michod D, Annibaldi A, Schaefer S, Dapples C, Rochat B, Widmann C. Effect of RasGAP N2 Fragment–Derived Peptide on Tumor Growth in Mice. Journal of the National Cancer Institute. 2009 June 2, 2009; 101(11):828–32. doi: 10.1093/jnci/djp100 PMID: 19470951

14. Pittet O, Petermann D, Michod D, Krueger T, Cheng C, Ris H-B, et al. Effect of the TAT-RasGAP317–326 peptide on apoptosis of human malignant mesothelioma cells and fibroblasts exposed to meso-tetra-hydroxyphenyl-chlorin and light. Journal of Photochemistry and Photobiology B: Biology. 2007 7/27/; 88(1):29–35.

15. Barras D, Lorusso G, Ruegg C, Widmann C. Inhibition of cell migration and invasion mediated by the TAT-RasGAP peptide requires the DLC1 tumor suppressor. Oncogene. 2013 Nov 11. PMID: 24213569.

16. Barras D, Chevalier N, Zoete V, Dempsey R, Lapouge K, Olayioye MA, et al. A WxW Motif is required for the Anticancer Activity of TAT-RasGAP317-326. Journal of Biological Chemistry. 2014 July 9, 2014.

17. Barras D, Lorusso G, Lhermitte B, Viertl D, Rüegg C, Widmann C. Fragment N2, a caspase-3-generated RasGAP fragment, inhibits breast cancer metastatic progression. International Journal of Cancer. 2014; 135(1):242–7. doi: 10.1002/ijc.28674 PMID: 24347041

18. Yang J-Y, Widmann C. The RasGAP N-terminal Fragment Generated by Caspase Cleavage Protects Cells in a Ras/PI3K/Akt-dependent Manner That Does Not Rely on NFκB Activation. Journal of Biological Chemistry. 2002 April 26, 2002; 277(17):14641–6. PMID: 11847220

19. Michod D, Widmann C. TAT-RasGAP317-326 Requires p53 and PUMA to Sensitize Tumor Cells to Genotoxins. Molecular Cancer Research. 2007 May 1, 2007; 5(5):497–507. PMID: 17510315

20. Annibaldi A, Heulot M, Martinou J-C, Widmann C. TAT-RasGAP317–326-mediated tumor cell death sensitization can occur independently of Bax and Bak. Apoptosis. 2014 2014/04/01; 19(4):719–33. English. doi: 10.1007/s10495-013-0958-8 PMID: 24362790

21. Lawlor ER, Thiele CJ. Epigenetic Changes in Pediatric Solid Tumors: Promising New Targets. Clinical Cancer Research. 2012 May 15, 2012; 18(10):2768–79. doi: 10.1158/1078-0432.CCR-11-1921 PMID: 22589485

22. DePinho RA. The age of cancer. Nature. 2000 11/09/print; 408(6809):248–54. PMID: 11089982

23. McKenna ES, Roberts CWM. Epigenetics and cancer without genomic instability. Cell Cycle. 2009 01/01; 8(1):23–6. PMID: 19098432

24. Foley GE, Lazarus H, Farber S, Uzman BG, Boone BA, McCarthy RE. Continuous culture of human lymphoblasts from peripheral blood of a child with acute leukemia. Cancer. 1965; 18 522–9. l. PMID: 14278051

25. Tsuchiya S, Yamabe M, Yamaguchi Y, Kobayashi Y, Konno T, Tada K. Establishment and characterization of a human acute monocytic leukemia cell line (THP-1). International journal of cancer. 1980; 26 (2):171–6. PMID: 6970727

26. DJ G, SA A, GJ T, P A, JH K, H D, et al. In vitro cultivation of human tumors: establishment of cell lines derived from a series of solid tumors. Journal of the National Cancer Institute. 1973; 51(5):1417–23. PMID: 4357758

27. Seeger RC, Rayner SA, Banerjee A, Chung H, Laug WE, Neustein HB, et al. Morphology, growth, chromosomal pattern and fibrinolytic activity of two new human neuroblastoma cell lines. Cancer research. 1977; 37(5):1364–71. PMID: 856461

28. Avanzi GC, Lista P, Giovinazzo B, Miniero R, Saglio G, Benetton G, et al. Selective growth response to IL-3 of a human leukaemic cell line with megakaryoblastic features. British journal of haematology. 1988; 69(3):359–66. PMID: 3261598

29. Turc-Carel C, Philip I, Berger MP, Philip T, Lenoir GM. Chromosome study of Ewing's sarcoma (ES) cell lines. Consistency of a reciprocal translocation t(11;22)(q24;q12). Cancer Genet Cytogenet. 1984; 12(1):1–19. PMID: 6713356

30. De Vito C, Riggi N, Cornaz S, Suvà M- L, Baumer K, Provero P, et al. A TARBP2-Dependent miRNA Expression Profile Underlies Cancer Stem Cell Properties and Provides Candidate Therapeutic Reagents in Ewing Sarcoma. Cancer Cell. 2012 6/12/; 21(6):807–21. doi: 10.1016/j.ccr.2012.04.023 PMID: 22698405

31. Coulon A, Flahaut M, Mühlethaler-Mottet A, Meier R, Liberman J, Balmas-Bourloud K, et al. Functional sphere profiling reveals the complexity of neuroblastoma tumor-initiating cell model. Neoplasia. 2011; 13(10):991–1004. PMID: 22028624

32. Shen F, Chu S, Bence AK, Bailey B, Xue X, Erickson PA, et al. Quantitation of Doxorubicin Uptake, Efflux, and Modulation of Multidrug Resistance (MDR) in MDR Human Cancer Cells. Journal of Pharmacology and Experimental Therapeutics. 2008 January 1, 2008; 324(1):95–102. PMID: 17947497

33. Cheung NV, Zhang J, Lu C, et al. ASsociation of age at diagnosis and genetic mutations in patients with neuroblastoma. JAMA. 2012; 307(10):1062–71. doi: 10.1001/jama.2012.228 PMID: 22416102

34. Keshelava N, Seeger RC, Reynolds CP. Drug resistance in human neuroblastoma cell lines correlates with clinical therapy. European Journal of Cancer. 1997 10//; 33(12):2002–6. PMID: 9516842

35. Maris JM, Hogarty MD, Bagatell R, Cohn SL. Neuroblastoma. The Lancet. //; 369(9579):2106–20. PMID: 17586306

36. Metayer C, Milne E, Clavel J, Infante-Rivard C, Petridou E, Taylor M, et al. The Childhood Leukemia International Consortium. Cancer Epidemiology. 2013 6//; 37(3):336–47. doi: 10.1016/j.canep.2012.12.011 PMID: 23403126

37. Balamuth NJ, Womer RB. Ewing's sarcoma. The Lancet Oncology. 2010 2//; 11(2):184–92. doi: 10.1016/S1470-2045(09)70286-4 PMID: 20152770

38. Marshall GM, Carter DR, Cheung BB, Liu T, Mateos MK, Meyerowitz JG, et al. The prenatal origins of cancer. Nat Rev Cancer. 2014 04//print; 14(4):277–89. doi: 10.1038/nrc3679 PMID: 24599217

39. Cheung N-KV, Dyer MA. Neuroblastoma: developmental biology, cancer genomics and immunotherapy. Nat Rev Cancer. 2013 06//print; 13(6):397–411. doi: 10.1038/nrc3526 PMID: 23702928

40. Kilk K, Mahlapuu R, Soomets U, Langel Ü. Analysis of in vitro toxicity of five cell-penetrating peptides by metabolic profiling. Toxicology. 2009 11/30/; 265(3):87–95. doi: 10.1016/j.tox.2009.09.016 PMID: 19799958

41. Zhao Y, Butler EB, Tan M. Targeting cellular metabolism to improve cancer therapeutics. Cell Death Dis. 2013 03/07/online; 4:e532. doi: 10.1038/cddis.2013.60 PMID: 23470539

42. Shiozawa Y, Takita J, Kato M, Sotomatsu M, Koh K, Ida K, et al. Prognostic significance of leukopenia in childhood acute lymphoblastic leukemia. oncology letters. 2014; 7(4):1169–74. PMID: 24944687

43. Emadi A, Jones R, Brodsky R. Cyclophosphamide and cancer: golden anniversary. Nature. 2009; 6 (11):638–47. doi: 10.1038/nrclinonc.2009.146 PMID: 19786984

44. Hayes F, Short R, JE G. A correlation between cyclophosphamide induced leukopenia in mice and the presence of alkylating metabolites. Proc Soc Exp Biol Med. 1972; 139(2):417–21. PMID: 5059031

45. Wang T, Wei JJ, Sabatini DM, Lander ES. Genetic Screens in Human Cells Using the CRISPR-Cas9 System. Science. 2014 January 3, 2014; 343(6166):80–4. doi: 10.1126/science.1246981 PMID: 24336569

46. Shalem O, Sanjana NE, Hartenian E, Shi X, Scott DA, Mikkelsen TS, et al. Genome-Scale CRISPR-Cas9 Knockout Screening in Human Cells. Science. 2014 January 3, 2014; 343(6166):84–7. doi: 10.1126/science.1247005 PMID: 24336571

PART II

THE TAT-RASGAP$_{317-326}$ ANTI-CANCER PEPTIDE CAN KILL IN A CASPASE-, APOPTOSIS-, AND NECROPTOSIS-INDEPENDENT MANNER.

Cancer cell resistance to apoptosis, which is triggered by many anti-tumour therapies, remains a major clinical problem. Henceforth, the development of novel and more efficient therapies is a priority to improve cancer prognosis. We have previously shown that TAT-RasGAP$_{317-326}$ bears anti-malignant activities *in vitro* and *in vivo,* such as inhibition of metastatic progression and tumour cell sensitization to cell death induced by anti-cancer therapies. Recently, we have discovered that this RasGAP-derived peptide possesses the ability to directly kill some cancer cells (e.g. the NB1 neuroblastoma and the Raji Burkitt lymphoma cell lines).

The characterization of the type of cell death triggered by the peptide is the subject of a first author paper published in Oncotarget in September 2016: “The TAT-RasGAP$_{317-326}$ anti-cancer peptide can kill in a caspase-, apoptosis-, and necroptosis-independent manner”. Of note, this study was carried out in collaboration with Mathieu Heulot. We equally contributed to the data presented in this section. I performed all the experiments in NB1 cells.

Our results showed that TAT-RasGAP$_{317-326}$ can activate both caspase-dependent and caspase-independent cell death. Indeed, TAT-RasGAP$_{317-326}$-induced cell death was not or only partially prevented when apoptosis was inhibited, either genetically or pharmacologically. Moreover, blocking other forms of cell death, such as necroptosis, autophagy, parthanatos, or pyroptosis, did not hamper the killing activity of the peptide. TAT-RasGAP$_{317-326}$ is, therefore, able to trigger a type of cell death, which is distinct from those known forms of regulated death. Our finding has potentially important clinical relevance because uncovering a newly described form of death in tumour cells could lead to the generation of anti-cancer drugs that target pathways not yet considered for cancer treatment.

Although these results allow a better understanding of the mode of action of the peptide, additional investigations were required to decipher the mechanisms involved in TAT-RasGAP$_{317-326}$ toxicity. For this purpose, CRISPR/Cas9-based screens were performed to identify genes that are required for the peptide to kill. The validation and the study of the role of the various candidates highlighted by these screenings are exposed in the next part of this manuscript.

Research Paper

The TAT-RasGAP$_{317-326}$ anti-cancer peptide can kill in a caspase-, apoptosis-, and necroptosis-independent manner

Mathieu Heulot[1,*], Nadja Chevalier[1,*], Julien Puyal[2], Christiane Margue[3], Sébastien Michel[1], Stephanie Kreis[3], Dagmar Kulms[4,5], David Barras[6], Aimable Nahimana[7], Christian Widmann[1]

[1]Department of Physiology, University of Lausanne, Lausanne, Switzerland

[2]Department of Fundamental Neurosciences, University of Lausanne, Lausanne, Switzerland

[3]Signal Transduction Laboratory, Life Sciences Research Unit, University of Luxembourg, Luxembourg, Luxembourg

[4]Experimental Dermatology, Department of Dermatology, TU-Dresden, Dresden, Germany

[5]Center for Regenerative Therapies, TU-Dresden, Dresden, Germany

[6]Bioinformatics Core Facility, Swiss Institute of Bioinformatics, Lausanne, Switzerland

[7]Service and Central Laboratory of Hematology, University Hospital of Lausanne, Lausanne, Switzerland

[*]These authors have contributed equally to this work

Correspondence to: *Christian Widmann,* ***email:*** *Christian.Widmann@unil.ch*

Keywords: *tumor cell death, non-apoptotic death, cell-permeable peptides, RasGAP*

Received: *April 21, 2016* ***Accepted:*** *August 24, 2016* ***Published:*** *September 02, 2016*

ABSTRACT

Tumor cell resistance to apoptosis, which is triggered by many anti-tumor therapies, remains a major clinical problem. Therefore, development of more efficient therapies is a priority to improve cancer prognosis. We have previously shown that a cell-permeable peptide derived from the p120 Ras GTPase-activating protein (RasGAP), called TAT-RasGAP$_{317-326}$, bears anti-malignant activities *in vitro* and *in vivo*, such as inhibition of metastatic progression and tumor cell sensitization to cell death induced by various anti-cancer treatments. Recently, we discovered that this RasGAP-derived peptide possesses the ability to directly kill some cancer cells. TAT-RasGAP$_{317-326}$ can cause cell death in a manner that can be either partially caspase-dependent or fully caspase-independent. Indeed, TAT-RasGAP$_{317-326}$-induced toxicity was not or only partially prevented when apoptosis was inhibited. Moreover, blocking other forms of cell death, such as necroptosis, parthanatos, pyroptosis and autophagy did not hamper the killing activity of the peptide. The death induced by TAT-RasGAP$_{317-326}$ can therefore proceed independently from these modes of death. Our finding has potentially interesting clinical relevance because activation of a death pathway that is distinct from apoptosis and necroptosis in tumor cells could lead to the generation of anti-cancer drugs that target pathways not yet considered for cancer treatment.

INTRODUCTION

Cancer ranks among the leading causes of death worldwide [1]; this makes the development of novel and improved anti-cancer treatment a priority. Current oncological therapeutics aim to activate apoptosis to achieve disease control. However, cancer cells can adapt and become refractory to therapy by mutating and acquiring the ability to resist apoptotic stimuli [2]. The ability to evade apoptosis is one of the hallmarks of cancer [3]. Resistance leads to cancer cell survival and relapse. Consequently, development of treatments able to trigger non-apoptotic forms of death in cancer cells is of prime interest. There are many ways for mammalian cells to die, which could be divided into two main categories: accidental cell death (ACD) or regulated cell death (RCD) [4-6]. ACD is a form of death that is not induced by physiological or pathological insults and that does not involve the signaling machinery of cells. For example, ACD can result from exposure to extreme mechanical or chemical stimuli. In contrast, RCD requires genetically encoded molecular signaling

pathways and consequently can be modulated by genetic or pharmacologic interventions. Regulated forms of cell death include the intensively studied apoptosis, necroptosis and autophagy but also less known forms of death such as pyroptosis and parthanatos. These different types of cell death diverge at the level of the morphological changes and biochemical features triggered by death stimuli [4-6].

TAT-RasGAP$_{317-326}$, a cell-permeable peptide derived from the p120 GTPase-activating protein (RasGAP), bears anti-malignant activities, including inhibition of metastatic progression and tumor cell sensitization to cell death induced by anti-cancer therapies [7-12]. This compound, in the initial tumor cell lines tested and at the given doses assessed was not found to affect their viability [7]. By screening additional tumor cells, however, we discovered that some cancer cell lines are directly killed by the RasGAP-derived peptide. The aim of the present study was to investigate which type of death was activated by TAT-RasGAP$_{317-326}$ in the cells that are directly eliminated by the peptide.

RESULTS

TAT-RasGAP$_{317-326}$ directly kills a subset of cancer cells

By screening a variety of cancer cell lines for their ability to become more sensitive to genotoxins in the presence of TAT-RasGAP$_{317-326}$, we found 13 tumor cell lines that were directly killed by the peptide (Table 1). Among these, five are B-cell-derived cell lines (Daudi, Namalwa, Raji, Ramos and SKW6.4). To determine if non-transformed B cells were affected by the peptide, purified B cells (CD19$^+$ cells) from healthy donors were tested. Supplementary Figure S1 shows that normal B cells were killed by TAT-RasGAP$_{317-326}$ while peripheral blood lymphocytes (PBL) were barely affected. This indicates that the RasGAP-derived peptide can be detrimental to a fraction of immune circulating cells and this will have to be taken into account in case the peptide is therapeutically used.

Two of the tumor cells that were efficiently killed by the peptide, the Raji Burkitt lymphoma and the NB1 neuroblastoma cell lines, were used to investigate the manner by which the peptide induced death. Supplementary Figure S2 shows that the peptide did not alter the proportion of cells in a given cell cycle stage, suggesting that cell cycle regulators are not targeted by the peptide. When treated with an inactive point mutant of the peptide [TAT-RasGAP$_{317-326}$ (W317A)] [13], or with the TAT cell-penetrating peptide alone, viability of Raji and NB1 cells was not affected (Figure 1A). This demonstrates that the direct killing ability of TAT-RasGAP$_{317-326}$ is not carried solely by the TAT moiety but depends on specific RasGAP sequences. TAT-RasGAP$_{317-326}$ induced membrane permeabilization in a dose-dependent manner in both Raji and NB1 cells (Supplementary Figure S3A). The kinetic of death, induced by the peptide was assessed using Annexin-V and 7AAD staining. Annexin-V binds to phosphatidylserine (PS) exposed at the cell surface, a phenomenon that is generally characteristic of apoptosis. The 7AAD dye is plasma membrane impermeable and thus only labels cells with compromised cell permeability, which is typically seen in necrotic cells. Apoptotic cells bind Annexin-V but remain initially 7AAD negative [14]. Figure 1B-1C shows that Annexin-V and 7AAD positivity occurred concomitantly in Raji and NB1 cells when incubated with TAT-RasGAP$_{317-326}$. In contrast and as expected, apoptotic inducers in these cells (e.g. Fas ligand (FasL) or etoposide) induced PS exposure before membrane impermeability was compromised (Figure 1D). Of note, in both Raji and NB1 cells, TAT-RasGAP$_{317-326}$ induced a drop in mitochondrial membrane potential (Supplementary Figure S3B).

Reactive oxygen species (ROS) production upon peptide treatment was investigated. Intracellular hydrogen peroxide (H_2O_2) and cytosolic superoxide ($CO_2^{\bullet-}$) were not augmented by TAT-RasGAP$_{317-326}$ (Supplementary Figure S4A). The sensors for these ROS were functional as shown in Jurkat cells treated with APO866, a nicotinamide phosphoribosyltransferase inhibitor (Supplementary Figure S4B). In contrast to hydrogen peroxide and cytosolic superoxide, mitochondrial superoxide ($mO_2^{\bullet-}$) was increased in NB1 and, less markedly, in Raji cells in response to TAT-RasGAP$_{317-326}$ treatment (Supplementary Figure S4A). To assess the impact of mitochondrial ROS production on the viability of these cells, they were incubated with MitoTEMPO, a mitochondria-specific ROS scavenger. Supplementary Figure S4C shows that MitoTEMPO efficiently reduced TAT-RasGAP$_{317-326}$-induced $mO_2^{\bullet-}$ production in NB1 cells and this lowered death induced by the peptide. However, in Raji cells, MitoTEMPO did neither reduce the level of $mO_2^{\bullet-}$ nor TAT-RasGAP$_{317-326}$-induced death. While it is not clear why MitoTEMPO failed to inhibit mitochondrial superoxide production in Raji cells, the data obtained in NB1 cells indicate that TAT-RasGAP$_{317-326}$ might kill some cells via production of mitochondrial ROS.

As the RasGAP-derived peptide impacted the functionality of mitochondria, we determined if it modulated cellular ATP levels. As shown in Supplementary Figure S4D, the peptide induced a drop in ATP levels in Raji and NB1 cells. Intriguingly, this drop started to occur before any detectable cell death, suggesting that the peptide impacts cellular metabolism before inducing membrane permeabilization.

To evaluate the morphological changes involved in TAT-RasGAP$_{317-326}$-induced cell death, we performed ultrastructural analyses in Raji and NB1 cells using electron microcopy (Figures 2 and 3). To have a comparison with apoptosis, we also treated Raji cells

Table 1: Cell lines tested for their sensitivity to TAT-RasGAP$_{317-326}$.

	TAT-RasGAP$_{317-326}$ (μM)					
Cell line	**10**	**20**	**40**	**60**	**80**	**Ref**
293T (embryonic kidney)	ND	-	-	ND	+	Unpublished
501Mel (melanoma)	ND	-	-	ND	ND	Unpublished
A375 (melanoma)	-	-	++	++	ND	Unpublished
A673 (Ewing sarcoma)	-	ND	ND	ND	ND	[12]
CCRF-CEM (acute T cell leukemia)	-	ND	ND	ND	ND	[12]
Daudi (Burkitt lymphoma)	-	++	++	ND	ND	Unpublished
EW-11 (Ewing sarcoma)	-	ND	ND	ND	ND	[12]
H1299 (non-small cell lung carcinoma)	ND	-	ND	ND	ND	[46]
HaCat (non-tumor keratinocyte)	ND	-	ND	ND	ND	[7]
HCT116 (colorectal carcinoma)	ND	-	ND	ND	ND	[7]
HeLa (cervical cancer)	-	-	+	ND	++	[7] / Unpublished
H-meso1 (lung mesothelioma)	ND	-	ND	ND	ND	[7]
HUVECC (non-tumor endothelial cells)	ND	-	ND	ND	ND	[7]
IGr37 (melanoma)	ND	-	-	ND	ND	Unpublished
IPC298 (melanoma)	ND	-	-	ND	ND	Unpublished
Jurkat (acute T cell leukemia)	-	-	ND	ND	ND	Unpublished
LAN-1 (neuroblastoma)	-	ND	ND	ND	ND	[12]
Lymphocytes (human PBL)	-	-	+	ND	+	[12] / Unpublished
MCF-7 (breast cancer)	ND	-	ND	ND	ND	[7]
MEF (mouse embryo fibroblast)	ND	-	ND	ND	ND	[44]
MelJuso (melanoma)	ND	-	-	ND	ND	Unpublished
MO7e (acute myeloid leukemia)	-	ND	ND	ND	ND	[12]
Namalwa (Burkitt lymphoma)	-	-	-	+	++	Unpublished
NB1 (neuroblastoma)	-	++	++	++	++	[12]/This study
PC3 (prostate cancer)	ND	-	ND	ND	ND	Unpublished
Raji (Burkitt lymphoma)	-	++	++	++	++	This study
Ramos (Burkitt lymphoma)	-	+	++	ND	++	Unpublished
RPMI-8226 (myeloma)	-	-	ND	ND	ND	Unpublished
SAOS (osteosarcoma)	ND	-	ND	ND	ND	[46]
SkMel30 (melanoma)	ND	-	-	ND	ND	Unpublished
SK-N-Be(2)c (neuroblastoma)	-	ND	ND	ND	ND	[12]
SKW6.4 (transformed B-lymphoblastoid)	-	++	++	++	++	Unpublished

(*Continued*)

	TAT-RasGAP$_{317-326}$ (μM)					
Cell line	**10**	**20**	**40**	**60**	**80**	**Ref**
TC252 (Ewing sarcoma)	-	ND	ND	ND	ND	[12]
THP-1 (acute myeloid leukemia)	-	-	++	++	++	[12] / Unpublished
U2OS (osteosacroma)	-	-	-	-	-	[7] / Unpublished
Vero (monkey kidney)	-	-	-	ND	+	Unpublished
WM1366 (melanoma)	ND	+	++	ND	++	Unpublished
WM3248 (melanoma)	ND	+	++	ND	++	Unpublished

ND: not determined. -: not killed. +: < 20% killed. ++: > 20% killed.

with FasL, a well-known apoptotic inducer (Figure 2). FasL treatment induced apoptotic cell death with classical morphological criteria including nuclear and cytoplasmic condensation, chromatin condensation throughout the nucleus (pyknosis), nuclear fragmentation, and minimal alterations of organelles (including mitochondria). TAT-RasGAP$_{317-326}$-treated Raji cells displayed different morphological features than those seen in FasL-treated cells (Figure 2). At first, slight and heterogeneous chromatin condensation without nuclear fragmentation, shrinkage of the cytoplasm and accumulation of cytoplasmic materials around the nucleus were observed. Organelles aggregated in distinct portions of the cytoplasm whereas some cytoplasmic areas seemed to be devoid of organelles. Organelles displayed a relatively good preservation but some mitochondria showed condensed features. Then, at later stages, Raji cells displayed a necrotic-like phenotype such as huge organelle swelling and loss of plasma membrane integrity. The inactive TAT-RasGAP$_{317-326}$ (W317A) mutant did not alter the ultrastructural morphology of Raji cells.

Whereas TAT-RasGAP$_{317-326}$-induced Raji cell death displayed a non-canonical morphological phenotype, TAT-RasGAP$_{317-326}$-induced NB1 cell death showed some morphological features of apoptosis including chromatin condensation, nuclear fragmentation and condensed mitochondria at early stage and then secondary necrosis morphological features at later stage (Figure 3). Morphological features in TAT-RasGAP$_{317-326}$-induced NB1 cell death are therefore relatively similar to those observed when NB1 cells were exposed to the pro-apoptotic drug etoposide. However, clear differences were detected at the ultrastructural level between TAT-RasGAP$_{317-326}$- and etoposide-treated NB1 cells. For example, the peptide never induced pyknosis in NB1 cells while etoposide almost always did so. Moreover, cytoplasmic materials often accumulated close to the nucleus in response to TAT-RasGAP$_{317-326}$, while this was rarely the case when cells were incubated with etoposide. As seen in Raji cells, the inactive TAT-RasGAP$_{317-326}$ (W317A) mutant had no effect on the ultrastructure of NB1 cells.

The data shown in Figures 2 and 3 indicate that TAT-RasGAP$_{317-326}$ is inducing a form of death that is sharing some characteristics with apoptosis, at least in some cell lines, but which does not seem to be strictly equivalent to this mode of death. We therefore aimed to determine if other types of cell death were triggered by the RasGAP-derived peptide.

Apoptosis inhibition does not protect against TAT-RasGAP$_{317-326}$-induced cell death in Raji cells and only partially in NB1 cells

TAT-RasGAP$_{317-326}$ induced caspase-3 activation and PARP1 cleavage in both Raji and NB1 cells (Figure 4A), indicating that the peptide can trigger an apoptotic program. However, inhibition of caspase activity with the pan-caspase Z-VD-fmk inhibitor [15, 16] (Figure 4A), while efficiently blocking apoptosis triggered by FasL, had no effect on death induced by TAT-RasGAP$_{317-326}$ in Raji cells (Figure 4B). In NB1 cells, however, a partial protection was observed (Figure 4B). Intrinsic mitochondrial apoptosis is characterized by the release of cytochrome *c* into the cytosol, which depends on the pore forming proteins Bax and Bak. Unlike tBid, TAT-RasGAP$_{317-326}$ did not induce cytochrome *c* release from isolated mitochondria (Supplementary Figure S5), suggesting no direct action at the mitochondria level. The activity of Bax and Bak can be inhibited by over-expression of anti-apoptotic Bcl-2 family members, such as Bcl-X$_L$ [17, 18]. Bcl-X$_L$ over expression (Figure 4C) partially prevented TAT-RasGAP$_{317-326}$-induced apoptosis in NB1 cells (Figure 4D). In Raji cells, etoposide, even at high doses, only induced a slight increase in apoptosis, most probably because Raji cells express high basal level of Bcl-2 [19]. However, Bcl-X$_L$ overexpression did not protect Raji cells against

TAT-RasGAP$_{317-326}$-induced death (Figure 4D). Similar results were obtained when Bax and Bak expression were removed by gene disruption using the CRISPR/Cas9 technology (Figure 4E-4F). Combining Bcl-X$_L$ overexpression and Z-VD-fmk treatment did not induce a stronger inhibition of TAT-RasGAP$_{317-326}$-induced death in NB1 cells as compared to individual inhibitor applications (Figure 4G).

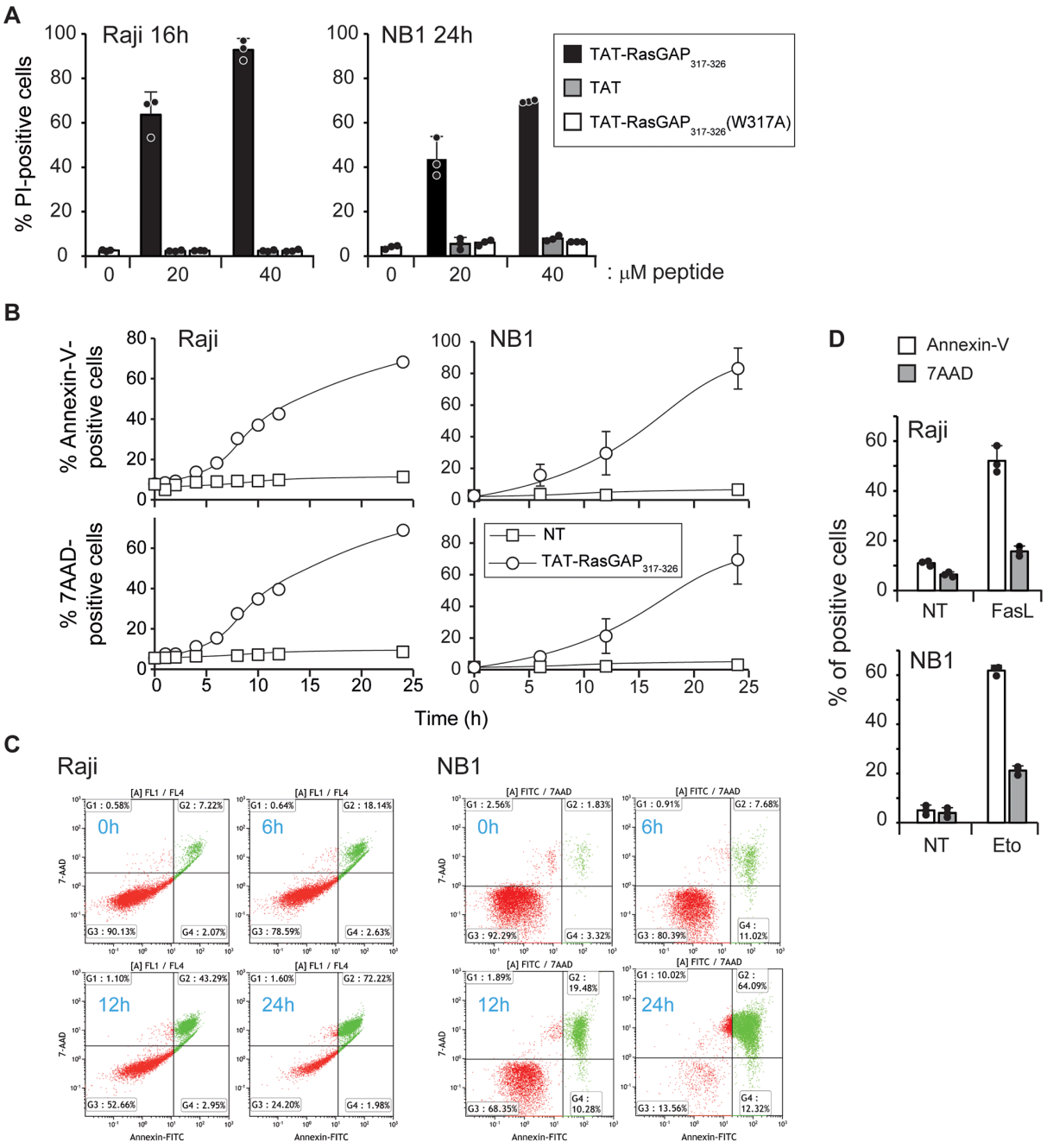

Figure 1: TAT-RasGAP$_{317-326}$ directly kills Raji and NB1 cells A. Raji cells and NB1 cells were treated for 16 and 24 hours, respectively, with 0, 20 and 40 µM TAT-RasGAP$_{317-326}$, TAT or TAT-RasGAP$_{317-326}$(W317A). Cell death, corresponding to the percentage of propidium iodide (PI)-positive cells, was determined by flow cytometry. Results correspond to the mean +/- 95% confidence interval (CI) of 3 independent experiments. **B.** Raji and NB1 cells were treated with 20 µM and 40 µM TAT-RasGAP$_{317-326}$, respectively, for the indicated periods of time. Phosphatidylserine exposure and plasma membrane permeabilization were then analyzed by flow cytometry using Annexin-V and 7AAD staining, respectively. **C.** Double stain analysis of 7AAD- and Annexin-V positive cells in Raji and NB1 cells after the indicated periods of time of TAT-RasGAP$_{317-326}$ treatment. **D.** Raji and NB1 cells were treated with 150 ng/mL FasL for 16 hours and 10 µg/mL etoposide for 9 hours, respectively. Cell death was analyzed as in panel B. The results correspond to the mean +/- 95% CI of 3 independent experiments.

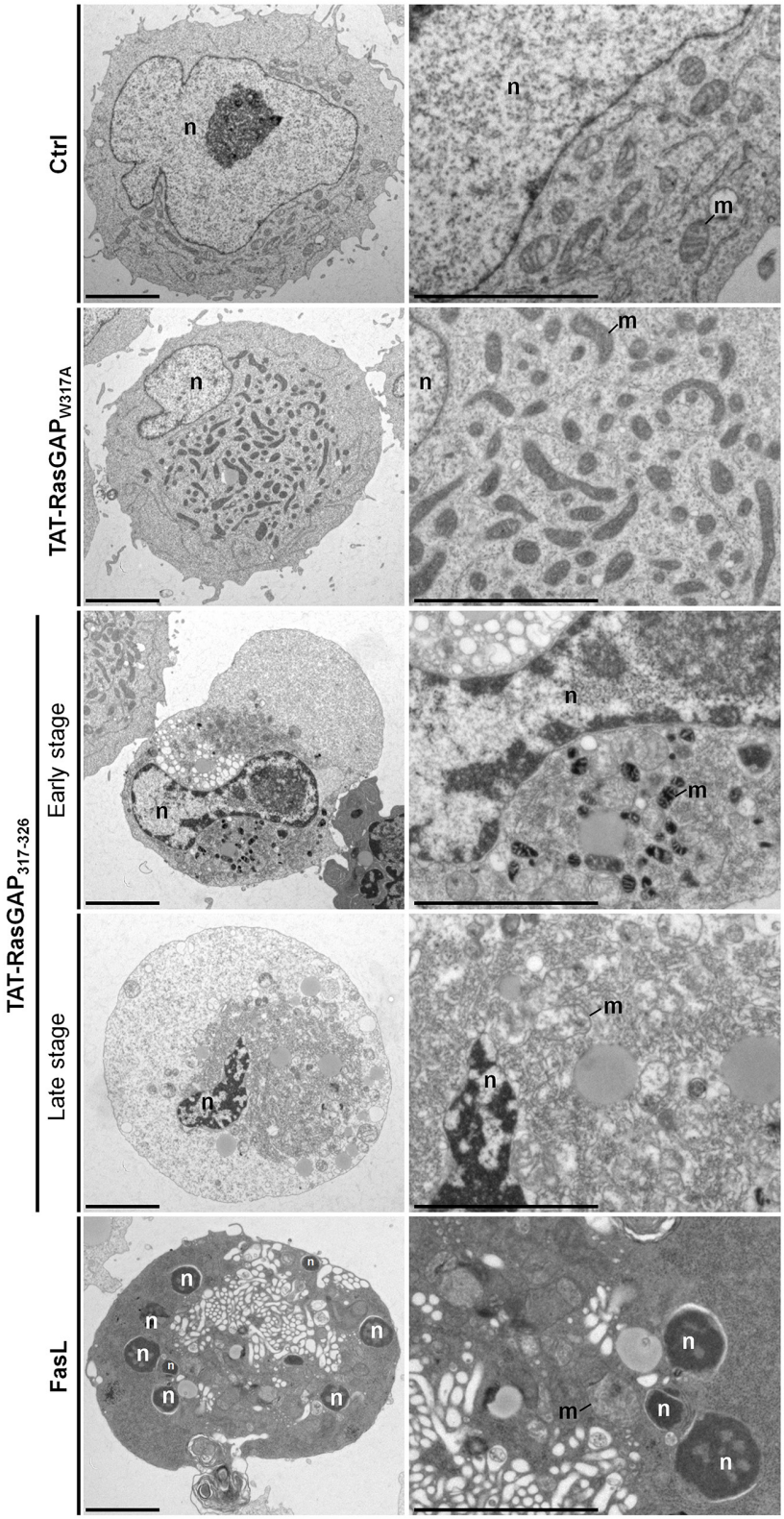

Figure 2: Ultrastructural analysis of TAT-RasGAP$_{317-326}$-induced cell death in Raji cells. Representative electron micrographs showing the morphological ultrastructural features in Raji cells left untreated (Ctrl) or incubated with 20 µM TAT-RasGAP$_{317-326}$ (W317) (24 hours), 20 µM TAT-RasGAP$_{317-326}$ (24 hours) or with 150 ng/mL FasL (16 hours). Scale bars: 5 µm. n: nucleus; m: mitochondria.

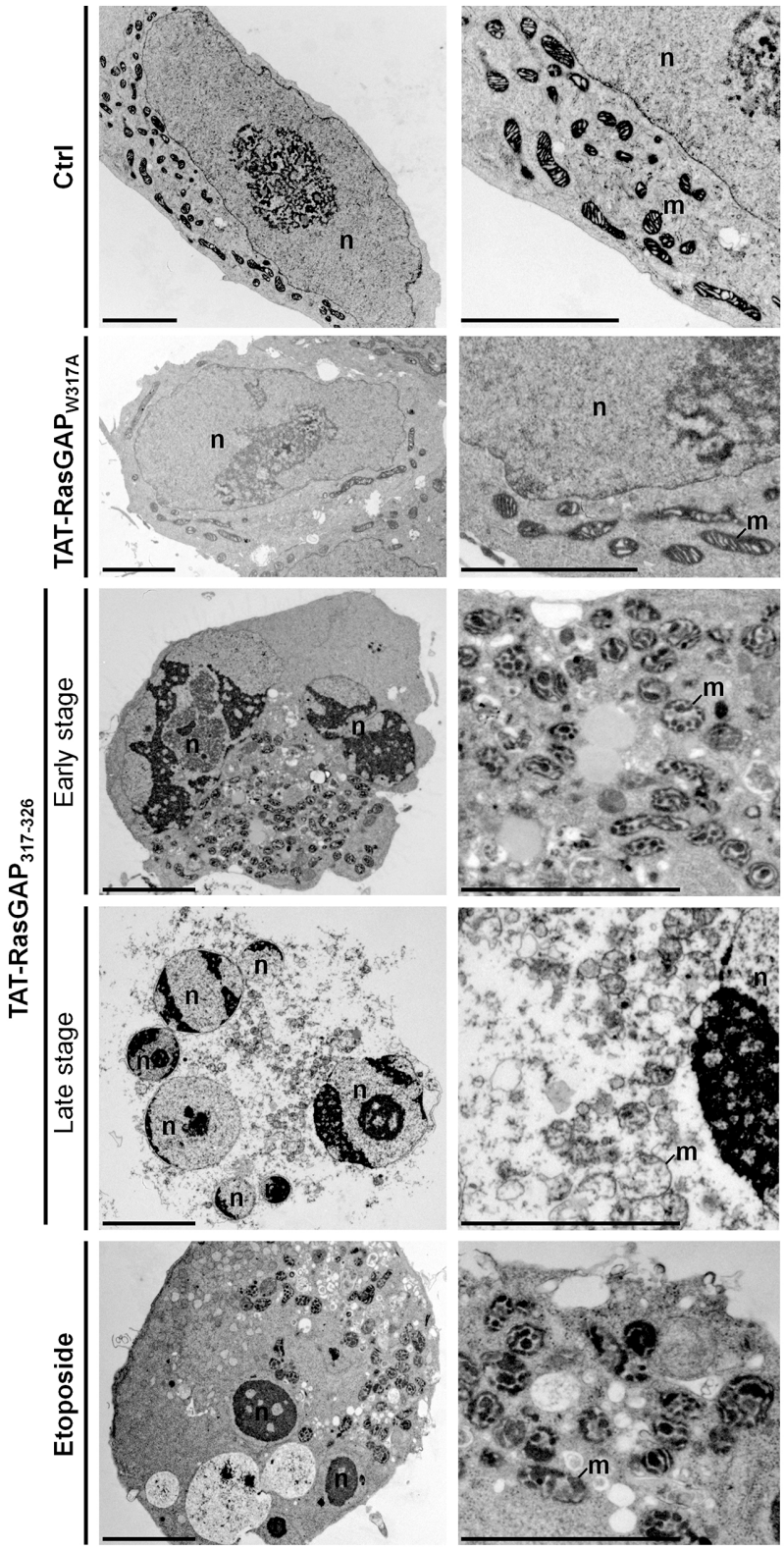

Figure 3: Ultrastructural analysis of TAT-RasGAP$_{317-326}$-induced cell death in NB1 cells. Representative electron micrographs showing the morphological ultrastructural features in NB1 cells in control condition (Ctrl) or after 40 µM TAT-RasGAP$_{317-326}$ (w317A) (24 hours), 40 µM TAT-RasGAP$_{317-326}$ (24 hours) or 10 µg/mL etoposide (8 hours) treatments. Scale bar: 5 µm. n: nucleus; m: mitochondria.

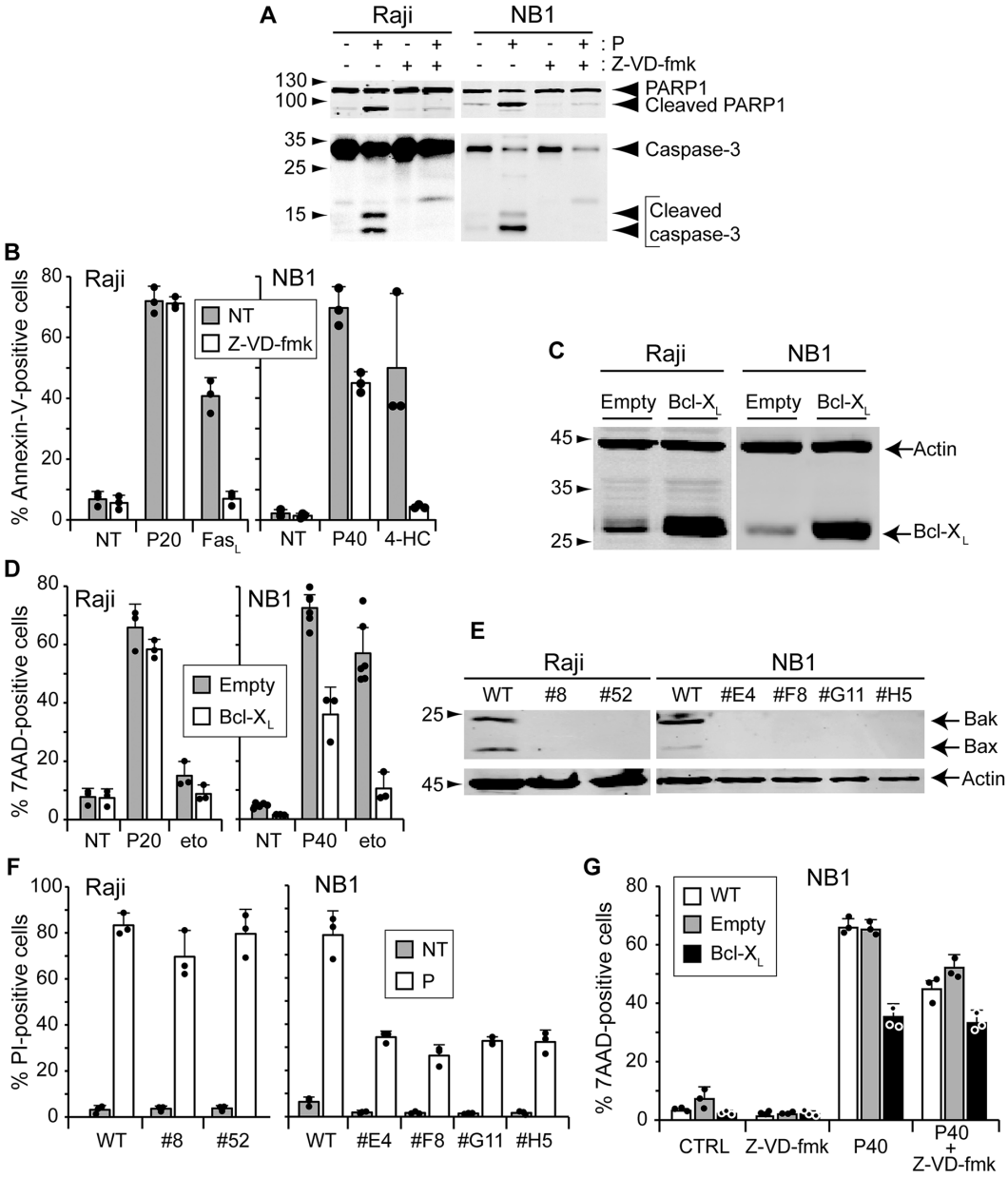

Figure 4: Inhibition of apoptosis does not prevent TAT-RasGAP$_{317-326}$-induced cell death. A. Raji cells and NB1 cells were pre-incubated or not 1 hour with 10 µM of the pan-caspase inhibitor Z-VD-fmk. Raji cells were then treated with 20 µM TAT-RasGAP$_{317-326}$ for 16 hours and NB1 cells with 40 µM TAT-RasGAP$_{317-326}$ for 24 hours. Cells were lysed and cleavage of PARP and caspase-3 analyzed by Western blotting. **B.** Raji and NB1 cells were pre-incubated or not 1 hour with 10 µM of the pan-caspase inhibitor Z-VD-fmk. Raji cells were then treated with 20 µM TAT-RasGAP$_{317-326}$ (P20) and 150 ng/mL Fas-ligand (FasL) for 16 hours. NB1 cells were treated with 40 µM TAT-RasGAP$_{317-326}$ (P40) and 30 µM 4-HC, the active form of cyclophosphamide, for 24 hours. Cell death (corresponding to the % of Annexin-V positive cells) was determined by FACS. Results correspond to the mean +/- 95% CI of 3 independent experiments. **C.** Raji and NB1 cells were infected with empty viruses or viruses encoding Bcl-X$_L$. Bcl-X$_L$ expression levels were assessed by Western blotting. **D.** Raji cells overexpressing or not Bcl-X$_L$ were treated with 20 µM TAT-RasGAP$_{317-326}$ and 250 µM etoposide (eto) for 16 hours. NB1 cells overexpressing or not Bcl-X$_L$ were treated with 40 µM TAT-RasGAP$_{317-326}$ and 50 µM etoposide for 24 hours. Cell death (corresponding to the % of 7AAD positive cells) was determined by FACS. The results correspond to the mean +/- 95% CI of at least three independent experiments. **E.** Bax and Bak were disrupted in Raji and NB1 cells using the CRISPR/Cas9 technology. Loss of expression was confirmed by Western blotting. **F.** Wild-type and Bax/Bak double-knock-out Raji and NB1 cells were treated with 20 µM TAT-RasGAP$_{317-326}$ for 16 hours and 40 µM TAT-RasGAP$_{317-326}$ for 24 hours, respectively. Cell death (corresponding to the % of PI-positive cells) was determined by FACS. Results correspond to the mean +/- 95% CI of 3 independent experiments. **G.** NB1 cells overexpressing or not Bcl-X$_L$ were pre-incubated or not 1 hour with 10 µM of the pan-caspase inhibitor Z-VD-fmk and then treated with 40 µM TAT-RasGAP$_{317-326}$. After 24 hours incubation, cell death (corresponding to the % of 7AAD-positive cells) was determined by FACS.

TAT-RasGAP$_{317-326}$ does not trigger necroptosis

As apoptosis was not, or only partially, involved in the death induced by TAT-RasGAP$_{317-326}$, we investigated whether other forms of death could be involved. Necroptosis, also called programmed necrosis, is a form of cell death that differs from apoptosis at morphological and signaling levels [20, 21]. It is characterized by cell rounding, gain in cell volume, organelle swelling and plasma membrane rupture. Necroptosis requires receptor-interacting protein (RIP) 1 and 3. The downstream target of the complex formed by RIP1/RIP3 was identified as mixed lineage kinase domain-like protein (MLKL) [22, 23]. Activation of MLKL leads to its translocation from the cytosol to plasma and intracellular membranes, and subsequent loss of membrane integrity [24]. In cells such as the HT29 colorectal adenocarcinoma, necroptosis can be triggered by tumor necrosis factor alpha (TNF-α) stimulation when caspases and translation are inhibited [25]. We were however unable to induce Raji and NB1 necroptosis using this protocol. This could be the consequence of a low MLKL expression (Figure 5A). To assess the involvement of necroptosis in TAT-RasGAP$_{317-326}$-induced death, Raji cells were treated with necrosulfonamide (NSA), an MLKL inhibitor [23]. NSA efficiently prevented necroptosis in HT29 cells (Figure 5B) but had no effect on the death provoked by the RasGAP-derived peptide (Figure 5C). One could argue that NSA might not be efficient in Raji cells, even at concentrations shown to be efficient in sensitive cell lines such as HT29. We therefore knocked out MLKL in Raji and NB1 cells as another approach to prevent necroptosis. Because endogenous levels of MLKL in these cells were low and could not be detected in Raji and NB1 cells (Figure 5A), the targeted DNA region by the Cas9 endonuclease was sequenced. Figure 5D shows that both alleles of Raji clones #2 and #6 and NB1 clones #B3 and #A6 were disrupted, engendering frameshift mutations. These MLKL disrupted clones were then treated with the TAT-RasGAP$_{317-326}$ peptide but this did not prevent cell death (Figure 5E). Collectively, these data demonstrate that TAT-RasGAP$_{317-326}$ does not require the molecular machinery of necroptosis to kill Raji and NB1 cells.

TAT-RasGAP$_{317-326}$ does not trigger pyroptosis

We next examined the implication of pyroptosis. This form of programmed cell death is stimulated by microbial and viral infections but also by stroke and cancer [26]. Morphological features displayed by pyroptotic cells are common with apoptosis and/or necrosis [26, 27]. Defined as a caspase-1-dependent cell death, pyroptosis results in the production of inflammatory cytokines such as interleukin-1β (IL-1β) and IL-18 and ends up in cell lysis. To determine whether pyroptosis is a type of cell death induced by TAT-RasGAP$_{317-326}$, Raji and NB1 cells lacking caspase-1 were generated. Loss of caspase-1 expression was confirmed in different clones by Western blotting (Figure 6A). The ability of the peptide to cause cell death was not abrogated in caspase-1 knock-out Raji and NB1 cells (Figure 6B). This is in line with the caspase inhibition results shown above (Figure 4B) as Z-VD-fmk is also expected to prevent caspase-1 activity [16]. Altogether, this indicates that the RasGAP-derived peptide does not elicit pyroptosis.

TAT-RasGAP$_{317-326}$ does not trigger parthanatos

Parthanatos is a cell death mode that is initiated by over-activation of poly (ADP-ribose)-polymerase 1 (PARP1). Under physiological conditions, PARP1 is involved in DNA repair. To maintain genomic homeostasis, PARP1 detects single strand DNA breaks, uses NAD^+ to synthetize poly (ADP-ribose) (PAR) and attaches PAR on itself and other target proteins [28, 29]. This leads to the recruitment of critical proteins for DNA repair [30, 31]. Hyperactivation of PARP1 contributes to NAD^+ and ATP depletion and translocation of apoptosis-inducing factor (AIF) from the mitochondria to the nucleus [32-34]. To investigate if TAT-RasGAP$_{317-326}$ triggers parthanatos, PARP1 knock-out cells were generated. Loss of PARP1 expression was controlled by Western blotting (Figure 6C). Figure 6D shows that in the absence of PARP1, Raji and NB1 cells are still killed by the peptide. Hence, the peptide does not trigger parthanatos.

Autophagy and TAT-RasGAP$_{317-326}$-induced death

Autophagy is a process of self-degradation. During starvation, it allows cells to maintain energy levels via the degradation and recycling of cellular cytoplasmic constituents, allowing cell survival. Autophagosome formation involves the lipidation of the LC3 protein [35]. This pro-survival function of autophagy is well accepted [36, 37]. Autophagy may in some conditions trigger cell death [38]. To test if the peptide modulates autophagy, the autophagic marker lipidatino of LC3 was examined by Western blotting. Figure 7A shows that conversion of the LC3-I unlipidated form to the LC3-II lipidated form is similar in untreated cells and in cells treated with TAT-RasGAP$_{317-326}$. To rule out the involvement of autophagy in TAT-RasGAP$_{317-326}$-triggered death, two autophagic genes, ATG5 and ATG6, were disrupted (Figures 7B and 7D). Disruption of ATG5 fully prevented autophagy in Raji cells, as assessed by the absence of LC3 lipidation in serum deprivated conditions (Figure 7F). Moreover, autophagy induced by serum starvation fully prevented in cells lacking ATG6 (Figure 7F). However, the absence of ATG5 and ATG6 did not prevent TAT-RasGAP$_{317-326}$-induced cell death in Raji and NB1 cells (Figures 7C and 7E), suggesting that autophagy plays no role in TAT-RasGAP$_{317-326}$-mediated death.

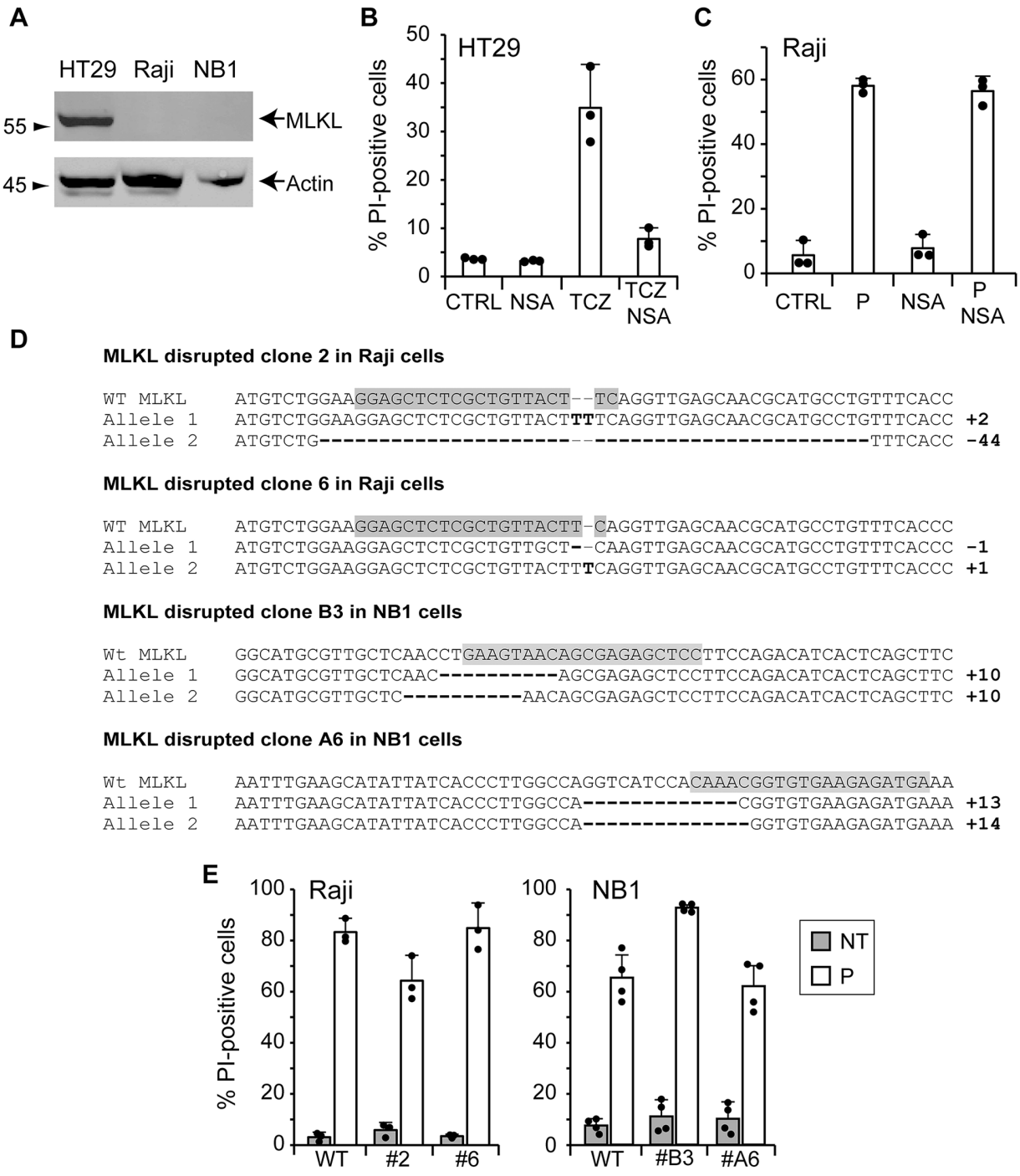

Figure 5: TAT-RasGAP$_{317-326}$-induced cell death does not require the necroptosis machinery. A. Expression of MLKL in wild-type HT29 cells, Raji cells and NB1 cells assessed by Western blotting. **B.** HT29 cells were pretreated for 1 hour with 10 μM necrosulfonamide (NSA) and necroptosis was induced by the addition of 30 ng/ml TNF-α (T), 2 μg/ml cycloheximide (C) and 10 μM Z-VD-fmk (Z). After 24 hours, cell death was determined by FACS after staining with PI. **C.** Raji cells were pretreated for 1 hour with 10 μM NSA before the addition of 20 μM TAT-RasGAP$_{317-326}$ (P). After 16 hours incubation, cell death (corresponding to the % of PI-positive cells) was determined by FACS. The results correspond to the mean +/- 95% CI of three independent experiments. **D.** DNA sequences of wild-type MLKL gene and MLKL alleles of clones 2 and 8 and clones B3 and A6 of Raji cells and NB1 cells, respectively. Differences with the wild-type MLKL sequence are highlighted in bold. The sgRNAs directed against MLKL are highlighted in grey. **E.** Wild-type and MLKL disrupted Raji and NB1 cells were treated for 16 and 24 hours, respectively. Cell death (corresponding to the % of PI-positive cells) was measured by FACS. The results correspond to the mean +/- 95% CI of minimum three independent experiments.

It is possible that the peptide triggers cell death via the activation of several pathways in parallel. We therefore investigated the effect of multiple cell death inhibition on TAT-RasGAP$_{317-326}$ toxicity. Figure 7G shows that inhibition of apoptosis and necroptosis in autophagy-deficient Raji and NB1 cells did not protect against the cytotoxic effect of the peptide. Taken together, these results indicate that none of the "classical" death pathways mediate the killing activity of TAT-RasGAP$_{317-326}$.

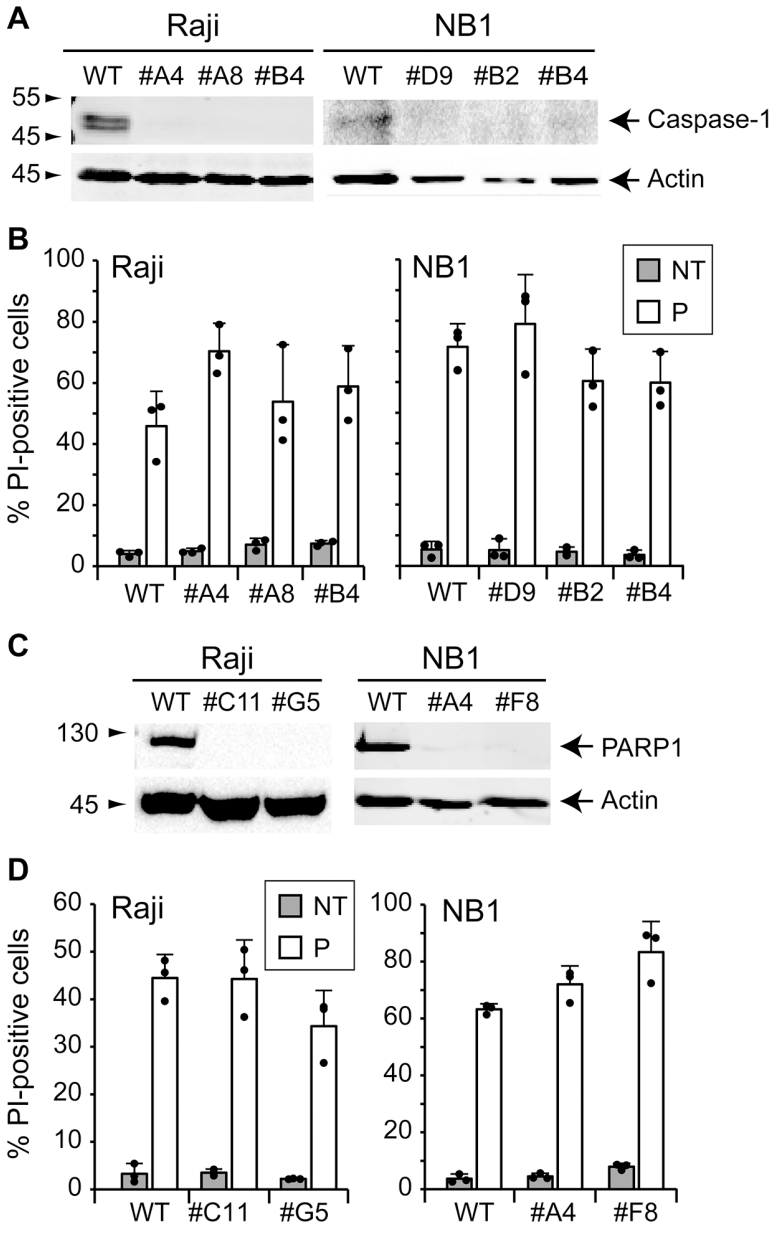

Figure 6: TAT-RasGAP$_{317-326}$-induced cell death is caspase-1- and PARP1-independent. A. Caspase-1 was disrupted in Raji and NB1 cells using the CRISPR/Cas9 technology. Loss of expression was confirmed by Western blotting. **B.** Wild-type and caspase-1 knock-out Raji cells were treated or not with 20 μM TAT-RasGAP$_{317-326}$ (P) for 16 hours. Wild-type and caspase-1 knock-out NB1 cells were treated or not with 40 μM TAT-RasGAP$_{317-326}$ (P) for 24 hours. Cell death was then assessed by flow cytometry after PI staining. Results correspond to the mean +/- 95% CI of 3 independent experiments. **C.** PARP1 was disrupted in wild-type Raji and NB1 cells using CRISPR/Cas9 technology. Loss of expression was confirmed by Western blotting. **D.** Wild-type and PARP1 knock-out Raji cells were treated or not with 20 μM TAT-RasGAP$_{317-326}$ (P) for 16 hours. NB1 cells were treated or not with 40 μM TAT-RasGAP$_{317-326}$ (P) for 24 hours. Cell death was then assessed by flow cytometry after PI staining. Results correspond to the mean +/- 95% CI of 3 independent experiments.

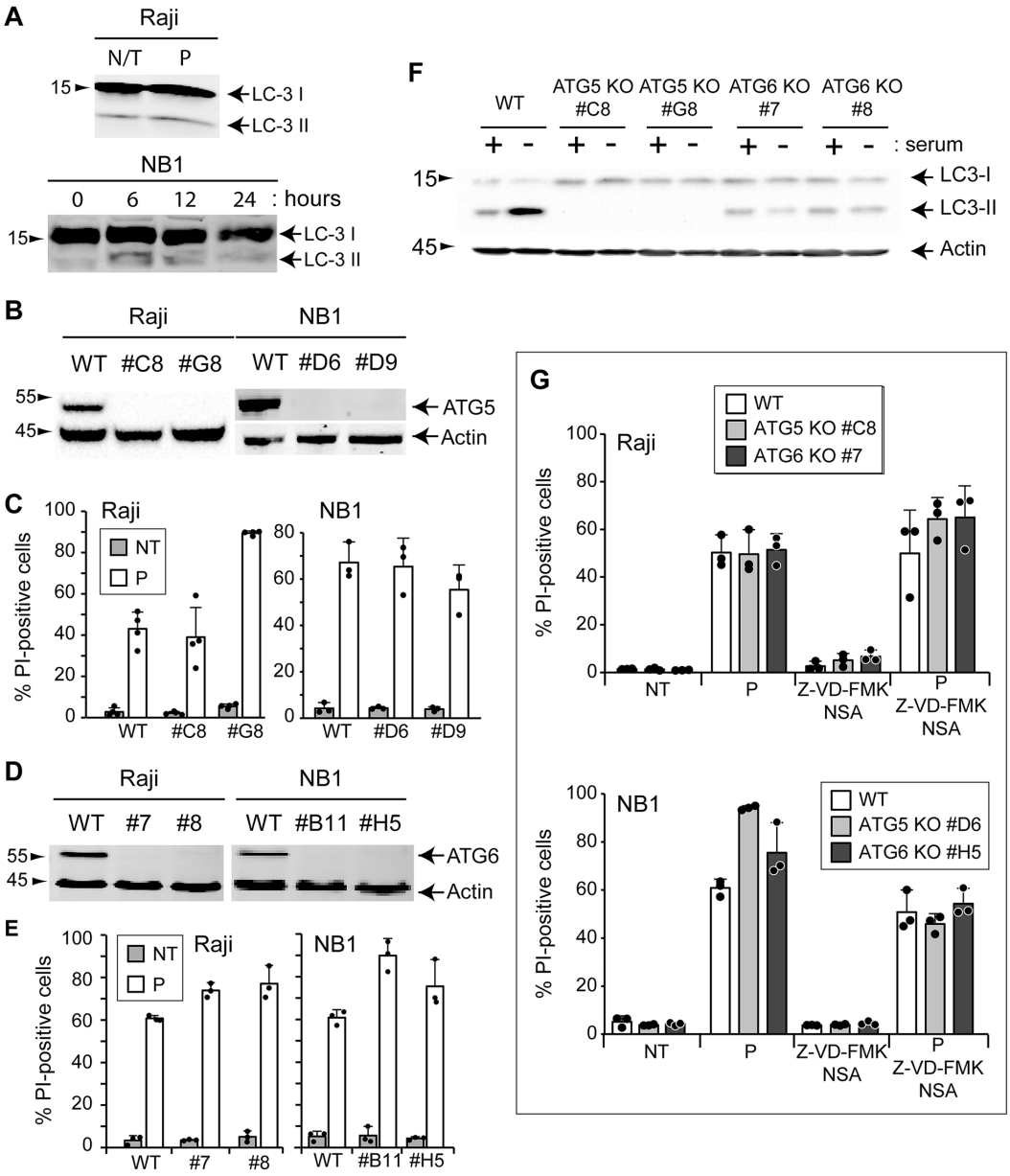

Figure 7: Autophagy is not involved in TAT-RasGAP$_{317-326}$-induced cell death. A. Raji cells were treated during 16 hours with 20 µM TAT-RasGAP$_{317-326}$ (P) or not (N/T) and LC3 expression was analyzed by Western blotting. NB1 cells were treated during the indicated periods of time with 40 µM TAT-RasGAP$_{317-326}$ and LC3 expression was analyzed by Western blotting. **B.** and **D.** ATG5 and ATG6 were individually disrupted in Raji and NB1 cells using the CRISPR/Cas9 technology. Loss of expression was confirmed by Western blotting. **C.** Wild-type and ATG5 knock-out Raji cells were treated or not with 20 µM TAT-RasGAP$_{317-326}$ (P) for 16 hours. Wild-type and ATG5 knock-out NB1 cells were treated or not with 40 µM TAT-RasGAP$_{317-326}$ (P) for 24 hours. Cell death was then assessed by flow cytometry after PI staining. Results correspond to the mean +/- 95% CI of 3 independent experiments. **E.** Wild-type and ATG6 knock-out Raji and NB1 cells were treated as described in panel D. Cell death was then assessed by flow cytometry after PI staining. Results correspond to the mean +/- 95% CI of 3 independent experiments. **F.** Wild-type, ATG5 knock-out and ATG6 knock-out Raji cells were cultured for 48 hours in presence or absence of serum. LC3 conversion was analyzed by Western blotting. **G.** Wild-type, ATG5 knock-out and ATG6 knock-out Raji cells were pretreated or not with 10 µM Z-VD-fmk and 10 µM necrosulfonamide (NSA) for 1 hour and then treated or not with 20 µM TAT-RasGAP$_{317-326}$ (P) for 16 hours. Wild-type, ATG5 knock-out and ATG6 knock-out NB1 cells were pretreated or not with 10 µM Z-VD-fmk and 10 µM necrosulfonamide (NSA) for 1 hour and then treated or not with 40 µM TAT-RasGAP$_{317-326}$ (P) for 24 hours. Cell death was then assessed by flow cytometry after PI staining. Results correspond to the mean +/- 95% CI of 3 independent experiments.

DISCUSSION

Apoptosis had been the most intensively studied mode of regulated cell death for years. Thus, apoptotic inducers were and are largely used in the clinic as cancer therapies. However, tumor cell resistance to apoptosis, leading to cancer progression, is currently a major clinical problem. Some strategies could overcome this problem. For example, restoring the sensitivity of cancer cells to apoptosis might improve the efficacy of anti-tumor drugs. Another possibility would be to trigger alternate modes of death to which cancer cells are not resistant. The results presented here indicate that the TAT-RasGAP$_{317-326}$ peptide has the capacity to kill some tumor cells in a manner distinct from the known characterized forms of death.

Our data show that necroptosis, autophagy, parthanatos and pyroptosis are neither activated nor involved in the toxicity induced by TAT-RasGAP$_{317-326}$. In contrast, the apoptotic pathway is efficiently stimulated by the peptide. However, inhibiting apoptosis, either pharmacologically or genetically, did not (Raji cells), or only partially (NB1 cells), prevent TAT-RasGAP$_{317-326}$ cytotoxicity. Hence, TAT-RasGAP$_{317-326}$ has the potential to activate apoptosis and another form of cell death that is distinct from the above mentioned death pathways. The ability of triggering multiple forms of death has been reported for other compounds. Indeed, shikonin and cisplatin, depending on the concentrations used, stimulate either apoptosis or necroptosis/necrosis [39, 40]. Another example is the lipophilic mitochondria-targeted F16 compound that was shown to elicit death via apoptosis [41]. However, Bcl-2 overexpression did not block the capacity of F16 to trigger a necrotic cell death, demonstrating that one compound can have a dual ability to kill through both apoptosis and necrosis.

Our results clearly indicate that TAT-RasGAP$_{317-326}$ has the potential to stimulate both apoptosis and an alternative form of death in tumor cells of various origins. However, it is currently not known whether these two forms of death are activated independently or whether the triggering event leading to the alternative form of death has the capacity to also stimulate apoptosis.

In Raji cells, the sensitivity to the alternative form of death stimulated by TAT-RasGAP$_{317-326}$ is seemingly high and the apoptotic pathway can be blocked without affecting the overall death response. In NB1 cells, activation of the alternate form of death appears suboptimal and efficient killing requires concomitant activation of apoptosis. Consequently, it seems that there is a continuum of sensitivities among cancer cell lines to the direct killing action of TAT-RasGAP$_{317-326}$.

Only a fraction of the tested cell lines were found to be sensitive to the killing activity of the peptide. To assess if those cells share common biological features that were not present in the resistant cell lines, we performed mutational and transcriptomics bioinformatical analyses on six sensitive and six resistant cell lines (subjected to 40 µM TAT-RasGAP$_{317-326}$). Supplementary Figure S6A lists the 6 genes with the strongest differential mutational status between resistant and sensitive cell lines. Even in these genes, there was no strict association between the mutation status and the sensitivity of the cell lines to the peptide. It is unlikely that these genes, individually at least, drive the peptide sensitivity of a cell line. In agreement with this is the absence of correlation between their expression and the sensitivity of a cell line to be killed by the peptide (Supplementary Figure S6B). Moreover, there is no statistical support for a difference in the overall mutational rate of these cell lines (Supplementary Figures S6C-S6D). Gene profiling analysis revealed that cell lines cluster according to their origin rather than their sensitivity to TAT-RasGAP$_{317-326}$ (Supplementary Figure S6E). We finally performed a differential expression analysis to find whether the expression of certain genes was specifically associated with TAT-RasGAP$_{317-326}$ sensitivity but failed to detect any (Supplementary Figure S6F). These results suggest that neither mutation nor transcriptional regulation are involved in the regulation of TAT-RasGAP$_{317-326}$ sensitivity. However, we should take into account that the cell lines were not always tested in identical experimental conditions (e.g. different culture media used for the experimentation). Moreover, as the peptide requires entry into cells via the HIV-TAT$_{48-57}$ portion, it is also possible that variations in peptide intake could explain some of the differences in the sensitivity observed between the cell lines.

At present, we cannot rule out the possibility that the alternate form of death triggered by the peptide is a form of necrosis. One hypothesis that we cannot dismiss is that TAT-RasGAP$_{317-326}$ enters cells and then once in the cytoplasm alters, directly or indirectly, plasma membrane integrity by interacting with specific molecules that are enriched in the inner leaflet of the membrane. This mode of action has been reported for defensin NaD1, a host defense peptide [42]. NaD1 was shown to enter mammalian cells and bind to phosphatidylinositol 4,5-bisphosphate (PIP2), leading to rapid membrane destabilization and permeabilization. As highlighted in this example, cell death induced by a peptide may not, or not only, depend on protein binding but also on specific membrane lipid interaction.

To conclude, our finding could potentially have interesting clinical relevance since current anti-cancer therapies are mostly based on drugs that induce tumor cell apoptosis. Consequently, determining that a peptide is able to induce a distinct form of death in tumor cells could lead to the generation of innovative anti-cancer drugs that complement or be combined with existing ones.

MATERIALS AND METHODS

Cell lines

All cell lines were cultured in 5% CO_2 at 37 °C. 293T, 501Mel, PC3, HT29, U2OS and Vero were cultured in DMEM (Invitrogen, ref. no. 61965) supplemented with 10% heat-inactivated fetal bovine serum (FBS; Invitrogen, ref. no. 10270-106). Raji, A375, Daudi, HeLa, IGr37, IPC298, Jurkat, MelJuso, Namalwa, Ramos, RPMI-8226, SKMel30, SKW6.4, THP-1, WM1366 and WM3248 were cultured in RPMI (Invitrogen, ref. no. 61870) supplemented with 10% FBS. The NB1 neuroblastoma cells were maintained in neural basic medium composed of DMEM/F12 (Invitrogen, ref. no. 31331-028) supplemented with 2% B27 serum-free supplement (Invitrogen, ref. no. 17504044), 20 ng/ml human recombinant basic fibroblast growth factor (bFGF) (Peprotech, ref. no. 100-18B) and 20 ng/ml human recombinant epidermal growth factor (EGF) (Peprotech, ref. no. AF-100-15). Human peripheral blood lymphocytes (PBLs) were isolated by density centrifugation over a Ficoll-Paque gradient (Lymphoprep; Stemcell Technologies) from buffy coats of healthy human donors, obtained from the state of Vaud blood transfusion service. The donors gave written consent for potential use of their blood for medical research. B cells present in PBLs were positively stained with mouse FITC-labelled anti-CD19 antibody for 30 min at 4°C before flow cytometry analysis.

Chemicals

TNFα and the protease inhibitor tablets were from Roche (ref. no. 11088939001 and 4693132001, respectively). Cycloheximide and etoposide were from Sigma (ref. no. C7698 and E1383 respectively). Necrosulfonamide was from Tocris bioscience (ref. no. 5025). The pan-caspase inhibitor Z-VD-fmk was a kind gift from Maxim Pharmaceuticals. Hexameric Fas ligand, resulting from the aggregation of 6 fusion proteins between Fas ligand and the Fc portion of IgG1 [43], was provided by Pascal Schneider (University of Lausanne). Puromycin was from Life technologies (ref. no. A11138-02) and 4-hydroperoxycyclophosphamide (4-HC) was from Niomech, (ref. no. D-18864).

Peptides

TAT and TAT-$RasGAP_{317–326}$ are retro-inverso peptides (i.e. synthesized with D-amino acids in the opposite direction compared to the natural sequence). The TAT moiety corresponds to amino acids 48–57 of the HIV TAT protein (RRRQRRKKRG) and the $RasGAP_{317–326}$ moiety corresponds to amino acids 317–326 of the human RasGAP protein (DTRLNTVWMW). These two moieties are separated by two glycine linker residues in the TAT-Ras-$GAP_{317–326}$ peptide. TAT-$RasGAP_{317-326}$(W317A) has the tryptophan at position 317 mutated into an alanine. The peptides were synthesized at the department of biochemistry, University of Lausanne, Switzerland, using FMOC technology, purified by HPLC and tested by mass spectrometry.

Cell death measurement

Cell death was measured with an Annexin-V-FITC / 7AAD kit (Beckman Coulter, ref. no. IM3614) or with propidium iodide (PI) (Sigma, ref. no. 81845) and used according to the manufacturer's instructions. Cells were scanned using a Beckman Coulter FC500 flow cytometer and data were analyzed with the Kaluza Version 1.3 software (Beckman Coulter).

Cell cycle analysis

Cells were collected, washed once in PBS and fixed in 70 % ethanol at 4°C for 2 hours and then washed twice with PBS. DNA was stained with PI solution (10 µg/mL PI, 150 µg/mL RNase A in water) at 37°C for 30 minutes. Samples were analyzed by flow cytometry using a Beckman Coulter FC500 flow cytometer.

TMRM staining

Cells were collected, washed once in PBS and stained with 100 µL of 150 nM tetramethylrhodamine methyl ester (TMRM) solution by incubating during 20 min at 37°C. 500 µL of PBS were added and then transferred to a sample tube which was analyzed by flow cytometry using a Beckman Coulter FC500 flow cytometer.

Mitochondria isolation and cytochrome *c* release

Cells were harvested in PBS and centrifuged 10 min at 1,000xg. Cells were then resuspended in isotonic mitochondrial buffer (MB) (10 mM HEPES pH 7.4, 210 mM mannitol, 70 mM sucrose, 1 mM EDTA supplemented with one tablet of protease inhibitor cocktail per 50 mL), broken by five passages through a 25G1 0.5- by 2.5-mm needle fitted on a 2 mL syringe and centrifuged at 1,500xg for 5 min. This procedure was repeated twice and supernatants from each step were pooled and centrifuged 5 min at 1,500xg. Supernatant was collected, centrifuged 5 min at 2,000xg and further centrifuged 10 min at 9,000xg. Pellet was resuspended in MB (100 µL), centrifuged 10 min at 7,000xg and the pellet, representing the mitochondrial fraction, was finally resuspended in a volume of 100 µL of MB. 40 µg of mitochondria were incubated in KCl buffer (10 mM HEPES pH 7.4; 125 mM KCl; 0.5 mM EGTA; 4 mM $MgCl_2$; 5 mM KH_2PO_4) and left untreated or treated with 20 µM TAT-$RasGAP_{317–326}$, 20 µM TAT-$RasGAP_{317–326}$ (W317A) or 40 nM tBid for 30 min at 37°C. Samples

were then centrifuged 5 min at 16,000xg and supernatant and pellet analyzed by Western blotting for the presence of cytochrome *c*.

Antibodies

The rabbit anti-Bcl-X_L, the rabbit anti-caspase-3, the rabbit anti-LC3, the mouse anti-PARP1, the rabbit anti-actin antibodies were from Cell Signaling (ref. no. 2764, 9662, 2775, 9546, 4970 respectively). The rabbit anti-ATG6, the rabbit anti-total Bax and the rabbit anti-total Bak were from Santa Cruz Biotechnology (ref. no. sc-11427, sc-493 and sc-832 respectively). The mouse anti-caspase-1 was from Adipogen (ref. no. AG-20B-0048). The rabbit anti-ATG5 was from Abcam (ref. no. ab108327). The rat anti-MLKL was from Merck Millipore (ref. no. MABC604). The mouse FITC-labelled anti-CD19 was from Beckman Coulter (ref. no. A07768).

Detection of cellular and mitochondrial ROS

Intracellular levels of cytosolic and mitochondrial superoxide as well as H_2O_2 production were determined by flow cytometry using live-cell permeant-specific fluorogenic probes, dihydroethidium (DHE; Marker Gene Technologies Inc, ref. no MGT-M1241-M010), MitoSOX (Molecular Probes, ref. no M36008) and 6-carboxy-20,70-dichlorodihydrofluorescein diacetate (carboxy-H2DCFDA; Molecular Probes, ref. no C-400), respectively. DHE is oxidized to red fluorescent ethidium by cytosolic superoxide, MitoSOX is selectively targeted to mitochondria, where it is oxidized by superoxide and exhibits red fluorescence and carboxy-H2DCFDA becomes green-fluorescent when oxidized with intracellular H_2O_2. After drug treatment, cells were harvested and transferred to flow cytometry tubes and incubated with 5 µM of specific probe at 37 °C for 30 min. Cells were washed twice with PBS, resuspended in 500 µL PBS and, for visualization of the intracellular fluorescence, probes were excited at 488 nm and fluorescence emission were analyzed by flow cytometry.

Determination of intracellular ATP content

Intracellular ATP content was measured with the ATP determination kit (Molecular Probes, ref. no A22066) according to manufacturer's instructions. Briefly, after drug treatment, cells were collected, washed twice in PBS, resuspended in 100 µL lysis buffer ($NaHCO_3$ 20 mM + Na_2CO_3 100 mM) and kept at -80°C for at least 4h. Cell lysates and ATP standards (10 µL) were mixed with standard reaction solution (90 µL) and luminescence was determined using an automatized bioluminometer (Promega Glomax 96 microplate luminometer). ATP level for each sample was normalized to protein content.

Plasmids

The lentiviral vector lentiCRISPRv2 [44] was obtained from Addgene (#868, Addgene, ref. no. 52961). The pMD2.G plasmid (#554, Addgene, ref. no. 12259) encodes the envelope of lentivirus. The psPAX2 plasmid (#842, Addgene, ref. no. 12260) encodes the packaging system. The hBclXL.LEGO-iG2 plasmid (#863) was constructed by subcloning the 771 bp EcoRI fragment from hBcl-XL. dn3 (#274) into LeGO-iG2 (#807; Addgene: plasmid 27341).

Lentivirus production

Recombinant lentiviruses hBclXL.LEGO-iG2 were produced as described [45] with the following modifications: pMD.G (#218) and pCMVDR8.91 (#219) were replaced by pMD2.G and psPAX2 respectively.

Genome editing by CRISPR method

Single guide RNAs targeting the early exon of the protein of interest were chosen in the sgRNA library [46] and are listed in Table 2. LentiCRISPR plasmids specific for a gene were created according to the provided instructions. Oligos were designed as follow: Forward 5'-CACCGnnnnnnnnnnnnnnnnnn-3'; Reverse-3'-Cnnnnnnnnnnnnnnnnnnnn-CAA-5', where nnnnnnnnnnnnnnnnnnnn in the forward oligo corresponds to the 20 bp sgRNA. Oligos were synthetized, then phosphorylated and annealed to form oligo complexes. LentiCRISPR vector was BsmBI digested and dephosphorylated. Linearized vector was purified and gel extracted and ligated to oligo complexes. The lentiCRISPR vector containing the sgRNA was then used for lentivirus production. Cells were infected and selected with the appropriate dose of puromycin (2 µg/ml for Raji, 1 µg/ml for NB1). Clone isolation was performed by limiting dilution in 96 well-plate.

TA cloning

TA cloning kit (Life technologies, ref. no. K202020) was used according to manufacturer's instructions to sequence DNA fragment containing the region where Cas9 was guided by a sgRNA.

Electron microscopy

NB1 cells were plated in poly-L-lysine (0.01%, Sigma-Aldrich, ref. no. P4832)-coated glass slides (LabTek Chamber Slides, ref. no. 177399) at a density of 300,000 cells per slide (area = 1.8 cm^2), cultured for 24 hours. The Raji Burkitt lymphoma cells were cultured at a density of 200,000 cells per ml. The cells were treated as described in the figures. Cells were then fixed 2 hours in 2.5% glutaraldehyde (Electron

Table 2: List of sgRNAs used to disrupt the indicated target genes (and in which exons)

Target gene	sgRNA name	sgRNA sequence	Exon number
ATG5	sgATG5.3	AAGATGTGCTTCGAGATGTG	3
ATG5	sgATG5.5	AAGAGTAAGTTATTTGACGT	4
ATG6	sgATG6.1	ATTTATTGAAACTCCTCGCC	7
ATG6	sgATG6.2	ATCTGCGAGAGACACCATCC	7
Bak	sgBak.1	GCTCACCTGCTAGGTTGCAG	3
Bak	sgBak.2	CTCCTACAGCACCATGGGGC	3
Bax	sgBax.2	CCATTCGCCCTGCTCGATCC	3
Caspase-1	sgCasp1.2	GACATTCCCTTCTGAGCCTG	4
MLKL	sgMLKL.3	GGAGCTCTCGCTGTTACTTC	2
MLKL	sgMLKL.6	TCATCTCTTCACACCGTTTG	2
PARP1	sgPARP1.1	TTCTAGTCGCCCATGTTTGA	2

Microscopy Sciences, ref. no. 16220) dissolved in 100 mM phosphate buffer (PB), pH7.4. After three washes in PB, cells were postfixed for 1 hour in 1% osmium tetroxide (Electron Microscopy Sciences, ref. no. 19150) in PB and then stained with ethanol 70% containing 1% uranyl acetate (Sigma-Aldrich, ref. no. 73943) for 20 min. Raji and NB1 cells were dehydrated in graded alcohol series and embedded in epon (Electron Microscopy Sciences, ref. no. 13940). Ultrathin sections (with silver to gray interference) were cut with a diamond knife (Diatome), mounted on Formvar-coated single slot grids, and then counterstained with 3% uranyl acetate for 10 min and then with lead citrate (0.2%, Sigma-Aldrich, ref. no. 15326) for 10 min. Sections were visualized using a Philips CM100 transmission electron microscope.

ACKNOWLEDGMENTS

The authors thank the following persons: Jean Daraspe (University of Lausanne, Switzerland) for technical assistance and the Electron Microscopy Facility at the University of Lausanne for the use of electron microscopes, Camilla Jandus (University of Lausanne) for preparing PBLs, Jean-Claude Martinou (University of Geneva, Switzerland) for providing recombinant tBid, Pascal Schneider (University of Lausanne, Switzerland) for providing FasL, and Olivier Dormond (University of Lausanne) for sharing HT29 cells.

CONFLICTS OF INTEREST

The authors declare that they have no conflict of interest.

GRANT SUPPORT

This study was funded by Swiss National Science Foundation (grant n°31003A_160181/1 and 31003A_141242/1), Swiss South African Joint Research Programme (grant n°IZLSZ3_148907/1), Swiss Cancer League grant n°KFS - 02543-02-2010 and MD-PhD fellowship from the Swiss National Science Foundation (n°158116).

REFERENCES

1. Torre LA, Bray F, Siegel RL, Ferlay J, Lortet-Tieulent J and Jemal A. Global cancer statistics, 2012. CA: a cancer journal for clinicians. 2015; 65:87-108.
2. Fernald K and Kurokawa M. Evading apoptosis in cancer. Trends Cell Biol. 2013; 23:620-633.
3. Hanahan D and Weinberg RA. The Hallmarks of Cancer. Cell. 2000; 100:57-70.
4. Kroemer G, Galluzzi L, Vandenabeele P, Abrams J, Alnemri ES, Baehrecke EH, Blagosklonny MV, El-Deiry WS, Golstein P, Green DR, Hengartner M, Knight RA, Kumar S, Lipton SA, Malorni W, Nunez G, et al. Classification of cell death: recommendations of the Nomenclature Committee on Cell Death 2009. Cell Death Differ. 2008; 16:3-11.
5. Galluzzi L, Bravo-San Pedro JM, Vitale I, Aaronson SA, Abrams JM, Adam D, Alnemri ES, Altucci L, Andrews D, Annicchiarico-Petruzzelli M, Baehrecke EH, Bazan NG, Bertrand MJ, Bianchi K, Blagosklonny MV, Blomgren K, et al. Essential versus accessory aspects of cell death: recommendations of the NCCD 2015. Cell Death Differ. 2014.
6. Galluzzi L, Vitale I, Abrams JM, Alnemri ES, Baehrecke EH, Blagosklonny MV, Dawson TM, Dawson VL, El-Deiry WS, Fulda S, Gottlieb E, Green DR, Hengartner MO, Kepp O, Knight RA, Kumar S, et al. Molecular definitions of cell

death subroutines: recommendations of the Nomenclature Committee on Cell Death 2012. Cell Death Differ. 2012; 19:107-120.

7. Michod D, Yang J-Y, Chen J, Bonny C and Widmann C. A RasGAP-derived cell permeable peptide potently enhances genotoxin-induced cytotoxicity in tumor cells. Oncogene. 2004; 23:8971-8978.
8. Pittet O, Petermann D, Michod D, Krueger T, Cheng C, Ris H-B and Widmann C. Effect of the TAT-RasGAP317–326 peptide on apoptosis of human malignant mesothelioma cells and fibroblasts exposed to meso-tetra-hydroxyphenyl-chlorin and light. Journal of Photochemistry and Photobiology B: Biology. 2007; 88:29-35.
9. Michod D, Annibaldi A, Schaefer S, Dapples C, Rochat B and Widmann C. Effect of RasGAP N2 Fragment–Derived Peptide on Tumor Growth in Mice. Journal of the National Cancer Institute. 2009; 101:828-832.
10. Barras D, Lorusso G, Lhermitte B, Viertl D, Rüegg C and Widmann C. Fragment N2, a caspase-3-generated RasGAP fragment, inhibits breast cancer metastatic progression. International Journal of Cancer. 2014; 135:242-247.
11. Annibaldi A, Heulot M, Martinou JC and Widmann C. TAT-RasGAP317-326-mediated tumor cell death sensitization can occur independently of Bax and Bak. Apoptosis : an international journal on programmed cell death. 2014; 19:719-733.
12. Chevalier N, Gross N and Widmann C. Assessment of the Chemosensitizing Activity of TAT-RasGAP(317-326) in Childhood Cancers. PloS one. 2015; 10.
13. Barras D, Chevalier N, Zoete V, Dempsey R, Lapouge K, Olayioye MA, Michielin O and Widmann C. A WXW Motif Is Required for the Anticancer Activity of the TAT-RasGAP317-326 Peptide. J Biol Chem. 2014; 289:23701-23711.
14. Zimmermann M and Meyer N. (2011). Annexin V/7-AAD Staining in Keratinocytes. In: Stoddart MJ, ed. Mammalian Cell Viability: Humana Press), pp. 57-63.
15. Jaeschke H, Farhood A, Cai SX, Tseng BY and Bajt ML. Protection against TNF-induced liver parenchymal cell apoptosis during endotoxemia by a novel caspase inhibitor in mice. Toxicol Appl Pharmacol. 2000; 169:77-83.
16. Yang W, Guastella J, Huang JC, Wang Y, Zhang L, Xue D, Tran M, Woodward R, Kasibhatla S, Tseng B, Drewe J and Cai SX. MX1013, a dipeptide caspase inhibitor with potent in vivo antiapoptotic activity. British journal of pharmacology. 2003; 140:402-412.
17. Cheng EH, Wei MC, Weiler S, Flavell RA, Mak TW, Lindsten T and Korsmeyer SJ. BCL-2, BCL-X(L) sequester BH3 domain-only molecules preventing BAX- and BAK-mediated mitochondrial apoptosis. Mol Cell. 2001; 8:705-711.
18. Upreti M, Chu R, Galitovskaya E, Smart SK and Chambers TC. Key role for Bak activation and Bak-Bax interaction in the apoptotic response to vinblastine. Mol Cancer Ther. 2008; 7:2224-2232.
19. Finke J, Fritzen R, Ternes P, Trivedi P, Bross KJ, Lange W, Mertelsmann R and Dolken G. Expression of bcl-2 in Burkitt's lymphoma cell lines: induction by latent Epstein-Barr virus genes. Blood. 1992; 80:459-469.
20. Christofferson DE and Yuan JY. Necroptosis as an alternative form of programmed cell death. Current Opinion in Cell Biology. 2010; 22:263-268.
21. Linkermann A and Green DR. Necroptosis. New Engl J Med. 2014; 370:455-465.
22. Zhao J, Jitkaew S, Cai Z, Choksi S, Li Q, Luo J and Liu ZG. Mixed lineage kinase domain-like is a key receptor interacting protein 3 downstream component of TNF-induced necrosis. Proc Natl Acad Sci U S A. 2012; 109:5322-5327.
23. Sun L, Wang H, Wang Z, He S, Chen S, Liao D, Wang L, Yan J, Liu W, Lei X and Wang X. Mixed lineage kinase domain-like protein mediates necrosis signaling downstream of RIP3 kinase. Cell. 2012; 148:213-227.
24. Wang H, Sun L, Su L, Rizo J, Liu L, Wang LF, Wang FS and Wang X. Mixed Lineage Kinase Domain-like Protein MLKL Causes Necrotic Membrane Disruption upon Phosphorylation by RIP3. Mol Cell. 2014; 54:133-146.
25. Linkermann A, Brasen JH, Himmerkus N, Liu S, Huber TB, Kunzendorf U and Krautwald S. Rip1 (receptor-interacting protein kinase 1) mediates necroptosis and contributes to renal ischemia/reperfusion injury. Kidney international. 2012; 81:751-761.
26. Bergsbaken T, Fink SL and Cookson BT. Pyroptosis: host cell death and inflammation. Nature reviews Microbiology. 2009; 7:99-109.
27. Labbe K and Saleh M. Cell death in the host response to infection. Cell Death Differ. 2008; 15:1339-1349.
28. D'Amours D, Desnoyers S, D'Silva I and Poirier GG. Poly(ADP-ribosyl)ation reactions in the regulation of nuclear functions. The Biochemical journal. 1999; 342:249-268.
29. Durkacz BW, Omidiji O, Gray DA and Shall S. (ADP-ribose) n participates in DNA excision repair. Nature. 1980; 283:593-596.
30. El-Khamisy SF, Masutani M, Suzuki H and Caldecott KW. A requirement for PARP-1 for the assembly or stability of XRCC1 nuclear foci at sites of oxidative DNA damage. Nucleic Acids Res. 2003; 31:5526-5533.
31. de Murcia G, Schreiber V, Molinete M, Saulier B, Poch O, Masson M, Niedergang C and Menissier de Murcia J. Structure and function of poly(ADP-ribose) polymerase. Mol Cell Biochem. 1994; 138:15-24.
32. Yu SW, Wang HM, Poitras MF, Coombs C, Bowers WJ, Federoff HJ, Poirier GG, Dawson TM and Dawson VL. Mediation of poly(ADP-ribose) polymerase-1-dependent cell death by apoptosis-inducing factor. Science. 2002; 297:259-263.
33. Yu SW, Andrabi SA, Wang H, Kim NS, Poirier GG, Dawson TM and Dawson VL. Apoptosis-inducing factor mediates poly(ADP-ribose) (PAR) polymer-induced cell

death. Proceedings of the National Academy of Sciences of the United States of America. 2006; 103:18314-18319.

34. Andrabi SA, Kim NS, Yu SW, Wang H, Koh DW, Sasaki M, Klaus JA, Otsuka T, Zhang Z, Koehler RC, Hurn PD, Poirier GG, Dawson VL and Dawson TM. Poly(ADP-ribose) (PAR) polymer is a death signal. Proceedings of the National Academy of Sciences of the United States of America. 2006; 103:18308-18313.
35. Tanida I, Ueno T and Kominami E. LC3 and Autophagy. Methods in molecular biology (Clifton, NJ). 2008; 445:77-88.
36. Imaizumi K. Autophagy is activated for cell survival after ER stress. J Pharmacol Sci. 2007; 103:45p-45p.
37. Mizushima N. Autophagy: process and function. Genes Dev. 2007; 21:2861-2873.
38. Tsujimoto Y and Shimizu S. Another way to die: autophagic programmed cell death. Cell Death Differ. 0000; 12:1528-1534.
39. Wada N, Kawano Y, Fujiwara S, Kikukawa Y, Okuno Y, Tasaki M, Ueda M, Ando Y, Yoshinaga K, Ri M, Iida S, Nakashima T, Shiotsu Y, Mitsuya H and Hata H. Shikonin, dually functions as a proteasome inhibitor and a necroptosis inducer in multiple myeloma cells. International journal of oncology. 2015; 46:963-972.
40. Sancho-Martinez SM, Piedrafita FJ, Cannata-Andia JB, Lopez-Novoa JM and Lopez-Hernandez FJ. Necrotic concentrations of cisplatin activate the apoptotic machinery but inhibit effector caspases and interfere with the execution of apoptosis. Toxicological sciences : an official journal of the Society of Toxicology. 2011; 122:73-85.
41. Fantin VR and Leder P. F16, a mitochondriotoxic compound, triggers apoptosis or necrosis depending on the genetic background of the target carcinoma cell. Cancer Res. 2004; 64:329-336.
42. Poon I, Baxter AA, Lay FT, Mills GD, Adda CG, Payne JA, Phan TK, Ryan GF, White JA, Veneer PK, van der Weerden NL, Anderson MA, Kvansakul M and Hulett MD. Phosphoinositide-mediated oligomerization of a defensin induces cell lysis. Elife. 2014; 3:e01808.
43. Holler N, Tardivel A, Kovacsovics-Bankowski M, Hertig S, Gaide O, Martinon F, Tinel A, Deperthes D, Calderara S, Schulthess T, Engel J, Schneider P and Tschopp J. Two adjacent trimeric Fas ligands are required for Fas signaling and formation of a death-inducing signaling complex. Mol Cell Biol. 2003; 23:1428-1440.
44. Sanjana NE, Shalem O and Zhang F. Improved vectors and genome-wide libraries for CRISPR screening. Nature methods. 2014; 11:783-784.
45. Annibaldi A, Dousse A, Martin S, Tazi J and Widmann C. Revisiting G3BP1 as a RasGAP Binding Protein: Sensitization of Tumor Cells to Chemotherapy by the RasGAP 317-326 Sequence Does Not Involve G3BP1. PloS one. 2011; 6.
46. Shalem O, Sanjana NE, Hartenian E, Shi X, Scott DA, Mikkelsen TS, Heckl D, Ebert BL, Root DE, Doench JG and Zhang F. Genome-scale CRISPR-Cas9 knockout screening in human cells. Science. 2014; 343:84-87.
47. Michod D and Widmann C. TAT-RasGAP317-326 Requires p53 and PUMA to Sensitize Tumor Cells to Genotoxins. Molecular Cancer Research. 2007; 5:497-507.

The TAT-RasGAP$_{317-326}$ anti-cancer peptide can kill in a caspase-, apoptosis-, and necroptosis-independent manner

SUPPLEMENTARY FIGURES

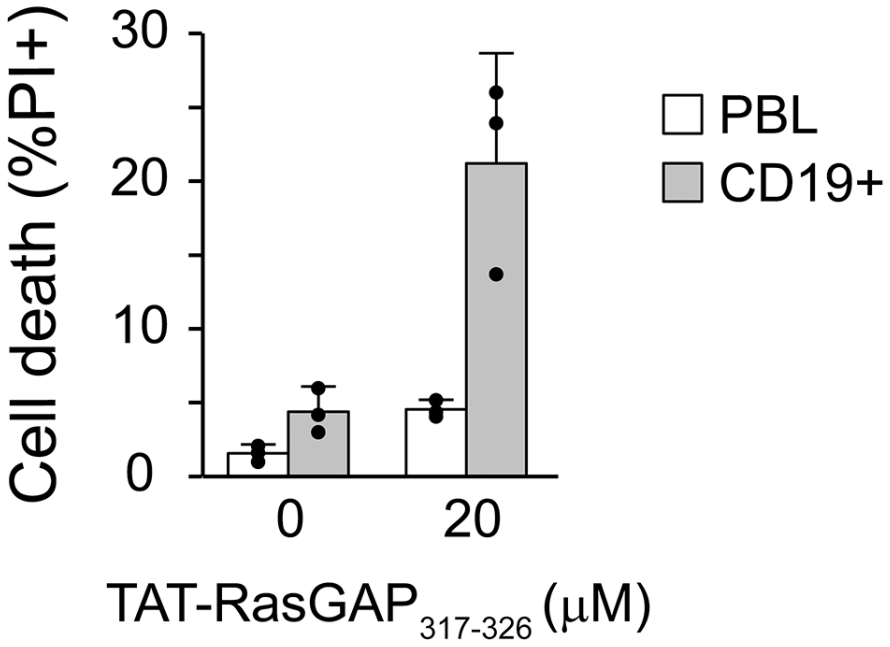

Supplementary Figure S1: Effect of TAT-RasGAP$_{317-326}$ on the survival of PBLs and B cells. PBLs from 3 different healthy donors were left untreated or treated with 20 μM TAT-RasGAP$_{317-326}$ for 16 hours. Then, cells were washed twice with PBS and B cells were stained with FITC-labelled anti-CD19 antibody. Cell death was assessed by flow cytometry after PI staining.

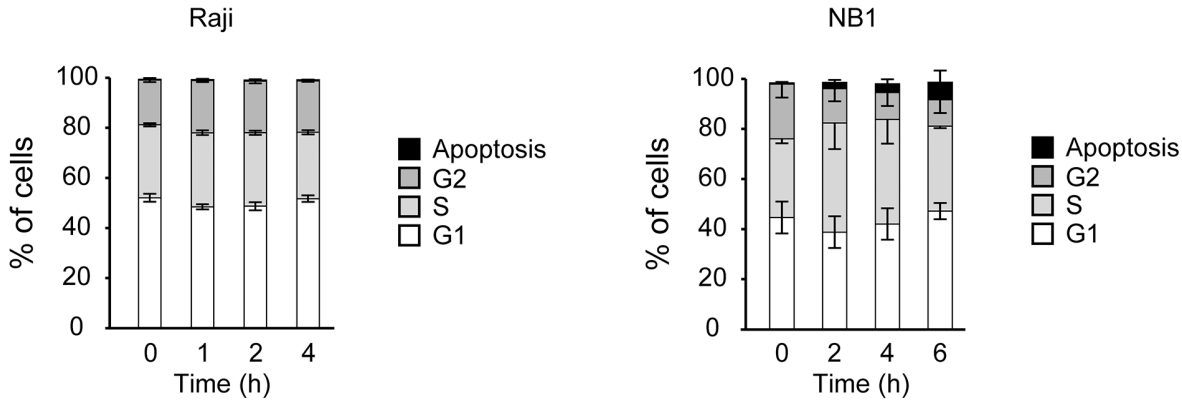

Supplementary Figure S2: Effect of TAT-RasGAP$_{317-326}$ on cell cycle. Raji cells and NB1 cells were treated for the indicated periods of time with 20 and 40 μM TAT-RasGAP$_{317-326}$, respectively. Cells were collected and cell cycle analyzed by flow cytometry. Results correspond to the mean +/- 95% CI of 3 independent experiments.

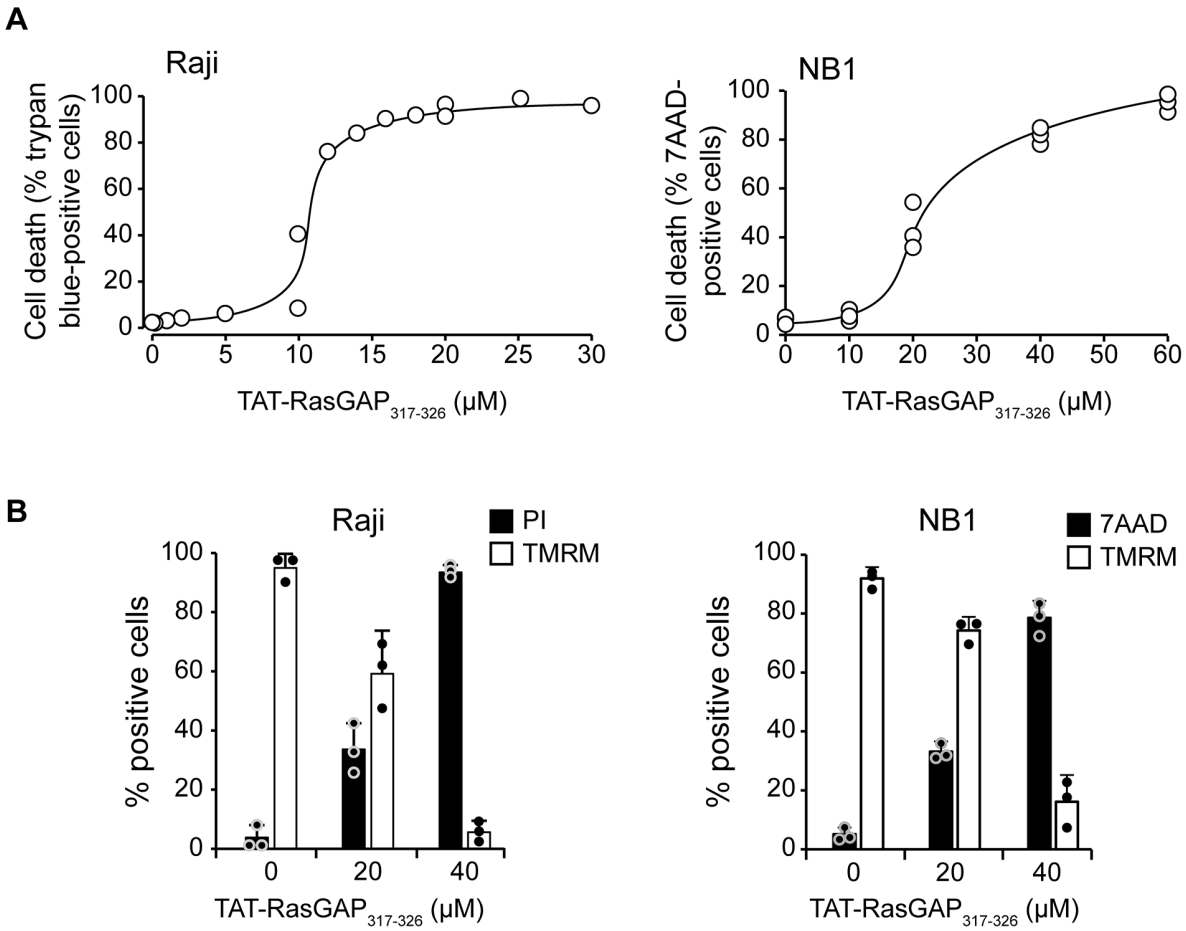

Supplementary Figure S3: Sensitivity of Raji and NB1 cells to TAT-RasGAP$_{317-326}$-mediated death and effect of the peptide on mitochondrial potential. A. Raji cells were treated with different concentrations of TAT-RasGAP$_{317-326}$ for 72 hours and cell death was determined by trypan blue exclusion. NB1 cells were treated with different concentrations TAT-RasGAP$_{317-326}$ for 24 hours and cell death was determined by flow cytometry using 7AAD. **B.** Raji and NB1 cells were treated with 0, 20 and 40 μM TAT-RasGAP$_{317-326}$ for 16 and 24 hours, respectively. Cell death and mitochondrial membrane potential were then analyzed by PI and TMRM staining using flow cytometry. Results correspond to the mean +/- 95% CI of 3 independent experiments.

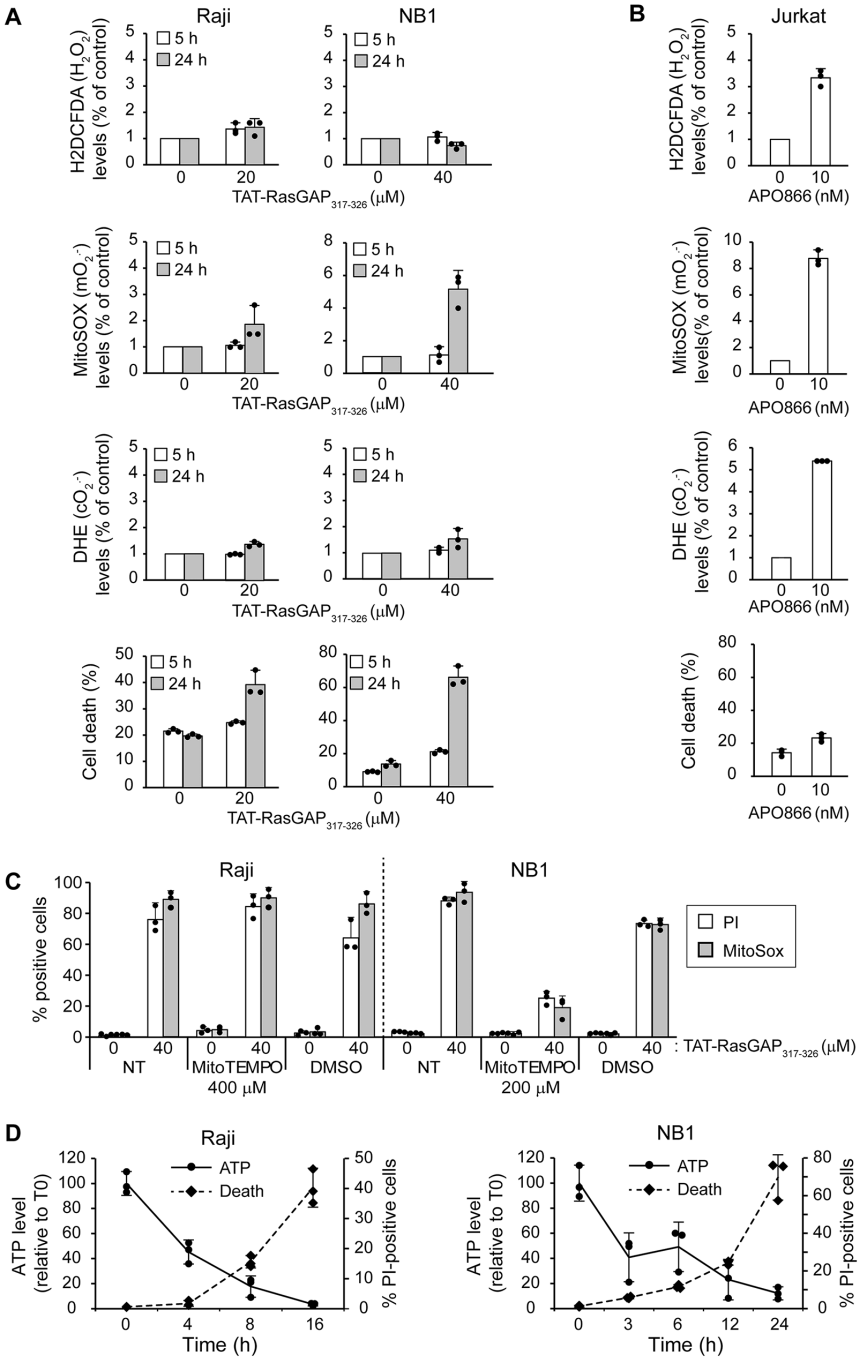

Supplementary Figure S4: Effect of TAT-RasGAP$_{317-326}$ on ROS production. A. Intracellular ROS production was detected in Raji or NB1 cells after treatment with 20 and 40 μM TAT-RasGAP$_{317-326}$, respectively. Cell death (corresponding to the % of Annexin-V and/or 7AAD-positive cells) was determined by flow cytometry. H_2O_2, $cO_2^{\cdot-}$ and $mO_2^{\cdot-}$ superoxides were detected for the indicated periods of time by flow cytometry staining using carboxy-H2DCFDA, DHE and MitoSOX fluorescent probe, respectively. **B.** Jurkat cells were treated for 48 hours with 10 nM APO866 (a potent ROS inducing agent). Cell death and ROS production were determined by flow cytometry using specific probes as described above. **C.** Cells were pretreated for 2 hours with or without the indicated concentrations of MitoTEMPO and then treated or not with 40 μM TAT-RasGAP$_{317-326}$ for 24 hours. Cell death and $mO_2^{\cdot-}$ were measured by flow cytometry using PI and MitoSox, respectively. The results are expressed as percentage of cells that are PI-positive (PI) or MitoSox-positive. **D.** Intracellular ATP levels were determined at the indicated periods of time for Raji and NB1 cells treated with 20 and 40 μM TAT-RasGAP$_{317-326}$, respectively. Each sample was normalized to protein content and to the mean basal ATP level (T0). Cell death was assessed by flow cytometry after PI staining. Results correspond to the mean +/- 95% CI of 3 independent experiments.

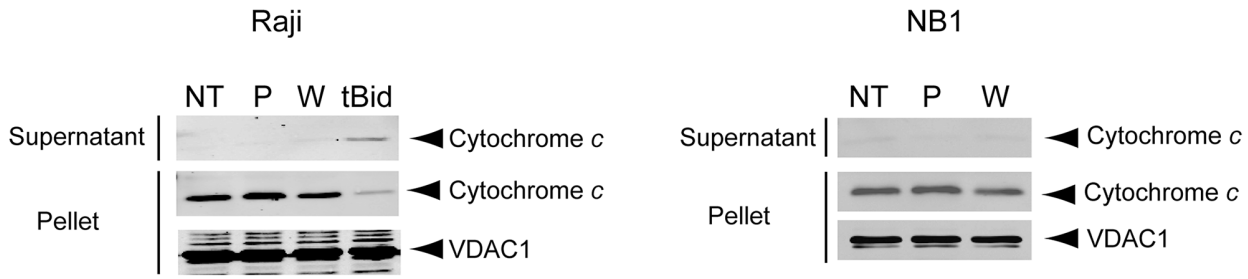

Supplementary Figure S5: Effect of TAT-RasGAP$_{317-326}$ on isolated mitochondria. Isolated mitochondria were left untreated or treated with 20 µM TAT-RasGAP$_{317–326}$ (P), 20 µM TAT-RasGAP$_{317–326}$ (W317A) (W) or 40 nM tBid for 30 min at 37°C. After centrifugation, supernatant and pellet were analyzed by Western blotting.

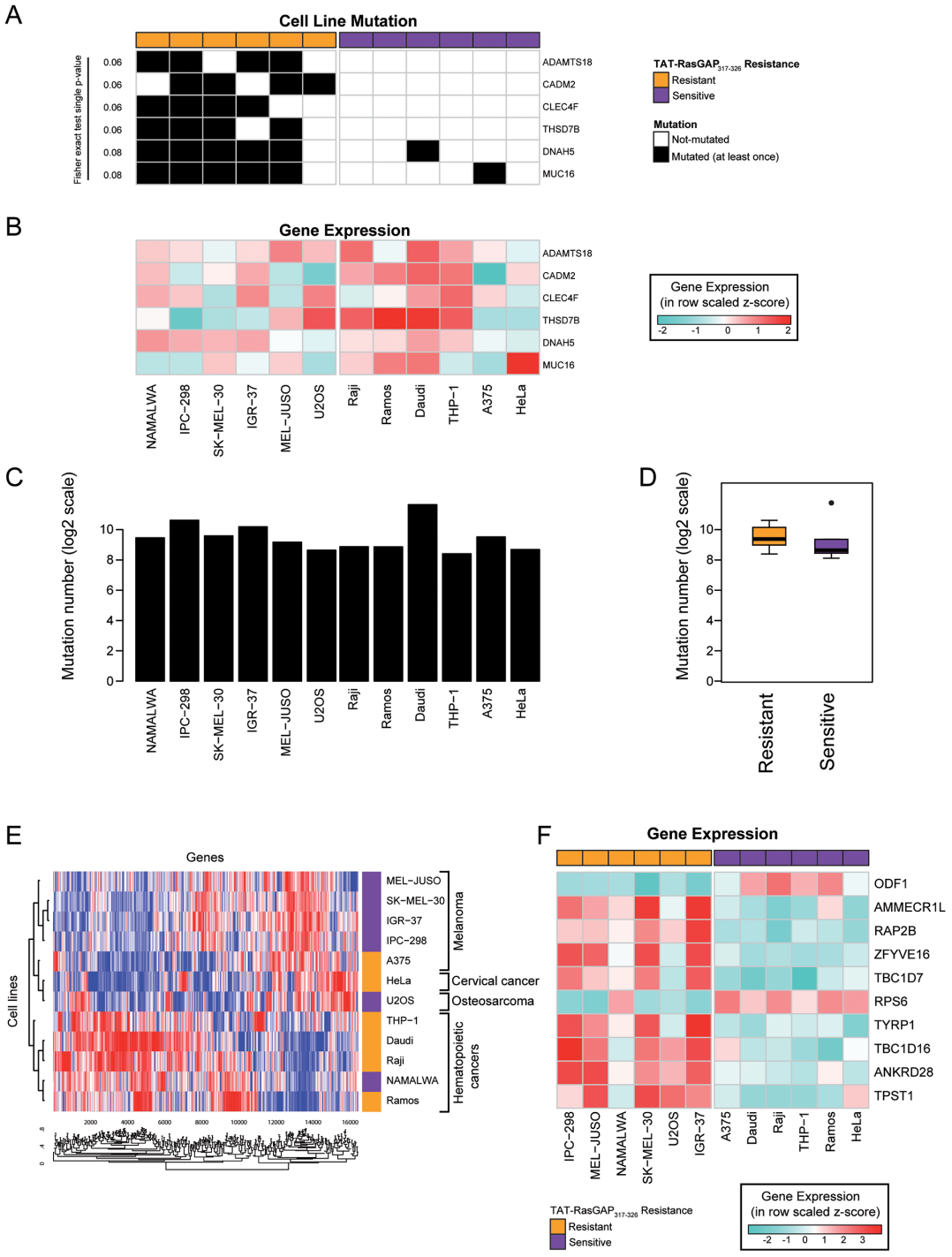

Supplementary Figure S6: Comparison of mutational count and gene expression profiles between TAT-RasGAP$_{317-326}$-sensitive and -resistant cell lines. A. Assessment of mutational enrichment according to TAT-RasGAP$_{317-326}$ sensitivity with black representing mutated genes and white denoting no mutation. The six most highly enriched genes are displayed. **B.** Heatmap representing the expression of the six most mutated genes. **C.** Number of non-synonymous somatic mutations among the twelve cell lines. **D.** Distribution of somatic mutation number in resistant and sensitive cell lines. **E.** Heatmap representing gene expression of the twelve different cell lines, with a gradient from blue (low expression) to red (high expression). **F.** Heatmap displaying the ten most differentially expressed genes between resistant and sensitive cell lines.

RELATED UNPUBLISHED DATA

To characterize the mode of cell death induced by TAT-RasGAP$_{317-326}$, I performed several experiments that were not published and that I report here.

Does TAT-RasGAP$_{317-326}$-induced cell death require the translation process?

To define at which level the peptide acts, transcription and translation were inhibited by actinomycin D and cycloheximide (CHX), respectively. Figure R1A shows that TAT-RasGAP$_{317-326}$-induced cell death still occurs in the presence of CHX at a concentration allowing the inhibition of c-Myc translation, as illustrated by the dose-dependent decrease of its protein abundance (Figure R1B). Results obtained with actinomycin D are not depicted due to the basal high toxicity of this compound rendering results hardly interpretable. Nevertheless, these data suggest that TAT-RasGAP$_{317-326}$ acts post-translationally. To better characterize at which step the RasGAP-derived peptide works, the requirement of the proteasome (using the MG-132 proteasome inhibitor) or the involvement of the kinases (using staurosporine) remain to be investigated.

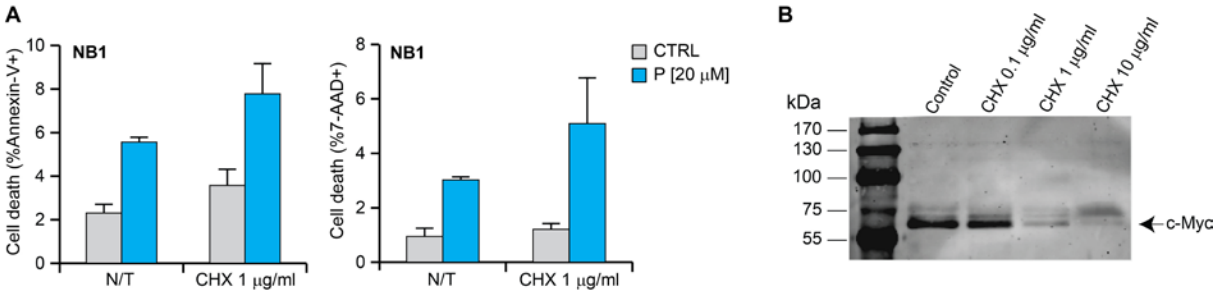

Figure R1. TAT-RasGAP$_{317-326}$ does not require the translation process. **A.** WT NB1 cells were preincubated or not (N/T) for 1 hour with cycloheximide (CHX), before being treated or not (CTRL) with 20 µM TAT-RAsGAP$_{317-326}$ (P) for 9 hours. Cell death, corresponding to the percentage of Annexin-V positive cells (apoptosis) or the percentage of 7-AAD positive cells (necrosis and late apoptosis), was determined by flow cytometry. Results correspond to the mean +/- 95% CI of at least 3 independent experiments. **B.** Abundance of c-Myc in NB1 cells treated or not for 9 hours with cycloheximide at the indicated concentrations was assessed by western blotting.

Does TAT-RasGAP$_{317-326}$ trigger necroptosis?

In order to answer this question, we used in parallel two approaches. First, we inhibited necroptosis using two different pharmacological inhibitors, a RIPK1 inhibitor called necrostatin-1 (Nec-1) and a MLKL inhibitor termed necrosulfonamide (NSA). Figures R2A and R2B indicate that NB1 cells treated with Nec-1 and NSA were not protected against the peptide toxicity. However, as mentioned in the Oncotarget paper, we were unable to induce necroptosis in NB1 cells rendering the generation of a positive control for these two experiments difficult. Consequently, the second approach was to generate MLKL knockout cells and to test them in the presence of the peptide as depicted in Figure 5

of the Oncotarget paper [196]. Results acquired with the MLKL knockout cells were in agreement with those obtained with the pharmacological inhibitors.

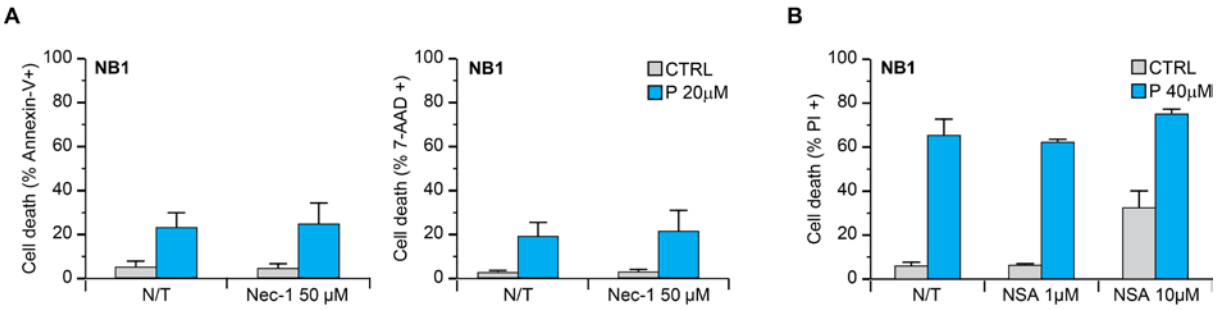

Figure R2. Inhibition of necroptosis does not prevent TAT-RasGAP$_{317-326}$-induced cell death. A. WT NB1 cells were preincubated or not (N/T) for 1 hour with necrostatin-1 (Nec-1), before being treated or not (CTRL) with 20 µM TAT-RAsGAP$_{317-326}$ (P) for 24 hours. Cell death, corresponding to the percentage of Annexin-V positive cells (apoptosis) or the percentage of 7-AAD positive cells (necrosis), was determined by flow cytometry. **B.** WT NB1 cells were preincubated or not (N/T) for 1 hour with 1 µM or 10 µM necrosulfonamide (NSA), before being treated or not (CTRL) with 40 µM TAT-RasGAP317-326 (P). After 24 hours incubation, cell death (corresponding to the % of PI positive cells) was determined by flow cytometry. Results correspond to the mean +/- 95% CI of at least 3 independent experiments.

Does TAT-RasGAP$_{317-326}$ require CAPNS1 to kill NB1 cells or to sensitize HCT116 cells to cisplatin?

The calpains are a family of calcium-dependent cysteine proteases that are implicated in several physiological processes, such as cell motility and apoptosis [197]. Furthermore, it has been demonstrated that calpain activity may affect cancer progression and anti-tumour therapies [198, 199]. Although the calpain family consists of more than ten members, the best characterized ones are the ubiquitously expressed µ-calpain and m-calpain. They are heterodimers consisting of an unique large subunit (CAPN1 and CAPN2 respectively) and a common small regulatory subunit (CAPNS1) [200]. CAPNS1 was identified as a RasGAP SH3 binding protein [201]. In order to investigate whether TAT-RasGAP$_{317-326}$ targets calpains to mediate cell death, CAPNS1 knockout NB1 and HCT116 cells were generated (Figure R5A). As illustrated in Figure R5B, the deletion of CAPNS1 in NB1 did not protect cells against the toxicity of the peptide. In addition, CAPNS1 disruption in HCT116 cell line did not abrogate the chemosensitizing activity of TAT-RasGAP$_{317-326}$ in the presence of cisplatin (Figure R5C). However, as already described in the literature, the absence of CAPNS1 in HCT116 renders those cells partially resistant to cisplatin (Figure R5C) [199].

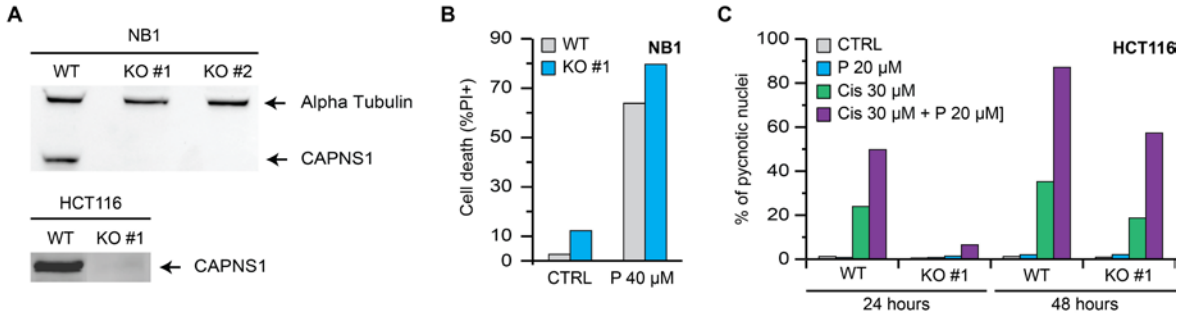

Figure R5. CAPNS1 is not required to sensitize HCT116 cells neither to kill NB1 cells. **A.** CAPNS1 was disrupted in NB1 and HCT116 cells using the CRISPR/Cas9 technology. Loss of expression was confirmed by western blotting. **B.** Wild-type (WT) and CAPNS1 knockout (KO) NB1 cells were treated or not with 40 µM TAT-RAsGAP$_{317-326}$ (P) for 24 hours. Cell death, corresponding to the % of PI positive cells, was determined by flow cytometry. The experiment was performed only once. **C.** WT and CAPNS1 KO HCT116 cells were treated or not with 30 µM cisplatin in the presence or in the absence of 20 µM TAT-RAsGAP$_{317-326}$ (P). After 24 or 48 hours, Hoechst 33342 staining was performed to determine the proportion of apoptotic cells by manually counting pycnotic nuclei. This experiment was performed only once.

Does TAT-RasGAP$_{317-326}$ induce cell death in HEK293T, Vero, HeLa, WM3248, and WM1366 cells?

In order to complete the Table 1 published in the Oncotarget paper, we tested several different cell lines for their sensitivity to TAT-RasGAP$_{317-326}$-induced cell death. Figure R6 depicts the sensitivity of five cell lines (293T, Vero, HeLa, WM3248, and WM1366) to the peptide. Of note, 293T and Vero cells were cultured in DMEM supplemented with 10% fetal bovine serum (FBS), whereas the three other cell lines were grown in RPMI supplemented with 10% FBS.

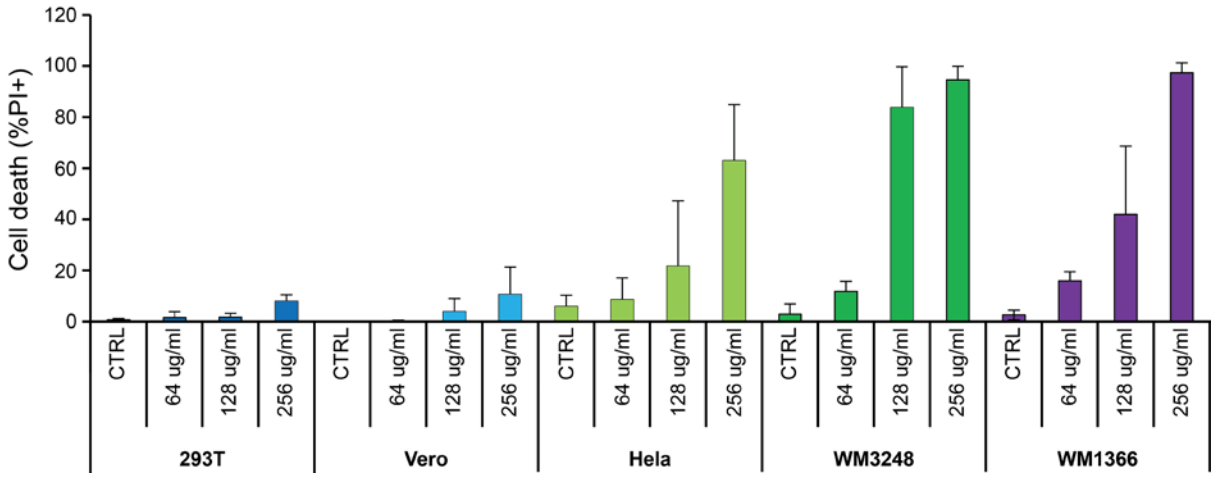

Figure R6. TAT-RasGAP$_{317-326}$ toxicity in 293T, Vero, HeLa, WM3248, and WM1366 cells. 293T, Vero, HeLa, WM3248, and WM1366 cell lines were treated with the indicated concentrations of TAT-RasGAP$_{317-326}$ for 24 hours. Cell death was then assessed using the Cytation 3 cell imaging multi-mode reader after PI and Hoechst 33342 staining. Results correspond to the mean +/- 95% CI of 3 independent experiments.

PART III

The third part of the results is dedicated to the identification of regulators of TAT-RasGAP$_{317-326}$-induced cell death. As reported in the previous part, the RasGAP-derived peptide can kill some tumour cells in a manner that differs from known regulated forms of death. To identify proteins involved in the killing activity of the peptide, a CRISPR/Cas9 screening was performed on two cell lines (SKW6.4 and Raji). Results of CRISPR/Cas9 screens, the validation of the top candidate genes, and the role of their proteins in the activity of TAT-RasGAP$_{317-326}$ are presented in the following manuscript.

This study was carried out in collaboration with several colleagues. The work was shared as following: Mathieu Heulot performed the screening on Raji cells and most of the experiments with those cells, except the cytosolic access assay (TAT-PNA), and the membrane potential and intracellular potassium measurements that were done by Dr. Sébastien Michel. Giulia Torriani, a PhD student in Prof. Stefan Kunz laboratory at the Institute of Microbiology, generated all the data with pseudotyped viruses. I performed the CRISPR/Cas9 screen on the SKW6.4 cells and validated all the yielded candidates of this screening. I did most of the experiments in SKW6.4 cells, except the cytosolic access assay (TAT-PNA) and the membrane potential measurement that were done by Dr. Sébastien Michel. In addition, I performed the majority of the experiments presented in the supplementary figures of the manuscript. Finally, I wrote the following manuscript.

GENOME-WIDE CRISPR/CAS9 SCREEN IDENTIFIES THE INVOLVEMENT OF POTASSIUM CHANNELS AND THE NA^+/K^+-ATPASE PUMP IN THE CYTOSOLIC ACCESS OF TAT-CONSTRUCTS AND VIRUSES.

INTRODUCTION

Drug delivery into cells remains a challenge due to selective permeability of the cell membrane. To improve the intracellular carriage of promising therapeutic molecules, such as proteins or nucleic acids, cell-penetrating peptides (CPPs) can be conjugated to these compounds of interest. CPPs are short peptides (usually less than 30 amino acids) able to spontaneously and ubiquitously transport various biochemically active molecules inside living cells. The first CPP described was the full length Trans-Activator of Transcription (TAT) protein of the HIV, in 1988 [140]. Some years later, it was found that a truncated version of TAT, TAT_{48-57}, was sufficient to deliver cargoes into cells [142]. Although the TAT CPP has been studied for almost 30 years, its mechanism of entry into cells remains debated due to the disparity of results among the different authors. It has been reported that the internalization of TAT can occur by direct translocation, endocytosis, or both simultaneously [153, 188-190, 193]. This discrepancy is mainly attributed to the fact that a CPP enters cells via a singular mechanism according to its sequence, structure, or amphipathicity. Moreover, cellular uptake of a single CPP is dependent on variable factors such as peptide concentration, time of incubation, local lipid composition, or characteristics of the cargo [147].

Direct translocation can happen at 4°C and in ATP depletion condition. It requires destabilization of the plasma membrane through different ways that result most of the time in the formation of pores allowing the passage of the CPP. In contrast to direct translocation, endocytosis is a generic name describing different processes that allow cells to absorb material via an ATP-depend manner [160]. Molecules can trigger endocytosis by the direct contact with the cell membrane, its binding to a receptor, or by their electrostatic interactions with the proteoglycans. There are several endocytic routes to reach the cytoplasm including macropinocytosis, clathrin-mediated endocytosis, caveolae-mediated endocytosis, or clathrin- and caveolae-independent endocytosis [161]. According to its size and biochemical properties, a cargo is internalized through specifically one or several of these routes. Once the cargo is sequestered into a vesicle, it is then internalized and sorted into a series of tubulovesicular compartments, named endosomes. Cargoes can have various fates including their recycling back to the cytoplasmic membrane, their delivery and degradation to the lysosomes, or their endosomal escape to reach the cytosol [180].

In this study, we performed gene disruption CRISPR-based genetic screens to better understand the mode of action of a peptide called TAT-$RasGAP_{317-326}$. The latter was derived from the p120 Ras GTPase-activating protein (RasGAP) and was fused to the TAT_{48-57} CPP. TAT-$RasGAP_{317-326}$ has various anti-cancer properties. It potently sensitizes tumour cells to various chemotherapeutic agents and hampers metastatic progression *in vitro* and *in vivo* [122-124, 202]. Recently, we have shown that this RasGAP-derived peptide possesses also the ability to directly kill some neoplastic cells [196]. Moreover, in these cells blocking any known mode of cell death, such as apoptosis, necroptosis,

autophagy, parthanatos, or pyroptosis, did not (or only partially) inhibit the toxicity of the peptide [196]. By using the CRISPR/Cas9 approach, we expected to decipher which genes were involved in TAT-$RasGAP_{317-326}$-induced cell death. The screens yielded as the top candidates several potassium channels (KCNQ5, KCNN4, and KCNK5) and a subunit of the Na^+/K^+-ATPase pump (ATP1B3), whose loss rendered the cells resistant to the peptide toxicity. However, we showed that the disruption of these genes hampers the cytosolic access of the RasGAP-derived peptide rather than inhibits its pro-death activity. In addition, we validated the involvement of these targets in the regulation of the cytosolic access of two other TAT-constructs called TAT-PNA and TAT-Cre. Finally, this ability to inhibit the intracellular delivery was also validated for several viruses.

This new property of potassium channels and the Na^+/K^+-ATPase pump could allow a better understanding of the mode of entry of TAT CPP and could lead to development of prophylactic inhibition of viral infections.

MATERIALS AND METHODS

Cell lines

All cell lines were cultured in 5 % CO_2 at 37 °C. The Raji and Daudi Burkitt lymphoma cells, the HeLa cervical cancer cells, the THP-1 acute monocytic leukemia cells, and the SKW6.4 lymphoblastoid cells were cultured in RPMI (Invitrogen, ref. no. 61870) supplemented with 10 % heat-inactivated fetal bovine serum (FBS; Invitrogen, ref. no. 10270-106). The NB1 neuroblastoma cells were maintained in neural basic medium composed of DMEM/F12 (Invitrogen, ref. no. 31331-028) supplemented with 2% B27 serum-free complement (Invitrogen, ref. no. 17504044), 20 ng/ml human recombinant basic fibroblast growth (bFGF) (Peprotech, ref. no. 100-18B) and 20 ng/ml human recombinant epidermal growth factor (EGF) (Peprotech, ref. no. AF-100-15). Human lung carcinoma alveolar epithelial (A549) cells were grown in DMEM (Invitrogen, ref. no. 61965) supplemented with 10 % heat-inactivated FBS, glutamine, and penicillin-streptomycin.

Chemicals

Puromycin was from Life technologies (ref. no. A11138-02). Blasticidin was from Applichem (ref. no. A3784). TRAM-34 and XE991 were from Alomone labs (ref. no. T-105 and X-100, respectively). Ouabain, digoxin, pyrenebutyrate, gramicidin, Live Hoechst 33342, and dasatinib were from Sigma (ref. no. O3125, O4599, 257354, 50845, B3361, and CDS023389, respectively). Okadaic acid was from LC laboratories (ref. no. O-2220).

Peptides

TAT-$RasGAP_{317–326}$ is a retro-inverso peptide (i.e. synthesized with D-amino acids in the opposite direction compared to the natural sequence). The TAT moiety corresponds to amino acids 48–57 of the HIV TAT protein (RRRQRRKKRG) and the $RasGAP_{317–326}$ moiety corresponds to amino acids 317–326 of the human RasGAP protein (DTRLNTVWMW). These two moieties are separated by two glycine linker residues in the TAT-Ras-$GAP_{317–326}$ peptide. TAT-$RasGAP_{317-326}$ (W317A) has the

tryptophan at position 317 mutated into an alanine. All the peptides, including the FITC-TAT-$RasGAP_{317-326}$ ([FITC]DTRLNTVWMWGGRRRQRRKKRG), were synthesized at the department of biochemistry, University of Lausanne, Switzerland, using FMOC technology, purified by HPLC and tested by mass spectrometry.

Cell death measurement

Cell death was measured with propidium iodide (PI) (Sigma, ref. no. 81845). Cells were analyzed using a Beckman Coulter FC500 flow cytometer and data were analyzed with the Kaluza Version 1.2 software (Beckman Coulter).

Plasmids

The lentiviral vector lentiCRISPR [203] was obtained from Addgene (#868, Addgene, ref. no. 52961). The pMD2.G plasmid (#554, Addgene, ref. no. 12259) encodes the envelope of lentivirus. The psPAX2 plasmid (#842, Addgene, ref. no. 12260) encodes the packaging system. pLUC705 (#876, gift from Bing Yang) [204] was HindIII/XhoI digested and blunted with T4 DNA polymerase. LeGOIG2 (#807, Addgene, ref. no. 27341) was StuI digested, dephosphorylated and ligated to the blunted insert to make LeGOiG2-LUC705 (#875). pTAT-Cre (#917, Addgene, ref. no. 35619) encodes the Histidine-tagged TAT-Cre recombinase. Cre-reporter plasmid (#918, Addgene, ref. no. 62732) encodes a LOXP-RFP-STOP-LOXP-GFP. After infection, cells are red. If Cre-recombinase is able to reach the nucleus, recombination will occur and the RFP-STOP fragment will be excised and GFP will be produced.

Lentivirus production

Recombinant lentiviruses were produced as described [205] with the following modification: pMD.G and pCMVDR8.91 were replaced by pMD2.G and psPAX2, respectively.

Genome-scale CRISPR/Cas9 Knockout screening

The human GeCKO v2 library (2 plasmid system) (Addgene ref. no. 1000000049) was amplified by electroporation using the electroporation system (Bio-Rad Gene Pulser II ref. no. 165-2105) and the Lucigen Endura cells (ref. no. 60242). Cells were plated on LB Agar plate containing 100 µg/ml ampicillin. After 14 h at 32°C, colonies were scrapped and plasmids recovered with the Plasmid Maxi kit (Qiagen, ref. no. 12162). To produce lentivirus library, 12 T-225 flasks were seeded with $12x10^6$ of HEK293T cells / flask. The day after, each flask was treated as follows: 10 µg pMD2.G, 30 µg psPAX2 and 25 µg GeCKO plasmid library were mixed with 250 mM $CaCl_2$. This solution was mixed (v/v) with 2x HEPES buffer (NaCl 280 mM, KCl 10 mM, Na_2HPO_4 1.5 mM, D-glucose 12 mM, HEPES 50 mM), incubated for 1 minute and added to the culture medium. Seven hours later, the medium was removed and replaced by DMEM supplemented with 10 % FBS and 1 % penicillin-streptomycin. Forty-eight hours later, the medium was collected and centrifuged for 5 min at 2000 g to pellet the cells. Supernatant was filtered through a 0.45 µm HV/PVDF (Millipore, ref. no. SE1M003M00) and

concentrated 100x by ultracentrifugation (Beckman) at 24.000 rpm for 2 hours at 4°C. Virus pellet was resuspended in ice-cold PBS, aliquoted and stored at -80°C.

To express the Cas9 endonuclease, SKW6.4 and Raji cells were infected with lentiCas9-Blast (Addgene, ref. no. 52962) and selected with 10 µg/ml blasticidin for a week.

The multiplicity of infection (MOI) of the GeCKO virus library was determined as follows: different volumes of virus library were added to $3x10^6$ cells expressing Cas9 plated in a 12-well plate. Twenty-four hours later, each well was split into duplicate and one replicate received 10 µg/ml puromycin for 3 days. Cell viability was determined by trypan blue exclusion and MOI was considered as the percentage of living cells. The virus volume yielding to MOI close to 0.3 was chosen. Large-scale infection of $12x10^7$ cells was carried out in 12-well plates with $3x10^6$ cells per well. Twenty-four hours later, wells were pooled in a T-225 flask and infected cells selected with 10 µg/ml puromycin for a week. $3x10^7$ infected untreated SKW6.4 and Raji cells were frozen for genomic DNA analysis. $1x10^8$ infected SKW6.4 cells and $6x10^7$ infected Raji cells were treated with 60 µM and 40 µM TAT-$RasGAP_{317-326}$ for 17 days and 8 days respectively, with a medium and peptide renewal every 2-3 days. $3x10^7$ peptide-selected SKW6.4 and Raji cells were frozen for genomic DNA analysis. Genomic DNA was extracted with Blood & Cell Culture DNA Midi Kit according to manufacturer's instructions (Qiagen, ref. no. 13343). A first PCR was performed to amplify the lentiCRISPR sgRNA region with the following primers:

F1: 5'-AATGGACTATCATATGCTTACCGTAACTTGAAAGTATTTCG-3'

R1: 5'-CTTTAGTTTGTATGTCTGTTGCTATTATGTCTACTATTCTTTCC-3

A second PCR was performed to attach Illumina adaptors and barcodes (green) to samples. 5 µL of the first PCR product was used. Primers for the second PCR include both a variable length sequence (red) to increase library complexity and an 8bp barcode for multiplexing of different biological samples. Of note, R2_iA_06 and R2_iA_12 were used for the PCR in SKW6.4 samples, whereas R2_iA_12 and R2_iC_26 were used for the PCR in Raji samples.

F2a	AATGATACGGCGACCACCGAGATCTACACTCTTTCCCTACACGACGCTCTTCCGATCTTCTTGTGGAAAGGACGAAACACCG
F2b	AATGATACGGCGACCACCGAGATCTACACTCTTTCCCTACACGACGCTCTTCCGATCTAGCTCTTGTGGAAAGGACGAAACACCG
F2c	AATGATACGGCGACCACCGAGATCTACACTCTTTCCCTACACGACGCTCTTCCGATCTCGAGCTCTTGTGGAAAGGACGAAACACCG
F2d	AATGATACGGCGACCACCGAGATCTACACTCTTTCCCTACACGACGCTCTTCCGATCTCATAACCTCTTGTGGAAAGGACGAAACACCG
F2e	AATGATACGGCGACCACCGAGATCTACACTCTTTCCCTACACGACGCTCTTCCGATCTGTGCTAACGTCTTGTGGAAAGGACGAAACACCG
R2_iA_06	CAAGCAGAAGACGGCATACGAGATATTGGCGTGACTGGAGTTCAGACGTGTGCTCTTCCGATCTTCTACTATTCTTTCCCCTGCACTGT
R2_iA_ 12	CAAGCAGAAGACGGCATACGAGATTACAAGGTGACTGGAGTTCAGACGTGTGCTCTTCCGATCTTCTACTATTCTTTCCCCTGCACTGT
R2_iC_26	CAAGCAGAAGACGGCATACGAGATGCTCATGTGACTGGAGTTCAGACGTGTGCTCTTCCGATCTTCTACTATTCTTTCCCCTGCACTGT

Table I. Primer sequences for the second PCR

Both PCR were performed in 100 µL with the Herculase II Fusion DNA Polymerase (Agilent, ref. no. 600675). Amplicons were gel extracted, quantified, mixed and sequenced with a MiSeq (Illumina). Raw FASTQ files were demultiplexed and processed to contain only the unique sgRNA sequence. The number of reads of each sgRNA was normalized as described [206]. The MAGeCK algorithm

[207] was used to rank screening hits by the consistent enrichment among multiple sgRNAs targeting the same gene.

Genome editing by CRISPR/Cas9 system

Single guide RNAs targeting the early exon of the protein of interest were chosen in the sgRNA library [206] and are listed in table I. LentiCRISPR plasmids specific for a gene were created according to the provided instructions. Oligos were designed as follow: Forward 5'-CACCGnnnnnnnnnnnnnnnnnnnn-3'; Reverse-3'-CnnnnnnnnnnnnnnnnnnnnCAA-5', where nnnnnnnnnnnnnnnnnnnn in the forward oligo corresponds to the 20 bp sgRNA. Oligos were synthetized, then phosphorylated and annealed to form oligo complex. LentiCRISPR vector was BsmBI digested and dephosphorylated. Linearized vector was purified and gel extracted and ligated to oligo complex. The lentiCRISPR vector containing the sgRNA was then used for virus production. Cells were infected and selected with the appropriate dose of puromycin (0.5 μg/ml for SKW6.4, 2 μg/ml for Raji). Clone isolation was performed by limiting dilution in 96 well-plate.

Table I. List of sgRNAs used to disrupt target genes

Target gene	**sgRNA name**	**sgRNA sequence**
KCNN4	sgKCNN4.1	CTGCCCGAGTGCTACAAGAA
KCNN4	sgKCNN4.2	CATGGTGCCCGGCACCACGT
KCNK5	sgKCNK5.1	ATGGTGGTAATGACGGTCGC
KCNK5	sgKCNK5.2	CTCTGCCTGACGTGGATCAG
ATP1B3	sgATP1B3.1	ATGCGGTCACTGGTTTTGGA
ATP1B3	sgATP1B3.2	ACTTCGTATGCAGGGTACAT
SLC39A14	sgSLC39A14.1	ATATCAGAGTAGCGGACACC
SLC39A14	sgSLC39A14.2	CGACTGCTCGCTGAAATTGT
KCNQ5	sgKCNQ5.1	TCTAGGAATTAATTCACAGC
KCNQ5	sgKCNQ5.2	ACAGATCCTCCGCATGGTCG
PIP5K1A	sgPIP5K1A.1	CATGCAAGATTTCTACGTGG
PIP5K1A	sgPIP5K1A.2	GGATACTACATGGTAAGGGA

Antibodies

The rabbit anti-PIP5K1A, anti-pSrc Tyr416, anti-pAKT S473, anti-pAKT T308, and anti-actin antibodies were purchased from Cell Signaling (ref. no. 9693, 6943, 9271, 9275, and 4970, respectively). The mouse anti-PP2Ac and anti-ATP1B3 antibodies were purchased from Santa Cruz (ref.no. sc56950 and sc135998, respectively). The mouse anti-vinculin antibody was purchased from Sigma (ref. no. v9131).

TA cloning

TA cloning kit (Life technologies, ref. no. K202020) was used according to manufacturer's instructions to sequence DNA fragment containing the region where Cas9 was guided by a sgRNA.

Cytosolic access assay

WT, KCNN4 KO, KCNK5 KO, and ATP1B3 KO SKW6.4 cells, as well as WT, KCNQ5 KO and PIP5K1A Raji cells were infected with the LeGOiG2-LUC705 lentivirus. Then, 200,000 cells were treated with 5 µM peptide nucleic acid (PNA) GRKKRRQRRR-CCTCCTACCTCAGTTACA (PNAbio). This PNA is composed of the protein TAT sequence and the oligonucleotide sequence able to mask the aberrant splicing site at the position 705 in order to restore proper luciferase splicing and expression. After 16 hours incubation, cells were washed twice in HKR buffer (119 mM NaCl, 2.5 mM KCl, 1 mM NaH2PO4, 2.5 mM CaCl2, 1.3 mM MgCl2, 20 mM HEPES, 11 mM dextrose, pH 7.4) and lysed in 40 µL HKR + 0.1 % Triton X-100 for 15 min at room temperature. Luciferase activity was measured using Dual-Luciferase Reporter Assay (Promega) and normalized to the protein content. Results are expressed as the ratio of PNA treated over PNA untreated luciferase activity. Signals were detected with GLOMAXTM 96 Microplate Luminometer (Promega), analyzed with Glomax version 1.7.0 program.

TAT-Cre-recombinase production, purification and recombination

WT and KCNQ5 KO Raji cells were infected with the lentivirus encoding Cre-reporter described in [208]. TAT-Cre-recombinase was produced as described in [188]. Briefly, *E. coli* BL21 transformed with pTAT-Cre were grown overnight in LB containing 100 µg/ml kanamycin. Overnight culture was used to inoculate fresh LB medium at OD600 nm 0.2. Protein production was induced at OD600 nm 0.6 with 500 µM IPTG for 3 hours. Bacteria were collected by centrifugation at 5000xg and kept at -20°C. Purification was performed on Äkta prime (GE, Healthcare, USA) equipped with a 1 ml HisTrap FF column equilibrated with binding buffer (20 mM sodium phosphate, 500 mM NaCl, 5 mM imidazole pH 7.4). The day of the purification, bacterial pellet was resuspended in lysis buffer (Binding buffer + protease inhibitor tablets (Roche, ref. no. 4693132001) + DNase 1 (Roche, ref. no. 04716728001) + Lysozyme 2 mg/ml (Roche, ref. no. 10 837 059 001)) and sonicated 6 x 30sec. After 20 minutes centrifugation at 5000xg, the supernatant was filtered with Steriflip 0.45 µm and loaded on the column. Elution buffer (20 mM sodium phosphate, 500 mM NaCl, 500 mM imidazole pH 7.4) was used to detach His-tagged proteins from the column. Imidazole was removed from collected fractions by overnight dialysis using 10K MWCO cassette (Thermo Scientific, ref. no. 66807) in PBS. WT and KCNQ5 KO Raji cells encoding the Cre-reported were treated for 48 hours with 20 µM TAT-Cre-recombinase. Fluorescence was observed using a Nikon Eclipse TS100 microscope.

Confocal microscopy

Cells were seeded onto glass bottom culture dishes (MatTek, corporation ref. no. P35G-1.5-14-C) and treated with FITC-TAT-RasGAP$_{317-326}$. For nuclear staining, 1 µl/ml live Hoechst 33342 (Molecular probes, ref. no. H21492) was added into culture medium 15 minutes before washing cells twice with PBS. After washing, cells were examined under a Zeiss LSM 710 Quasar laser scanning fluorescence confocal microscope.

Direct translocation with pyrenebutyrate

Cells were washed twice with serum-free medium and treated for 10 minutes with 50 µM pyrenebutyrate at 37°C. Then cells were treated with TAT-RasGAP$_{317-326}$ or the inactive point mutant TAT-RasGAP$_{317-326}$ (W317A) for the indicated period of time.

Potassium-rich buffer

40 mM KCl, 100 mM potassium glutamate, 1 mM $MgCl_2$, 1 mM $CaCl_2$, 5 mM glucose, 20 mM HEPES, pH7.4 from [193].

Membrane potential and intracellular potassium measurements

The membrane potential (V_m) was determined by incubating the cells with the fluorescent probe DiBAC4(3) 100 nM during 40 minutes (molecular probe, ref. no. B438) Median fluorescence intensity was directly assessed by flow cytometry. For intracellular potassium concentration [K+]i determination, cells were incubated with the K+-sensistive probe Asante Potassium Green 2 (APG-2) (Abcam, ref. no. ab142806) 1 uM during 30 minutes, followed by flow cytometry analysis.

Virus infection

WT and KCNN4 KO HeLa cells or A549 cells were plated in 96-well plates at a density of $2x10^4$ cells per well and grown into confluent monolayers in 16 to 20 h. The cells were treated or not with 10 µM TRAM-34 or 10 µM XE991 for 1 hour, followed by infection with the indicated pseudotyped virus that contained a luciferase reporter in their genome for 1 h at 37°C. Unbound virus was removed, the cells were washed twice with DMEM, and fresh medium was added. Sixteen hours after the infection, cells were lysed in 1X Cell Culture Lysis Reagent (Promega) according to the manufacturer's instructions. The activity of the Luciferase gene reporter was measured using the Luciferase Assay System (Promega) according to manufacturer's instructions and using a Lumat LB 9507 (Berthold Technologies) luminometer.

RESULTS

CRISPR/Cas9 screening highlighted several genes involved in the modulation of TAT-RasGAP$_{317-326}$ toxicity

To identify proteins required for the peptide toxicity, we performed CRISPR/Cas9 screens on two cell lines, the SKW6.4 B-lymphoblastoid EBV-transformed cells and the Raji Burkitt lymphoma cells. Both cell lines were directly killed by the peptide (Figures 1A and 1B). The CRISPR/Cas9 system uses single-guide RNAs (sgRNAs) that direct the Cas9 DNA endonuclease to their complementary sequences, located at specific loci, and disrupt them [209, 210]. We used the GeCKO v2 human CRISPR/Cas9 lentiviral library, where each plasmid encodes a different sgRNA, targeting a total of 19,050 human genes (with 6 sgRNAs per target) and 1,864 miRNAs (with 4 sgRNAs per target) [203] (Figure 1C). The two cell lines were infected with the lentivirus library. Half of the infected SKW6.4 or Raji cells were treated with TAT-RasGAP$_{317-326}$ for 17 or 8 days with 60 µM or 40 µM TAT-RasGAP$_{317-326}$ respectively, a dose of peptide known to induce close to 100% cell death within 48 hours. This allowed to positively select only the cells bearing sgRNAs that target genes required for the toxicity of the peptide. The other half of the cells was left untreated to serve as a control. Then, the sgRNAs in the resistant population and those of the control population were sequenced by high-throughput sequencing, to determine their relative abundance. The initial distribution of the sgRNAs observed in the control population is expecting to change in the treated one. This is because the positive selection leads to the enrichment of the resistant subpopulation and therefore to an overall increase abundance of only the sgRNAs which confer resistance against the peptide (Figure 1C). Figures 1D and 1E represent the TAT-RasGAP$_{317-326}$-induced cell death sensitivity of both cell lines infected with the CRISPR/Cas9 library before and after selection with the peptide. As expected, after positive selection with TAT-RasGAP$_{317-326}$, the two cell lines were rendered resistant to its toxicity.

Results of massively parallel sequencing for SKW6.4 and Raji cells in both the control and the peptide selected populations are presented in Supplementary Table S1. The screens identified several candidate genes. The frequency of each sgRNA in both control and peptide selected populations for the two cell lines is displayed in Figures 1F and 1G. The four top candidate genes with the highest sgRNA enrichment in the treated population are labeled. The dots with the same color indicate sgRNAs targeting the same gene. The plots of Figures 1H and 1I depict the four top genes in SKW6.4 and in Raji cells respectively obtained using the Model-based Analysis of Genome-wide CRISPR-Cas9 Knockout (MAGeCK) algorithm. Interestingly, three potassium channels were found among the top candidates (KCNN4, KCNK5, and KCNQ5). In addition, the screen on SKW6.4 cells identified one subunit of the Na^+/K^+-ATPase pump (ATP1B3) and a divalent metal transporter for zinc, manganese, iron, and cadmium (SLC39A14). In Raji cells, an enzyme that catalyzes the phosphorylation of phosphatidylinositol 4-phosphate (PI4P) to form phosphatidylinositol 4,5-biphosphate (PI(4,5)P2) called PIP5K1A, an adaptor protein termed Arrestin domain-containing protein 3 (ARRDC3), and a MAGE family member protein (MAGEB5) were highlighted as putative regulators of the peptide. The absence of these candidates is expected to render SKW6.4 cells and Raji cells resistant to the peptide toxicity.

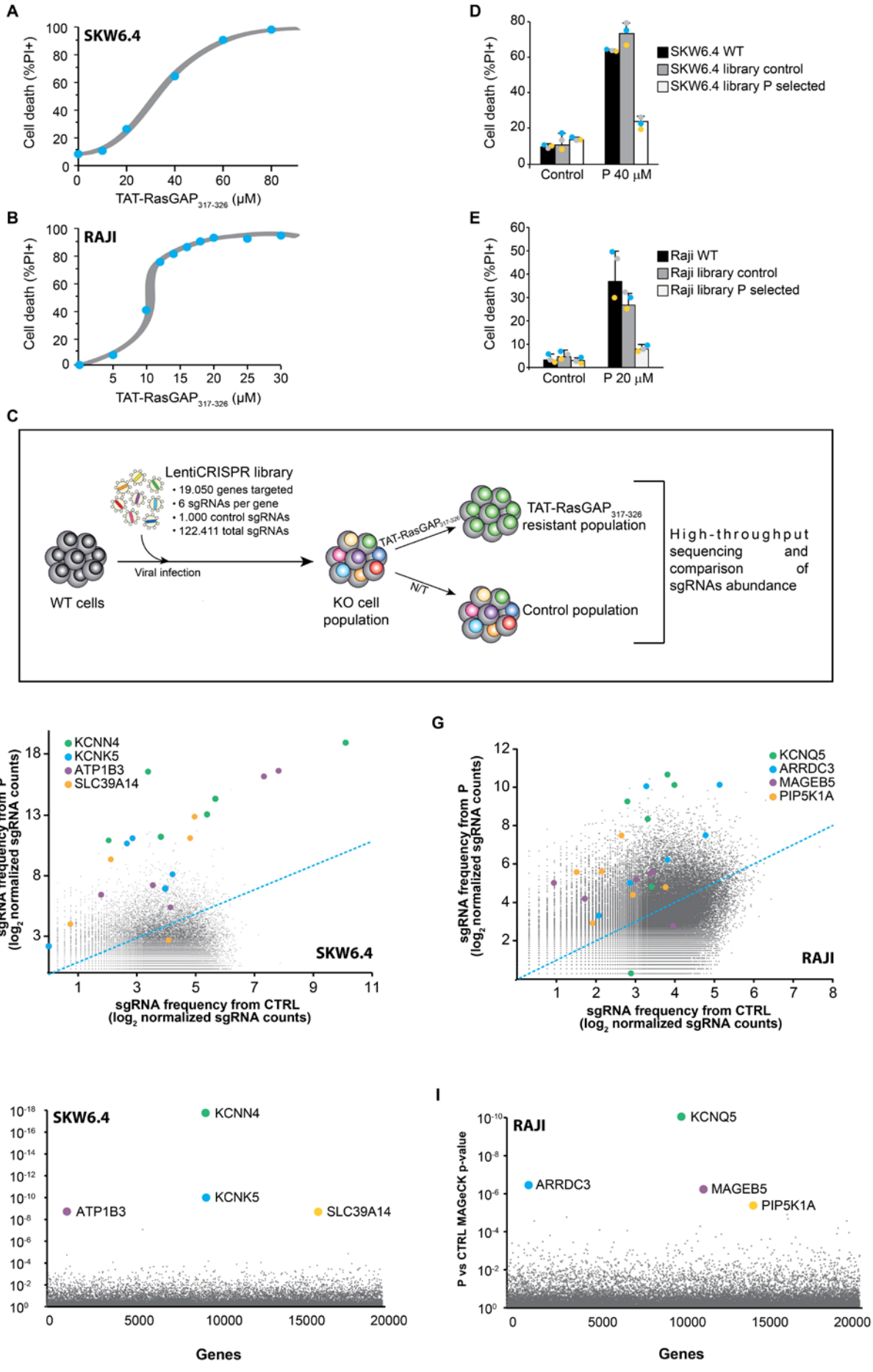
A
SKW6.4
Cell death (%PI+)
TAT-RasGAP317-326 (μM)
B
RAJI
Cell death (%PI+)
TAT-RasGAP317-326 (μM)
D
Cell death (%PI+)
SKW6.4 WT
SKW6.4 library control
SKW6.4 library P selected
Control
P 40 μM
E
Cell death (%PI+)
Raji WT
Raji library control
Raji library P selected
Control
P 20 μM
C
LentiCRISPR library
• 19.050 genes targeted
• 6 sgRNAs per gene
• 1.000 control sgRNAs
• 122.411 total sgRNAs
Viral infection
WT cells
KO cell population
TAT-RasGAP317-326
N/T
TAT-RasGAP317-326 resistant population
Control population
High-throughput sequencing and comparison of sgRNAs abundance
F
KCNN4
KCNK5
ATP1B3
SLC39A14
sgRNA frequency from P (log2 normalized sgRNA counts)
SKW6.4
sgRNA frequency from CTRL (log2 normalized sgRNA counts)
G
KCNQ5
ARRDC3
MAGEB5
PIP5K1A
sgRNA frequency from P (log2 normalized sgRNA counts)
RAJI
sgRNA frequency from CTRL (log2 normalized sgRNA counts)
H
SKW6.4
KCNN4
KCNK5
ATP1B3
SLC39A14
P vs CTRL MAGeCK p-value
Genes
I
RAJI
KCNQ5
ARRDC3
MAGEB5
PIP5K1A
P vs CTRL MAGeCK p-value
Genes

Figure 1. Identification of candidate genes, whose depletion confers TAT-RasGAP$_{317-326}$ resistance. **A.** SKW6.4 cells were treated for 24 hours with indicated concentrations of TAT-RasGAP$_{317-326}$. Cell death, corresponding to the percentage of propidium iodide (PI)-positive cells, was assessed using flow cytometry. **B.** Raji cells were treated for 16 hours as described in panel A. Cell death was then assessed by flow cytometry after PI staining. **C.** The lentiCRISPR library is a pool of lentiviruses used to infect wild-type (WT) cells. Half of the infected knockout cell population is then treated with TAT-RasGAP$_{317-326}$ to select the resistant cells, while the other half remains untreated. The abundance of each sgRNA is then compared between the two populations using high-throughput sequencing. **D-E.** SKW6.4 WT, SKW6.4 GeCKO library control, and SKW6.4 GeCKO library TAT-RasGAP$_{317-326}$ (P)-selected cells, or Raji WT, Raji GeCKO library control, and Raji GeCKO library TAT-RasGAP$_{317-326}$ (P)-selected cells were treated or not with 40 µM or 20 µM TAT-RasGAP$_{317-326}$ for 24 or 16 hours, respectively. Cell death was then assessed by flow cytometry after PI staining. Results correspond to the mean +/- 95% CI of three independent experiments. **F-G.** Scatterplot showing enrichment of specific sgRNAs after TAT-RasGAP$_{317-326}$ treatment in SKW6.4 and Raji cells, respectively. Dots with the same color indicate sgRNAs targeting the same gene. The blue dashed-line represents the equal frequency in both control (CTRL) and TAT-RasGAP$_{317-326}$ (P) populations. **H-I.** Identification of the four top candidate genes implicated in resistance to TAT-RasGAP$_{317-326}$ in SKW6.4 and Raji cells respectively using the Model-based Analysis of Genome-wide CRISPR/Cas9 Knockout (MAGeCK) p-value.

To validate the top candidates, we knocked them out in the two corresponding cell lines using the CRISPR/Cas9 technology. The level of expression of ATP1B3 in wild-type and knockout SKW6.4 cells was detected by western blot (Figure 2D), however, endogenous levels of KCNN4, KCNK5, and SLC39A14 could not be assessed in that way. Consequently, the DNA region targeted by the Cas9 endonuclease was sequenced for these genes (Figures 2A and 2G and Supplementary Figure S1A). Of note, KCNK5 disrupted clone #2 and SLC39A14 disrupted clone #1 bear a frameshift on allele 2 and on allele 1 respectively, which could mean that KCNK5 and SLC39A14 might still be functional in these clones.

All the knockout clones were treated with TAT-RasGAP$_{317-326}$. The absence of each of the four top genes yielded by the CRISPR/Cas9 screening in SKW6.4 cell line protects, at least partially, against the peptide toxicity (Figures 2B, 2E, 2H, and Supplementary Figure S1B). As a complementary approach, we used pharmacological inhibitors whenever they were available, such as TRAM-34, a KCNN4 blocker and digoxin/ouabain, two Na^+/K^+-ATPase pump potent inhibitors (Figures 2C and 2F) [211-213].

As shown in Figures 2J and 2M, only the two candidates KCNQ5 and PIP5K1A were validated in Raji cells. Knockout cells for both genes (Figures 2I and 2L) fully prevent TAT-RasGAP$_{317-326}$-induced cell death. Moreover, the pharmacological inhibitor XE991, which acts on the five members of the KCNQ family, was able to block the peptide toxicity in Raji cells (Figure 2K) [214].

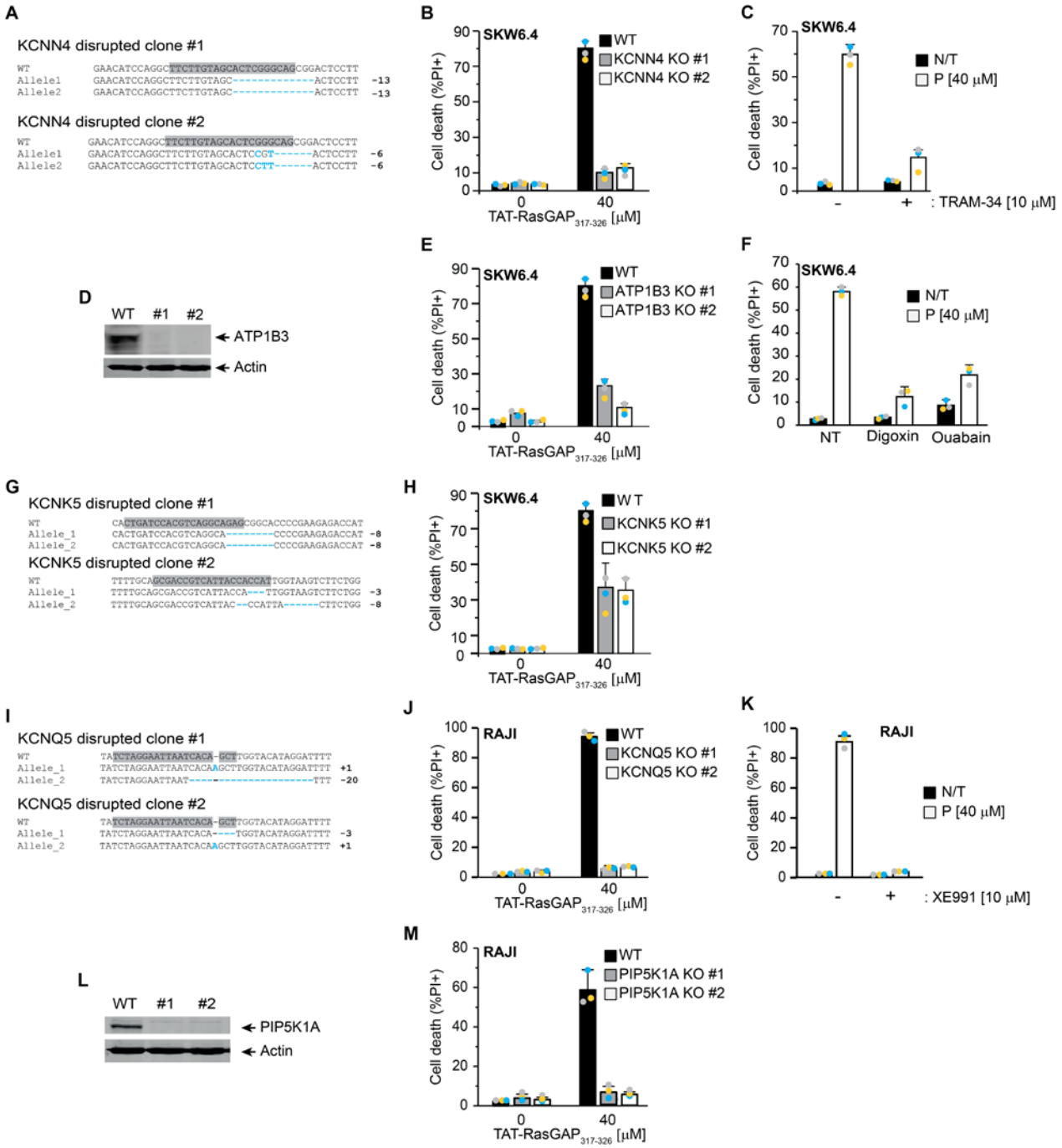

Figure 2. Validation of the top candidate genes in SKW6.4 and Raji cells. **A, G.** DNA sequences of WT KCNN4 and KCNK5 genes in SKW6.4 cells and KCNN4 and KCNK5 alleles of corresponding knockout clones #1 and #2. Differences with WT and disrupted clones are in blue. The sgRNAs directed against each gene are highlighted in grey. **B, E, H.** WT and KCNN4, ATP1B3, KCNK5 disrupted SKW6.4 cells respectively were treated or not with 40 µM TAT-RasGAP$_{317-326}$ for 24 hours. Cell death was then assessed by flow cytometry after PI staining. **C, F.** SKW6.4 WT cells were pretreated or not with 10 µM TRAM-34 (C) and 100 nM digoxin or 100 nM ouabain (F) for 1 hour and then treated with 40 µM TAT-RasGAP$_{317-326}$ for 24 hours. Cell death was assessed by flow cytometry after PI staining. **D, L.** Expression of ATP1B3 and PIPK1A in WT and knockout SKW6.4 and Raji cells, respectively. **I.** Same as panel A for KCNQ5 gene in Raji cells. **J, M.** WT and KCNQ5, PIP5K1A disrupted Raji cells respectively were treated or not with 40 µM TAT-RasGAP$_{317-326}$ for 16 hours. Cell death was assessed as in panel B. **K.** Raji cells were pretreated or not with 10 µM XE991 for 1 hour and then treated with 40 µM TAT-RasGAP$_{317-326}$ for 16 hours. Cell death was assessed by flow cytometry after PI staining. Results for panels B, C, E, F, H, J, K, and M correspond to the mean +/- 95% CI of three independent experiments.

To determine if the candidates generated by the two CRISPR/Cas9 screens were required for the peptide to exert its toxicity on other cell lines, we tested the inhibitors on several cell types which were also killed by the RasGAP-derived peptide. Supplementary Figure S1C depicts that the KCNN4 inhibitor TRAM-34 can prevent TAT-RasGAP$_{317-326}$-induced cell death in the acute monocytic leukemia THP-1 cell line and the cervix adenocarcinoma HeLa cell line, but not in Raji cells. However, ouabain and digoxin, by inhibiting the Na^+/K^+-ATPase pump, were able to block the toxicity of the peptide in three (Raji, THP-1, and Daudi) out of the four cell lines tested (Supplementary Figure S1D). Of note, Raji, THP-1, and Daudi (Burkitt Lymphoma) cells all belong to the peripheral blood mononuclear cell type, whereas the non-responder NB1 cell line is derived from a neuroblastoma tumour. Finally, the KCNQ inhibitor XE991 was able to reduce the killing efficiency of the peptide in SKW6.4 and Daudi cells, but not in NB1 and HeLa cell lines (Supplementary Figure S1E). To confirm some of these results KCNQ5, ATP1B3, and KCNN4 disrupted clones were generated in NB1, Raji, and HeLa cells, respectively (Supplementary Figures S1F, S1H, and S1H). Supplementary Figures S1G, S1I, and S1K support the conclusion that disruption of KCNQ5 does not protect NB1 cells against TAT-RasGAP$_{317-326}$, whereas in ATP1B3 knockout Raji cells and in KCNN4 knockout HeLa cells the killing efficiency of the peptide is decreased. These results suggest that the involvement of the top candidates in TAT-RasGAP$_{317-326}$-induced cell death is cell type dependent.

Regulators of TAT-RasGAP$_{317-326}$-induced cell death are not involved in the pro-death activity of the peptide

KCNN4, KCNK5, ATP1B3, SLC39A14, KCNQ5 and PIP5K1A can be implicated in the activity of TAT-RasGAP$_{317-326}$ at three different cellular steps, which are the entry of the peptide into the cell either through direct translocation or endocytosis, its endosomal escape (only if it gains access to the cytosol by endocytosis), and the pro-death activity of the peptide once having reached the cytoplasm (Figure 3A).

To determine how these proteins participate in the inhibition of the peptide toxicity, we first assessed whether they were implicated in the pro-death activity of the peptide. To bypass the step of the intracellular delivery of the peptide, we used the counteranion pyrenebutyrate (PB). The latter allows the direct membrane translocation of arginine-rich peptides such as TAT within a few minutes, through an electrostatic interaction between the guanidium groups of arginines and the negative charges of PB [215]. We first compared the kinetics of TAT-RasGAP$_{317-326}$-induced death in the presence or in the absence of PB. Figures 3B and 3C show that in the presence of PB death occurs within ten minutes, while in the absence of the counteranion it takes about 24 hours for the peptide to exert the same killing efficiency. These results reveal that the forced direct translocation of TAT-RasGAP$_{317-326}$ by PB accelerates the capacity of the peptide to kill SKW6.4 and Raji wild-type cells. As shown in Figure 3D, PB leads to the rapid diffuse cytosolic accumulation of FITC-labeled TAT-RasGAP$_{317-326}$ in Raji cells. However, when treated only with fluorescent peptide, the signal consists of punctate endocytic-like structures.

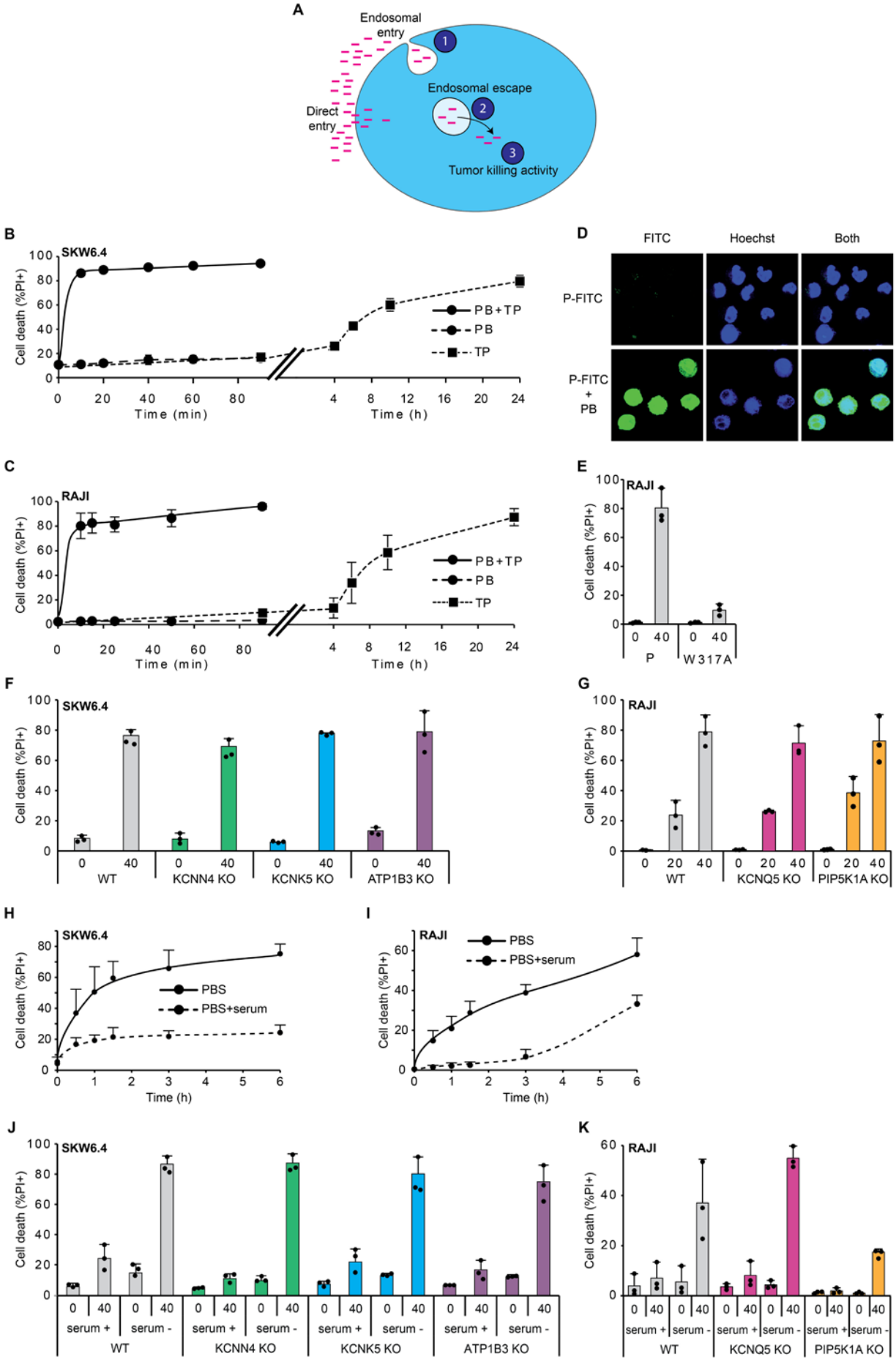

Figure 3. The disrupted cells for regulators of TAT-RasGAP$_{317-326}$-induced cell death are not

anymore protected when the peptide enters through forced direct translocation. A. Scheme depicting the three different cellular steps, on which the regulators of TAT-RasGAP$_{317-326}$-induced cell death can potentially act. They could modulate the entry of the peptide into the cells (step 1), its endosomal escape (step 2), or the pro-death activity of the peptide once having reached the cytoplasm (step 3). **B.** WT SKW6.4 cells were treated with 40 µM TAT-RasGAP$_{317-326}$ (TP) and 50 µM pyrenebutyrate (PB) alone or in combination. Cell death was analyzed by flow cytometry using PI as membrane permeabilization marker. **C.** Same than in panel B in Raji cells. **D.** Confocal images of Raji cells treated with 40 µM TAT-RasGAP$_{317-326}$-FITC (P-FITC) for 30 minutes in the presence or in the absence of 50 µM PB. Of note, in conditions where PB was added, experiments were performed in serum-free medium. **E.** WT Raji cells were treated with 50 µM PB and the indicated concentration of peptide, either TAT-RasGAP$_{317-326}$ or TAT-RasGAP$_{317-326}$ (W317A) for 30 minutes. Cell death was analyzed by flow cytometry using PI. **F.** WT, KCNN4 KO, KCNK5 KO, and ATP1B3 KO SKW6.4 cells were treated or not with 40 µM TAT-RasGAP$_{317-326}$ and 50 µM PB for 30 minutes and cell death was determined using PI. **G.** Same as panel F in WT, KCNQ5 KO, and PIP5K1A KO Raji cells. **H**. WT SKW6.4 cells were treated with 40 µM TAT-RasGAP$_{317-326}$ for indicated periods of time in PBS containing or not 10% serum. Cell death was analyzed by flow cytometry using PI. **I.** Same as H with WT Raji cells. Cell death was analyzed by flow cytometry using PI. **J.** WT, KCNN4 KO, KCNK5 KO, and ATP1B3 KO SKW6.4 cells were incubated in medium containing or not 10% serum and treated for 3 hours with 40 µM TAT-RasGAP$_{317-326}$. Cell death was analyzed by flow cytometry using PI. **K.** Same as J with WT, KCNQ5 KO, and PIP5K1A KO cells treated for 1h30 with 40 µM TAT-RasGAP$_{317-326}$. Results represent 3 independent experiments +/- 95% CI.

Importantly, forced translocation of the inactive point mutant TAT-RasGAP$_{317-326}$ (W317A) with PB did not lead to significant increase of cell death (Figure 3E). We then assessed the effect of TAT-RasGAP$_{317-326}$ direct translocation on the SKW6.4 and Raji knockout cells. Figures 3F and 3G show that in the presence of PB TAT-RasGAP$_{317-326}$-induced death occurs to the same extent in wild-type and KCNN4, KCNK5, ATP1B3 knockout SKW6.4 cells or in wild-type and KCNQ5 and PIP5K1A Raji cells, respectively. Furthermore, Supplementary Figure S2A supports the same conclusion for SLC39A14 knockout clone and wild-type SKW6.4 cells pretreated with TRAM-34, digoxin, or ouabain.

In addition, as a complementary approach, we investigated the toxicity of the RasGAP-derived peptide in serum-free conditions. Indeed, it was reported that serum proteins act on the internalization mechanism of arginine-rich peptides, inducing their cellular uptake preferentially through endocytosis. [216]. On the contrary, serum-free media have been shown to favor the direct translocation process of these peptides [217]. To verify this assertion, HeLa cells were incubated in phosphate-buffered saline (PBS) with or without serum and treated with the FITC-labeled peptide. Supplementary Figure S2B shows that the cytoplasmic accumulation of the fluorescent RasGAP-derived peptide is much more pronounced in cells in serum-free medium compared to the ones in medium supplemented with serum. Of note, the same observation was shown in SKW6.4 cells (Supplementary Figure S2B).
We, therefore, examined the effect of serum in SKW6.4 and Raji cells treated with the peptide. When incubated in PBS without serum, death kinetics in both wild-type SKW6.4 and Raji cells were accelerated compared to the serum-rich conditions (Figures 3H and 3I). Figures 3J and 3K show that in the absence of serum, the KCNN4, KCNK5, and ATP1B3 disrupted clones in SKW6.4 cells and the KCNQ5 and PIP5K1A disrupted clones in Raji cells were efficiently killed within 3 and 1.5 hours, respectively. The same result was depicted in SLC39A14 knockout SKW6.4 cells (Supplementary Figure S2C).

Altogether these results indicate that the regulators of TAT-RasGAP$_{317-326}$-induced cell death are not involved in the pro-death activity of the peptide. Indeed, knockout clones for six different targets can be killed if the route taken by TAT-RasGAP$_{317-326}$ to reach the cytosol is forced translocation.

Nevertheless, our data do not allow us to conclude if these observations are due to an increased amount of peptide reaching the cytoplasm, or a change in the route of entry of the peptide, or both.

Regulators of TAT-RasGAP$_{317-326}$-induced cell death prevent its cytosolic access and that of other TAT-constructs

After having shown that the six validated candidates were not involved in the pro-death activity of TAT-RasGAP$_{317-326}$, we investigated if they were implicated in its cytosolic access. We used the fluorescent FITC-coupled version of TAT-RasGAP$_{317-326}$ to assess the peptide uptake into wild-type and knockout cells. Of note, the FITC-coupled peptide increases cell adhesion and directly kills cells with the same efficiency as the TAT-RasGAP$_{317-326}$ peptide. As illustrated by confocal microscopy images in Figure 4A, in wild-type cells the fluorescent peptide accumulates with time, whereas in KCNQ5 knockout Raji cells, no or only a slight distribution of the FITC-peptide is observed. These results were confirmed by the measurement of the median fluorescence intensity by flow cytometry in wild-type and KCNQ5 knockout Raji cells treated with the fluorescent version of the peptide (Figure 4B).
Moreover, to assess the mode of entry of the peptide, we performed the same experiment at 4°C, the temperature at which active cellular processes such as endocytosis are blocked (Figure 4B). In low temperature, the signal of FITC-TAT-RasGAP$_{317-326}$ was greatly reduced in both wild-type and KCNQ5 knockout Raji cells compared to the conditions at 37°C (Figure 4B). This suggests that the peptide enters cells mainly through endocytosis. To exclude a potential membrane-bound defect of the peptide in KCNQ5 knockout Raji clone that could induce misinterpretation of the results, we assessed the fluorescent intensity at shorter time points (Figure 4C). The increased fluorescence present in both wild-type and knockout cells after 1 minute of incubation with the labeled peptide suggests indirectly that the capacity of the peptide to bind to plasma membrane is not affected in knockout cells. Observations made in Raji cells were partially supported in wild-type and knockout SKW6.4 cells. Indeed, the inhibition of the FITC-peptide intracellular delivery was less pronounced at 37°C in the KCNN4, KCNK5, and ATP1B3 knockout SKW6.4 cells than in KCNQ5 knockout Raji cells (Figure 4G). Finally, the confocal microscopy images of HeLa wild-type cells pretreated or not with TRAM-34 and HeLa KCNN4 knockout cells show that at 4°C the peptide is blocked at the membrane (Supplementary Figure 3A). Though, at 37°C, the intracellular accumulation of the peptide with time is diminished and delayed in KCNN4 knockout and TRAM-34 pretreated cells compared to wild-type HeLa cells. In addition, the plasma membrane is partially delimited by the fluorescent peptide after one hour of incubation in the knockout and pretreated cells, but not in the wild-type cells (Supplementary Figure 3A). This observation suggests that some of the peptide accumulates at the membrane and its entry is partially prevented when the KCNN4 potassium channel is non-functional.
Thus far, data indicate that the FITC-TAT-RasGAP$_{317-326}$ peptide mainly enters through endocytosis. However, the slight increase in the median fluorescence intensity in Raji and SKW6.4 cells at 4°C suggests that the labeled peptide can marginally translocates directly into cells (Figures 4B and 4G).

Consequently, we cannot formally rule out the possibility that both direct translocation and endocytosis happen simultaneously at 37°C.

As the uptake of TAT-RasGAP$_{317-326}$ was affected in the knockout cells, we next assessed if the candidates could also be involved in the intracellular delivery of other TAT-constructs such as TAT-PNA and TAT-Cre (Supplementary Figures S4A and S4B).

For the former construct, wild-type and knockout SKW6.4 and Raji cells were infected with a virus encoding for a luciferase gene disrupted by the mutated β-globin intron 2. These cells produce a mRNA that encodes a truncated non-functional luciferase. However, the luciferase pre-mRNA can be properly processed if the splice site generated by the mutation at position 705 is masked by a matching oligonucleotide (ON-705) (Supplementary Figure S4A). ON-705 was covalently coupled to the cell-permeable peptide TAT. The resulting so-called TAT-peptide nucleic acid (TAT-PNA), when incubated with cells, triggers the correct splicing of the mutated luciferase pre-RNA but only if the PNA is gaining access to the cytosol [204, 218]. Figure 4D shows that in Raji KCNQ5 and PIP5K1A knockout cells, the fold induction of luciferase is decreased compared to wild-type Raji cells. This result was confirmed in Raji wild-type cells treated with XE991 (Figure 4E). However, as expected, there was no reduction of the luciferase activity in Raji wild-type cells treated with the KCNN4 inhibitor TRAM-34 (Figure 4E). Moreover, the luciferase activity was restored with TAT-PNA in wild-type SKW6.4 cells, whereas in KCNN4 as well as in SKW6.4 wild-type cells treated with TRAM-34 the activity of the luciferase was not fully restored (Figures 4H and 4I). In contrast to KCNN4, the disruption of KCNK5 and ATP1B3 as well as the chemical inhibition of KCNQ5 in SKW6.4 did not significantly decrease the fold induction of luciferase compared to wild-type cells. Finally, we observed in wild-type HeLa cells pretreated with the KCNN4 inhibitor a decrease of the luciferase activity compared to the non-treated wild-type HeLa cells (Supplementary Figure S4C). These results indicate that the absence of KCNQ5 and KCNN4 prevent at least partially the cytosolic access of the TAT-PNA construct, whereas the disruption of the other candidates do not affect significantly the intracellular delivery of the TAT-construct.

To investigate the delivery into cells of the TAT-Cre construct, we used a second assay based on the TAT-Cre-mediated recombination of a loxP-RFP-STOP-loxP-GFP construct (Supplementary Figure S4B) [188, 208]. Cells stably infected with the loxP-RFP-STOP-loxP-GFP construct express the red fluorescence protein. When exogenous TAT-Cre recombinase enters cells and translocates to the nucleus, RFP-STOP is excised and GFP expression is initiated. The switch from red to green fluorescence consequently attests for cytosolic access of TAT-Cre recombinase. Accordingly, the lentiviral loxP-RFP-STOP-loxP-GFP construct was stably introduced into wild-type, KCNQ5, and PIP5K1A knockout Raji cells. These cells were then left untreated or treated with TAT-Cre recombinase. As expected, the absence of TAT-Cre did not induce GFP production (Figure 4F). After 48 hours of treatment, many GFP-positive cells were visible in wild-type Raji cells, while only one or two GFP-positive cells were observed in the knockout Raji clones (Figure 4F). These preliminary data suggest that KCNQ5 and PIP5K1A are required for efficient cytosolic access of TAT-Cre recombinase in Raji cells.

Taken together, the above experiments indicate that regulators of TAT-RasGAP$_{317-326}$-induced death play a role in the regulation of the cytosolic access of the RasGAP-derived peptide but also of other TAT-constructs of different sizes, ranging from 3.3 kDa to ~40 kDa.

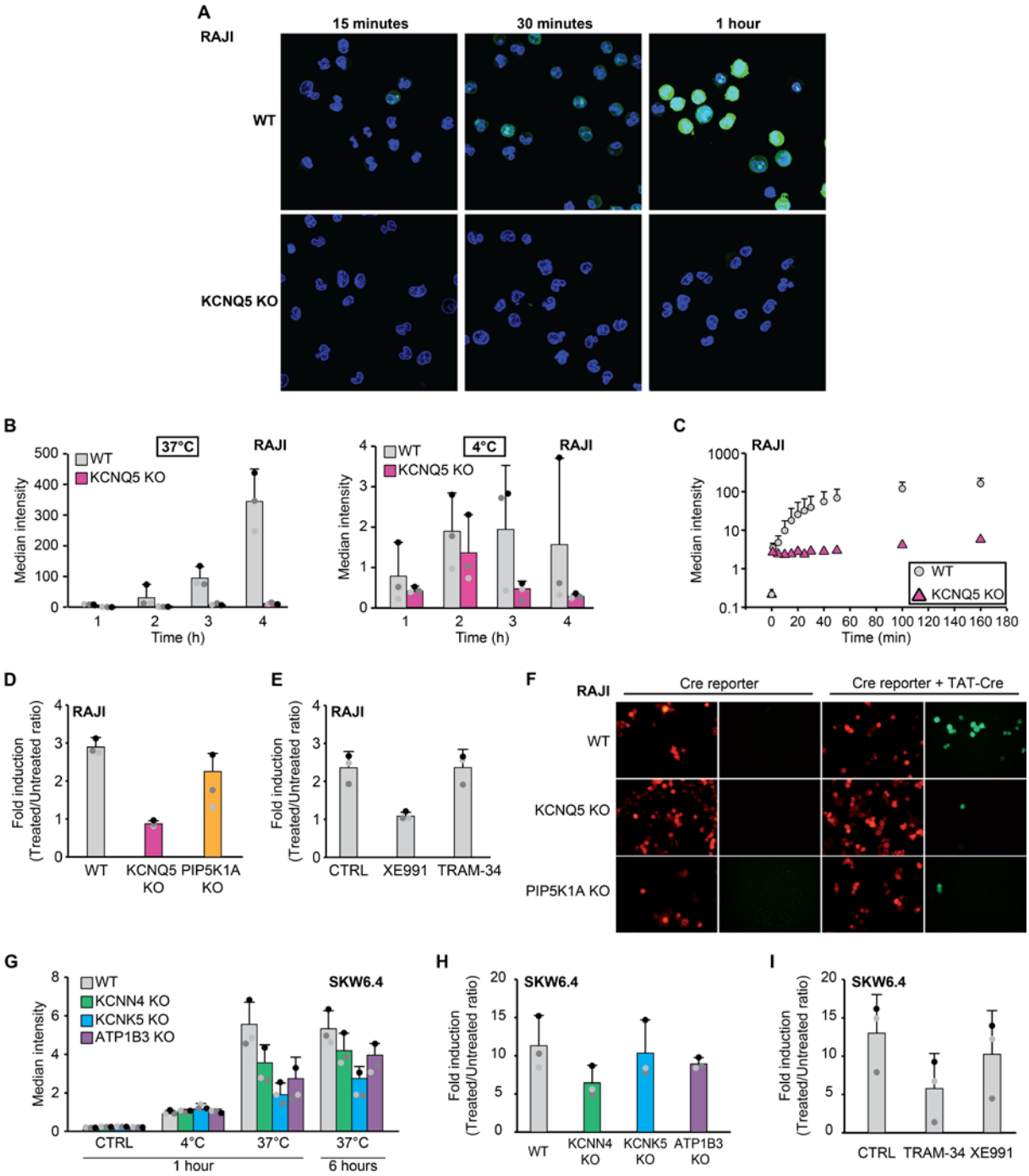

Figure 4. Regulators of TAT-RasGAP$_{317-326}$ toxicity prevent its cytosolic access and that of other TAT-constructs. **A.** Confocal microscopy images of WT and KCNQ5 KO Raji cells treated for indicated periods of time with 40 µM FITC-coupled TAT-RasGAP$_{317-328}$ (green) at 37°C. The nucleus is stained with live Hoechst 33342 1 µg/ml for 15 minutes (blue). **B.** WT and KCNQ5 KO Raji cells were treated with 40 µM TAT-RasGAP$_{317-326}$-FITC for indicated periods of time at 37°C (left panel) or 4°C (right panel). Cells were then collected and washed three times with cold phosphate-buffered saline (PBS). The median fluorescence intensity

of viable cells was then measured by flow cytometry. **C.** WT and KCNQ5 KO Raji cells were treated with 40 µM TAT-RasGAP$_{317-326}$-FITC for indicated periods of time at 37°C and then washed once with ice-cold PBS. Cells were then analyzed by flow cytometry. **D.** Cytosolic access was assessed using a luciferase rescue reporter assay [204]. WT, KCNQ5 KO, and PIP5K1A KO Raji cells were infected with a virus encoding for the luciferase-coding sequence, interrupted by a mutated human β-globin intron and treated with 10 µM TAT-ON-705, a TAT-peptide nucleic acid (TAT-PNA). After 24 hours, luciferase activity was measured and normalized to the protein content. **E.** WT Raji cells were pretreated or not with 10 µM XE991 or 10 µM TRAM-34 for 1 hour and treated for 24 hours with TAT-PNA. The cells were then processed as in panel D.**F.** WT, KCNQ5 KO and PIP5K1A KO Raji cells stably expressing loxP-RFP-STOP-loxP-GFP construct were treated or not with TAT-Cre for 48 hours. Fluorescence was observed on microscope. **G.** WT, KCNN4 KO, KCNK5 KO, and ATP1B3 KO SKW6.4 cells were treated with 40 µM TAT-RasGAP$_{317-326}$-FITC for indicated periods of time at 4°C or 37°C. Cells were then processed as for panel B. **H.** WT, KCNN4 KO, KCNK5 KO, and ATP1B3 KO SKW6.4 cells expressing the mutated luciferase mRNA were treated with 10 µM TAT-PNA and analyzed as in panel D. **I.** Same as panel E with SKW6.4 cells. Results for panels B, C, D, E, G, H and I correspond to the mean +/- 95% CI of 3 independent experiments.

The plasma membrane depolarization induced by the disruption of the KCNQ5 potassium channel in Raji cells hampers the cytosolic access of TAT-RasGAP$_{317-326}$

To better understand the mechanisms by which the proteins revealed by CRISPR/Cas9 screens hamper the intracellular delivery of TAT-constructs, we investigated the effect of plasma membrane potential and intracellular potassium [K+]i modulations. Indeed, the candidate proteins mainly regulate the potassium flux either because they are potassium channels (KCNN4, KCNK5, and KCNQ5) or a subunit of the Na^+/K^+-ATPase pump (ATP1B3). Potassium plays a predominant role in the establishement of the resting cell membrane potential. Indeed, Rothbard and colleagues proposed a membrane potential-driven direct plasma membrane penetration hypothesis, whereas the rate of passage of molecules through the bilayer is directed by the membrane potential [219]. Moreover, another study showed that endocytosis depends on the membrane resting potential through a potential-dependent reorganization of actin [220]. Consequently, to disrupt the plasma membrane polarization, we incubated the SKW6.4 and Raji wild-type cells in a K^+-rich buffer and investigated whether TAT-RasGAP$_{317-326}$ was still able to kill cells. Figure 5A indicates that in Raji cells, but not in SKW6.4 cells, the disruption of the bilayer potential prevents the peptide toxicity. As a complementary approach to explore whether the candidate proteins were involved in the regulation of the membrane resting potential, we used the DiBAC4(3) potential-sensitive probe, where increased depolarization results in an increase in fluorescence. Although the gold standard to measure membrane potential is electrophysiology, this probe was shown to obtain similar values [221, 222]. We used the K^+/Na^+ ionophore gramicidin as a positive control for cell depolarization [223]. Figure 5B shows that KCNQ5 knockout Raji cells are more depolarized than wild-type cells. In addition, in the presence of the KCNQ family inhibitor XE991, wild-type cells are also depolarized. However, no significant changes in the plasma membrane potential of KCNN4, KCNK5, and ATP1B3 knockout SKW6.4 cells were observed compared to wild-type cells, although gramicidin was greatly able to depolarize those cells (Figure 5C). In order to study if the increase membrane potential of KCNQ5 knockout cells was correlated with an increase of $[K^+]i$ due to a decrease of K^+ export in disrupted cells, we employed the K^+-sensitive probe Asante Potassium Green 2 (APG-2). Figures 5D and 5E report that there is no significant variation of the $[K^+]i$ in KCNQ5 knockout or Raji wild-type cells treated with XE991 compared to non-treated wild-type cells. The same observation was made in KCNN4 knockout or SKW6.4 wild-type

cells treated with TRAM-34 (Figure 5F). As a positive control for the APG2 probe, we observed a slight decrease of the $[K^+]i$ in wild-type SKW6.4 treated with gramicidin, which is known to allow the efflux of K^+ out of the cells. Finally, to investigate a putative link between the plasma membrane potential and the peptide uptake, we assessed FITC-TAT-RasGAP$_{317-326}$ accumulation in cell depolarized with K^+-rich buffer or gramicidin. Figure 5G indicates that the Raji wild-type cells depolarization, due to both K^+-rich buffer and gramicidin, hampers the cytosolic access of TAT-RasGAP$_{317-326}$ independently of the $[K^+]i$. These results suggest that the disruption of KCNQ5 induces a depolarization of the membrane potential responsible for the inhibition of the peptide entry into the cells. However, the KCNN4, KCNK5 and ATP1B3 SKW6.4 disrupted cells did not prevent TAT-RasGAP$_{317-326}$-induced cell death through the modulation of the membrane resting potential. Accordingly, the mechanism by which those knockout cells are protected remains to be resolved.

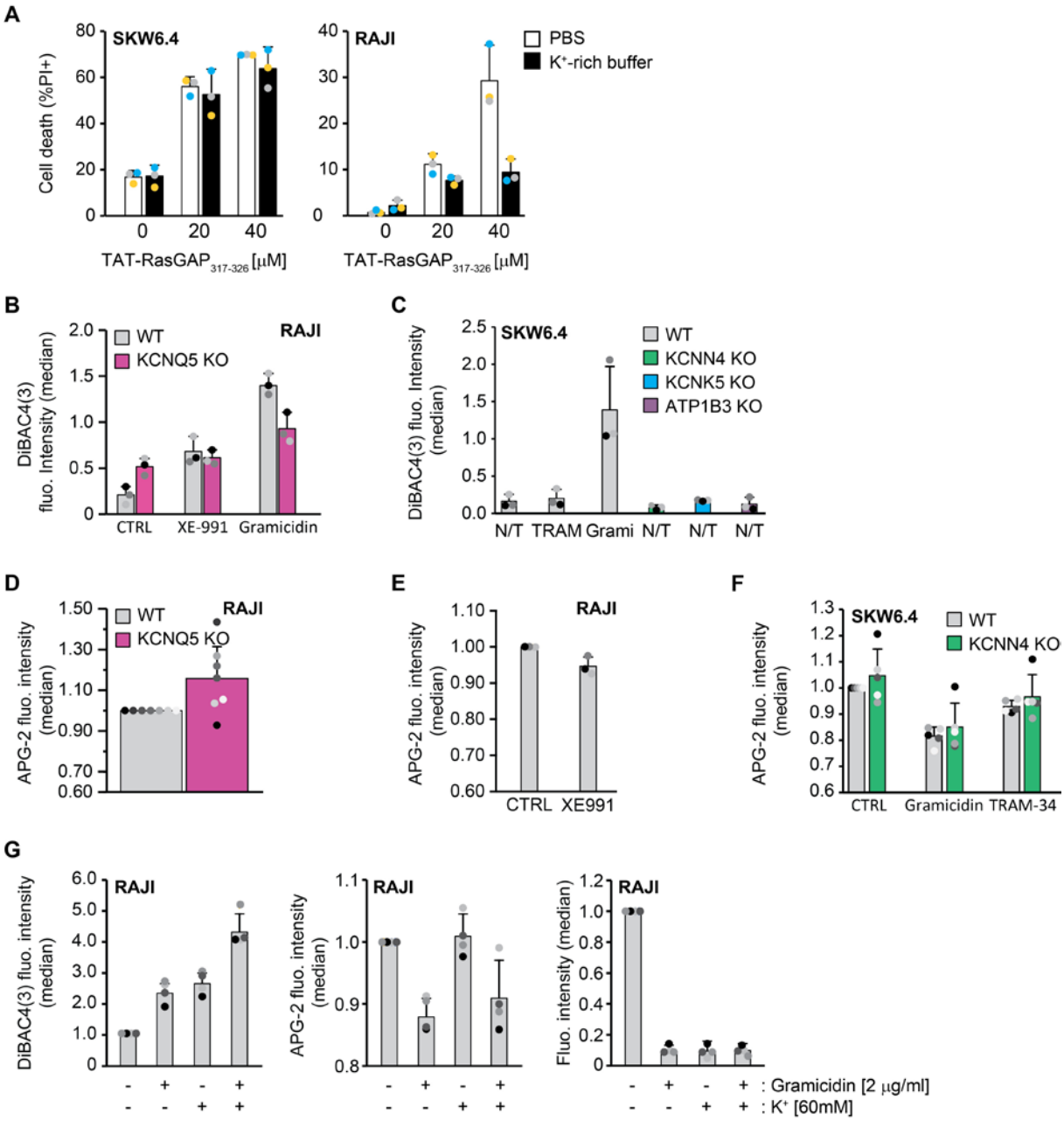

Figure 5. The disruption of KCNQ5, but not KCNN4, induces the depolarization of the plasma membrane preventing the cytosolic access of the TAT-RasGAP$_{317-326}$ peptide. **A.** To affect the resting potential of the plasma membrane, SKW6.4 WT and Raji WT cells were incubated in PBS or K^+-rich buffer before being treated with 0, 20, or 40 µM TAT-RasGAP$_{317-326}$ during 1h30. Cell death was then assessed by flow cytometry using PI as cell membrane permeabilization marker. **B.** Plasma membrane potential (V_m) in Raji WT and KCNQ5 KO cells that were pretreated or not with 10 µM XE991 or 2 µg/ml gramicidin for 30 or 5 minutes, respectively. The V_m was determined by incubating the cells with 100 nM fluorescent probe DiBAC4(3) for 40 minutes and median fluorescence intensity was directly assessed by flow cytometry. **C.** Same than in panel B, but in WT, KCNN4, KCNK5, and ATP1B3 SKW6.4 cells and WT cells were pretreated with 10 µM TRAM-34 (TRAM) instead of XE991. **D.** For the intracellular potassium concentration $[K^+]i$ in Raji WT and KCNQ5 KO cells, they were incubated with 1 µM K^+-sensitive probe Asante Potassium Green 2 (APG-2) for 30 minutes, followed by flow cytometry analysis. **E.** Same than in panel D, but in Raji WT cells that were pretreated for 30 minutes with 10 µM XE991. **F.** Same than in panels D and E but in WT and KCNN4 KO SKW6.4 cells treated or not with 10 µM TRAM-34. **G.** Cells incubated in K^+-rich buffer and/or treated with 2 µg/ml gramicidin were pre-incubated during 30 or 5 minutes, respectively, before the addition of the fluorescent probes. To monitor V_m, $[K^+]i$ and peptide uptake, cells were incubated with 100nM DiBAC4(3) for 40 minutes, 1 µM APG-2 for 30 minutes and 40 µM TAT-RasGAP$_{317-326}$-FITC for 1 hour, respectively. Fluorescence intensity was then assessed by flow cytometry, directly for DiBAC4(3) or APG2 and after one washing step with cold-PBS for peptide uptake. Results represent at least 3 independent experiments +/- 95% CI.

Disruption of KCNN4 hampers the cytosolic access of several arenaviruses

After having shown that regulators of TAT-RasGAP$_{317-326}$-induced death mediate the intracellular delivery of different TAT-constructs, we hypothesized that they might also be functionally required for proper internalization of other cargos, such as viruses. Indeed, many pathogens hijack the existing endocytic routes to mediate their internalization into the cytoplasmic compartment, thus maintaining their survival and activity [194, 195].

Here, we used the well-characterized human lung carcinoma alveolar epithelial A549 cell line that shares key characteristics with human epithelia and has been used extensively to study viral entry. We employed a safe pseudotyped vesicular stomatitis virus (VSV) system bearing the envelope glycoproteins (GPs) of viruses of interest. Such viral particles possess the tropism of the virus from which the GP was derived. We selected VSV and several arenaviruses, originating from both Old World (Eastern Hemisphere, e.g. Lassa, lymphocytic choriomeningitis virus (LCMV), and Lujo viruses) and New World (Western Hemisphere, e.g. Junin, Guanarito, Tacaribe, and Amapari viruses), because they gain access to the cytosol through different endocytic pathways (Supplementary Figures 5A and 5B). VSV associates to the low-density lipoprotein receptor (LDLR), as its principal receptor to enter cells via clathrin-mediated endocytosis (CME), and escapes from early endosomes at pH 6.2 to reach the cytoplasm (Supplementary Figure 5B) [224-226]. The New World arenaviruses utilize human transferrin receptor-1 (hTfR1) (Junin and Guanarito) or animal orthologs of TfR1 (Amapari and Tacaribe) to enter cells via CME and then exit late endosome at pH≈5.5 (Supplementary Figure 5B) [227-229]. The Old World LCMV and Lassa viruses use the cellular receptor α-dystroglycan (DG) to infect cells via a macropinocytosis-related pathway [230-232]. The latter belong both to acid-activated viruses, escaping late endosomes by acid-induced membrane fusion (pH <5). However, they are transported to intermediate multivesicular bodies (MVBs) by an unidentified organelle, which is not early endosomes as demonstrated by the persistence of infection in cells lacking the early endosome markers Rab5 and EEA1 (Supplementary Figure 4B) [231, 233]. Of note, Lassa virus has to engage the late endosomal resident protein LAMP-1 for efficient fusion, which is not the case for LCMV [234].

Finally, mechanisms of entry, including the receptor, have still not been highlighted for the newly identified Old World arenavirus Lujo, although Tani and colleagues demonstrated that TfR1 and DG were not involved [235]. Consequently, because those viruses use different endocytic routes to enter cells, they are valuable tools for characterizing at which step potassium channels regulate the cytoplasmic access.

To study the entry of the selected viruses in the presence of KCNN4 and KCNQ5 inhibitors, the viral genome employed encodes luciferase gene, and successful internalization into the cytosol of the host cell can be determined by luciferase activity measurement. Figure 6A shows that in A549 cells, the KCNN4 inhibitor TRAM-34 prevented entry of LCMV, Junin, Lujo, Guanarito, Tacaribe, and Amapari viruses in a dose-dependent manner. However, infections by VSV and Lassa viruses were not blocked by TRAM-34. These results suggest that KCNN4 could inhibit transferrin-mediated clathrin endocytosis, prevent LAMP-1-independent late endosomal escape, or both. Finally, we cannot rule out the possibility that TRAM-34 exerts a virucidal activity. Unlike TRAM-34, inhibition of KCNQ5 with XE991 in A549 did not protect significantly cells against tested virus infections (VSV, Lassa, LCMV, Junin, and Guanarito) (Figure 6B).

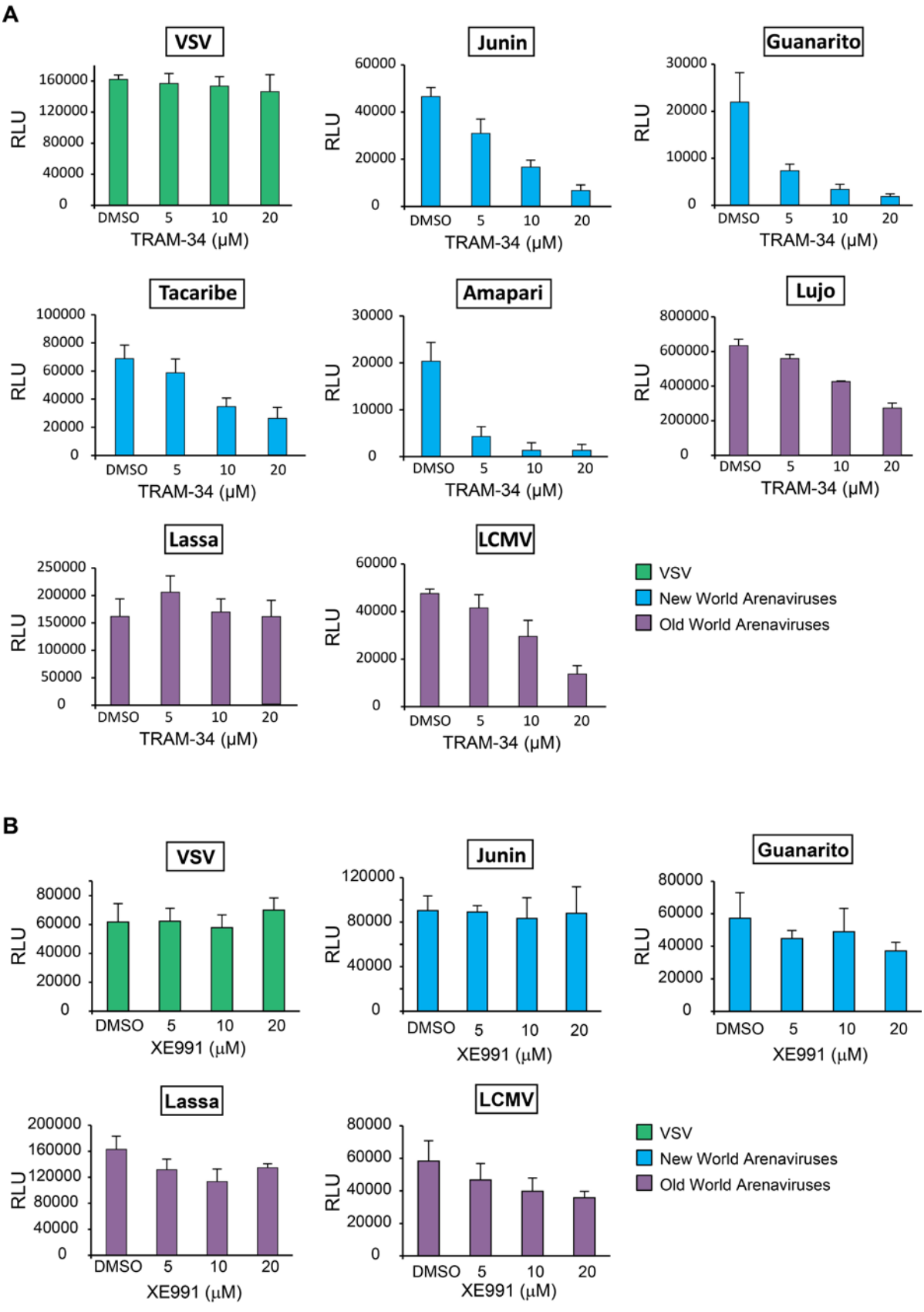

Figure 6. Inhibition of KCNN4 but not KCNQ5 prevents cytosolic access of certain viruses in A549 cells. **A.** A549 cells were pretreated for 1 hour with indicated concentration of TRAM-34 and infected with the mentioned pseudotyped virus containing a luciferase reporter in their genome. Luciferase activity was measured 16 hours post-infection. **B.** Same as in A with X991. Results represent 3 technical triplicate experiments +/- 95% CI.

DISCUSSION

In order to unravel the mechanism of action of the TAT-RasGAP$_{317-326}$ anti-cancer peptide, we performed genome-wide CRISPR/Cas9 screens in two distinct cell lines. The identified mediators of TAT-RasGAP$_{317-326}$-induced cell death in the SKW6.4 B-lymphoblastoid EBV-transformed cells are mainly involved in the regulation of potassium flux, as illustrated by the two potassium channels KCNN4, KCNK5 and the subunit of the Na^+/K^+-ATPase pump ATP1B3. In addition, we validated one more candidate in these cells, which is a divalent metal transporter SLC39A14 for which no association with potassium has yet been reported. The screen in the Raji Burkitt lymphoma cells identified another potassium channel named KCNQ5 and the PIP5K1A lipid kinase. As PIP5K1A generates the membrane lipid phosphatidylinositol 4,5-bisphosphate (PI(4,5)P2), which is required for KCNQ family channels opening, the two proteins revealed by screening Raji cells are probably both involved in the modulation of potassium flux [236, 237]. Furthermore, we show that the inhibition of KCNN4, KCNQ5, and ATP1B3 can prevent cell death induced by the peptide in other cell lines (Daudi, THP-1, NB1, and HeLa), meaning that the effect of these candidates can be transferred to cells from diverse origins. Nevertheless, although almost all the tested cell lines were protected by at least one of the three candidates, no relation can be deduced between the origin of cells and the protein able to rescue them from the peptide toxicity. This could be explained by cell line-dependent differences in the level of expression or in the activity of each candidate. Of note, the only refractory cell line to the protective effect of the validated targets is the neuroblastoma NB1 cells, which are cultured in the absence of serum. As shown in this study, in serum-free conditions the protection of knockout clones against the killing activity of the peptide is lost.

However, instead of being implicated in the death induction process *per se* as expected, we demonstrated that regulators of potassium flux are involved in the cytosolic access of TAT-RasGAP$_{317-326}$ and two other TAT-constructs, TAT-Cre and TAT-PNA. Indeed, when we force the entry of the peptide via direct translocation using PB or serum deprivation, cells lacking the validated targets are not anymore protected against the toxicity of the anti-cancer peptide. Thenceforth, the candidates can prevent the intracytoplasmic delivery of the TAT-constructs at two different levels, either they inhibit direct translocation and/or endocytosis or they hamper endosomal escape. The latter possibility can occur only if TAT-constructs gain access to the cytosol by an active vesicular uptake. Although endocytosis has been proposed as the general mode of entry of CPP constructs into cells, several studies show that TAT CPP can gain access to the cytoplasm by vesicular uptake, direct translocation, or both simultaneously depending mainly on the size, the biochemical nature of the cargo, and on the concentration used [188-190, 238, 239]. Our results indicate that TAT-RasGAP$_{317-326}$ penetrates the cell via both endocytosis and direct translocation. Indeed, confocal microscopy detects early diffuse distribution (after less than 5 minutes) followed by the accumulation of the fluorescent peptide in small vesicles. In addition, although there is a decrease of peptide uptake at 4°C, temperature at which endocytosis is blocked, the fluorescence does not go back to the basal intensity, meaning that a low amount of the peptide translocates directly into cells. Of note, although still occurring, it is well-established that the direct translocation is lowered at low temperatures due to decreases in cell

membrane dynamics and fluidity [240]. Another possibility to explain the slight increase in the fluorescence intensity at 4°C could be that the FITC-coupled peptide remains attached to the plasma membrane despite several washes. To exclude this hypothesis, trypan blue can be used to quench membrane-bound fluorescence instead of washes. Trypan blue is a non-permeant dye that was shown to quench the green fluorescence of membrane bound particles [241].

In contrast, TAT-Cre recombinase internalization was reported to occur purely by endocytosis via macropinocytosis [188, 242]. Although we cannot rule out that the targets revealed by the screens mediate the direct translocation of the peptide, we can argue that the KCNQ5 potassium channel and its regulator PIP5K1A block either endocytosis or endosomal escape as the disrupted clones for these genes hamper the cytosolic access of TAT-Cre. To better decipher the involvement of each candidate in the cytosolic access of some cargoes, the requirement of the candidates for different endocytosis pathways will have to be investigated. To this purpose, we could use fluorescent probe, such as dextran (70kDa) and transferrin, which have been shown to be internalized specifically via macropinocytosis and clathrin-mediated endocytosis, respectively [243-245].

Interestingly, the size of TAT-constructs studied here, ranging from 3.3 kDa to ~40kDa, does not affect the capacity of the candidates (at least KCNQ5 and PIP5K1A) to modulate their intracellular delivery. Though, it is well-described that the mechanism of entry depends on the size of the molecule fused to TAT, with smaller cargoes distributing throughout the cell and the bigger ones ending up in cytoplasmic vesicles [242].

The candidates highlighted in the screen performed on SKW6.4 prevent the cytosolic access of TAT-constructs to a lesser extent than KCNQ5 and PIP5K1A. Hypotheses to explain those results could be that they do not act at the same level, to the same efficiency, or depending on the cell line the mode of entry used by TAT-constructs can vary. Indeed, the composition of the plasma membrane, which differs from a cell line to another, affects the efficiency of cytosolic access [246]. Finally, although literature reports that the identified regulators are mainly sited in the plasma membrane, defining their exact location might shed light on the specific step of the cytosolic access where they act [247-250].

In order to better understand how the regulators of potassium flux modulate the cytosolic access of TAT, we show that the disruption of potassium channel KCNQ5 hampers the cytosolic access of the anti-cancer peptide via cytoplasmic membrane depolarization. The effect of the membrane potential on molecule internalization by endocytosis or direct translocation was already previously reported by incubating the cells with potassium-rich buffer [219, 251]. Strikingly, in Raji wild-type cells, incubation with potassium-rich buffer inducing depolarization of the bilayer membrane does not go with an increased intracellular potassium concentration. However, these results should be interpreted with caution due to the suboptimal specificity of the APG2 probe for potassium. Furthermore, electrophysiology would be required to confirm results obtained with the DiBAC4(3) potential-sensitive probe.

Interestingly, KCNN4, KCNK5, and ATP1B3 do not prevent the intracellular delivery of TAT-$RasGAP_{317-326}$ through the regulation of the membrane resting potential. Ben-Dov et al. demonstrated that intracellular uptake depends on the membrane resting potential through a potential-dependent

reorganization of actin [220]. Consequently, one can hypothesize that KCNN4, KCNK5, and ATP1B3 regulate cytosolic access by preventing actin depolymerization via another mechanism than depolarization of the plasma membrane. Indeed, it was reported that Ca^{2+}-sensitive K^+ channels, such as KCNN4, and the Na^+/K^+-ATPase pump modulate actin cytoskeleton [252, 253]. If the potassium flux regulators act on the actin cytoskeleton, it would suggest that their absence prevents endocytosis rather than endosomal escape. This assumption is supported by the stronger membrane association of the FITC peptide in HeLa cells treated with TRAM-34 or in KCNN4 knockout HeLa cells than in HeLa wild-type cells.

Finally, as a potential clinical relevance, we demonstrate that the KCNN4 inhibitor TRAM-34 blocks the cytosolic access of some arenaviruses. Among them Junin, Guanarito, and Lujo viruses are responsible for clinical disease associated with fever and bleeding referred to as viral hemorrhagic fevers (VHFs) [254]. VHFs have significant clinical and public health impact with high case mortality rate (10-30%) and only limited therapies and vaccines [255-257]. In the light of the results obtained with several viruses and because they use different endocytic routes, we can postulate that either the inhibition of KCNN4 potassium channel hamper transferrin-mediated clathrin endocytosis or modulate shared downstream processes of the endocytic pathway, including endosome maturation (i.e. acidification) or endosomal escape. It is nevertheless unlikely that TRAM-34 affects acidification of endosomes since Lassa virus infection, which exits from late endosome (pH≈5.5), was not hampered by the KCNN4 inhibitor [258]. It is, therefore, possible that TRAM-34 prevents the cytosolic access of viruses by blocking LAMP-1-independent late endosomal escape. Of note, it has been reported that some viruses can utilize several endocytic pathways to reach the cytosol, making the analysis of these data more complex [259]. However, one hypothesis that we cannot dismiss yet is the potential virucidal activity of TRAM-34. The KCNN4 inhibitor could indeed inactivate viral particles outside the cell. Furthermore, it has been reported that TRAM-34 can block the activity of other proteins such as cytochrome P450 [260]. Consequently, to exclude possible off-target effects, results should be confirmed in A549 KCNN4 knockout cells. In addition, these preliminary data obtained with pseudotyped viruses have to be confirmed with authentic viruses. Finally, the absence of protection against viral infection in cells treated with the KCNQ5 inhibitor XE991 suggests that either the expression of this potassium channel is not predominant in A549 cells or the activity of KCNQ5 is not required to regulate viral infections.

To conclude, we demonstrated that regulators of potassium flux play a key role in the cytosolic access of some TAT-constructs and arenaviruses. Although we show that the regulation of intracellular entry by KCNQ5 potassium channel is dependent on the plasma membrane potential, how the other candidates work remains still to be unravelled. Consequently, further experiments need to be performed in order to decipher at which steps the different validated targets act.

SUPPLEMENTARY TABLE AND FIGURES

	Metrics	Library control	Library P selected
SKW6.4	Reads number	4513118	4222777
	Targeted genes	20335	17203
	Targeted genes with >50 normalized counts	9427	706
	Targeted genes with >100 normalized counts	704	256
	Targeted sgRNAs	101852	34893
	Targeted sgRNAs with >50 normalized counts	453	618
	Targeted sgRNAs with >100 normalized counts	7	232
Raji	Reads number	4364742	4414584
	Targeted genes	20416	20330
	Targeted genes with >50 normalized counts	9866	6733
	Targeted genes with >100 normalized counts	267	1850
	Targeted sgRNAs	110962	99479
	Targeted sgRNAs with >50 normalized counts	102	2939
	Targeted sgRNAs with >100 normalized counts	1	890

Supplementary Table S1. Counts summary metrics of the CRISPR/Cas9 screens in SKW6.4 and Raji cells. SKW6.4 and Raji GeCKO library control populations and SKW6.4 and Raji GeCKO library TAT-RasGAP$_{317-326}$ (P) selected populations were sequenced with a MiSeq (Illumina). Raw FASTQ files were demultiplexed and processed to contain only the unique sgRNA sequence. The total number of reads, the number of reads for each sgRNA, and the number of reads per targeted genes are shown in this table.

Supplementary Figure S1. The involvement of candidate proteins in TAT-RasGAP$_{317-326}$-induced cell death is tumour type dependent. **A.** DNA sequences of WT SLC39A14 gene in SKW6.4 cells and SLC39A14 alleles of corresponding knockout clone #1. Differences between WT and the disrupted clone are in blue. The sgRNA directed against the gene is highlighted in grey. **B.** WT and SLC39A14 disrupted SKW6.4 cells were treated or not with 40 µM TAT-RasGAP$_{317-326}$ for 24 hours. Cell death was then assessed by flow cytometry after PI staining. **C.** Raji, THP-1, and HeLa WT cells were pretreated or not with 1 µM or 10 µM TRAM-34 for 1 hour and then treated with the indicated concentration of TAT-RasGAP$_{317-326}$ (P) for 16 (Raji) or 24 (THP-1/HeLa) hours. Cell death was assessed by flow cytometry after PI staining. **D.** Raji, THP-1, Daudi, and NB1 WT cells were preincubated with 100 nM digoxin or 100 nM ouabain for 1 hour and then treated with 40 µM TAT-RasGAP$_{317-326}$ for 16 (Raji) or 24 hours. Cell death was assessed by flow cytometry after PI staining. **E.** SKW6.4, HeLa, Daudi, and NB1 WT cells were preincubated with 10 µM XE991 for 1 hour and then treated with 40 or 80 (HeLa) µM TAT-RasGAP$_{317-326}$ for 24 hours. Cell death was assessed by flow cytometry after PI staining. **F.** Same as Panel A for KCNQ5 gene in NB1 cells. **G.** WT and KCNQ5 disrupted NB1 cells were treated or not with 40 µM TAT-RasGAP$_{317-326}$ for 24 hours. Cell death was then assessed by flow cytometry after PI staining. **H.** Expression of ATP1B3 in WT and knockout Raji cells. **I.** WT and ATP1B3 disrupted Raji cells were treated or not with 40 µM TAT-RasGAP$_{317-326}$ for 16 hours. Cell death was then assessed by flow cytometry after PI staining. **J.** Same as Panel A for KCNN4 gene in HeLa cell. **K.** WT and KCNN4 disrupted HeLa cells were treated or not with 80 µM TAT-RasGAP$_{317-326}$ for 24 hours. Cell death was then assessed by flow cytometry after PI staining. Results for panels B, C, D, E, G, I, and K correspond to the mean +/- 95% CI of three independent experiments.

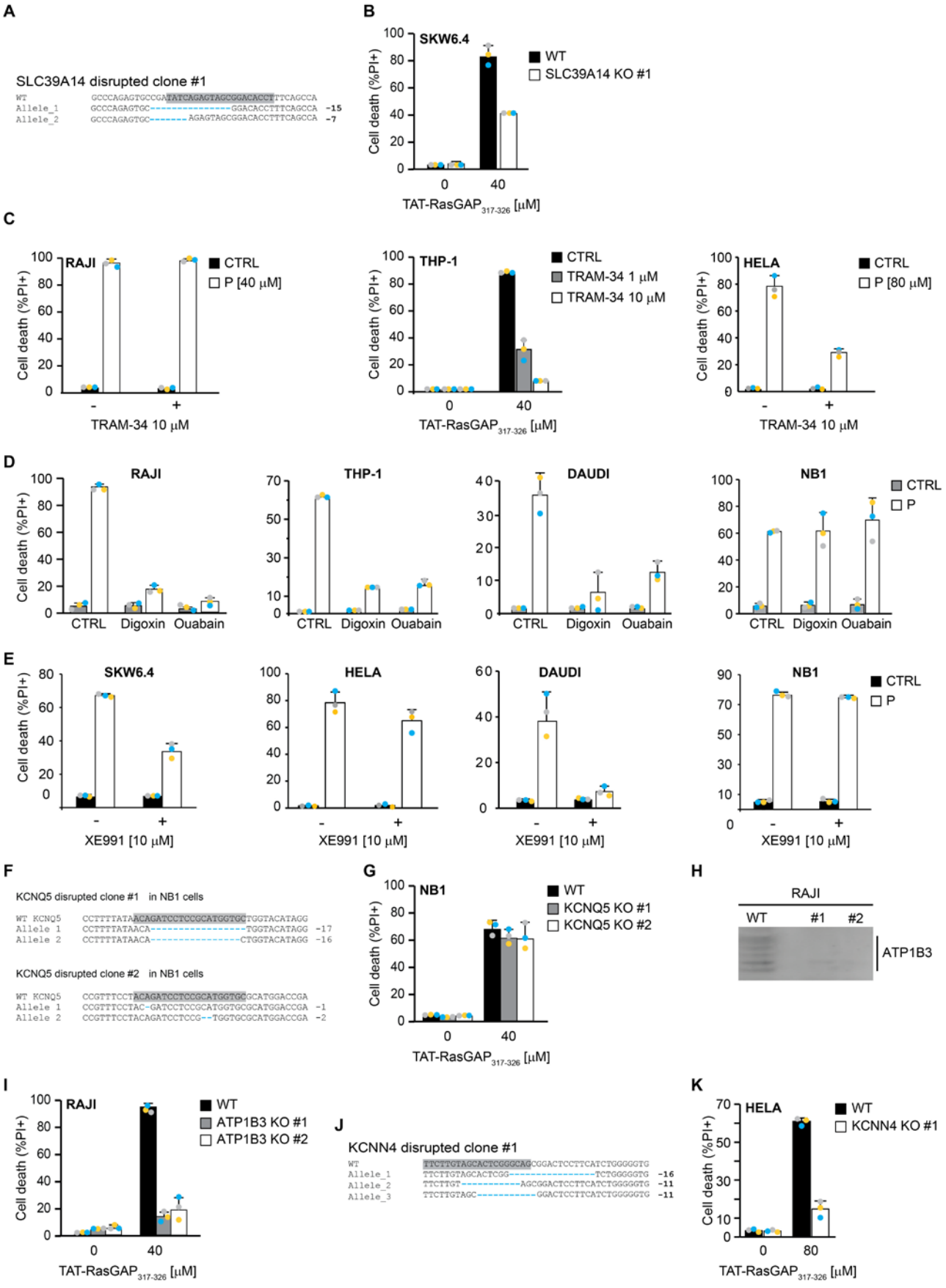

Supplementary Figure S1. The involvement of candidate proteins in TAT-RasGAP$_{317-326}$-induced cell death is tumour type dependent. (see legend on the previous page)

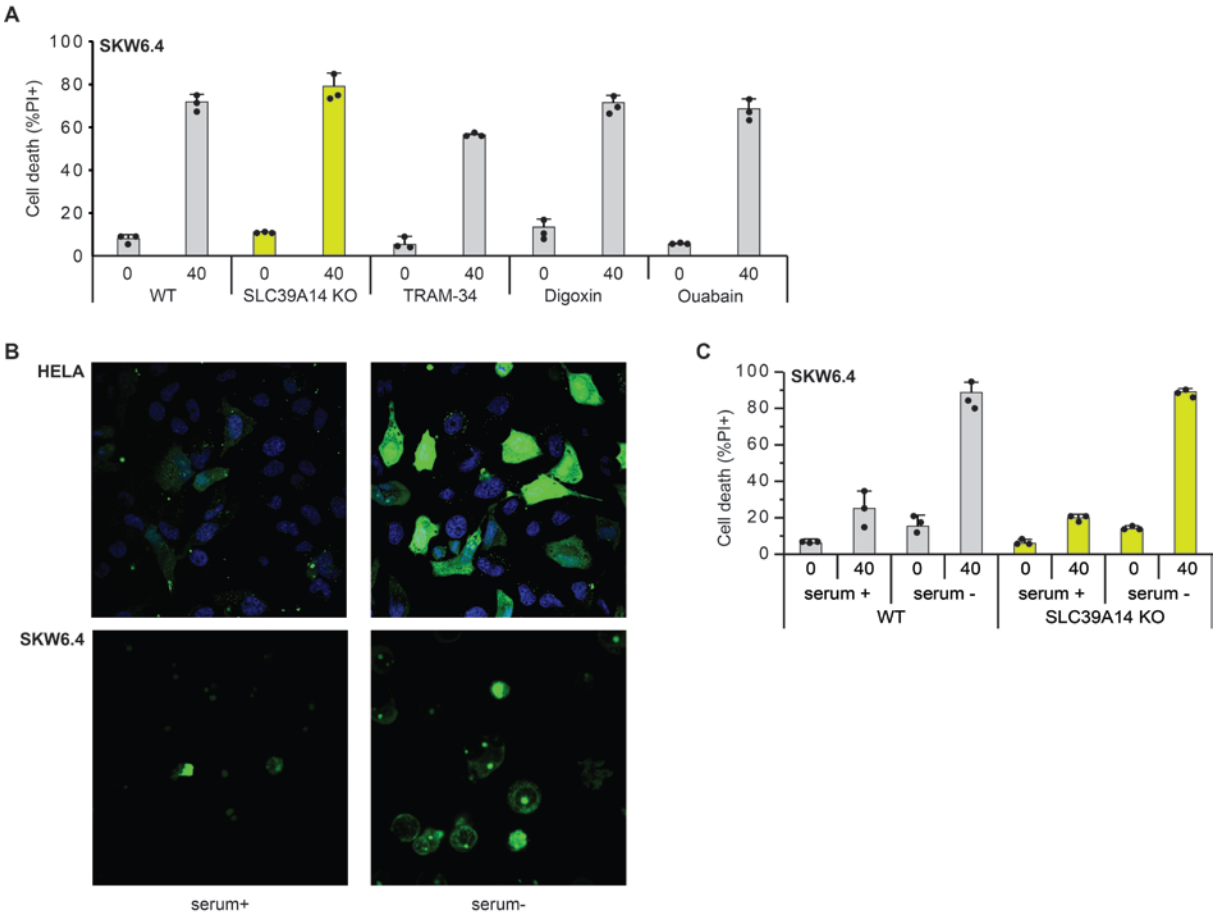

Supplementary Figure S2. Forced TAT-RasGAP$_{317-326}$ direct translocation induced death in SKW6.4 WT, SLC39A14 KO and treated with TRAM-34, digoxin, or ouabain. **A.** WT, SLC39A14 KO, and SKW6.4 cells pretreated with TRAM-34, digoxin, or ouabain were treated or not with 40 µM TAT-RasGAP$_{317-326}$ and 50 µM PB for 30 minutes and cell death was determined using PI. **B.** Live confocal microscopy imaging of HeLa and SKW6.4 WT cells incubated in medium containing or not 10% serum and treated for 1 hour with 20 µM FITC fused TAT-RasGAP$_{317-328}$ (green). The nuclei of HeLa cells are stained with live Hoechst 33342 1 µg/ml for 15 minutes (blue). **C.** WT and SLC39A14 KO SKW6.4 cells were incubated in medium containing or not 10% serum and treated for 3 hours with 40 µM TAT-RasGAP$_{317-326}$. Cell death was analyzed by flow cytometry using PI.

Supplementary Figure S3. Assessment of the FITC-TAT-RasGAP$_{317-326}$ cytosolic access in KCNN4 KO, HeLa cells treated with TRAM-34 and WT HeLa cells. **A.** Live confocal microscopy imaging of HeLa WT, HeLa WT pretreated with 10 µM TRAM-34 for 1 hour, and HeLa KCNN4 KO treated for the indicated periods of time with 80 µM FITC fused TAT-RasGAP$_{317-328}$ (green) at 4°C and 37°C. The nucleus is stained with live Hoechst 33342 1 µg/ml for 15 minutes (blue).

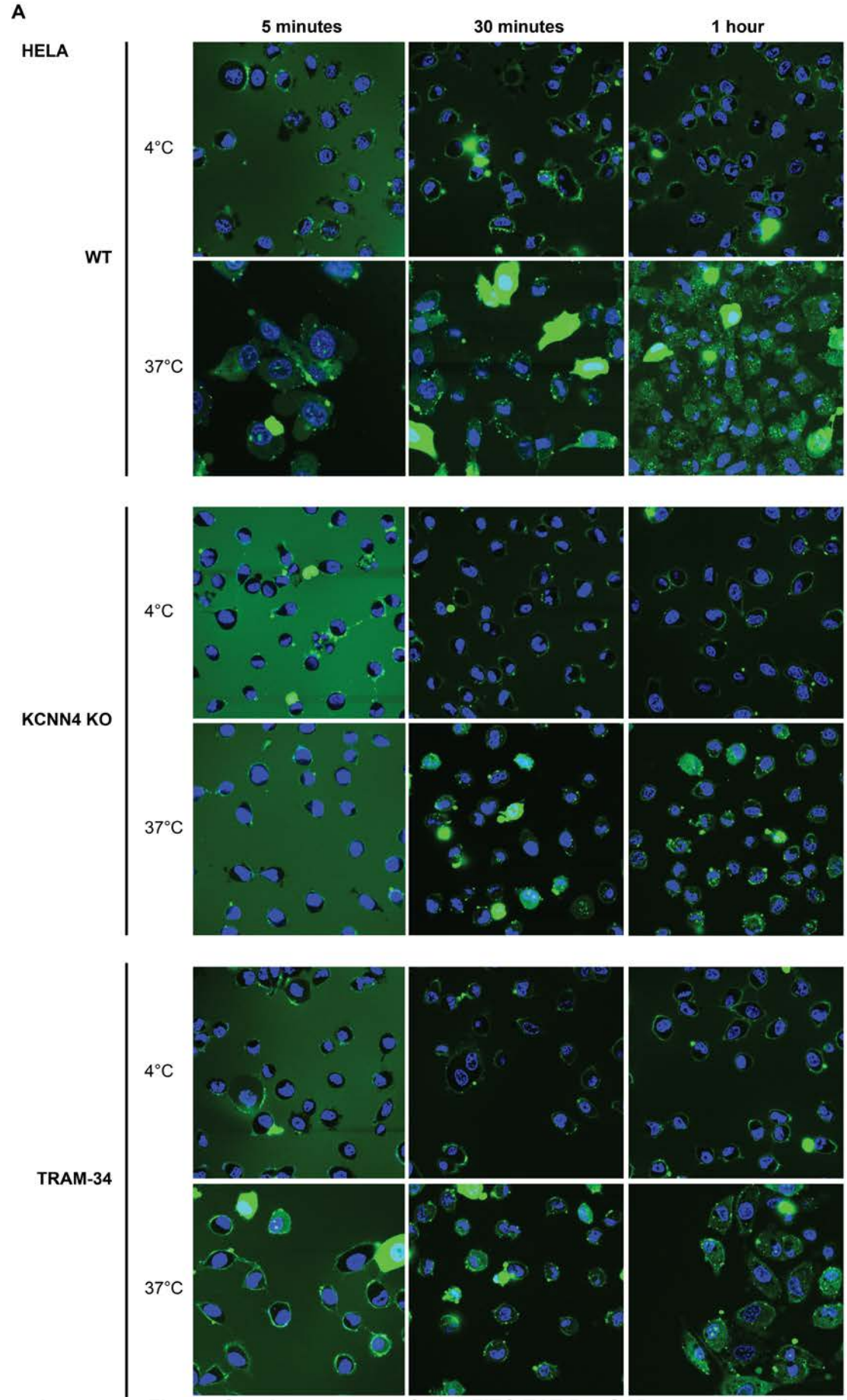

Supplementary Figure S3. Assessment of the FITC-TAT-RasGAP$_{317-326}$ cytosolic access in KCNN4 KO, HeLa cells treated with TRAM-34 and WT HeLa cells. (see legend on the previous page)

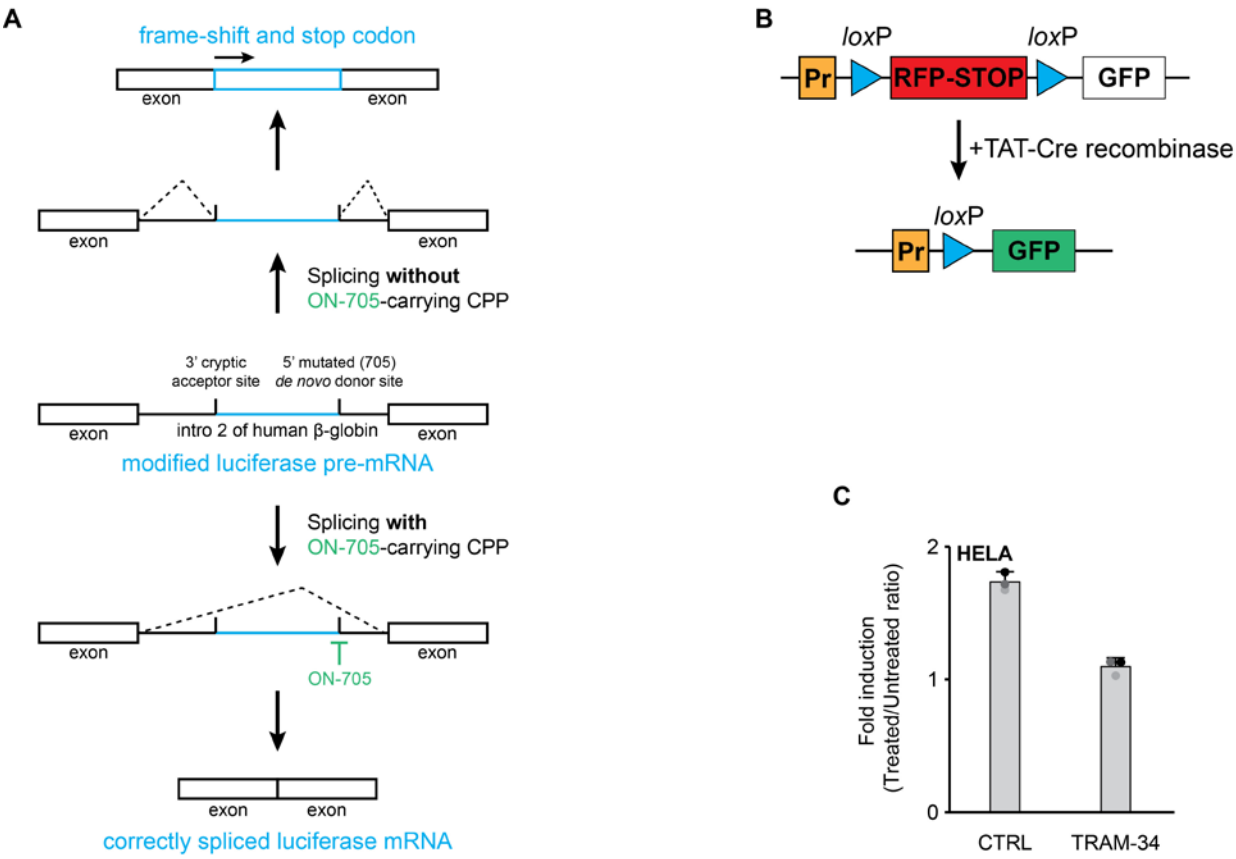

Supplementary Figure S4. Cytosolic access assays. **A.** The scheme represents the luciferase rescue reporter assay. This assay employs cells expressing a plasmid carrying the luciferase-coding sequence interrupted by a mutated human β-globin intron 2. This mutation creates a new splicing site that is targeted by the splicing machinery of the cells, together with a cryptic site that is now also used, to produce an mRNA that encodes a truncated non-functional luciferase. However, the luciferase pre-mRNA can be properly processed if the splice site generated by the mutation at position 705 is masked by a matching oligonucleotide (ON-705). ON-705 can be covalently coupled to a cell-penetrating peptide (CPP) (e.g. TAT). The resulting so-called peptide nucleic acid (PNA), when incubated with cells, triggers the correct splicing of the mutated luciferase pre-RNA but only if the PNA is gaining access to the cytosol. **B.** TAT-Cre mediated excision of transcriptional RFP-STOP region flanked by two *lox*P sites induces constitutive GFP expression. Pr, promoter. **C.** Cytosolic access was assessed using a luciferase rescue reporter assay [261]. WT HeLa cells were infected with a virus encoding for the luciferase-coding sequence, interrupted by a mutated human β-globin intron. They were then pretreated or not with 10 μM TRAM-34 for 1 hour and treated for 24 hours with 10 μM TAT-PNA. After 24 hours, luciferase activity was measured and normalized to the protein content. Results correspond to the mean +/- 95% CI of three independent experiments.

Supplementary Figure S5. VSV and Arenaviruses entry and transport. **A.** Phylogenic tree of Arenaviruses. Modified from Urata et al., Viruses, 2012, [262]. **B.** Viruses bind to specific receptors before entering the cell by hijacking endocytic pathways. VSV (in green) associates to the low-density lipoprotein receptor (LDLR) to enter cells via clathrin-mediated endocytosis (CME), and escapes from early endosomes to reach the cytoplasm. The New World arenaviruses (in blue) utilize transferrin receptor-1 to enter cells via CME and then exit late endosome. The Old World (in purple) LCMV and Lassa viruses use the cellular receptor α-dystroglycan to infect cells via a macropinocytosis-related pathway and escape late endosomes by acid-induced membrane fusion. However, they are transported to intermediate multivesicular bodies by an unidentified organelle, which is not early endosomes. Of note, Lassa virus has to engage the late endosomal resident protein LAMP-1 for efficient fusion, which is not the case for LCMV. Finally, mechanisms of entry, including the receptor, have still not been highlighted for the newly identified Old World arenavirus Lujo (in purple).

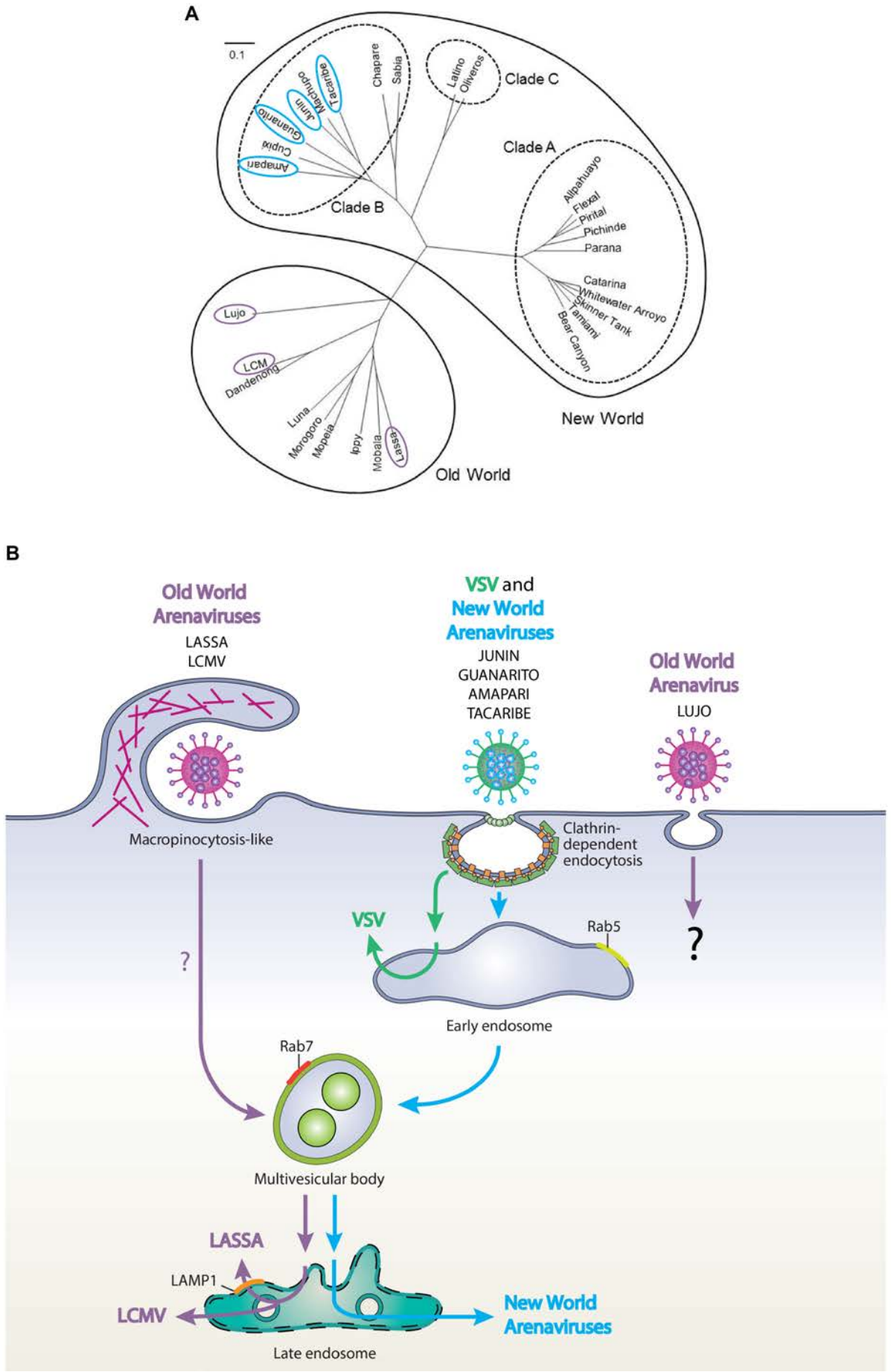

Supplementary Figure S5. VSV and Arenaviruses entry and transport. (see legend on the previous page)

RELATED DATA

This part is dedicated to results that I obtained by working on the mode of action of TAT-RasGAP$_{317-326}$ and the involvement of the candidates highlighted by CRISPR/Cas9 screens in the cytosolic access of the peptide. As they are either negative results or preliminary data, they were not added to the previous manuscript.

CRISPR/Cas9 screening in NB1 cells

As we did not succeed in the Oncotarget paper to decipher how TAT-RasGAP$_{317-326}$ could kill NB1 cells (Figure R1A), a gene disruption CRISPR/based genetic screen was performed to identify genes whose loss increases resistance to the peptide in this cell line. The rational of using the NB1 cells for the screen, in addition to the SKW6.4 and the Raji cells, was to favor the identification of the core proteins required for the peptide to kill in cell lines of different origins. Table R1 compares the results of massive parallel sequencing for NB1 and Raji cells in both control and peptide-selected populations. The screen identified more than 20,000 targeted genes with more than 100,000 targeted sgRNAs in the control population of Raji and NB1 cells (in grey and red respectively in Table R1). These data demonstrate that the infection with the CRISPR/Cas9 GeCKO library worked well. However, whereas the number of targeted genes and sgRNAs in control and peptide selected populations are quite similar in Raji cells (in grey and bold grey respectively in Table R1), they differ in NB1 control and peptide selected populations (in red and bold red respectively in Table R1). One explanation for the loss of around 40% of targeted genes in the NB1 peptide selected population could be that these genes were not involved in inducing cell resistance to the peptide toxicity. Another explanation would be that a large number of cells were lost during the splitting steps of the treated population. Indeed, one of the properties of TAT-RasGAP$_{317-326}$ is to greatly increase cell adherence rendering the cells very difficult to be detached with trypsin. The latter explanation seems to be the right one, according to the large and unexpected decrease of the targeted sgRNAs number in the peptide-selected population compared to the control population (>80%). As a consequence of this technical issue, the results of the sequencing performed on NB1 cells are not directly interpretable as shown in Figure R1. Although after positive selection with TAT-RasGAP$_{317-326}$, the NB1 cells infected with the library were rendered resistant to its toxicity (Figure R1B), SNAP29, the top candidate yielded by the screen, was not required for the peptide to kill NB1 cells (Figures R1C, D, and E).

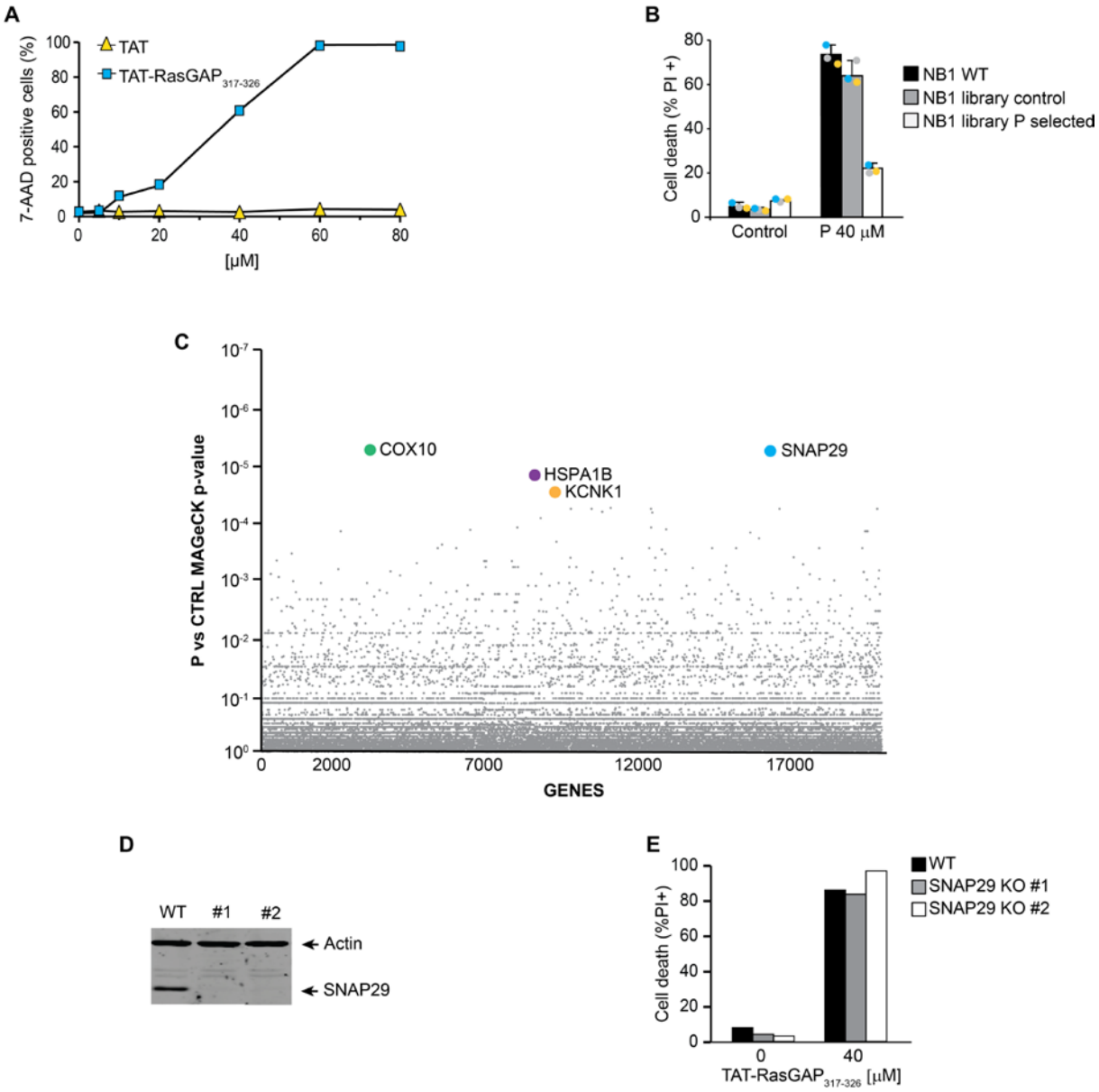

Figure R1. Identification of candidate genes, whose loss-of-function should confer TAT-RasGAP$_{317-326}$ resistance. **A.** NB1 cells were incubated for 24 hours with indicated concentrations of TAT-RasGAP$_{317-326}$ or TAT, as a control. Cell death was then assessed by flow cytometry after 7-AminoActinomycin D (7-AAD) staining. **B.** NB1 WT, NB1 GeCKO library control and NB1 GeCKO library TAT-RasGAP$_{317-326}$ (P) selected cells were treated or not with 40 µM TAT-RasGAP$_{317-326}$ for 24 hours. Cell death was then assessed by flow cytometry after PI staining. Results correspond to the mean +/- 95% CI of 3 independent experiments. **C.** Identification of the four top candidate genes implicated in resistance to TAT-RasGAP$_{317-326}$ in NB1 cells using the Model-based Analysis of Genome-wide CRISPR/Cas9 Knockout (MAGeCK) p-value. **D.** Expression of SNAP29 in NB1 WT and KO clones #1 and #2. **E.** WT and SNAP29 disrupted NB1 cells were treated or not with 40 µM TAT-RasGAP$_{317-326}$ for 24 hours. Cell death was then assessed by flow cytometry after PI staining.

	Metrics	Library control	Library P selected
Raji	Reads number	4364742	4414584
	Targeted genes	20416	20330
	Targeted genes with >50 normalized counts	9866	6733
	Targeted genes with >100 normalized counts	267	1850
	Targeted sgRNAs	110962	99479
	Targeted sgRNAs with >50 normalized counts	102	2939
	Targeted sgRNAs with >100 normalized counts	1	890
NB1	Reads number	4205848	4180577
	Targeted genes	20410	12569
	Targeted genes with >50 normalized counts	9004	551
	Targeted genes with >100 normalized counts	327	402
	Targeted sgRNAs	109129	18055
	Targeted sgRNAs with >50 normalized counts	402	553
	Targeted sgRNAs with >100 normalized counts	16	400

Table RI. Counts summary metrics of the CRISPR-Cas9 screen in Raji and NB1 cells. Raji and NB1 GeCKO library control populations and Raji and NB1 GeCKO library TAT-RasGAP$_{317-326}$ (P) selected populations were sequenced with a MiSeq (Illumina). Raw FASTQ files were demultiplexed and processed to contain only the unique sgRNA sequence. The total number of reads, the number of reads for each sgRNA, and the number of reads per targeted genes are shown in this table.

Are ATP1A1 knockout SKW6.4 clones resistant to TAT-RasGAP$_{317-326}$-induced cell death?

Na^+/K^+-ATPase pump transforms the energy of ATP to maintain the sodium and potassium gradients across the plasma membrane. This pump transports three Na^+ from inside the cell to the outside and two K^+ from outside to the inside. The minimal functional Na^+/K^+-ATPase pump is composed of two subunits: the alpha subunit that hydrolyses ATP and transports the cations, and the beta subunit that is required for the stability and trafficking of the pump [263]. Whereas three different isoforms of the beta subunit have been found in humans, the alpha subunit possesses four isoforms (ATP1A1, ATP1A2, ATP1A3 and ATP1A4) [264, 265]. In contrast to the other subunits, ATP1A1 is expressed in all tissues.

As the CRISPR/Cas9 screen on SKW6.4 cells highlighted ATP1B3, which is an isoform of the beta subunit of the Na^+/K^+-ATPase pump, we then investigated if the alpha subunit of the pump was equally able to regulate TAT-RasGAP$_{317-326}$-induced cell death. We, therefore, generated ATP1A1 knockout clones in parallel to ATP1B3 knockout cells (Figure R2A). Figure R2B indicates that the alpha subunit ATP1A1 of the Na^+/K^+-ATPase pump is also involved in the regulation of the peptide toxicity.

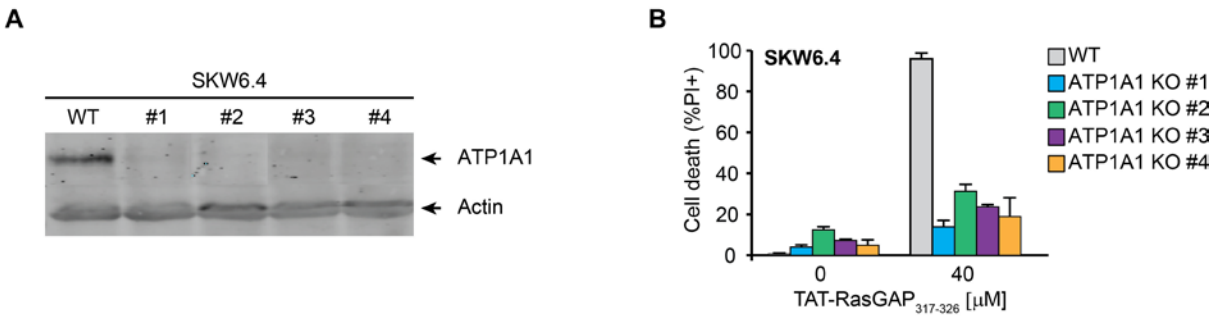

Figure R2. ATP1A1 knockout SKW6.4 cells are protected against TAT-RasGAP$_{317-326}$ toxicity. A. ATP1A1 was disrupted in SKW6.4 cells using the CRISPR/Cas9 technology. Loss of expression was confirmed

by western blotting. **B.** Wild-type (WT) and ATP1A1 knockout (KO) SKW6.4 cells were treated or not with 40 µM TAT-RAsGAP$_{317-326}$ for 24 hours. Cell death, corresponding to the % of PI positive cells, was determined by flow cytometry. Results correspond to the mean +/- 95% CI of 3 independent experiments.

Does TAT-RasGAP$_{317-326}$ colocalize with Rab5 in HeLa cells?

To assess if TAT-RasGAP$_{317-326}$ enters cells through endocytosis, we investigated whether the FITC fluorescent-labelled peptide colocalized with the marker of early endosomes, Rab5. As depicted in Figure R3, TAT-RasGAP$_{317-326}$ and Rab5 colocalize, suggesting that the peptide enters cells at least partially through endocytosis.

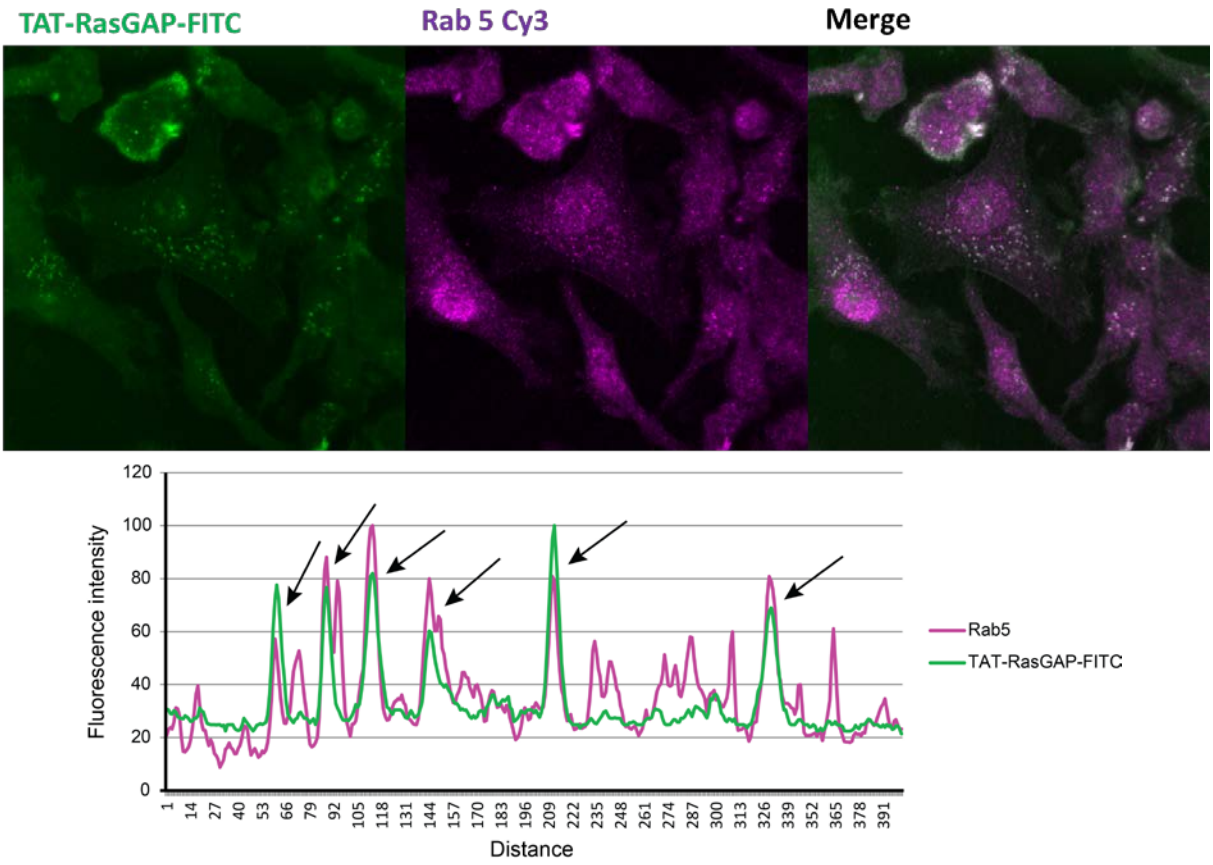

Figure R3. TAT-RasGAP$_{317-326}$ colocalizes with the early endosome marker Rab5. A. Fluorescent confocal microscopy analysis of HeLa cells treated with 40 µM FITC-TAT-RasGAP$_{317-326}$ (upper left panel, green) for 12 hours and then stained with an anti-Rab5 antibody (upper central panel, purple) indicates that TAT-RasGAP$_{317-326}$ and Rab5 colocalize (upper right panel, white). A histogram (lower panel) showing colocalization of FITC-TAT-RasGAP$_{317-326}$ with Rab5 along a line that was drawn on one of the cells was generated from the image using ImageJ software. Black arrows indicate colocalization in aggregates.

Does TAT-RasGAP$_{317-326}$ colocalize with LAMP1 in HeLa cells?

Once trapped into endosomes, TAT-RasGAP$_{317-326}$ has to escape them to access to the cytoplasm and exerts its activity. Endosomal escape can occur in early or late endosomes. One way to assess if the peptide gains access to the cytosol from early endosomes is to determine whether it is or not

present in the late endosomes. Therefore, we studied if the peptide colocalized with the late endosomal marker, LAMP-1. Figure R4 illustrates that TAT-RasGAP$_{317-326}$ and LAMP-1 colocalize. This suggests that the peptide does not escape early endosomes. Consequently, either the peptide is able to escape late endosomes or it is sequestrated into endosomes, hampering it to reach the cytosol. The second hypothesize would mean that the killing efficiency of the peptide is only based on its entry via direct translocation.

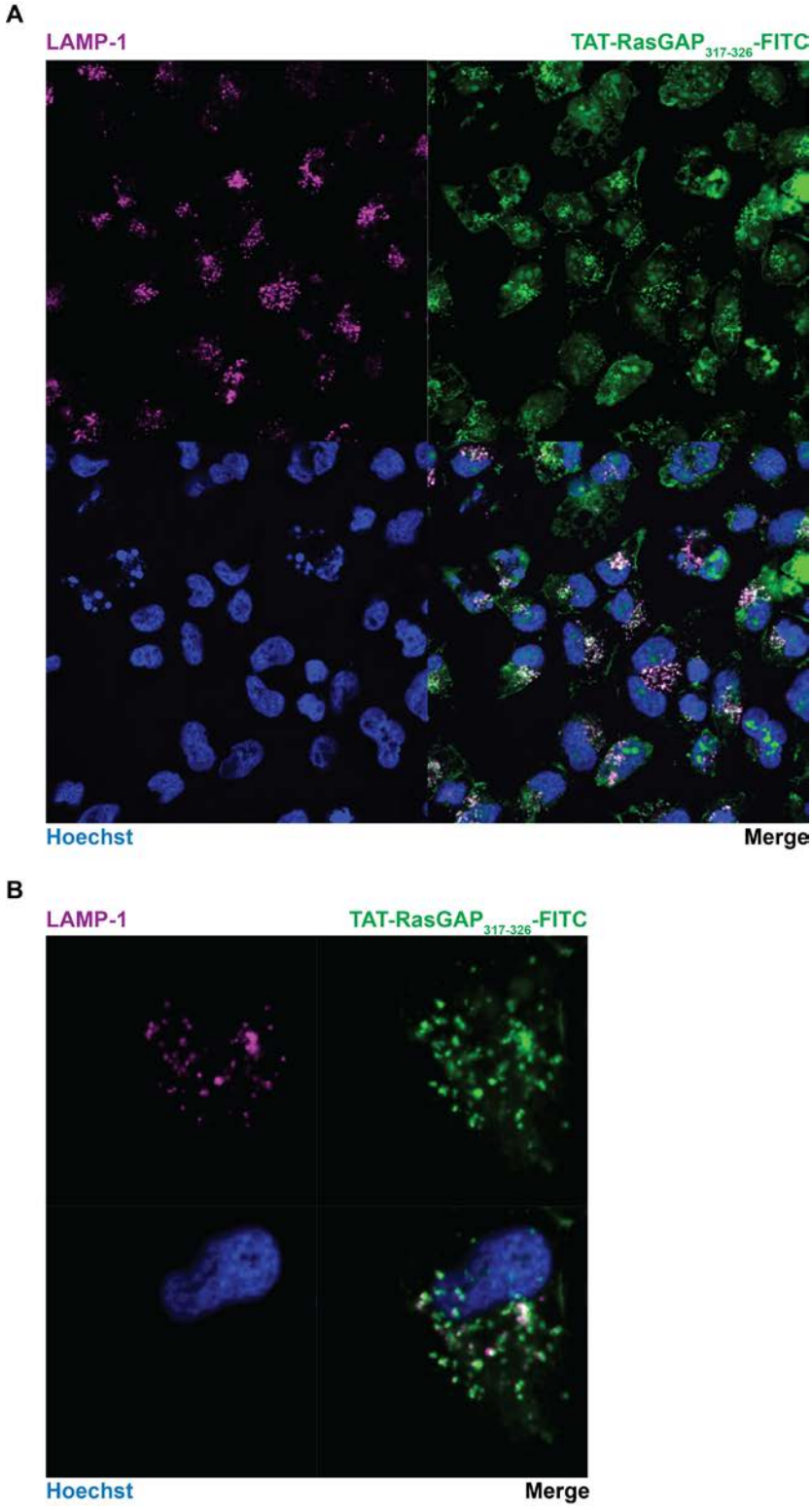

Figure R4. TAT-RasGAP$_{317-326}$ colocalizes with the late endosome marker LAMP-1. **A.** Fluorescent confocal microscopy analysis of HeLa cells treated with 80 µM FITC-TAT-RasGAP$_{317-326}$ (upper right panel, green) for 24 hours and then stained with an anti-LAMP-1 antibody (upper left panel, purple) and with the nuclei marker Hoechst 33343 (lower right panel, blue) indicates that TAT-RasGAP$_{317-326}$ and LAMP-1 partially colocalize (lower left panel, white). **B.** Picture magnifications of what was represented in panel A.

Does the absence of KCNN4 and KCNQ5 potassium channels inhibit endocytosis of TAT-RasGAP$_{317-326}$ through the activation of PP2A?

Recently, Eil and colleagues demonstrated that increased intracellular potassium concentration could limit the activation of T cells through the activation of the serine/threonine phosphatase PP2A and the subsequent inhibition of Akt [266]. Moreover, by overexpressing KCNN4 as well as another potassium channel KCNA3 in T-cells, the intracellular potassium concentration was reduced and consequently PP2A was inhibited. Consequently, they have demonstrated that potassium channels, via the modulation of intracellular potassium concentration, can regulate T-cell activation through PP2A.

PP2A is known to negatively regulate Akt activity as well as Src kinase, two proteins that were shown to be involved in endocytosis [267-271]. The PP2A protein consists of the structural subunit (A), catalytic subunit (C), and a variable regulatory subunit (B) [272].

Consequently, we hypothesized that the absence of KCNN4 or KCNQ5 would increase the intracellular potassium concentration and subsequently stimulates PP2A activation that represses Akt or Src kinase. This would result finally in the inhibition of TAT-RasGAP$_{317-326}$ endocytosis (Figure R5).

In order to validate this assumption, we used a serine/threonine phosphatase (PP1 and PP2A) inhibitor named okadaic acid (OA). Figures R5B and R5C show that, in the presence of OA, the KCNN4 and KCNQ5 knockout cells are re-sensitized to TAT-RasGAP$_{317-326}$-induced cell death at the same extent as wild-type cells treated with the peptide. Then, to investigate if the absence of KCNN4 and KCNQ5 potassium channels impacted the abundance of the catalytic subunit of PP2A (PP2Ac) or the extent of Src and Akt phosphorylation, we performed western blot analyses. The first phosphorylation site of Akt at the threonine 308 residue stimulates only partially the kinase, which requires a second phosphorylation at serine 473 residue for its full activation [273, 274]. Figures R5D and R5E illustrate that neither the abundance of PP2Ac nor Src or Akt phosphorylation are deregulated in knockout cells or wild-type cells treated with the KCNN4 inhibitor TRAM-34 or the KCNQ5 inhibitor XE991 compared to the non-treated wild-type cells. These results suggest that the effect of OA is independent of Akt or Src kinase phosphorylation. Of note, although it seems that there is a decrease of Src and Akt (at S473 residue only) phosphorylation in Raji treated with XE991 or in KCNQ5 knockout Raji cells (Figure R5E), it is an artifact due to an inefficient exposure of the membrane. In addition, the increased phosphorylation of Akt at T308 residue in KCNN4 knockout SKW6.4 cells was not related to the protective effect against the peptide toxicity observed in those cells, as no similar observation was made in wild-type cells treated with the TRAM-34 inhibitor (Figure R5D). The same assertion can be done regarding to the increased abundance of PP2Ac in KCNQ5 knockout Raji cells (Figure R5E). Finally, we treated wild-type SKW6.4 and Raji cells with an efficient dose of the Src kinase inhibitor dasatinib (Figure R5F) in the presence of TAT-RasGAP$_{317-326}$. Figure

R5G shows that the inhibition of Src kinase does not protect wild-type cells against the peptide toxicity, supporting western blotting results.

Ultimately, we assessed if the re-sensitizing effect of OA in knockout cells was associated with an increased intracellular uptake of the peptide. Strikingly, in the presence of OA, the entry of the FITC-coupled TAT-RasGAP$_{317-326}$ peptide remained blocked in KCNQ5 knockout Raji cells (Figure R5H). This suggests that, upon OA treatment, the peptide is able to kill cells directly from the outside. Another assumption would be that OA is able to very efficiently potentiate the effect of the peptide which, therefore, requires only very few molecules inside the cell to induce its death.

In order to better understand how OA is able to rescue the phenotype of knockout cells, we could silence PP2A. This would allow us to assess if the observed effect of OA is due to PP2A inhibition. Alternatively, we could stimulate PP2A in wild-type cells and assess whether its activation prevents TAT-RasGAP$_{317-326}$-induced cell death.

Figure R5. Okadaic acid can re-sensitize KCNN4 and KCNQ5 knockout cells to TAT-RasGAP$_{317-326}$ independently of Akt and Src kinase modulation. **A.** Scheme depicting the possible mechanisms by which okadaic acid (OA) could re-sensitize KCNN4 and KCNQ5 knockout cells to TAT-RasGAP$_{317-326}$-induced cell death. OA is a specific inhibitor of PP1 and PP2A. Src as well as Akt kinases are inhibited by PP1 and PP2A. The sequential inhibitions activate Src and Akt kinases that induce endocytosis. The presence of potassium channels could inhibit PP2A activation or stimulate both kinases, either directly or by modulating the intracellular potassium concentrations, resulting in endocytosis stimulation. Consequently, in cells specifically disrupted for KCNN4 or KCNQ5, endocytosis could not occur correctly. According to this hypothesize, Dasatinib, a Src Kinase inhibitor, should protect wild-type cells against the peptide toxicity via the TAT-RasGAP$_{317-326}$ endocytosis inhibition. **B.** KCNN4 KO or WT SKW6.4 cells were preincubated one hour with different concentrations (0, 12.5, 25, 50, and 100 µM) of OA, before being treated or not (CTRL) with 40 µM TAT-RasGAP$_{317-326}$ for 24 hours. Cell death, corresponding to the % of PI positive cells, was determined by flow cytometry. **C.** KCNQ5 KO or WT Raji cells were preincubated one hour with different concentrations (0, 50, 100, 200, and 400 µM) of OA, before being treated or not (CTRL) with 40 µM TAT-RasGAP$_{317-326}$ for 16 hours. Cell death was assessed as in panel B. **D.** SKW6.4 WT cells were pretreated one hour with 10 µM TRAM-34 (TRAM) or 10 µM XE991. The abundance of PP2Ac as well as the extent of Src and Akt phosphorylation at serine 473 and threonine 308 were assessed by western blot in the indicated cells. Vinculin was used as protein loading control. **E.** Same as panel D with WT and KCNQ5 KO Raji cells. **F.** Abundance of Src kinase in SKW6.4 and Raji WT cells treated or not for 1 hour with dasatinib at the indicated concentrations was assessed by western blotting. **G.** WT SKW6.4 and Raji cells were preincubated or not (N/T) one hour with 125 nM or 1 µM dasatinib, before being treated or not with 40 µM TAT-RasGAP$_{317-326}$ for 24 hours (SKW6.4) or 16 hours (Raji). Cell death was assessed as in panel B. **H.** KCNQ5 KO and WT Raji cells were treated as in panel C with FITC-TAT-RasGAP$_{317-326}$ for 1 hour. Cells were then collected and washed three times with cold phosphate-buffered saline (PBS). The median fluorescence intensity of viable cells was then measured by flow cytometry. Results of panel B and C correspond to the mean +/- 95% CI of 3 independent experiments.

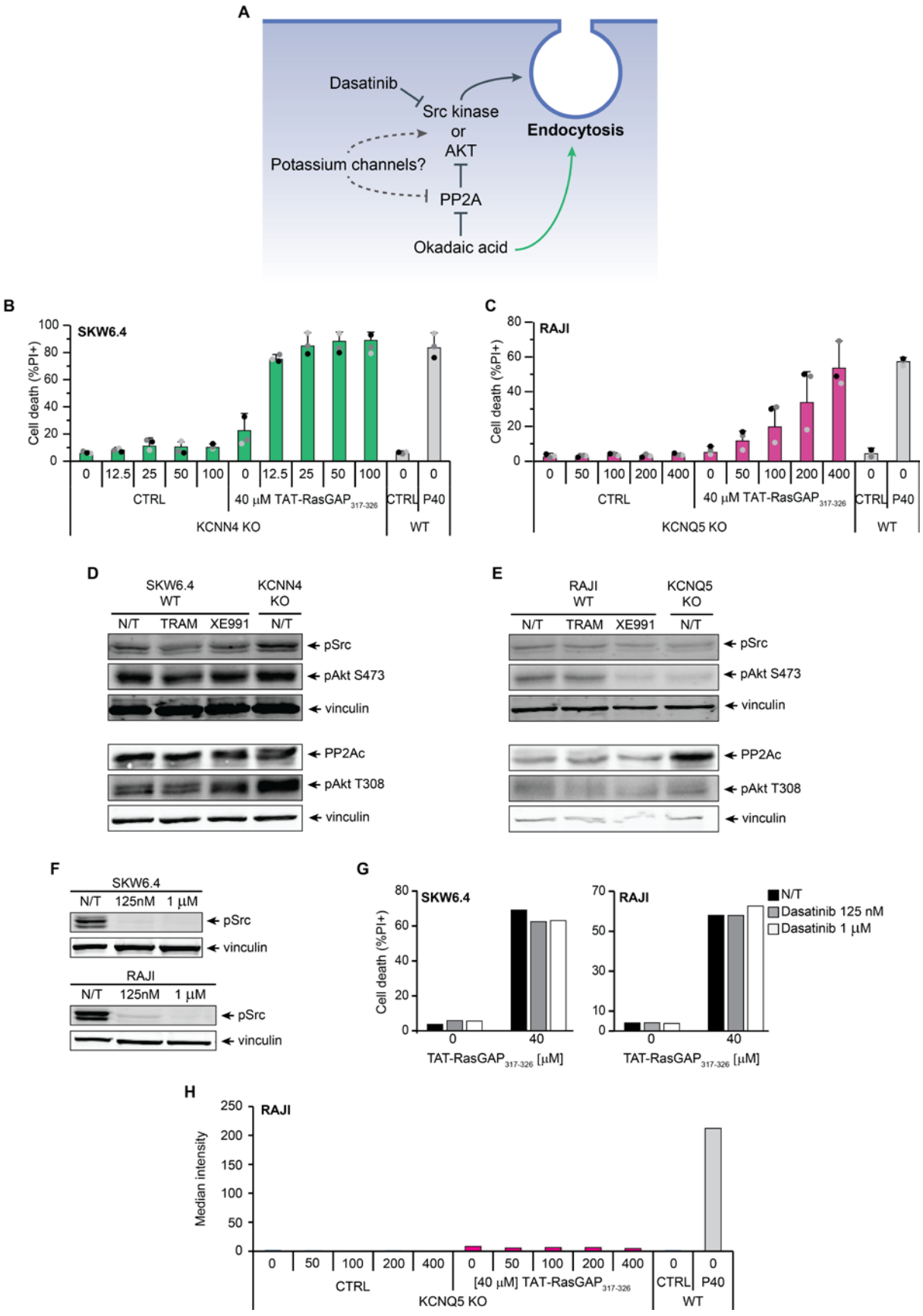

Figure R5. Okadaic acid can resensitize KCNN4 and KCNQ5 knockout cells to TAT-RasGAP$_{317-326}$ independently of Akt and Src kinase modulation. (see legend on the previous page)

DMEM protects cells against TAT-RasGAP$_{317-326}$-induced cell death.

By working with several cell lines that were cultured in different media, we observed that the sensitivity of cells toward TAT-RasGAP$_{317-326}$ toxicity was medium-dependent. Figure R6A show that SKW6.4 wild-type cells are partially protected against the peptide in DMEM compared to RPMI. Same results were observed in other cell lines such as here in the melanoma cell lines WM3248 and WM1366 (Figure R6B). Comparison of media composition revealed that the concentration of calcium was higher in DMEM than in RPMI. Consequently, the complementation of RPMI with calcium partially blocked TAT-RasGAP$_{317-326}$-induced death (Figure R6C).

To investigate if DMEM was still able to protect cells once the peptide has gained access to the cytoplasm, we used pyrenebutyrate (PB) to force its direct translocation. Figure R6C shows that in the presence of PB, cells were not any more protected in DMEM. This suggests that the calcium concentration of the medium is an important parameter modulating the peptide toxicity, although it does not regulate its direct pro-death activity.

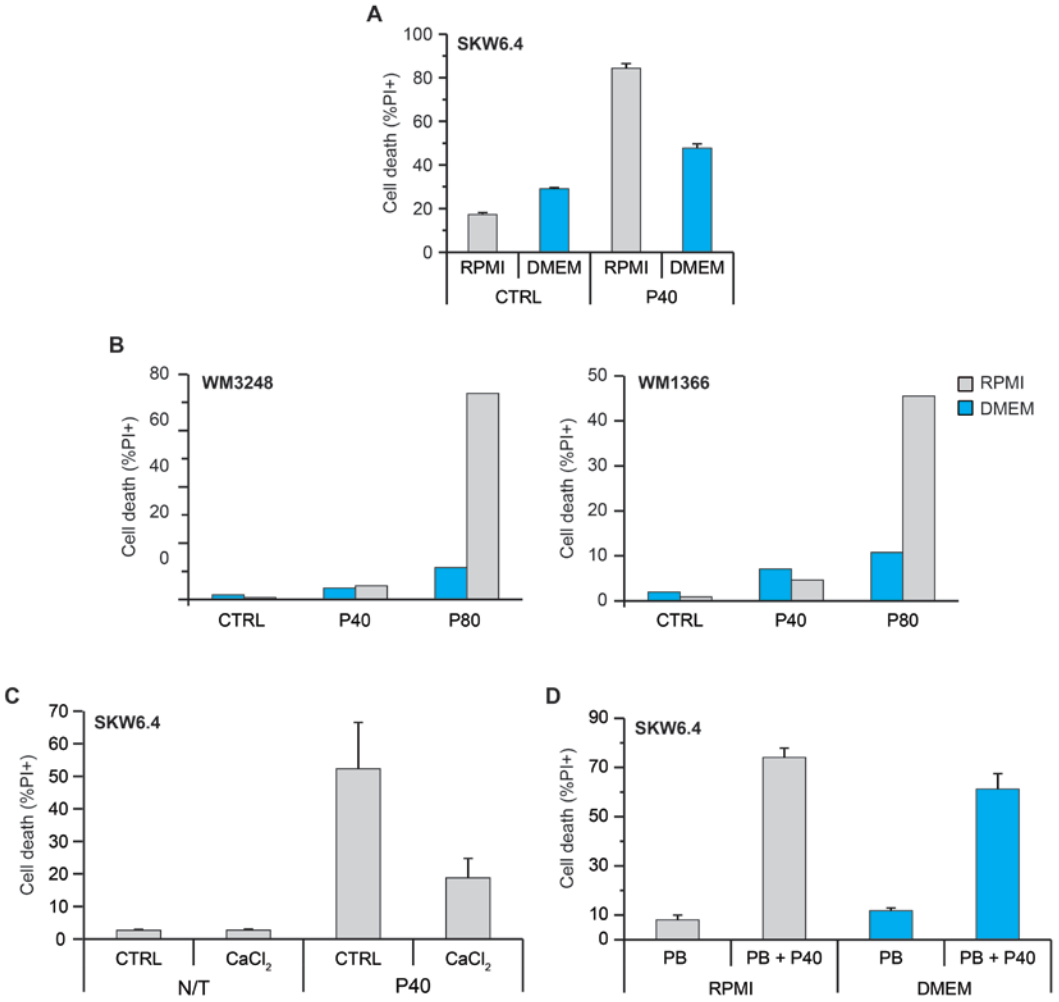

Figure R6. DMEM protects against TAT-RasGAP$_{317-326}$-induced cell death. **A.** SKW6.4 cells cultured in RPMI or in DMEM were treated or not (CTRL) with 40 µM TAT-RasGAP$_{317-326}$ (P40) for 24 hours. Cell death, corresponding to the % of PI positive cells, was determined by flow cytometry. **B.** Same as Panel A in WM3248 and WM1366 cell lines treated with 40 or 80 µM TAT-RasGAP$_{317-326}$. **C.** SKW6.4 cells cultured in RPMI were treated or not (CTRL) with 1.38mM $CaCl_2$ and 40 µM TAT-RasGAP$_{317-326}$ for 24 hours. Cell death was determined using PI. **D.** SKW6.4 cells cultured in RPMI or in DMEM were treated or not with 40 µM TAT-RasGAP$_{317-326}$ and

50 µM PB for 30 minutes and cell death was determined using PI. Results of panel A, C and D correspond to the mean +/- 95% CI of at least 3 independent experiments.

A549 is the only tested cancer cell line that is not killed by TAT-RasGAP$_{317-326}$.

Among about 40 tested cell lines, the human lung carcinoma A549 cells are the only ones that were not killed by the peptide when cultured in RPMI. Of note, the scale of the y-axis goes only until 4% cell death. Accordingly, these cells could be useful for future experiments designed to find the mechanism of action of the peptide or its mode of entry. As a first experiment, we could assess the uptake of the FITC-TAT-RasGAP$_{317-326}$ in those cells.

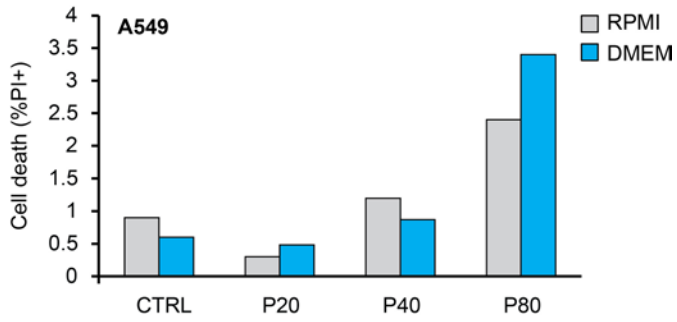

Figure R7. A549 cells are not killed by TAT-RasGAP$_{317-326}$. A. A549 cells cultured in RPMI or in DMEM were treated or not (CTRL) with 20, 40, and 80 µM TAT-RasGAP$_{317-326}$ for 24 hours. Cell death, corresponding to the % of PI positive cells, was determined by flow cytometry.

There is no difference in intracellular calcium concentration between wild-type and KCNN4 or KCNQ5 knockout cells.

Perturbations of intracellular calcium compartmentalization and concentration have been shown to induce cytotoxicity [275]. Moreover, we showed that cells cultured in DMEM, which contains more calcium than RPMI, are protected against the peptide toxicity. Finally, the absence of KCNN4, which is a potassium calcium-activated channel, blocks TAT-RasGAP$_{317-326}$-induced death. We, therefore, hypothesize that calcium could play a key role in the mode of action of the RasGAP-derived peptide. We used the chemical calcium indicator Fluo-4/AM to assess intracellular calcium concentration in various conditions [276]. We employed the ionophore ionomycin and the intracellular calcium chelator Bapta/AM as positive and negative control, respectively [277, 278]. Figure R8A shows that there is no difference in intracellular calcium concentration between wild-type and KCNN4 knockout SKW6.4 cells. Furthermore, cells preincubated in OA, calcium chloride ($CaCl_2$), and DMEM did not display any changes in intracellular calcium concentration compared to non-treated cells. Same observations were reported in wild-type and KCNQ5 knockout Raji cells (Figure R8B).

These results do not exclude that calcium is involved in TAT-RasGAP$_{317-326}$-induced cell death. Indeed, as Fluo-4 is blocked in the cytoplasm, it cannot measure precisely perturbation of calcium

compartmentalization. Moreover, Fluo-4 probe might not be enough sensitive to detect small localized variations of calcium that could be sufficient to modulate the peptide toxicity. We could, therefore, perform confocal microscopy to better investigate calcium localization.

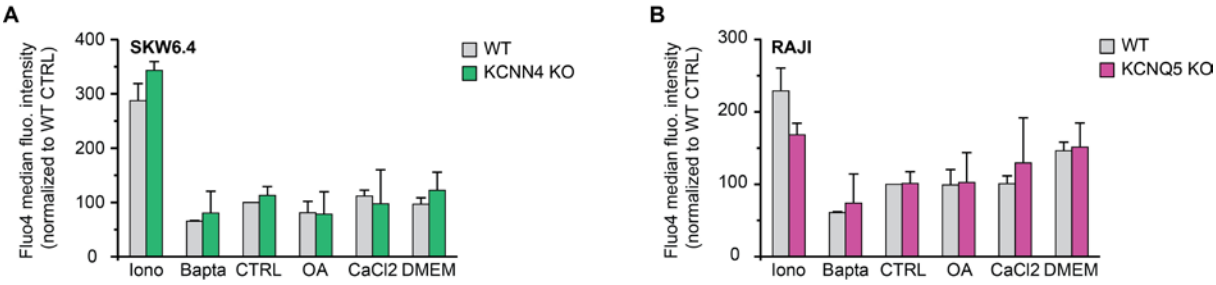

Figure R8. There is no difference in intracellular calcium concentration between wild-type and KCNN4 or KCNQ5 knockout cells. **A.** WT and KCNN4 KO SKW6.4 cells were preincubated one hour in 10 µM Bapta/AM, 200 µM okadaic acid (OA), 200 µg/ml $CaCl_2$, or DMEM. 5 µM Fluo-4/AM was then added for 1 hour. The cells were washed once and 20 minutes later, the median fluorescence intensity of viable cells was measured by flow cytometry. For the positive control, ionomycin plus 200 µg/ml $CaCl_2$ were added five minutes before analyzing the cells by flow cytometry. **B.** As in panel A with WT and KCNQ5 KO Raji cells. Results correspond to the mean +/- 95% CI of 3 independent experiments.

PART IV

The fourth part of the results is dedicated to a recent project unrelated to TAT-RasGAP$_{317-326}$.
In this part, we took advantage of the well-implemented CRISPR/Cas9 technology in the lab to apply it to a project about resistance mechanisms of hepatocellular carcinoma (HCC) to sorafenib. In addition, we used exome sequencing analysis to identify novel pathways that lead to sorafenib resistance. The latter could be targeted to treat HCC. Preliminary results obtained with the two technologies are presented in the following section in form of manuscript.
Of note and as illustrated in the manuscript, we have encountered some technical issues in the course of this project. This study was based on three HCC cell lines that were rendered resistant to sorafenib by our collaborators. Once we received them, we directly performed exome sequencing analyses. In the meantime, we assessed if cells were still resistant to sorafenib in our hands. Unexpectedly, two out of the three cell lines had lost their resistant phenotype suggesting the occurrence of a genetic drift. However, the latter happened most probably after we had performed exome sequencing. Indeed, the results depict some mutations already described in the literature suggesting that cells were still resistant at that time. Unfortunately, as our collaborators did not keep frozen resistant cells, we were unable to validate mutations highlighted by exome sequencing analyses. Accordingly, certain results presented in this part should be cautiously interpreted.

This study was carried out in collaboration with Dr. Olivier Dormond from the department of Visceral Surgery of Centre Hospitalier Universitaire Vaudois (CHUV). Dr. Emilie Uldry, from his laboratory, established and validated the three sorafenib resistant cell lines used in this study (Figure 1 of the following manuscript). Dr. David Barras from the Swiss Institute of Bioinformatics (SIB) analyzed the exome sequencing data. I performed all the other experiments.

IDENTIFICATION OF GENES INVOLVED IN ACQUIRED SORAFENIB RESISTANCE IN HEPATOCELLULAR CARCINOMA.

INTRODUCTION

Worldwide, liver cancer is the second most common cause of cancer death and the fifth most common tumour [39]. The five-year survival rate of hepatocellular carcinoma (HCC), which is the most frequent liver cancer, is around 10%. The global mortality rate is proportional to the global incidence, highlighting the aggressiveness of the tumour and the poor efficacy of current therapies. Sorafenib, a multikinase inhibitor (VEGFR, PDGFR, RET, c-KIT, C-Raf, B-Raf), is the sole approved drug for patients with advanced HCC. In addition to its ability to induce cancer cell death, sorafenib is a potent anti-proliferative agent via the inhibition of growth factor receptors [279]. However, despite clinical trials showing that the median overall survival time with sorafenib is higher than with placebo (10.7 months vs 7.9 months), the outcomes are far from satisfactory [52]. Genetic heterogeneity of HCC and resistance to sorafenib are part of the explanations of the poor prognosis. To date, many mechanisms have been implicated in the failure to respond to sorafenib [57]. One of them is activation of the escape pathway of canonical RAF/MERK/ERK cascade. In addition, EGFR aberrant activation and the subsequent stimulation of PI3K/AKT pathway are such examples [58]. In this context, other mechanisms, such as JNK, Mcl-1, Mapk14, SDF-1α, Galectin-1, and Sirtuin 1 activations, have been reported as well [59-64]. Sorafenib resistance can also be acquired through its antiangiogenic activity as sustained sorafenib treatment induces an increased intratumour hypoxia, which leads to cell survival in a HIF-1α-dependent manner [65].

Despite the fact that several signalling pathways have been shown to be implicated in sorafenib primary and acquired resistance, the exact mechanisms are still incompletely understood. A better knowledge of chemoresistance mechanisms is primordial to improve the outcome of advanced-stage HCC patients. Indeed, unraveling new genes involved in sorafenib resistance in HCC could lead to the identification of new targetable candidates to treat HCC. In this study, we rendered three different HCC cell lines (HUH-7, PLC/PRF/5, and HepG2/C3A) resistant to sorafenib by long-term exposure to the drug. To identify novel mutations responsible for the resistance to sorafenib, exome sequencing was conducted on the parental cell lines and their matched sorafenib resistant counterpart. The results highlighted two already known genetic alterations, including p53 Y220C structural mutation and EGFR amplification. As a complementary approach, we performed a CRISPR/Cas9 screen to identify additional potential regulators of sorafenib-induced resistance. The screen highlighted KEAP1 as the top candidate. Dysregulation of KEAP1 cellular pathway has been shown to promote proliferation and chemoresistance in several cancer types including HCC [112, 280, 281].

MATERIALS AND METHODS

Cell lines

All cell lines were cultured in 5 % CO_2 at 37 °C. HepG2/C3A, PLC/PRF/5, and HUH-7 cells were cultured in Dulbecco's modified Eagle Medium (DMEM) (Gibco, Paisley, UK) supplemented with 10% heat-inactivated fetal bovine serum (FBS; Invitrogen, ref. no. 10270-106). The sorafenib resistant HepG2/C3A, PLC/PRF/5, and HUH-7 cells were maintained in DMEM plus 10% FBS with 5 μM sorafenib. They were rendered resistant by three months exposure to 5 μM sorafenib, a clinically relevant dose.

Chemical and antibodies

Sorafenib was purchased from LC laboratories (ref. no. S8502). The mouse anti-vinculin and the goat anti-vimentin antibodies were purchased from Sigma (ref. no. v9131 and v4630, respectively). The goat anti-EGFR antibody was purchased from Santa Cruz (ref. no. sc-03-G). The rabbit anti-p53 and anti-E-cadherin antibodies were purchased from Cell Signaling (ref. no. 9282 and 3195, respectively).

MTS (3-[4,5 dimethylthiazol-2-yl]-5-(3-carboxymethoxyphenyl)-2-(4-sulfophenyl)-2H-tetrazolium) assay

The MTS is a colorimetric assay that functions as an indicator of cell metabolic activity. The assay determines the presence of live cells with functional mitochondria and is commonly used to detect cell growth and proliferation. Briefly, cells were placed into 96-well plates. Subsequent to incubation overnight, the cultured cells were treated with varying concentrations of sorafenib for 72 hours. The combined MTS/PMS (phenazine methosulfate) solution (Promega ref. no. G5421) was added to each well and incubated for an additional 1 hour at 37ºC. The absorption was then measured at a wavelength of 490 nm by the Cytation 3 cell imaging multi-mode reader (BioTek Instruments).

Cell death measurement

Cell death was measured with propidium iodide (Sigma, ref. no. 81845). Cells were analyzed using a Beckman Coulter FC500 flow cytometer and data were analyzed with the Kaluza Version 1.2 software (Beckman Coulter).

Exome sequencing

All six cell lines were subjected to exome sequencing. Genomic DNA was extracted with Blood & Cell Culture DNA Midi Kit according to manufacturer's instructions (Qiagen, ref. no. 13343). Nucleic acid quality was assessed using the Fragment Analyzer (Advances Analytical Technologies Inc., Ankeny, USA). Exome sequencing libraries were performed as follows: 3 μg of genomic DNA was fragmented into 150-200 base pair fragments using the Covaris Sample Preparation System (S-series). Samples were prepared using SureSelect^{XT} library prep kit (Agilent, Santa Clara, USA). The resulting adaptor-tagged libraries were then hybridized with exons biotin-coated baits from the SureSelect V5 kit (Agilent) for 24 hours at 65°C. Hybrids were captured with streptavidin-coated beads, PCR amplified and indexed. Cluster generation was performed with the libraries using the Illumina HiSeq PE Cluster Kit v4 cBot reagents (Catalog number PE-401-400) and sequenced on the Illumina HiSeq 2500 using

HiSeq SBS Kit V4 reagents (Catalog number FC-401-4002). Sequencing data were processed using the Illumina Pipeline Software version 1.84.

Somatic mutation and copy number variation calling

Exome sequences were processed according to the Genome Analysis Toolkit (GATK) best practices pipeline, which involves trimming, alignment using BWA-MEM, marking of duplicates, local realignment around indels, and base recalibration [282]. Somatic single nucleotide polymorphisms (SNP) calling for each cell line was then achieved by comparing every resistant cell lines to its matched sensitive counterpart using both MuTect [283] and VarScan 2 [284] with default settings. Only the variants that were shared between MuTect and Varscan2 filtered output were kept and annotated using ANNOVAR [285]. Somatic copy number variation between resistant cell lines and their sensitive counterparts was achieved using the VEGAWES R package [286] and these calls were then used to create Circos plots [287]. In order to determine whether important genes were contained in the amplified and lost chromosomal regions, we made the intersection between the gain/lost genes and a cancer curated driver gene database from Rubio-Perez et al. [288].

Lentivirus production

Recombinant lentiviruses were produced as described [205] with the following modification: pMD.G and pCMVDR8.91 were replaced by pMD2.G and psPAX2, respectively.

Genome-scale CRISPR/Cas9 Knockout screening

The human GeCKO v2 library (2 plasmid system) (Addgene ref. no. 1000000049) was amplified by electroporation using the electroporation system (Bio-Rad Gene Pulser II ref. no. 165-2105) and the Lucigen Endura cells (ref. no. 60242). Cells were plated on LB Agar plate containing 100 µg/mL ampicillin. After 14 hours at 32°C, colonies were scrapped and plasmids recovered with the Plasmid Maxi kit (Qiagen, ref. no. 12162). To produce lentivirus library, 12 T-225 flasks were seeded with $12x10^6$ of HEK293T cells/flask. The day after, each flask was treated as follows: 10 µg pMD2.G, 30 µg psPAX2 and 25 µg GeCKO plasmid library were mixed with 250 mM $CaCl_2$. This solution was mixed (v/v) with 2x HEPES buffer (NaCl 280 mM, KCl 10 mM, Na_2HPO_4 1.5 mM, D-glucose 12 mM, HEPES 50 mM), incubated for 1 minute and added to the culture medium. Seven hours later, the medium was removed and replaced by DMEM supplemented with 10 % FBS and 1 % penicillin-streptomycin. Forty-eight hours later, the medium was collected and centrifuged for 5 min at 2000 g to pellet the cells. The supernatant was filtered through a 0.45 µm HV/PVDF (Millipore, ref. no. SE1M003M00) and concentrated 100x by ultracentrifugation (Beckman) at 24.000 rpm for 2 hours at 4°C. Virus pellet was resuspended in ice-cold PBS, aliquoted and stored at -80°C.

To express the Cas9 endonuclease, HUH-7 SR cells were infected with lentiCas9-Blast (Addgene, ref. no. 52962) and selected with 35 µg/mL blasticidin for a week.

The multiplicity of infection (MOI) of the GeCKO virus library was determined as follows: different volumes of virus library were added to 250,000 HUH-7 SR cells expressing Cas9 plated in a 6-well plate. Twenty-four hours later, each well was split into duplicate and one replicate received 10 µg/mL

puromycin for 3 days. Cell viability was determined by trypan blue exclusion and MOI was considered as the percentage of living cells. The virus volume yielding to MOI close to 0.3 was chosen. Large-scale infection of $12x10^7$ HUH-7 cells was carried out in 6-well plates with 250,000 cells per well. Twenty-four hours later, wells were pooled in a T-225 flask and infected cells selected with 10 µg/mL puromycin for a week. After puromycin selection, the cells were split into two. One part ($6x10^7$ cells) was left untreated. The second part ($6x10^7$ cells) was treated with 5 µM Sorafenib for 12 population doublings with a sorafenib renewal every 3 days. After 12 doubling times, control and sorafenib-treated surviving cells were collected, and their genomic DNA was extracted with Blood & Cell Culture DNA Midi Kit according to manufacturer's instructions (Qiagen, ref. no. 13343). A first PCR was performed to amplify the lentiCRISPR sgRNA region with the following primers:

F1: 5'-AATGGACTATCATATGCTTACCGTAACTTGAAAGTATTTCG-3'

R1: 5'-CTTTAGTTTGTATGTCTGTTGCTATTATGTCTACTATTCTTTCC-3

A second PCR was performed to attach Illumina adaptors and barcodes (green) to samples. 5 µL of the first PCR product was used. Primers for the second PCR include both a variable length sequence (red) to increase library complexity and an 8bp barcode for multiplexing of different biological samples.

Table 1. Primer sequences for the second PCR

F2a	AATGATACGGCGACCACCGAGATCTACACTCTTTCCCTACACGACGCTCTTCCGATCTTCTTGTGGAAAGGACGAAACACCG
F2b	AATGATACGGCGACCACCGAGATCTACACTCTTTCCCTACACGACGCTCTTCCGATCTAGCTCTTGTGGAAAGGACGAAACACCG
F2c	AATGATACGGCGACCACCGAGATCTACACTCTTTCCCTACACGACGCTCTTCCGATCTCGAGCTCTTGTGGAAAGGACGAAACACCG
F2d	AATGATACGGCGACCACCGAGATCTACACTCTTTCCCTACACGACGCTCTTCCGATCTCATAACCTCTTGTGGAAAGGACGAAACACCG
F2e	AATGATACGGCGACCACCGAGATCTACACTCTTTCCCTACACGACGCTCTTCCGATCTGTGCTAACGTCTTGTGGAAAGGACGAAACACCG
R2_iC_26	CAAGCAGAAGACGGCATACGAGATGCTCATGTGACTGGAGTTCAGACGTGTGCTCTTCCGATCTTCTACTATTCTTTCCCCTGCACTGT
R2_iA_12	CAAGCAGAAGACGGCATACGAGATTACAAGGTGACTGGAGTTCAGACGTGTGCTCTTCCGATCTTCTACTATTCTTTCCCCTGCACTGT

Both PCR were performed in 100 µL with the Herculase II Fusion DNA Polymerase (Agilent, ref. no. 600675). Amplicons were gel extracted, quantified, mixed and sequenced with a MiSeq (Illumina). Raw FASTQ files were demultiplexed and processed to contain only the unique sgRNA sequence. The number of reads of each sgRNA was normalized as described [206]. The MAGeCK algorithm [207] was used to rank screening hits by the consistent enrichment among multiple sgRNAs targeting the same gene.

RESULTS

Establishment of sorafenib resistant PLC/PRF/5, HepG2/C3A, and HUH-7 cell lines

To investigate mechanisms of acquired sorafenib resistance, we established three sorafenib resistant (SR) HCC cell lines derived from wild-type PLC/PRF/5, HepG2/C3A, and HUH-7 cells by three months exposure to 5 μM sorafenib, a clinically relevant dose. As sorafenib can induce both decreased proliferation and tumour cell death, acquired resistance can target one of these two properties separately or at the same time. However, firstly only the acquisition of an anti-proliferative resistance was confirmed in the three populations using cell growth as a readout. Figure 1 shows that even though sorafenib affects greatly the growth of the wild-type cells in a dose-dependent manner, the matched resistant ones are almost not sensitive to the drug. These data indicate that after three months of treatment with sorafenib, PLC/PRF/5, HepG2/C3A, and HUH-7 became resistant to the drug. Of note, results depicted in Figure 1 are technical triplicates from a single experiment.

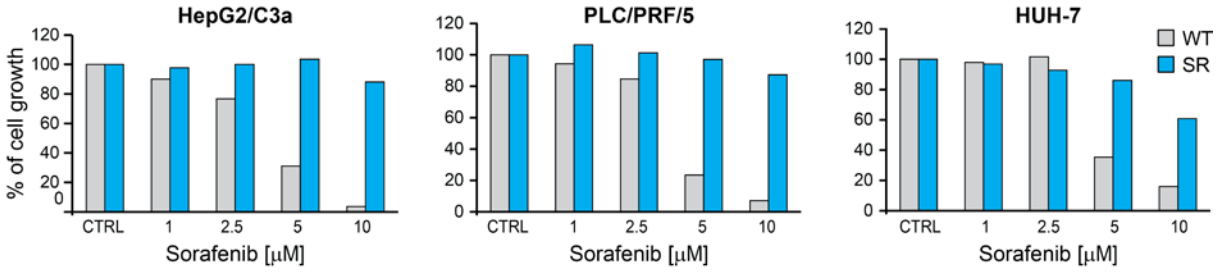

Figure 1. Validation of sorafenib resistant cell lines. Specified HCC cell lines were treated with sorafenib at indicated concentrations for 72 hours. Cell growth was assessed by MTS assay. Results correspond to the mean of technical triplicates compared to the respective control.

Genetic changes in sorafenib resistant cell lines compared to the matched sensitive ones

To assess the genetic alterations responsible for acquired resistance to sorafenib, we extracted DNA from three HCC wild-type cell lines (PLC/PRF/5, HepG2/C3A, and HUH-7) and their matched sorafenib resistant derivatives. We then conducted exome sequencing using the Illumina technology to compare mutation profiling of baseline and matched resistant cell lines. We achieved a median coverage above 50x. Supplementary figure S1 depicts the distribution of the depth of sequencing coverage. Characteristics of non-synonymous mutations present in sorafenib resistant cell lines are shown in the Supplementary Table S1.

Exome sequencing data revealed genetic alterations such as ATP7A and p53 Y220C structural mutations as putative causes of sorafenib resistance in HepG2/C3A SR cells

Exome sequencing analyses on HepG2/C3A SR and wild-type cells identified four somatic mutations. Among them, there was the p53 Y220C structural mutation (Figure 2). Y220C missense mutation causes conformational instability of p53 protein [289]. This genetic alteration has been reported to induce chemoresistance in many tumour types such as neuroblastoma or ovarian cancer [290, 291]. Although it has not been described to be involved in acquired resistance specifically, loss-of-function mutations in p53 were reported to confer intrinsic sorafenib resistance [292].

To study the involvement of p53 mutation in the resistant phenotype of HepG2/C3A SR cells, we planned to rescue mutated p53. In order to assess the effect of the rescue experiment in both anti-proliferative and cell death resistance to sorafenib, we measured cell death and cell growth in the presence of the drug. Unexpectedly, Supplementary Figure S2A illustrates that HepG2/C3A SR and PLC/PRF/5 SR cell lines lost their resistant phenotype, although all three SR cell lines were always kept in culture in the presence of sorafenib. Of note, results showed in Figure 1 and those represented in Supplementary Figure S2 were obtained in two different laboratories by two different experimenters at three months interval. To reach the same growth inhibitory effect in the three HCC wild-type cells as in Figure 1, the dose of sorafenib was 4-fold higher in Supplementary Figure S2A. We used, nevertheless, the same batch of sorafenib in both experiments. However, at concentrations where the wild-type cells have reduced cell growth, the HepG2/C3A SR and PLC/PRF/5 SR cells did not display any resistance to sorafenib. We observed the same effect regarding the cell death induced by the multikinase inhibitor, except in HepG2/C3A at 20 µM sorafenib (Supplementary Figure 2B). Two main hypotheses that are not mutually exclusives could explain these results. Either a genetic drift occurred in the two SR cell lines, or wild-type cells were not sensitive to sorafenib anymore, despite the fact that they have never been in contact with this drug previously. One could hypothesize that the serum used in the experiment depicted in Supplementary Figure S2 was less prone to promote the cellular entry of sorafenib than the one employed in the experiment illustrated in Figure 1. Interestingly, HUH-7 SR cells were still resistant to the drug compared to their sensitive counterpart (Supplementary Figures S2A and S2B).

Although we were unable to validate the involvement of p53 Y220C mutation by a rescue experiment, exome sequencing results in HepG2/C3A SR cells are not called into question by a potential genetic drift. Indeed, we extracted the DNA that was used to conduct exome sequencing directly after having received cells from Olivier Dormond laboratory. Henceforth, the contribution of the destabilised p53 in sorafenib resistance remains to be validated.

Importantly, Supplementary Table S1 reports that the frequency of the p53 Y220C mutation in the SR population is 21.57%. This means that only about one-fifth of HepG2/C3A SR cells bear the mutation. Accordingly, other genetic alterations should be involved in the acquired resistance to sorafenib. Among mutations revealed by exome sequencing data, the ATP7A copper-transporting P-type adenosine triphosphatase has been described to confer multidrug resistance [293-296]. Although it

was not reported to be directly implicated in sorafenib resistance, it could be a good candidate to investigate in more detail. These preliminary results suggest that sorafenib resistance is a complex, heterogeneous, and multifactorial phenomenon.

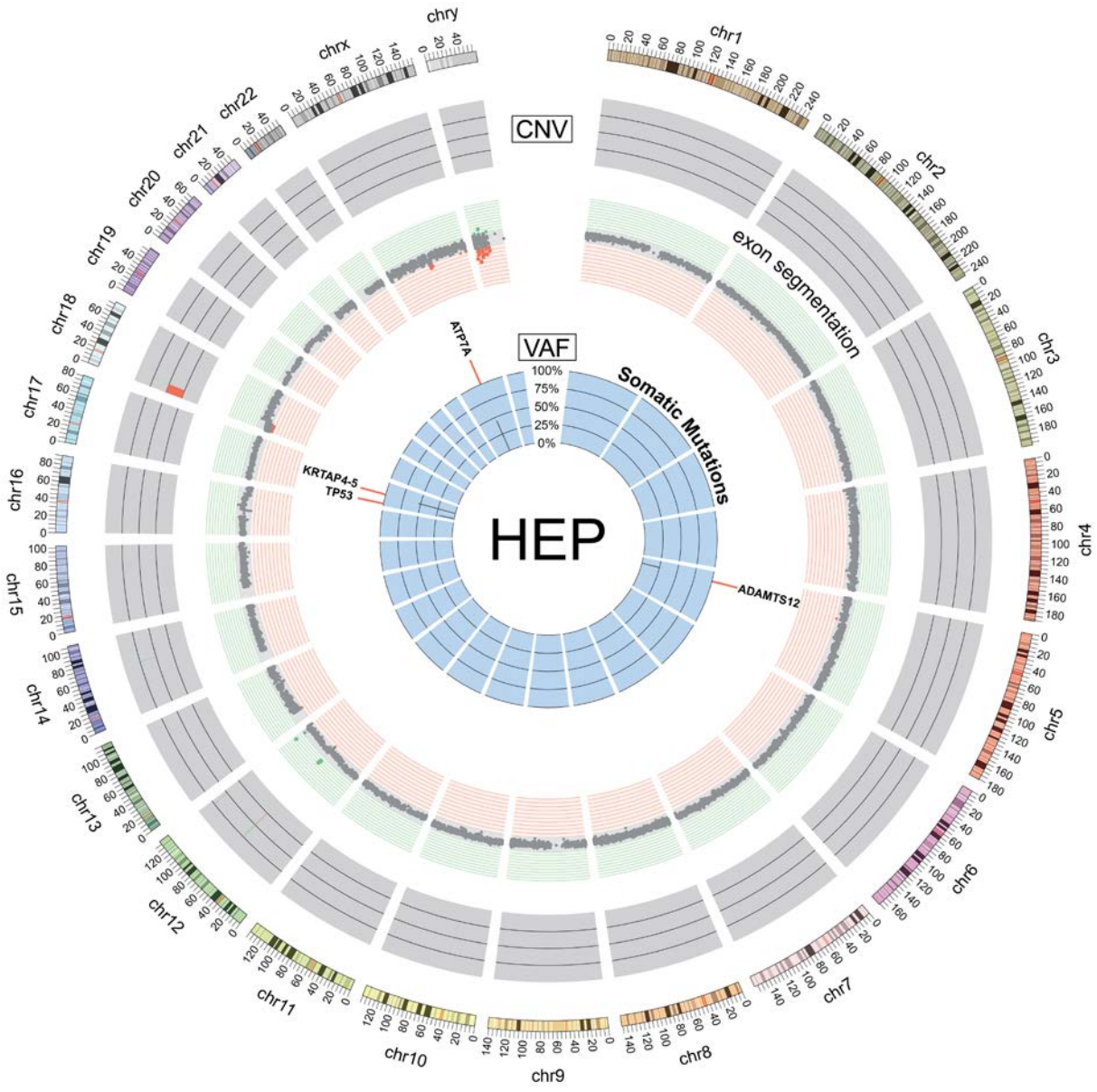

Figure 2. Circos plot depicting copy number variations and somatic mutations in HepG2/C3A SR cell line. Outer ideogram runs clockwise from chromosome 1 (chr1) to chromosome Y (chry) with labels in Mb of physical distance. The data are represented in several tracks. The innermost track represents somatic mutations with their respective variant allele frequency (VAF) detected in the exome sequencing data. The next central track shows exon segmentation (in log2 of the resistant/sensitive depth ratio). The outer track depicts somatic copy number variation (CNV) calls. Green bands represent amplifications and red bands represent loss/deletions.

PLC/PRF/5 acquired sorafenib resistance is probably due to several concomitant mutations including EGFR amplification

Exome sequencing results obtained from PLC/PRF/5 SR and wild-type cell lines identified several somatic mutations as well as the amplification and deletion of several regions of the exome (Figure 4).

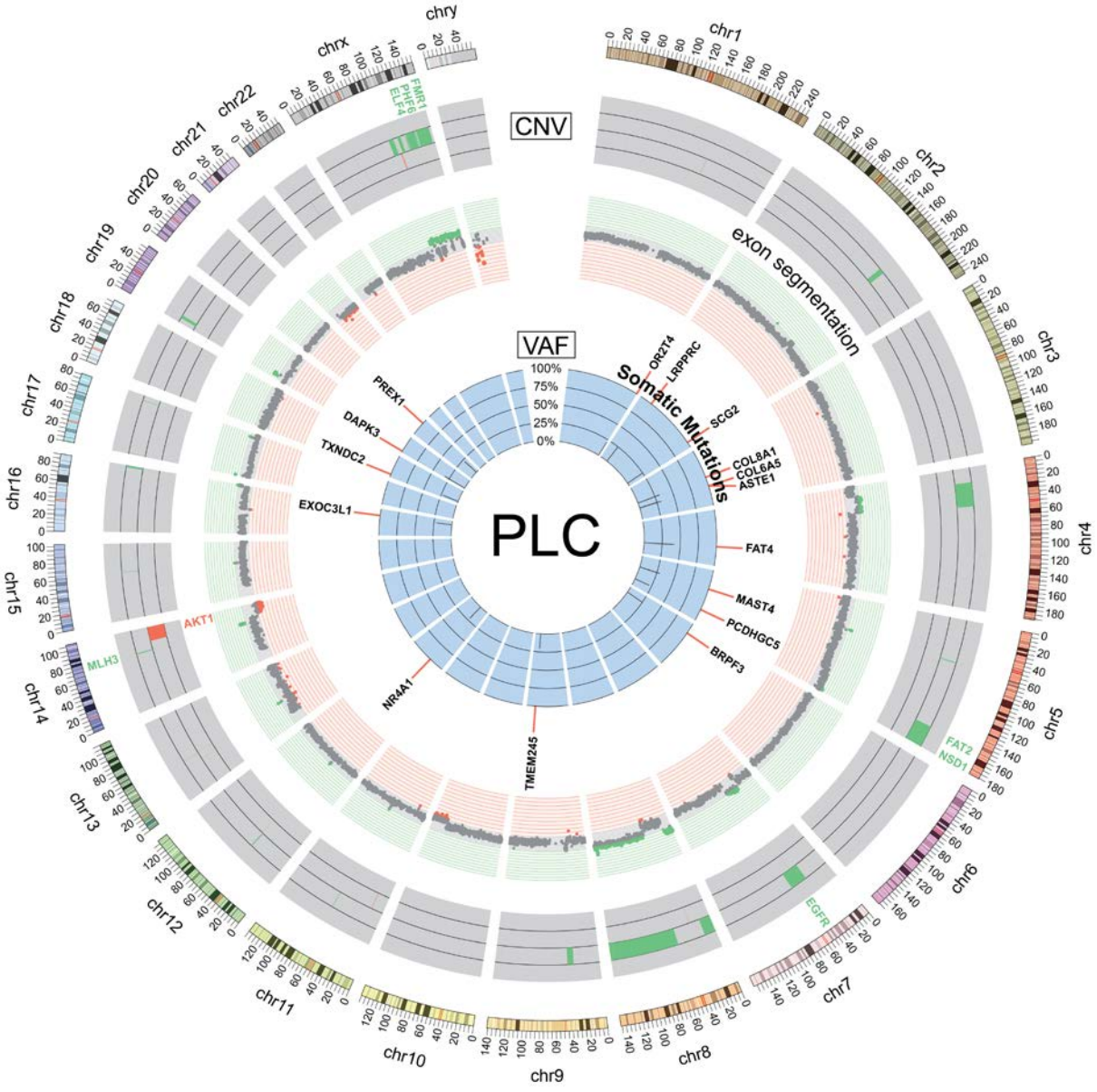

Figure 4. Circos plot depicting copy number variations and somatic mutations in PLC/PRF/5 SR cell line. Outer ideogram runs clockwise from chromosome 1 (chr1) to chromosome Y (chry) with labels in Mb of physical distance. The data are represented in several tracks. The innermost track represents somatic mutations with their respective variant allele frequency (VAF) detected in the exome sequencing data. The next central track shows exon segmentation (in log2 of the resistant/sensitive depth ratio). The outer track depicts somatic copy number variation (CNV) calls. Green bands represent amplifications and red bands represent loss/deletions. Potential driver genes contained within amplified or deleted regions are highlighted in green or red, respectively.

Among these genetic alterations, the amplification of the epidermal growth factor receptor (EGFR) gene has been already shown to be involved in primary and acquired resistance of HCC to sorafenib [58, 297, 298]. Unfortunately, likewise in HepG2/C3A cells, we were unable to validate the involvement of EGFR amplification in sorafenib resistance because of the occurrence of a potential genetic drift in PLC/PRF/5 SR cells (Supplementary Figure S2).
In addition, PREX1, DAPK3, NR4A1, LRPPRC, and NSD1, whose genomic alterations in PLC/PRF/5 SR cells were highlighted by exome sequencing, have been previously reported to play a role in resistance to several chemotherapeutic agents [299-304]. As the frequency of each specific mutation was not higher than 42% of PLC/PRF/5 SR cells, this means that the resistant phenotype of the population was secondary to several concomitant mutations. Consequently, further experiments are required to investigate the involvement of each genetic alteration in sorafenib resistance specifically.

The epithelial to mesenchymal transition is not involved in HUH-7 acquired sorafenib resistance

The circos plot of exome sequencing data conducted on HUH-7 wild-type and SR cells depicts numerous mutations induced by sorafenib treatment (Figure 6). Among them, we identified mutations in genes involved in the epithelial-mesenchymal transition (EMT) such as E-cadherin (CDH1), collagen (COL15A1), and laminin (LAMA4) (Figure 6). EMT referrers to the conversion of cells with an epithelial phenotype into cells with a mesenchymal phenotype [305]. It is the consequence of the loss of E-cadherin adhesion receptors that mediate cell-to-cell interaction [306]. The extracellular matrix (ECM), which is a network composed of proteoglycans, polysaccharides, and fibers mainly constituted by fibronectin, vitronectin, collagen, and laminin, plays a crucial role in EMT [307]. Indeed, ECM proteins promote EMT and are used as biomarkers of this process [308]. Finally, several reports highlight the major contribution of EMT to cancer drug resistance including sorafenib [59, 309-311].
In order to investigate whether EMT contributes to sorafenib resistance in HUH-7 cells, we evaluated the expression of EMT markers between HUH-7 SR cells and their matched sensitive counterpart. EMT is characterized by decrease in the expression of the epithelial marker E-cadherin and an increased expression of the mesenchymal marker vimentin. Western blot analyses indicated no change in the abundance of E-cadherin and vimentin proteins between both HUH-7 wilde-type and SR cell lines (Figures 7A and 7B). The absence of E-cadherin downregulation observed by western blot in HUH-7 SR cells, whereas exome sequencing results depicted a deletion of CDH1 in those cells, could be explained by the occurrence of some mechanisms of compensation (e.g. increased RNA stability, increased expression of other remaining gene copies).
Moreover, we tested the contribution of EMT in the two other SR cell lines and the matched wild-type cells. Figures 7A and 7B show that the SR cell lines do not display any EMT phenotype.

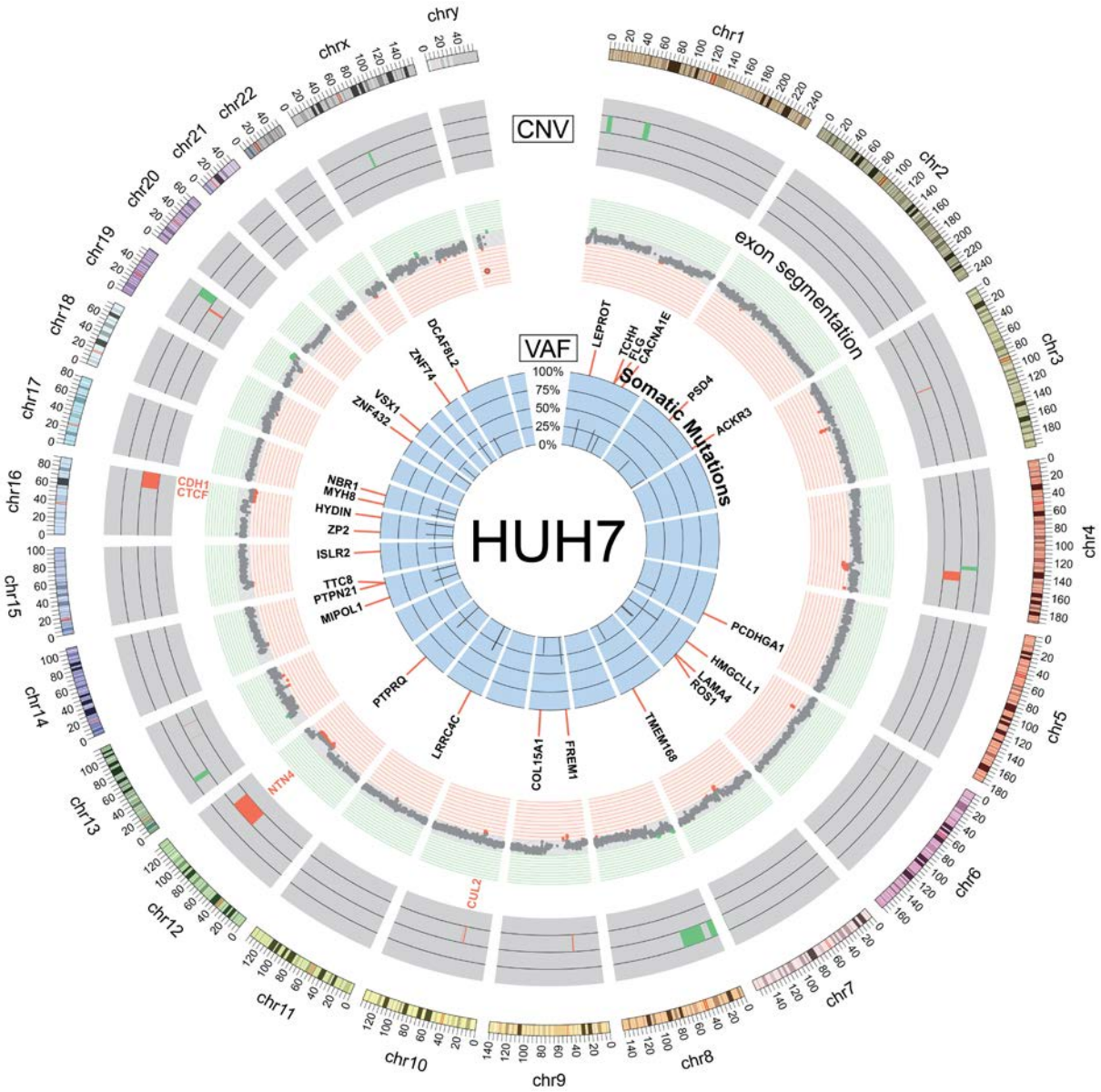

Figure 6. Circos plot depicting copy number variations and somatic mutations in HUH-7 SR cell line. Outer ideogram runs clockwise from chromosome 1 (chr1) to chromosome Y (chry) with labels in Mb of physical distance. The data are represented in several tracks. The innermost track represents somatic mutations with their respective variant allele frequency (VAF) detected in the exome sequencing data. The next central track shows exon segmentation (in log2 of the resistant/sensitive depth ratio). The outer track depicts somatic copy number variation (CNV) calls. Green bands represent amplifications and red bands represent loss/deletions. Potential driver genes contained within amplified or deleted regions are highlighted in green or red, respectively.

As for the two previous HCC cell lines, other genetic alterations that are illustrated in the HUH-7 circos plot have been shown to be involved in mechanisms of cancer resistance, such as NTN4, COL15A1, ROS1, and CACNA1E [312-315].

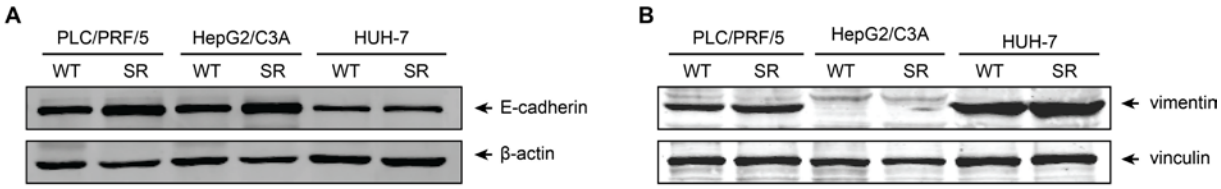

Figure 7. SR cell lines do not display an epithelial to mesenchymal transition phenotype. A. Western blot analyses of E-cadherin abundance in indicated cell lines. β-actin was used as protein loading control. **B.** Western blot analyses of vimentin abundance in indicated cell lines. Vinculin was used as protein loading control.

CRISPR/Cas9 screen identifies KEAP1 as a putative gene involved in sorafenib anti-proliferative activity

As a complementary approach to exome sequencing, we performed a loss-of-function CRISPR/Cas9 screen on HUH-7 SR cell line. By using a negative selection screen, we sought to identify genes whose inactivation is detrimental to the resistant cells. Such genes can be recognized by a decrease in the abundance of corresponding sgRNAs during the course of the sorafenib treatment. Consequently, genes for which the targeted sgRNAs would be depleted compared to the control are those required for the cell to be resistant to sorafenib.

HUH-7 SR cells were infected with the GeCKO v2 human CRISPR/Cas9 lentiviral library [203]. Half of the infected cells were treated with 5 µM sorafenib for 12 population doublings. According to the literature, this number of doubling times should ensure sufficient depletion of genes required for resistance [316]. The other half of the cells was left untreated for 12 population doublings to serve as a control. Then, the sgRNAs present in both the resistant and the control populations were sequenced by high-throughput sequencing to determine their relative abundance. As a supplementary control, the sgRNAs of $3x10^6$ HUH-7 SR infected cells were sequenced before starting the experiment. This ensures that the difference seen between both treated and non-treated HUH-7 SR after 12 doubling times is due to the effect of sorafenib, and not to a depletion of sgRNAs in the control population secondary to several splitting steps and long-term culture conditions.

Results of massively parallel sequencing did not reveal any significantly depleted genes in HUH-7 SR treated with sorafenib compared to the non-treated population. Nevertheless, one candidate gene named KEAP1 was significantly enriched in the sorafenib treated population after 12 doubling times. The plot of Figure 8A depicts the only significant candidate gene obtained using the Model-based Analysis of Genome-wide CRISPR/Cas9 Knockout (MAGeCK) algorithm. The frequency of each sgRNA in both untreated and treated populations is displayed in Figure 8B. The six sgRNAs for KEAP1 are labeled in blue.

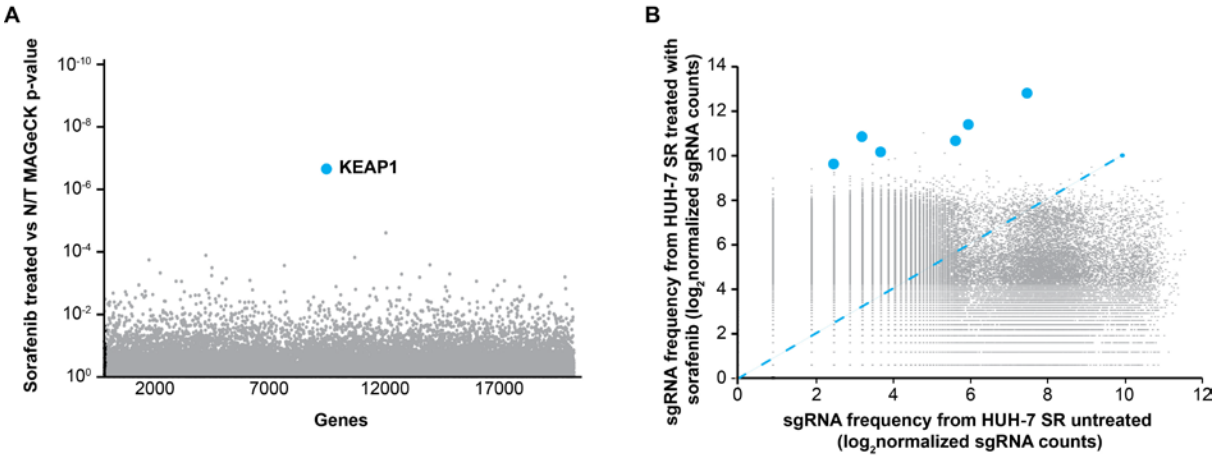

Figure 8. GeCKO screen in HUH-7 SR cells reveals KEAP1 whose loss confers sorafenib resistance. **A.** Identification of KEAP1 gene implicated in sorafenib resistance using the MAGeCK p-value in HUH-7 SR cells. **B.** Scatterplot showing enrichment of six sgRNAs targeting KEAP1 gene after sorafenib treatment in HUH-7 SR cells. Blue dots indicate the six sgRNAs targeting KEAP1 gene. The blue dashed line represents the equal frequency in both untreated and treated populations.

As the dose of sorafenib used for the screen (5 µM) was shown to not induce cell death in HUH-7 SR population (Supplementary Figure S2), the enrichment of sgRNAs targeting KEAP1 gene is due to the selective advantage of KEAP1 knockout cells to proliferate in sorafenib-rich conditions. Accordingly, in HUH-7 SR cells, KEAP1 is not responsible for acquired resistance to the killing activity of sorafenib but is involved in the anti-proliferative resistance to the tyrosine kinase inhibitor. Supplementary Figure S3 shows that there is no enrichment of sgRNAs targeting KEAP1 in untreated HUH-7 SR cells after 12 population doublings compared to the population that did not undergo any doublings. This means that the deletion of KEAP1 confers a proliferative advantage only in the presence of sorafenib.

To validate the involvement of KEAP1 in the anti-proliferative activity of sorafenib, HUH-7 as well as PLC/PRF/5 and HepG2/C3A KEAP1 knockout clones are currently being generated.

DISCUSSION

Intrinsic and acquired resistances to sorafenib are mainly responsible for the poor outcome of patients suffering from advanced-stage HCC. As the exact mechanisms of sorafenib resistance remain to be better understood, we conducted an analysis of genetic alterations occurring in cell lines that were previously rendered resistant to the multi-targeted tyrosine kinase inhibitor.

Results of exome sequencing in PLC/PRF/5 cell lines highlighted EGFR amplification as a potential genomic alteration responsible for sorafenib resistance. This mutation was already described to be involved in primary and acquired resistance of HCC to sorafenib [58, 297, 298]. Although these results lack innovation, they nevertheless validate the efficiency of exome sequencing approach to bring out genomic modification due to acquired sorafenib resistance. Unfortunately, we were unable to validate the involvement of EGFR amplification in sorafenib resistance, probably due to an occurrence of a genetic drift in two (PLC/PRF/5 and HepG2/C3A) out of the three cell types studied.

In HepG2/C3A SR cells, we identified Y220C mutation of p53 as a putative mechanism of sorafenib resistance. P53 is the most frequently altered gene in human cancers and up to 58% of HCCs may harbour mutations in this tumour suppressor gene [317]. Its role in treatment resistance was described in many cancer types [290, 291, 318]. Loss-of-function p53 mutations are responsible for intrinsic sorafenib resistance. Indeed, the inactivation of p53 gene decreases the susceptibility of cells to apoptosis in a hypoxic environment. Therefore, in the absence of p53, tumours may be less dependent on their vascular supply rendering them less responsive to antiangiogenic therapies [292]. Nevertheless, to our knowledge, this mutation was not yet described to be implicated in acquired sorafenib resistance. Again, because of the existence of a potential genetic drift, we could not perform the rescue experiment that would allow us to validate the role of p53 mutation in HepG2/C3A resistance to sorafenib. As an alternative approach, we could overexpress the Y220C p53 mutant in wild-type cells and assess whether it is sufficient to induce resistance.

Finally, exome sequencing data revealed several mutations present in HUH-7 SR cells but not in their wild-type sensitive counterpart. Except for mutations in E-cadherin, laminin, and collagen genes, none of them have been described in the literature to be involved in sorafenib resistance. E-cadherin, laminin, and collagen are known to mediate EMT process [305]. However, results suggest that the mechanism of sorafenib resistance in HUH-7 SR cells is independent of EMT. Consequently, to decipher which one(s) of all the mutations highlighted by exome sequencing is (are) more prone to mediate sorafenib resistance, we are going to use two Web open platforms cBioPortal (www.cbioportal.org) and COSMIC (cancer.sanger.ac.uk) that provide large-scale cancer genomics data sets, including annotations of mutations defined in the literature as resistance mutations [319, 320]. Of note, the same approach will be used for the mutations revealed in HepG2/C3A SR and PLC/PRF/5 SR cell lines.

As a complementary approach to exome sequencing, we performed genome-wide CRISPR/Cas9 screen on HUH-7 SR cell line. The aim was to identify genes required for the acquired resistance to sorafenib. However, the negative selection screen did not reveal any significantly depleted genes. Several reasons could explain this result. First, the dose of sorafenib used (5 µM) was shown (later) to be too low to induce cell death even in the wild-type sensitive HUH-7 cells (Supplementary Figure S2). Consequently, cells carrying the sgRNAs targeting genes involved in sorafenib resistance will not be killed by sorafenib at this concentration. Then, negative selection screen has to be carried out a large scale to guarantee that entire library is represented multiple times over, ensuring sufficient sensitivity for depleted sgRNAs to be deducted from the final cell population. Presumably, using $6x10^7$ cells per condition was not satisfactory to reach enough sensitivity. Finally, negative selection screen requires efficient sgRNAs. Indeed, depletion of a sgRNA can only be recognized if the targeted gene is cleaved and inactivated in a large proportion of the cells carrying the sgRNA. This third possibility seems less likely to be the cause of the screen failure since several papers report the use of the same CRISPR/Cas9 library to perform their successful negative selection screens [203, 209]. Nevertheless, the screening performed in HUH-7 SR cells revealed a significant enrichment of KEAP1 sgRNAs in the treated population. This suggests that KEAP1 knockout cells bear a selective advantage to proliferate under sorafenib treatment. Accordingly, KEAP1 seems to be involved in the anti-proliferative activity of sorafenib rather than in its capacity to induce cancer cell death.

The KEAP1-NRF2 regulatory pathway plays a central role in cell defense against oxidative damage. Upon exposure to oxidative stress, the nuclear factor erythroid 2-related factor 2 (NRF2) transcription factor activates the expression of many cytoprotective proteins, including drug-efflux pumps, antioxidant proteins, and drug-metabolizing enzymes [321-324]. The intracellular level of NRF2 is regulated by the Cul3-KEAP1 ubiquitin E3 ligase complex, which degrades NRF2 in proteasomes preventing it from moving to the nucleus [325, 326]. KEAP1 somatic mutations were detected in many tumour types including HCCs [327-329]. Cancer cells bearing loss-of-function KEAP1 mutations display NRF2 overexpression and subsequent transcriptional upregulation of cytoprotective proteins [329, 330]. The constitutive activation of NRF2, that stimulates detoxification and antioxidant enzymes, increases resistance against anti-cancer treatment including sorafenib [112, 280, 281]. Moreover, Zhang et al. report that NRF2 promotes proliferation in HCC [331]. Consequently, our results are in line with the literature and suggest that loss-of-function mutation of KEAP1 upregulates NRF2 that promotes cell proliferation in HCC. To validate this hypothesis HUH-7 as well as PLC/PRF/5 and HepG2/C3A KEAP1 knockout clones are currently being generated. In addition, we will assess if the proliferative effect of KEAP1 mutation depends on NRF2 activity.

To conclude, using exome sequencing analysis we identified EGFR amplification and Y220C destabilized mutation of p53 as already known causes of sorafenib resistance. In addition, we showed that, in the presence of sorafenib, KEAP1 knockout HUH-7 SR cells display selective proliferation advantage. Finally, we are still working on the analysis of the different genomic mutations revealed in the three SR HCC cell lines. Hopefully, we will unveil a novel mechanism of sorafenib resistance.

Interestingly, none of the genetic alterations was common to the three SR cell lines. These data shed light on the complexity and the multifactorial process of acquired sorafenib resistance.

SUPPLEMENTARY TABLE AND FIGURES

	chromosome	gene	exon	nt_normal	nt_variant	aa	comments
HepG2/C3A	5	ADAMTS12	23	C	A	p.K1532N	Var_Freq=25.53% ; NormRef=57;NormVar=0;TumRef=35;TumVar=12 ; pval=3.02276334925652e-05
	17	TP53	6	T	C	p.Y220C	Var_Freq=21.57% ; NormRef=43;NormVar=0;TumRef=40;TumVar=11 ; pval=0.000689808997416789
	17	KRTAP4-5	1	A	T	p.C79S	Var_Freq=52.94% ; NormRef=12;NormVar=0;TumRef=8;TumVar=9 ; pval=0.00242735774969656
	X	ATP7A	10	C	T	p.H741Y	Var_Freq=44.93% ; NormRef=63;NormVar=0;TumRef=38;TumVar=31 ; pval=2.75786606748935e-11
PLC/PRF/5	1	OR2T4	1	C	T	p.H208Y	Var_Freq=21.32% ; NormRef=205;NormVar=0;TumRef=107;TumVar=29 ; pval=3.60522885059006e-13
	2	LRPPRC	36	C	T	p.E1313K	Var_Freq=25% ; NormRef=43;NormVar=0;TumRef=33;TumVar=11 ; pval=0.000273853549899687
	2	SCG2	2	A	G	p.M147T	Var_Freq=25.84% ; NormRef=119;NormVar=0;TumRef=66;TumVar=23 ; pval=5.18518296722473e-10
	3	COL8A1	5	C	A	p.L236I	Var_Freq=31.58% ; NormRef=92;NormVar=0;TumRef=52;TumVar=24 ; pval=5.13625445082996e-10
	3	COL6A5	24	C	T	p.P1611L	Var_Freq=28% ; NormRef=26;NormVar=0;TumRef=18;TumVar=7 ; pval=0.00415201541609537
	3	ASTE1	3	T	G	p.I372L	Var_Freq=31.48% ; NormRef=45;NormVar=0;TumRef=37;TumVar=17 ; pval=8.54287570245387e-06
	4	FAT4	17	G	T	p.R4814M	Var_Freq=41.38% ; NormRef=33;NormVar=0;TumRef=17;TumVar=12 ; pval=2.40241927500685e-05
	5	MAST4	5	T	C	p.L134S	Var_Freq=28.77% ; NormRef=86;NormVar=0;TumRef=52;TumVar=21 ; pval=1.3010717388905e-08
	5	PCDHGC5	1	C	A	p.P569Q	Var_Freq=21.21% ; NormRef=68;NormVar=0;TumRef=52;TumVar=14 ; pval=2.26529529099562e-05
	6	BRPF3	5	C	G	p.P610A	Var_Freq=25.32% ; NormRef=67;NormVar=0;TumRef=59;TumVar=20 ; pval=1.30233798023623e-06
	9	TMEM245	8	T	C	p.S462G	Var_Freq=20% ; NormRef=27;NormVar=0;TumRef=16;TumVar=4 ; pval=0.0271634008914299
	12	NR4A1	3	C	G	p.L39V	Var_Freq=21.43% ; NormRef=111;NormVar=1;TumRef=99;TumVar=27 ; pval=1.22698734976333e-07
	16	EXOC3L1	5	C	T	p.A282T	Var_Freq=21.21% ; NormRef=45;NormVar=0;TumRef=26;TumVar=7 ; pval=0.00161703492633542
	18	TXNDC2	2	C	A	p.A394E	Var_Freq=22.02% ; NormRef=121;NormVar=1;TumRef=85;TumVar=24 ; pval=5.02051569717353e-08
	19	DAPK3	3	T	C	p.D81G	Var_Freq=31.58% ; NormRef=84;NormVar=0;TumRef=52;TumVar=24 ; pval=1.81421261591585e-09
	20	PREX1	30	T	G	p.Y1299S	Var_Freq=21.43% ; NormRef=22;NormVar=0;TumRef=22;TumVar=6 ; pval=0.0237082066869291
HUH-7	1	LEPROT	2	A	G	p.D3G	Var_Freq=38.14% ; NormRef=133;NormVar=0;TumRef=120;TumVar=74 ; pval=1.29621420350843e-20
	1	TCHH	3	T	C	p.D70G	Var_Freq=30.99% ; NormRef=67;NormVar=0;TumRef=49;TumVar=22 ; pval=6.8578681997738e-08
	1	FLG	3	T	C	p.K123R	Var_Freq=26.97% ; NormRef=104;NormVar=0;TumRef=65;TumVar=24 ; pval=1.24713756600968e-09
	1	CACNA1E	47	G	T	p.R2111I	Var_Freq=24.36% ; NormRef=60;NormVar=0;TumRef=59;TumVar=19 ; pval=6.58009999749085e-06
	1	CACNA1E	47	A	C	p.R2111S	Var_Freq=24.36% ; NormRef=58;NormVar=0;TumRef=59;TumVar=19 ; pval=8.85937690874239e-06
	2	PSD4	2	A	T	p.E124V	Var_Freq=21.61% ; NormRef=135;NormVar=0;TumRef=156;TumVar=43 ; pval=2.68391108649089e-11
	2	ACKR3	2	C	T	p.T341I	Var_Freq=21.05% ; NormRef=50;NormVar=0;TumRef=45;TumVar=12 ; pval=0.000285335917714085
	5	PCDHGA1	1	C	T	p.L505F	Var_Freq=27.94% ; NormRef=116;NormVar=1;TumRef=98;TumVar=38 ; pval=7.54555642503331e-11
	6	HMGCLL1	6	G	T	p.A209E	Var_Freq=51.43% ; NormRef=26;NormVar=0;TumRef=17;TumVar=18 ; pval=3.45784975955139e-06
	6	LAMA4	9	G	A	p.A326V	Var_Freq=21.59% ; NormRef=78;NormVar=0;TumRef=69;TumVar=19 ; pval=2.07936069440011e-06
	6	ROS1	29	G	A	p.P1607L	Var_Freq=20.48% ; NormRef=177;NormVar=0;TumRef=167;TumVar=43 ; pval=4.25113072871995e-13
	7	TMEM168	2	A	C	p.L20R	Var_Freq=22.92% ; NormRef=62;NormVar=0;TumRef=74;TumVar=22 ; pval=5.91900293031971e-06
	9	FREM1	17	C	G	p.G937R	Var_Freq=37.74% ; NormRef=61;NormVar=0;TumRef=33;TumVar=20 ; pval=2.10461395401582e-08
	9	COL15A1	16	G	T	p.E680X	Var_Freq=22.54% ; NormRef=59;NormVar=0;TumRef=55;TumVar=16 ; pval=2.63470174010994e-05
	11	LRRC4C	7	G	T	p.P389T	Var_Freq=36.89% ; NormRef=132;NormVar=0;TumRef=77;TumVar=45 ; pval=2.60838342230116e-17
	12	PTPRQ	2	A	G	p.I32M	Var_Freq=41.38% ; NormRef=39;NormVar=0;TumRef=17;TumVar=12 ; pval=7.12657956578534e-06
	14	MIPOL1	6	A	G	p.K41E	Var_Freq=34.19% ; NormRef=122;NormVar=1;TumRef=102;TumVar=53 ; pval=8.75765871130879e-15
	14	PTPN21	17	C	G	p.R1055T	Var_Freq=33.33% ; NormRef=66;NormVar=0;TumRef=58;TumVar=29 ; pval=6.73146329822748e-09
	14	TTC8	13	T	G	p.F383L	Var_Freq=29.41% ; NormRef=52;NormVar=0;TumRef=60;TumVar=25 ; pval=1.3335172208777e-06
	15	ISLR2	4	C	T	p.R458C	Var_Freq=33.33% ; NormRef=75;NormVar=0;TumRef=62;TumVar=31 ; pval=7.29446226296915e-10
	16	ZP2	19	T	C	p.E676G	Var_Freq=36.76% ; NormRef=66;NormVar=0;TumRef=43;TumVar=25 ; pval=2.97400278886949e-09
	16	HYDIN	74	G	T	p.Y4187X	Var_Freq=38.78% ; NormRef=53;NormVar=0;TumRef=30;TumVar=19 ; pval=9.4107509254498e-08
	17	MYH8	33	C	A	p.Q1510H	Var_Freq=33.09% ; NormRef=105;NormVar=1;TumRef=93;TumVar=46 ; pval=2.42556161290772e-12
	17	NBR1	21	A	G	p.T951A	Var_Freq=29.17% ; NormRef=63;NormVar=0;TumRef=51;TumVar=21 ; pval=3.73219376124505e-07
	19	ZNF432	5	C	T	p.G111R	Var_Freq=24.72% ; NormRef=45;NormVar=0;TumRef=67;TumVar=22 ; pval=4.48443891196936e-05
	20	VSX1	1	G	A	p.P46S	Var_Freq=21.62% ; NormRef=27;NormVar=0;TumRef=29;TumVar=8 ; pval=0.00872267906642771
	22	ZNF74	6	G	A	p.V249M	Var_Freq=34.19% ; NormRef=94;NormVar=1;TumRef=77;TumVar=40 ; pval=2.84743621850786e-11
	X	DCAF8L2	1	A	G	p.I346V	Var_Freq=27.4% ; NormRef=60;NormVar=0;TumRef=53;TumVar=20 ; pval=1.56870595424578e-06

Supplementary Table S1. Characteristics of nonsynonymous mutations present in sorafenib resistant cell lines. Var_Freq represents the frequency of the specific mutation in corresponding SR cell line (TumVar/(TumRef+TumVar)). Norm denotes wild-type cells and Tum denotes SR cells. Var represents the fold number that the mutation was detected either in wild-type (NormVar) or in SR (TumVar) cells. Ref represents the fold number that the non-mutated version of the gene was detected either in wild-type (NormRef) or in SR (TumRef) cells.

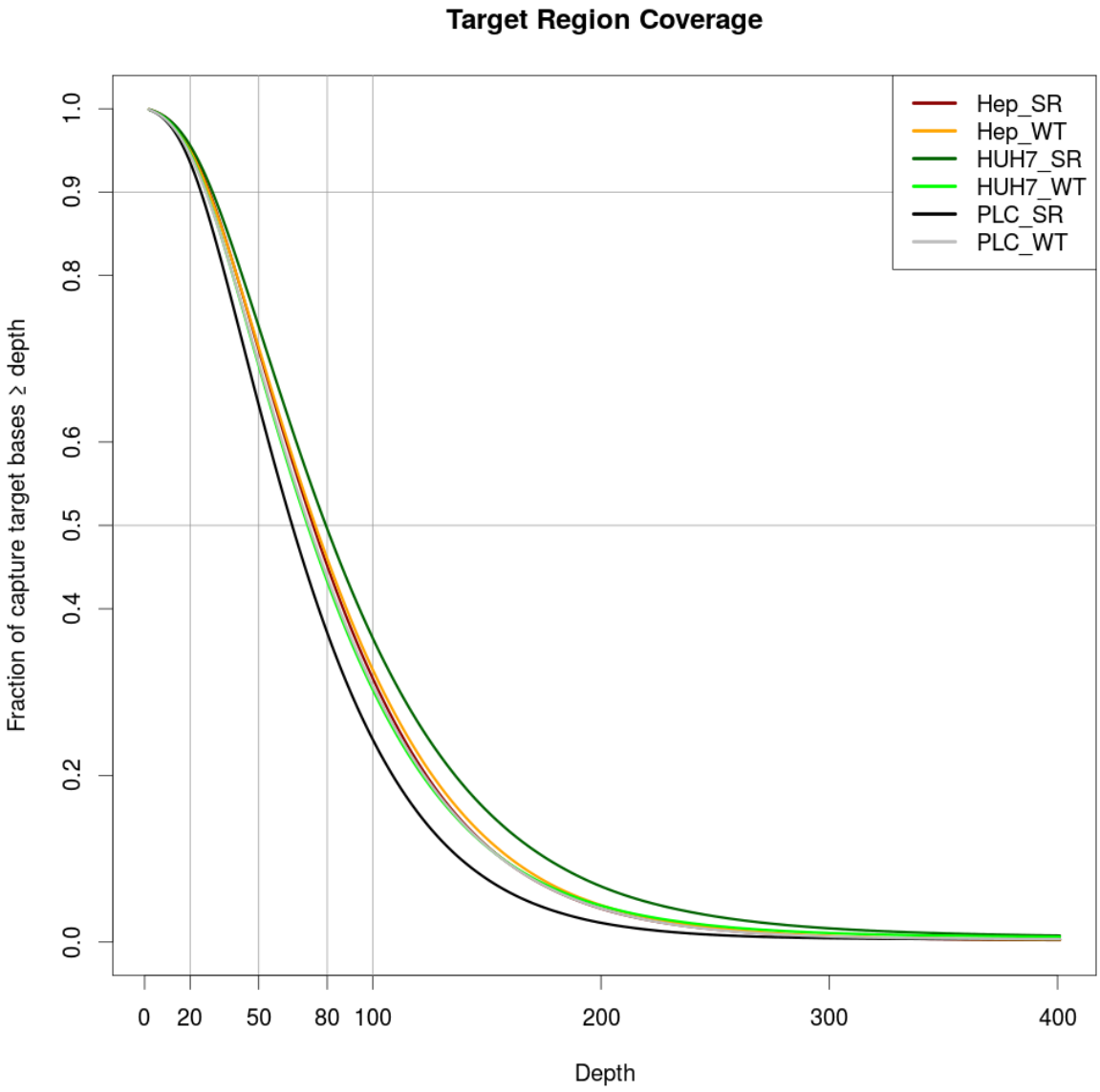

Supplementary Figure S1. Distribution of the depth of sequencing coverage. The lines depict the cumulative fraction of the target bases covered at or above the specified coverage. This shows that around 70% of target bases were covered with at least 50x sequencing reads.

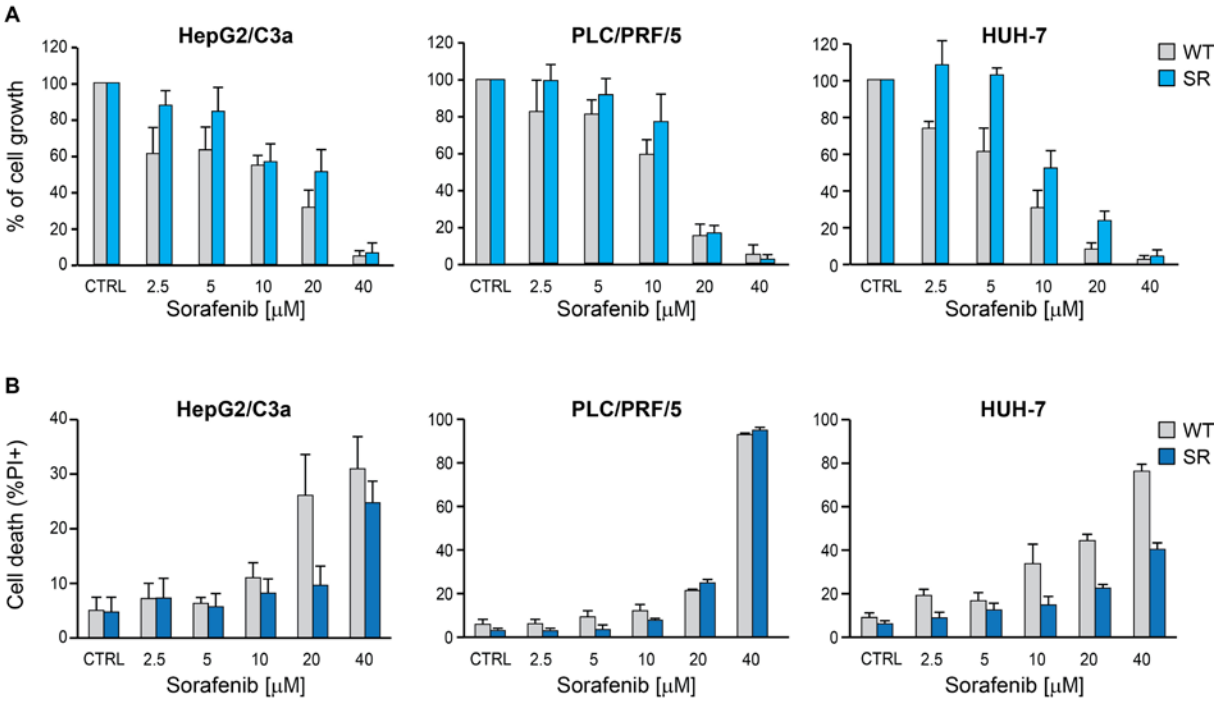

Supplementary Figure S2. HepG2/C3A and PLC/PRF/5 are subjected to a genetic drift inducing the loss of sorafenib resistant phenotype. **A.** Specified HCC cell lines were treated with sorafenib at indicated concentrations for 72 hours. Cell growth was assessed by MTS assay and compared to the control (CTRL). **B.** Specified HCC cell lines were treated with sorafenib at indicated concentrations for 48 hours. Cell death was assessed by flow cytometry after PI staining. Results correspond to the mean +/- 95% CI of three independent experiments.

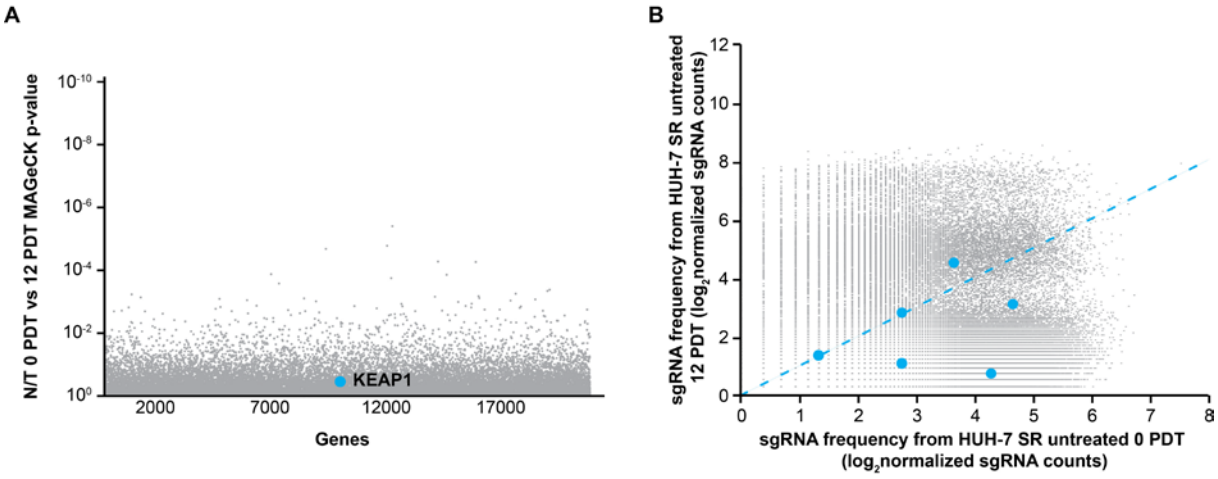

Supplementary Figure S3. GeCKO screen in HUH-7 SR PDT 0 vs PDT 12 reveals no enrichment of KEAP1. **A.** Identification of KEAP1 gene using the MAGeCK p-value in HUH-7 SR cells. **B.** Scatterplot showing the six sgRNAs targeting KEAP1 gene in HUH-7 SR cells at population doubling time (PDT) 0 versus PDT 12. Blue dots indicate the six sgRNAs targeting KEAP1 gene. The blue dashed line represents the equal frequency in both PDT 0 and PDT 12.

DISCUSSION

Cancer is one of the most dreadful diagnoses a patient can receive. Although many types of tumour are now considered curable thanks to advances in research, screening methods, and treatment modalities, cancer remains one of the deadliest diseases in the world. Fighting cancer starts with prevention strategies through the avoidance of risk factors (e.g. tobacco use, alcohol abuse, lack of physical activity, infection by HPV/HBV). However, whereas efficient, prevention is often not sufficient. Once diagnosed, several therapeutic strategies exist to treat malignant disease. Though, yet too many tumours are refractory to known treatments. To improve cancer outcome several approaches can be undertaken, including the improvement of the current anti-cancer therapies, the development of novel more efficient drugs, or the reduction of treatment associated long-term side effects.

Our laboratory developed more than ten years ago a peptide with anti-cancer potentials termed TAT-RasGAP$_{317-326}$. This ten amino acid peptide, derived from the RasGAP protein and coupled to the TAT cell-penetrating peptide, sensitizes adult cancer cells to various chemotherapies and radiotherapy [122]. In addition, it possesses the ability to prevent metastasis formation by hampering cell migration and invasion [124]. The present thesis reports the identification of two new features of TAT-RasGAP$_{317-326}$: its capacity to sensitize pediatric tumours to several chemotherapeutic agents and its ability to directly kill some cancer cells.

The biology and genetic of childhood cancers differ from adulthood tumours. Thus, most anti-cancer treatments developed to target specific pathways in adult malignancies may have only little or no benefit in pediatric patients. Moreover, childhood tumours are rare diseases with a subsequent slow rate of drug development [332]. One approach to overcome this hurdle is to study an anti-cancer drug for pediatric patients at the preclinical stage. We used this strategy in the first part of this thesis by studying the *in vitro* efficacy of TAT-RasGAP$_{317-326}$ to sensitize childhood tumours from various origins to chemotherapies. We show that the peptide sensitizes childhood cancer cells to genotoxins. However, it was not possible to predict the efficacy of this sensitization based on the tumour type and the drug used.

Moreover, we discovered a new feature of the RasGAP-derived peptide which is its ability to directly kill some adult and pediatric cancer cells. This novel property gave us the opportunity to investigate the mechanism of action of the peptide, which remained to be precisely determined, through the characterization of the mode of cell death triggered by it. Using pharmacological and genetic approaches, we found that cell death was not fully prevented when regulated forms of death including apoptosis, necroptosis, autophagy, parthanatos, and pyroptosis were inhibited. As a second approach to decipher the mode of action of the peptide, we performed a genome-scale knockout screen using CRISPR/Cas9 technology. The validated candidates highlighted by the screen were shown to be dispensable for the pro-death activity of the peptide. Indeed, results reported in the third part of this manuscript suggest that they are involved in the cytosolic access of the anti-cancer peptide. Consequently, how TAT-RasGAP$_{317-326}$ kills cancer cells remains unanswered. Our original hypothesis

that it induces regulated cell death rather than accidental death seems to be invalidated by our recent results. Some evidence suggest that the peptide triggers a form of necrosis. Thus, a new assumption is that TAT-RasGAP$_{317-326}$ once penetrated inside the cell could interact with some lipids of the inner leaflet of the plasma membrane, leading to membrane destabilization and cell lysis. NaD1, another cationic peptide is known to induce cell death by this mechanism [333]. This could explain the death kinetic of the peptide, which does not kill within minutes but requires few hours (between four and six) to induce cell death. Indeed, the peptide has to enter the cell and to accumulate sufficiently into the cytoplasm to display its cytotoxic activity. Another indication supporting the necrotic hypothesis is that the peptide is able to bind to several phosphatidylinositols (e.g. PIP2, PIP3, phosphatidylserine, and cardiolipin). These recent results were obtained by one of my colleague using membrane lipid strips. The peptide target being a lipid rather than a protein could explain the results obtained with the CRISPR/Cas9 screen, a technology not adapted to screen lipids. However, the absence of any proteins required for the pro-death activity in CRISPR/Cas9 screens could alternatively be explained by the fact that the target of TAT-RasGAP$_{317-326}$ is part of the pool of essential genes. Therefore, it will not be detectable through this unbiased approach. Of note, the results showing that the NB1 neuroblastoma cells treated with the peptide partially die through apoptosis are not necessarily in contradiction with the necrotic hypothesis. Indeed, it is possible that, in those particular cells, damages of the plasma membrane induced by the peptide trigger subsequently low level of apoptosis. Moreover, it has been described that changes in plasma membrane lipid composition occur in cancer cells [334-336]. This could explain why they are killed by the peptide, whereas healthy cells are not. Finally, another assumption to explain the peptide selectivity for cancer cells could be related to its uptake mechanism. Indeed, we have demonstrated that ion channels and pumps are involved in the cytoplasmic access of the peptide. They are also known to be implicated in the driving malignant cancer cell behaviour [337]. Accordingly, changes in their expression in tumour cells compared to normal cells have been described [338-341]. Thenceforward, their dysregulation in cancer cells could increase TAT-RasGAP$_{317-326}$ uptake allowing it to be in sufficient quantity to exert its toxicity. To investigate which one of the two speculations is correct, we could assess if the fluorescent version of the peptide is able to reach the cytoplasm of healthy cells as efficiently as it does in cancer cells.

One question that remains unanswered is to know whether the mechanisms used by TAT-RasGAP$_{317-326}$ to sensitize to chemotherapies are similar to those used to directly kill cancer cells. One evidence in favour of a distinct mechanism would be to find a cell line that is directly killed but not sensitize by the peptide or a cell line that is not killed even at high TAT-RasGAP$_{317-326}$ concentrations, but that is sensitized to chemotherapies. To address this point A549 cells could be used, since they are insensitive to high doses of peptide, and assess whether they are sensitized by it to chemotherapy. If the answer is positive this would argue in favour of a distinct mechanism. However, one hypothesis that would support a similar mode of action is that chemotherapeutic agents or radiotherapy could render peptide-induced cell death more efficient, for instance by lowering its IC_{50}. According to this assumption, it would be chemotherapeutic agents that would act as a sensitizer and not the opposite as we have always hypothesized. This would also explain why to sensitize cancer cells we usually use about four times lower dosage than to directly kill them.

One very interesting aspect revealed in the paper published in Oncotarget is that TAT-RasGAP$_{317-326}$ can kill in an apoptosis-independent manner. Indeed, most of the current non-surgical anti-cancer strategies are designed to induce cancer cell death, mainly through apoptosis. However, a cancer cell can mutate and adapt to become resistant to apoptosis. To decrease this risk of acquired resistance and consequently the relapse of the tumour, combinations of anti-cancer drugs have improved the success of some therapies. Another way to overcome cancer cell resistance to pro-apoptotic stimuli would be to trigger non-apoptotic cell death. Consequently, as TAT-RasGAP$_{317-326}$ has the ability to kill in a way distinct from apoptosis, it could efficiently complement the current anti-cancer strategies and hopefully would be less prone to treatment resistance.

Finally, TAT-RasGAP$_{317-326}$ could potentially have interesting clinical relevance. Indeed, it may benefit pediatric cancer patients by increasing the efficacy of anti-cancer therapies notably by allowing reductions in anti-cancer drug dosage and the associated treatment-induced side effects. As a direct cancer cell killer, it could also complement or be combined with existing anti-cancer drugs. However, some limitations still hamper its potential clinical use. As for peptides of less than 5 kDa, it is mostly extracted via the renal or hepatic routes preventing its sufficient accumulation into the tumour [342]. The bioavailability of the peptide has already been studied in nude mice bearing a xenograft HCT116 subcutaneous tumour. Although only 0.2% of the injected TAT-RasGAP$_{317-326}$ dose went into the tumour, this faint percentage was nevertheless sufficient to sensitize cancer cells to cisplatin toxicity [343]. However, the efficiency of this anti-cancer agent could be improved by preventing renal and hepatic excretion and by increasing the biodelivery of the peptide specifically into the tumour. Another major concern precluding the translation of this peptide into the clinics is the high concentration that we should use to reach an anti-tumour activity *in vitro*. Finally, we have recently observed that different calcium concentrations in the media can affect the direct killing activity of the peptide. This information is of importance since the calcemia can differ from one patient to another. Additional investigations are therefore required to improve the stability and the delivery of the peptide as well as the increase of our understanding of how it works with the final aim to one day translate this anti-cancer peptide into clinical applications.

One major concern in anti-cancer therapies is treatment resistance. An important factor behind treatment failure due to intrinsic and acquired resistance is intratumoral heterogeneity [344, 345]. Few remaining cells to certain treatment are then able to rebuild a tumour and their resistance is often associated with an increased aggressiveness and invasive behaviour. Cancer relapse secondary to drug resistance underscores the urgent need to better understand the mechanisms of resistance that could ultimately lead to the development of alternative therapies. In the fourth part of the present thesis, we aimed at finding out new genes involved in sorafenib resistance in hepatocellular carcinoma (HCC) using exome sequencing and CRISPR/Cas9 loss-of-function screening. Sorafenib is the only FDA-approved chemotherapeutic agent to treat advanced HCC. However, its efficacy is far from satisfactory with an overall survival of 11 months mostly due to its intrinsic and acquired resistance. Among the genetic alterations highlighted by exome sequencing data, p53 Y220C structural mutation and EGFR amplification have been already described to be involved in sorafenib resistance [58, 292,

297, 298]. Interestingly, the Y220C missense mutation causing conformational instability of the p53 protein is druggable. Indeed, the compounds PhiKan083 and PK7088 bind Y220C mutant with high affinity and stabilize the p53 protein [346-349]. Although they are not yet in clinical trials, they are very promising drugs, that could be used in combination with sorafenib. This strategy has been already applied to erlotinib, a potent EGFR inhibitor. A phase III clinical trial of sorafenib plus erlotinib in patients with advanced HCC concludes that erlotinib does not improve survival in patients with advanced HCC [350]. Although erlotinib does not seem to be indicated in first-line treatment, it could potentially benefit to patients with EGFR amplification as a second-line therapy. Therefore, tumour cells of each relapsed cancer should be sequenced in order to assess if the patient bears the EGFR amplification or not. Such therapeutic approach raised the new concept of personalized cancer medicine. Thanks to the drop in the cost of genome sequencing (from 1,000,000 in 2001 to around 1,000 nowadays), this concept will be achievable in a near future.

One limitation of our study is that we should have generated for each type of HCC cell line more than one sorafenib resistant derivative cell line. This would have allowed us to investigate whether, for a given cell line, it is always the same mutation that is responsible for the resistant phenotype or whether mutations are randomly acquired independently of the type of cell line.

Finally, in order to capture the full complexity of HCC, data generated by exome sequencing have to be ideally integrated with transcriptomic, proteomic, metabolic, and methylome analyses. Although we did not perform these analyses, as a complementary approach to exome sequencing we employed a CRISPR/Cas9 screening. It revealed the involvement of the KEAP1 protein in the anti-proliferative activity of sorafenib. Though, it was already reported that loss-of-function mutation of KEAP1 upregulates NRF2, that promotes cell proliferation in HCC [329-331].

Another CRISPR-based approach, using this time the CRISPR/deadCas9 transcriptional activation genome-wide screen, could provide a better understanding of the molecular mechanisms inducing sorafenib resistance [351]. This system can increase transcription of a gene through an inactive Cas9 (deadCas9) fused to a transcription activator peptide. A defined sgRNA is used to target the deadCas9-activator to a specific genomic sequence and subsequently to achieve high expression levels. Consequently, at a lethal concentration of sorafenib, a gain-of-function screen would detect genes whose overexpression lead to sorafenib resistance.

To bring innovation and consequently to increase the interest of this project, future experiments are planned to test the effect of a new multi-targeted tyrosine kinase inhibitor Lenvatinib (lenvima®) [352]. It has more potent inhibitory activity than sorafenib against several kinases including VEGFR, RET, FGFR, c-KIT, and PDGFR [353]. It is now FDA-approved for recurrent or metastatic thyroid cancer and a phase III clinical trial comparing lenvatinib to sorafenib has just been completed in HCC [354]. Accordingly, very few are known about its resistance mechanisms. Thenceforward, it is of high importance to assess whether the resistance mechanisms are similar to those of sorafenib. If lenvatinib is efficient in conditions where sorafenib is not, it could represent a breakthrough in the current crisis affecting advanced HCC treatment.

Whereas CRISPR/Cas9 negative selection screen in HCC cells was technically unsuccessful, the positive selection screens performed in order to identify regulators of TAT-RasGAP$_{317-326}$ were an accomplishment. As mentioned above, instead of being required in the death induction process *per se*, we demonstrated that validated candidates were involved in the cytosolic access of TAT-RasGAP$_{317-326}$ and two other TAT-constructs, TAT-Cre and TAT-PNA. This interesting discovery opens new fields of investigations and generates further questions. Indeed, how KCNN4, KCNK5, ATP1B3, SLC39A14, KCNQ5, and PIP5K1A which are mostly regulators of potassium flux manage cytosolic access, remains to be fully characterized. The preliminary results suggest that the absence of KCNQ5 prevents cytosolic access of the anti-cancer peptide through the depolarization of the plasma membrane. This observation was however not confirmed for the other candidates. Different experiments that could be done to elucidate what is the exact role of each candidate in the regulation of the cytosolic access of TAT-constructs are proposed in the discussion of the third part of the results. A better understanding of how TAT CPP enters cells is crucial for its clinical application and could lead to a subsequent modulation of its uptake or endosomal escape [355]. Indeed, although TAT has proceeded to different phases of clinical trials, no therapy employing this CPP has been yet approved by the FDA [356]. As a future perspective, it would be of interest to assess if the candidates yielded by the CRISPR-based screen modulate also the delivery of other CPP from different origins.
Finally, we demonstrated the property of the KCNN4 inhibitor TRAM-34 to efficiently prevent the cytosolic access of some arenaviruses. Among this family of viruses, some of them are causative agents of various severe viral hemorrhagic fevers with a high rate of mortality in humans [255]. Only suboptimal therapies and limited vaccines for some of these viruses exhibit the urgent need for novel therapeutic strategies [255-257]. Although these results are preliminary, they highlight a potential clinical relevance of KCNN4 chemical inhibitors to prevent viral infection. Therefore, it could be interesting to investigate whether the absence of KCNN4 can also inhibit the infection of other microorganisms, such as bacteria or other types of viruses.

To conclude, a better understanding of the mode of action of TAT-RasGAP$_{317-326}$ as well as the discovery of some new features could one day lead to the development of a compound with multiple anticancer properties. Furthermore, this work paves the ground to a better knowledge of sorafenib resistance. This could ultimately lead to the development of alternative therapies.

REMERCIEMENTS

Lors de ces quatre années de thèse, j'ai eu la chance de côtoyer et de travailler avec des personnes qui me sont précieuses tant pour leurs qualités humaines que scientifiques. Je souhaite tout particulièrement remercier Dr. Nicole Gross. C'est grâce à son soutien, sa disponibilité (même en étant aux quatre coins du monde) et à sa confiance que j'ai pu effectuer cette thèse. Je remercie également Pr. Christian Widmann pour m'avoir accueillie au sein de son laboratoire, pour ses conseils et pour son aide indispensable à l'obtention de mon MD-PhD.

J'aimerais remercier mes collègues qui sont devenus des amis et dont la présence quotidienne à participé au plaisir que j'ai eu à venir travailler. Merci aux Dr. Mathieu Heulot et Dr. David Barras pour tout ce qu'ils m'ont appris, pour leur patience, leurs précieux conseils, leur humour et bonne humeur. Merci à Gilles Dubuis pour les milliers de services qu'il m'a rendus, pour son soutien et pour toutes les petites discussions que nous avons eues. Merci au Dr. Sébastien Michel pour sa pédagogie, sa gentillesse, et pour avoir relu entièrement ma thèse. Merci aux Dr. Güliz Vanli Jaccard et Dr. Hadi Khalil pour leur accueil et aide lorsque je suis arrivée dans le laboratoire. Merci au Dr. Alvaro Cuesta Marban pour son aide et ses explications, ainsi que pour avoir résolu tous mes problèmes avec Illustrator et Photoshop. Merci au Dr. Sabine Rütti Roch pour sa bonne humeur communicative et pour nos nombreux entraînements de course. Merci à Daniel Constantin pour ses remarques scientifiques pertinentes et son humour noir. Merci à Maria de Carmen Condo Rubio, Evgeniya Trofimenko et Marc Serulla Llorens avec qui je n'ai travaillé que peu de temps, mais qui ont contribué aux bons moments passés dans le laboratoire.

Je souhaite également exprimer mon immense gratitude à tous les membres actuels et passés du Laboratoire d'Oncologie Pédiatrique du CHUV pour leur accueil et leur gentillesse. Merci à Katia Bourloud Balmas et Katja Nardou pour tout ce qu'elles m'ont appris. Merci au Dr. Jean-Marc Joseph pour son soutien, notamment pour l'obtention de ma bourse MD-PhD. Merci aux Dr. Julie Lieberman, Dr. Aurélie Coulon et Dr. Marjorie Flahaut pour leurs encouragements et leur bonne humeur. Merci au Dr. Annick Muehlethaler pour m'avoir intégrée dans la transition du laboratoire et pour son soutien.

Je tiens à remercier tout particulièrement le Pr. Ivan Stamenkovic et le Dr. Raffele Renella pour leurs conseils avisés, l'intérêt qu'ils ont porté à mon travail et leur immense soutien. Je suis très reconnaissante de tout ce qu'ils m'ont appris et de leur précieux mentorat.

Merci à tous les collaborateurs (Dr. Julien Puyal, Dr. Aimable Nahimana, Giulia Torriani, Pr. Stefan Kunz et Dr. Olivier Dormond) dont la participation et les échanges ont mené à l'accomplissement de ce travail. Merci également à mon jury de thèse pour leurs commentaires et discussions pertinents.

Je suis extrêmement reconnaissante envers ma famille et mes proches qui ont toujours été présents et très soutenants tout au long de mes études. Un immense merci à vous!

REFERENCES

1. Torre LA, Siegel RL, Ward EM and Jemal A. Global Cancer Incidence and Mortality Rates and Trends—An Update. Cancer Epidemiology Biomarkers & Prevention. 2016; 25(1):16-27.

2. J F, I S and M E. (2013). GLOBOCAN 2012 v1.0, Cancer incidence and mortality worldwide: IARC CancerBase No.11.

3. Jemal A, Bray F, Center MM, Ferlay J, Ward E and Forman D. Global cancer statistics. CA Cancer J Clin. 2011; 61(2):69-90.

4. Brawanski A. On the myth of the Edwin Smith papyrus: is it magic or science? Acta Neurochirurgica. 2012; 154(12):2285-2291.

5. Sudhakar A. History of Cancer, Ancient and Modern Treatment Methods. Journal of cancer science & therapy. 2009; 1(2):1-4.

6. Croce CM. Oncogenes and Cancer. New England Journal of Medicine. 2008; 358(5):502-511.

7. Stratton MR, Campbell PJ and Futreal PA. The cancer genome. Nature. 2009; 458(7239):719-724.

8. Feinberg AP, Koldobskiy MA and Gondor A. Epigenetic modulators, modifiers and mediators in cancer aetiology and progression. Nat Rev Genet. 2016; 17(5):284-299.

9. Alexandrov LB, Nik-Zainal S, Wedge DC, Aparicio SAJR, Behjati S, Biankin AV, Bignell GR, Bolli N, Borg A, Borresen-Dale A-L, Boyault S, Burkhardt B, Butler AP, Caldas C, Davies HR, Desmedt C, et al. Signatures of mutational processes in human cancer. Nature. 2013; 500(7463):415-421.

10. Hanahan D and Weinberg Robert A. Hallmarks of Cancer: The Next Generation. Cell. 144(5):646-674.

11. Alberts B JA, Lewis J, et al. . (2002). Signaling through Enzyme-Linked Cell-Surface Receptors.: Molecular Biology of the Cell.).

12. Hanahan D and Weinberg RA. The hallmarks of cancer. Cell. 2000; 100(1):57-70.

13. Lee EY and Muller WJ. Oncogenes and tumor suppressor genes. Cold Spring Harbor perspectives in biology. 2010; 2(10):a003236.

14. Adams JM and Cory S. The Bcl-2 apoptotic switch in cancer development and therapy. Oncogene. 2007; 26(9):1324-1337.

15. Collado M and Serrano M. Senescence in tumours: evidence from mice and humans. Nat Rev Cancer. 2010; 10(1):51-57.

16. Shay JW, Zou Y, Hiyama E and Wright WE. Telomerase and cancer. Human Molecular Genetics. 2001; 10(7):677-685.

17. Bergers G and Benjamin LE. Tumorigenesis and the angiogenic switch. Nat Rev Cancer. 2003; 3(6):401-410.

18. Goel HL and Mercurio AM. VEGF targets the tumour cell. Nat Rev Cancer. 2013; 13(12):871-882.

19. Mehlen P and Puisieux A. Metastasis: a question of life or death. Nat Rev Cancer. 2006; 6(6):449-458.

20. Larue L and Bellacosa A. Epithelial-mesenchymal transition in development and cancer: role of phosphatidylinositol 3[prime] kinase//AKT pathways. Oncogene. 0000; 24(50):7443-7454.

21. Steeg PS. Targeting metastasis. Nat Rev Cancer. 2016; 16(4):201-218.

22. Pavlova Natalya N and Thompson Craig B. The Emerging Hallmarks of Cancer Metabolism. Cell Metabolism. 2016; 23(1):27-47.

23. Raghunand N, He X, van Sluis R, Mahoney B, Baggett B, Taylor CW, Paine-Murrieta G, Roe D, Bhujwalla ZM and Gillies RJ. Enhancement of chemotherapy by manipulation of tumour pH. Br J Cancer. 1999; 80(7):1005-1011.

24. Rozhin J, Sameni M, Ziegler G and Sloane BF. Pericellular pH affects distribution and secretion of cathepsin B in malignant cells. Cancer Res. 1994; 54(24):6517-6525.

25. Grivennikov SI, Greten FR and Karin M. Immunity, Inflammation, and Cancer. Cell. 2010; 140(6):883-899.

26. Farber S and Diamond LK. Temporary remissions in acute leukemia in children produced by folic acid antagonist, 4-aminopteroyl-glutamic acid. The New England journal of medicine. 1948; 238(23):787-793.

27. Wyld L, Audisio RA and Poston GJ. The evolution of cancer surgery and future perspectives. Nat Rev Clin Oncol. 2015; 12(2):115-124.

28. Delaney G, Jacob S, Featherstone C and Barton M. The role of radiotherapy in cancer treatment: estimating optimal utilization from a review of evidence-based clinical guidelines. Cancer. 2005; 104(6):1129-1137.

29. Baskar R, Lee KA, Yeo R and Yeoh KW. Cancer and radiation therapy: current advances and future directions. International journal of medical sciences. 2012; 9(3):193-199.

30. Ralhan R and Kaur J. Alkylating agents and cancer therapy. Expert Opinion on Therapeutic Patents. 2007; 17(9):1061-1075.

31. Gmeiner WH. Antimetabolite incorporation into DNA: structural and thermodynamic basis for anticancer activity. Biopolymers. 2002; 65(3):180-189.

32. Minotti G, Menna P, Salvatorelli E, Cairo G and Gianni L. Anthracyclines: molecular advances and pharmacologic developments in antitumor activity and cardiotoxicity. Pharmacological reviews. 2004; 56(2):185-229.

33. Nitiss JL. Targeting DNA topoisomerase II in cancer chemotherapy. Nat Rev Cancer. 2009; 9(5):338-350.

34. Jordan MA and Wilson L. Microtubules as a target for anticancer drugs. Nat Rev Cancer. 2004; 4(4):253-265.

35. Walther V, Hiley CT, Shibata D, Swanton C, Turner PE and Maley CC. Can oncology recapitulate paleontology? Lessons from species extinctions. Nat Rev Clin Oncol. 2015; 12(5):273-285.

36. Gerber DE. Targeted therapies: a new generation of cancer treatments. American family physician. 2008; 77(3):311-319.

37. Khalil DN, Smith EL, Brentjens RJ and Wolchok JD. The future of cancer treatment: immunomodulation, CARs and combination immunotherapy. Nat Rev Clin Oncol. 2016; 13(5):273-290.

38. Lippert TH, Ruoff HJ and Volm M. Current status of methods to assess cancer drug resistance. International journal of medical sciences. 2011; 8(3):245-253.

39. Kim JU, Shariff MI, Crossey MM, Gomez-Romero M, Holmes E, Cox IJ, Fye HK, Njie R and Taylor-Robinson SD. Hepatocellular carcinoma: Review of disease and tumor biomarkers. World journal of hepatology. 2016; 8(10):471-484.

40. McGlynn KA and London WT. The Global Epidemiology of Hepatocellular Carcinoma, Present and Future. Clinics in liver disease. 2011; 15(2):223-x.

41. El-Serag HB. Hepatocellular carcinoma. The New England journal of medicine. 2011; 365(12):1118-1127.

42. Waller LP, Deshpande V and Pyrsopoulos N. Hepatocellular carcinoma: A comprehensive review. World journal of hepatology. 2015; 7(26):2648-2663.

43. Lee J-S. The mutational landscape of hepatocellular carcinoma. Clinical and Molecular Hepatology. 2015; 21(3):220-229.

44. Cleary SP, Jeck WR, Zhao X, Chen K, Selitsky SR, Savich GL, Tan TX, Wu MC, Getz G, Lawrence MS, Parker JS, Li J, Powers S, Kim H, Fischer S, Guindi M, et al. Identification of driver genes in hepatocellular carcinoma by exome sequencing. Hepatology (Baltimore, Md). 2013; 58(5):1693-1702.

45. Totoki Y, Tatsuno K, Covington KR, Ueda H, Creighton CJ, Kato M, Tsuji S, Donehower LA, Slagle BL, Nakamura H, Yamamoto S, Shinbrot E, Hama N, Lehmkuhl M, Hosoda F, Arai Y, et al. Trans-ancestry mutational landscape of hepatocellular carcinoma genomes. Nat Genet. 2014; 46(12):1267-1273.

46. Schulze K, Imbeaud S, Letouze E, Alexandrov LB, Calderaro J, Rebouissou S, Couchy G, Meiller C, Shinde J, Soysouvanh F, Calatayud AL, Pinyol R, Pelletier L, Balabaud C, Laurent A, Blanc JF, et al. Exome sequencing of hepatocellular carcinomas identifies new mutational signatures and potential therapeutic targets. Nat Genet. 2015; 47(5):505-511.

47. Ersahin T, Ozturk M and Cetin-Atalay R. (2006). Molecular Biology of Liver Cancer. Reviews in Cell Biology and Molecular Medicine: Wiley-VCH Verlag GmbH & Co. KGaA).

48. Forner A, Llovet JM and Bruix J. Hepatocellular carcinoma. The Lancet. 379(9822):1245-1255.

49. Forner A, Reig ME, de Lope CR and Bruix J. Current strategy for staging and treatment: the BCLC update and future prospects. Seminars in liver disease. 2010; 30(1):61-74.

50. Cholongitas E, Papatheodoridis GV, Vangeli M, Terreni N, Patch D and Burroughs AK. Systematic review: The model for end-stage liver disease--should it replace Child-Pugh's classification for assessing prognosis in cirrhosis? Alimentary pharmacology & therapeutics. 2005; 22(11-12):1079-1089.

51. Raza A and Sood GK. Hepatocellular carcinoma review: current treatment, and evidence-based medicine. World journal of gastroenterology. 2014; 20(15):4115-4127.

52. Llovet JM, Di Bisceglie AM, Bruix J, Kramer BS, Lencioni R, Zhu AX, Sherman M, Schwartz M, Lotze M, Talwalkar J and Gores GJ. Design and endpoints of clinical trials in hepatocellular carcinoma. Journal of the National Cancer Institute. 2008; 100(10):698-711.

53. Marin JJG, Castano B, Martinez-Becerra P, Rosales R and Monte MJ. Chemotherapy in the treatment of primary liver tumours. Cancer therapy. 2008; 6:711-728.

54. Llovet JM, Ricci S, Mazzaferro V, Hilgard P, Gane E, Blanc JF, de Oliveira AC, Santoro A, Raoul JL, Forner A, Schwartz M, Porta C, Zeuzem S, Bolondi L, Greten TF, Galle PR, et al. Sorafenib in advanced hepatocellular carcinoma. The New England journal of medicine. 2008; 359(4):378-390.

55. Cheng AL, Kang YK, Chen Z, Tsao CJ, Qin S, Kim JS, Luo R, Feng J, Ye S, Yang TS, Xu J, Sun Y, Liang H, Liu J, Wang J, Tak WY, et al. Efficacy and safety of sorafenib in patients in the Asia-Pacific region with advanced hepatocellular carcinoma: a phase III randomised, double-blind, placebo-controlled trial. The Lancet Oncology. 2009; 10(1):25-34.

56. Llovet JM, Villanueva A, Lachenmayer A and Finn RS. Advances in targeted therapies for hepatocellular carcinoma in the genomic era. Nat Rev Clin Oncol. 2015; 12(7):408-424.

57. Nishida N, Kitano M, Sakurai T and Kudo M. Molecular Mechanism and Prediction of Sorafenib Chemoresistance in Human Hepatocellular Carcinoma. Digestive Diseases. 2015; 33(6):771-779.

58. Blivet-Van Eggelpoel MJ, Chettouh H, Fartoux L, Aoudjehane L, Barbu V, Rey C, Priam S, Housset C, Rosmorduc O and Desbois-Mouthon C. Epidermal growth factor receptor and HER-3 restrict cell response to sorafenib in hepatocellular carcinoma cells. Journal of hepatology. 2012; 57(1):108-115.

59. Zhang PF, Li KS, Shen Yh, Gao PT, Dong ZR, Cai JB, Zhang C, Huang XY, Tian MX, Hu ZQ, Gao DM, Fan J, Ke AW and Shi GM. Galectin-1 induces hepatocellular carcinoma EMT and sorafenib resistance by activating FAK/PI3K/AKT signaling. Cell Death Dis. 2016; 7:e2201.

60. Chen W, Xiao W, Zhang K, Yin X, Lai J, Liang L and Chen D. Activation of c-Jun predicts a poor response to sorafenib in hepatocellular carcinoma: Preliminary Clinical Evidence. Scientific Reports. 2016; 6:22976.

61. Hagiwara S, Kudo M, Nagai T, Inoue T, Ueshima K, Nishida N, Watanabe T and Sakurai T. Activation of JNK and high expression level of CD133 predict a poor response to sorafenib in hepatocellular carcinoma. British Journal of Cancer. 2012; 106(12):1997-2003.

62. Rudalska R, Dauch D, Longerich T, McJunkin K, Wuestefeld T, Kang T-W, Hohmeyer A, Pesic M, Leibold J, von Thun A, Schirmacher P, Zuber J, Weiss K-H, Powers S, Malek NP, Eilers M, et al. In vivo RNAi screening identifies a mechanism of sorafenib resistance in liver cancer. Nature medicine. 2014; 20(10):1138-1146.

63. Personeni N, Rimassa L, Pressiani T, Destro A, Ligorio C, Tronconi MC, Bozzarelli S, Carnaghi C, Di Tommaso L, Giordano L, Roncalli M and Santoro A. Molecular determinants of outcome in sorafenib-treated patients with hepatocellular carcinoma. Journal of cancer research and clinical oncology. 2013; 139(7):1179-1187.

64. Chen H-C, Jeng Y-M, Yuan R-H, Hsu H-C and Chen Y-L. SIRT1 Promotes Tumorigenesis and Resistance to Chemotherapy in Hepatocellular Carcinoma and its Expression Predicts Poor Prognosis. Annals of Surgical Oncology. 2012; 19(6):2011-2019.

65. Liang Y, Zheng T, Song R, Wang J, Yin D, Wang L, Liu H, Tian L, Fang X, Meng X, Jiang H, Liu J and Liu L. Hypoxia-mediated sorafenib resistance can be overcome by EF24 through Von Hippel-Lindau tumor suppressor-dependent HIF-1alpha inhibition in hepatocellular carcinoma. Hepatology (Baltimore, Md). 2013; 57(5):1847-1857.

66. Puumala SE and Hoyme HE. Epigenetics in pediatrics. Pediatrics in review. 2015; 36(1):14-21.

67. Marshall GM, Carter DR, Cheung BB, Liu T, Mateos MK, Meyerowitz JG and Weiss WA. The prenatal origins of cancer. Nat Rev Cancer. 2014; 14(4):277-289.

68. Lawlor ER and Thiele CJ. Epigenetic changes in pediatric solid tumors: promising new targets. Clinical cancer research : an official journal of the American Association for Cancer Research. 2012; 18(10):2768-2779.

69. Stiller CA, Marcos-Gragera R, Ardanaz E, Pannelli F, Almar Marqués E, Cañada Martinez A and Steliarova-Foucher E. Geographical patterns of childhood cancer incidence in Europe, 1988–1997. Report from the Automated Childhood Cancer Information System project. European Journal of Cancer. 2006; 42(13):1952-1960.

70. Sullivan R, Kowalczyk JR, Agarwal B, Ladenstein R, Fitzgerald E, Barr R, Steliarova-Foucher E, Magrath I, Howard SC, Kruger M, Valsecchi MG, Biondi A, Grundy P, Smith MA, Adamson P, Vassal G, et al. New policies to address the global burden of childhood cancers. The Lancet Oncology. 2013; 14(3):e125-135.

71. Birch JM. Genes and cancer. Archives of disease in childhood. 1999; 80(1):1-3.

72. Lichtenstein P, Holm NV, Verkasalo PK, Iliadou A, Kaprio J, Koskenvuo M, Pukkala E, Skytthe A and Hemminki K. Environmental and heritable factors in the causation of cancer--analyses of cohorts of twins from Sweden, Denmark, and Finland. The New England journal of medicine. 2000; 343(2):78-85.

73. Stiller CA. Epidemiology and genetics of childhood cancer. Oncogene. 2004; 23(38):6429-6444.

74. Steliarova-Foucher E, Stiller C, Kaatsch P, Berrino F, Coebergh J-W, Lacour B and Perkin M. Geographical patterns and time trends of cancer incidence and survival among children and adolescents in Europe since the 1970s (the ACCIS project): an epidemiological study. The Lancet. 364(9451):2097-2105.

75. Reulen RC, Winter DL, Frobisher C, Lancashire ER, Stiller CA, Jenney ME, Skinner R, Stevens MC and Hawkins MM. Long-term cause-specific mortality among survivors of childhood cancer. JAMA. 2010; 304(2):172-179.

76. Melino G. The Sirens' song. Nature. 2001; 412(6842):23.

77. Hotchkiss RS, Strasser A, McDunn JE and Swanson PE. Cell Death. New England Journal of Medicine. 2009; 361(16):1570-1583.

78. Mattson MP. Apoptosis in neurodegenerative disorders. Nat Rev Mol Cell Biol. 2000; 1(2):120-129.

79. Nagata S. Apoptosis and autoimmune diseases. Annals of the New York Academy of Sciences. 2010; 1209:10-16.

80. Galluzzi L, Vitale I, Abrams JM, Alnemri ES, Baehrecke EH, Blagosklonny MV, Dawson TM, Dawson VL, El-Deiry WS, Fulda S, Gottlieb E, Green DR, Hengartner MO, Kepp O, Knight RA, Kumar S, et al. Molecular definitions of cell death subroutines: recommendations of the Nomenclature Committee on Cell Death 2012. Cell Death Differ. 2012; 19(1):107-120.

81. Galluzzi L, Bravo-San Pedro JM, Vitale I, Aaronson SA, Abrams JM, Adam D, Alnemri ES, Altucci L, Andrews D, Annicchiarico-Petruzzelli M, Baehrecke EH, Bazan NG, Bertrand MJ, Bianchi K, Blagosklonny MV, Blomgren K, et al. Essential versus accessory aspects of cell death: recommendations of the NCCD 2015. Cell Death Differ. 2015; 22(1):58-73.

82. Saraste A and Pulkki K. (2000). Morphologic and biochemical hallmarks of apoptosis.

83. Fadeel B. Plasma membrane alterations during apoptosis: role in corpse clearance. Antioxidants & redox signaling. 2004; 6(2):269-275.

84. Dickens Laura S, Boyd Robert S, Jukes-Jones R, Hughes Michelle A, Robinson Gemma L, Fairall L, Schwabe John W, Cain K and MacFarlane M. A Death Effector Domain Chain DISC Model Reveals a Crucial Role for Caspase-8 Chain Assembly in Mediating Apoptotic Cell Death. Molecular Cell. 2012; 47(2-2):291-305.

85. Taylor RC, Cullen SP and Martin SJ. Apoptosis: controlled demolition at the cellular level. Nat Rev Mol Cell Biol. 2008; 9(3):231-241.

86. Li H, Zhu H, Xu C-j and Yuan J. Cleavage of BID by Caspase 8 Mediates the Mitochondrial Damage in the Fas Pathway of Apoptosis. Cell. 1998; 94(4):491-501.

87. Elmore S. Apoptosis: a review of programmed cell death. Toxicologic pathology. 2007; 35(4):495-516.

88. Marino G, Niso-Santano M, Baehrecke EH and Kroemer G. Self-consumption: the interplay of autophagy and apoptosis. Nat Rev Mol Cell Biol. 2014; 15(2):81-94.

89. Ichim G and Tait SWG. A fate worse than death: apoptosis as an oncogenic process. Nat Rev Cancer. 2016; 16(8):539-548.

90. Kroemer G and Martin SJ. Caspase-independent cell death. Nature medicine. 2005; 11(7):725-730.

91. Vandenabeele P, Galluzzi L, Vanden Berghe T and Kroemer G. Molecular mechanisms of necroptosis: an ordered cellular explosion. Nat Rev Mol Cell Biol. 2010; 11(10):700-714.

92. Linkermann A and Green DR. Necroptosis. New England Journal of Medicine. 2014; 370(5):455-465.

93. Berghe TV, Linkermann A, Jouan-Lanhouet S, Walczak H and Vandenabeele P. Regulated necrosis: the expanding network of non-apoptotic cell death pathways. Nat Rev Mol Cell Biol. 2014; 15(2):135-147.

94. Linkermann A and Green DR. Necroptosis. New England Journal of Medicine. 2014; 370(5):455-465.

95. Zhao J, Jitkaew S, Cai Z, Choksi S, Li Q, Luo J and Liu Z-G. Mixed lineage kinase domain-like is a key receptor interacting protein 3 downstream component of TNF-induced necrosis. Proceedings of the National Academy of Sciences. 2012; 109(14):5322-5327.

96. Sun L, Wang H, Wang Z, He S, Chen S, Liao D, Wang L, Yan J, Liu W, Lei X and Wang X. Mixed Lineage Kinase Domain-like Protein Mediates Necrosis Signaling Downstream of RIP3 Kinase. Cell. 2012; 148(1–2):213-227.

97. Fuchs Y and Steller H. Live to die another way: modes of programmed cell death and the signals emanating from dying cells. Nat Rev Mol Cell Biol. 2015; 16(6):329-344.

98. Vandenabeele P, Grootjans S, Callewaert N and Takahashi N. Necrostatin-1 blocks both RIPK1 and IDO: consequences for the study of cell death in experimental disease models. Cell Death Differ. 2013; 20(2):185-187.

99. Curtin NJ and Szabo C. Therapeutic applications of PARP inhibitors: anticancer therapy and beyond. Molecular aspects of medicine. 2013; 34(6):1217-1256.

100. Isabelle M, Moreel X, Gagne JP, Rouleau M, Ethier C, Gagne P, Hendzel MJ and Poirier GG. Investigation of PARP-1, PARP-2, and PARG interactomes by affinity-purification mass spectrometry. Proteome science. 2010; 8:22.

101. Yu S-W, Wang H, Poitras MF, Coombs C, Bowers WJ, Federoff HJ, Poirier GG, Dawson TM and Dawson VL. Mediation of Poly(ADP-Ribose) Polymerase-1-Dependent Cell Death by Apoptosis-Inducing Factor. Science. 2002; 297(5579):259-263.

102. Andrabi SA, Kim NS, Yu S-W, Wang H, Koh DW, Sasaki M, Klaus JA, Otsuka T, Zhang Z, Koehler RC, Hurn PD, Poirier GG, Dawson VL and Dawson TM. Poly(ADP-ribose) (PAR) polymer is a death signal. Proceedings of the National Academy of Sciences. 2006; 103(48):18308-18313.

103. Fatokun AA, Dawson VL and Dawson TM. Parthanatos: mitochondrial-linked mechanisms and therapeutic opportunities. Br J Pharmacol. 2014; 171(8):2000-2016.

104. Tait SW, Ichim G and Green DR. Die another way--non-apoptotic mechanisms of cell death. Journal of cell science. 2014; 127(Pt 10):2135-2144.

105. Bergsbaken T, Fink SL and Cookson BT. Pyroptosis: host cell death and inflammation. Nature reviews Microbiology. 2009; 7(2):99-109.

106. Lee CY and Baehrecke EH. Steroid regulation of autophagic programmed cell death during development. Development. 2001; 128(8):1443-1455.

107. Dixon SJ, Lemberg KM, Lamprecht MR, Skouta R, Zaitsev EM, Gleason CE, Patel DN, Bauer AJ, Cantley AM, Yang WS, Morrison B and Stockwell BR. Ferroptosis: An Iron-Dependent Form of Non-Apoptotic Cell Death. Cell. 2012; 149(5):1060-1072.

108. Bridges RJ, Natale NR and Patel SA. System xc(-) cystine/glutamate antiporter: an update on molecular pharmacology and roles within the CNS. Br J Pharmacol. 2012; 165(1):20-34.

109. Yang WS and Stockwell BR. Ferroptosis: Death by Lipid Peroxidation. Trends in cell biology. 2016; 26(3):165-176.

110. Xie Y, Hou W, Song X, Yu Y, Huang J, Sun X, Kang R and Tang D. Ferroptosis: process and function. Cell Death Differ. 2016; 23(3):369-379.

111. Yang WS and Stockwell BR. Synthetic lethal screening identifies compounds activating iron-dependent, nonapoptotic cell death in oncogenic-RAS-harboring cancer cells. Chemistry & biology. 2008; 15(3):234-245.

112. Sun X, Ou Z, Chen R, Niu X, Chen D, Kang R and Tang D. Activation of the p62-Keap1-NRF2 pathway protects against ferroptosis in hepatocellular carcinoma cells. Hepatology (Baltimore, Md). 2016; 63(1):173-184.

113. Yu H, Guo P, Xie X, Wang Y and Chen G. Ferroptosis, a new form of cell death, and its relationships with tumourous diseases. Journal of cellular and molecular medicine. 2016.

114. Vanden Berghe T, Linkermann A, Jouan-Lanhouet S, Walczak H and Vandenabeele P. Regulated necrosis: the expanding network of non-apoptotic cell death pathways. Nat Rev Mol Cell Biol. 2014; 15(2):135-147.

115. Taylor RC, Cullen SP and Martin SJ. Apoptosis: controlled demolition at the cellular level. Nat Rev Mol Cell Biol. 2008; 9(3):231-241.

116. Kroemer G and Levine B. Autophagic cell death: the story of a misnomer. Nat Rev Mol Cell Biol. 2008; 9(12):1004-1010.

117. Yang J-Y and Widmann C. Antiapoptotic Signaling Generated by Caspase-Induced Cleavage of RasGAP. Molecular and Cellular Biology. 2001; 21(16):5346-5358.

118. Yang J-Y, Michod D, Walicki J, Murphy BM, Kasibhatla S, Martin SJ and Widmann C. Partial Cleavage of RasGAP by Caspases Is Required for Cell Survival in Mild Stress Conditions. Molecular and Cellular Biology. 2004; 24(23):10425-10436.

119. Khalil H, Peltzer N, Walicki J, Yang J-Y, Dubuis G, Gardiol N, Held W, Bigliardi P, Marsland B, Liaudet L and Widmann C. Caspase-3 Protects Stressed Organs against Cell Death. Molecular and Cellular Biology. 2012; 32(22):4523-4533.

120. Yang J-Y and Widmann C. The RasGAP N-terminal Fragment Generated by Caspase Cleavage Protects Cells in a Ras/PI3K/Akt-dependent Manner That Does Not Rely on NFκB Activation. Journal of Biological Chemistry. 2002; 277(17):14641-14646.

121. Yang J-Y, Walicki J, Michod D, Dubuis G and Widmann C. Impaired Akt Activity Down-Modulation, Caspase-3 Activation, and Apoptosis in Cells Expressing a Caspase-resistant Mutant of RasGAP at Position 157. Molecular Biology of the Cell. 2005; 16(8):3511-3520.

122. Michod D, Yang J-Y, Chen J, Bonny C and Widmann C. A RasGAP-derived cell permeable peptide potently enhances genotoxin-induced cytotoxicity in tumor cells. Oncogene. 2004; 23(55):8971-8978.

123. Michod D, Annibaldi A, Schaefer S, Dapples C, Rochat B and Widmann C. Effect of RasGAP N2 Fragment–Derived Peptide on Tumor Growth in Mice. Journal of the National Cancer Institute. 2009; 101(11):828-832.

124. Barras D, Lorusso G, Ruegg C and Widmann C. Inhibition of cell migration and invasion mediated by the TAT-RasGAP peptide requires the DLC1 tumor suppressor. Oncogene. 2013.

125. Barras D, Chevalier N, Zoete V, Dempsey R, Lapouge K, Olayioye MA, Michielin O and Widmann C. A WxW Motif is required for the Anticancer Activity of TAT-RasGAP317-326. Journal of Biological Chemistry. 2014.

126. Michod D and Widmann C. TAT-RasGAP317-326 Requires p53 and PUMA to Sensitize Tumor Cells to Genotoxins. Molecular Cancer Research. 2007; 5(5):497-507.

127. Debatin KM, Poncet D and Kroemer G. Chemotherapy: targeting the mitochondrial cell death pathway. Oncogene. 2002; 21(57):8786-8803.

128. Kaufmann SH, Lee SH, Meng XW, Loegering DA, Kottke TJ, Henzing AJ, Ruchaud S, Samejima K and Earnshaw WC. Apoptosis-associated caspase activation assays. Methods (San Diego, Calif). 2008; 44(3):262-272.

129. Fulda S and Debatin KM. Extrinsic versus intrinsic apoptosis pathways in anticancer chemotherapy. Oncogene. 2006; 25(34):4798-4811.

130. Annibaldi A, Heulot M, Martinou J-C and Widmann C. TAT-RasGAP317–326-mediated tumor cell death sensitization can occur independently of Bax and Bak. Apoptosis. 2014; 19(4):719-733.

131. Otvos L and Wade JD. Current challenges in peptide-based drug discovery. Frontiers in Chemistry. 2014; 2:62.

132. Uhlig T, Kyprianou T, Martinelli FG, Oppici CA, Heiligers D, Hills D, Calvo XR and Verhaert P. The emergence of peptides in the pharmaceutical business: From exploration to exploitation. EuPA Open Proteomics. 2014; 4:58-69.

133. Fosgerau K and Hoffmann T. Peptide therapeutics: current status and future directions. Drug Discovery Today. 2015; 20(1):122-128.

134. Fosgerau K and Hoffmann T. Peptide therapeutics: current status and future directions. Drug Discov Today. 2015; 20(1):122-128.

135. Vlieghe P, Lisowski V, Martinez J and Khrestchatisky M. Synthetic therapeutic peptides: science and market. Drug Discov Today. 2010; 15(1-2):40-56.

136. Kaspar AA and Reichert JM. Future directions for peptide therapeutics development. Drug Discov Today. 2013; 18(17-18):807-817.

137. Thundimadathil J. Cancer treatment using peptides: current therapies and future prospects. Journal of amino acids. 2012; 2012:967347.

138. Wurz GT, Kao CJ, Wolf M and DeGregorio MW. Tecemotide: an antigen-specific cancer immunotherapy. Human vaccines & immunotherapeutics. 2014; 10(11):3383-3393.

139. Deplanque G, Madhusudan S, Jones PH, Wellmann S, Christodoulos K, Talbot DC, Ganesan TS, Blann A and Harris AL. Phase II trial of the antiangiogenic agent IM862 in metastatic renal cell carcinoma. Br J Cancer. 2004; 91(9):1645-1650.

140. Milletti F. Cell-penetrating peptides: classes, origin, and current landscape. Drug Discov Today. 2012; 17(15-16):850-860.

141. Frankel AD and Pabo CO. Cellular uptake of the tat protein from human immunodeficiency virus. Cell. 1988; 55(6):1189-1193.

142. Vives E, Brodin P and Lebleu B. A truncated HIV-1 Tat protein basic domain rapidly translocates through the plasma membrane and accumulates in the cell nucleus. The Journal of biological chemistry. 1997; 272(25):16010-16017.

143. Derossi D, Joliot AH, Chassaing G and Prochiantz A. The third helix of the Antennapedia homeodomain translocates through biological membranes. The Journal of biological chemistry. 1994; 269(14):10444-10450.

144. Pooga M, Hallbrink M, Zorko M and Langel U. Cell penetration by transportan. FASEB journal : official publication of the Federation of American Societies for Experimental Biology. 1998; 12(1):67-77.

145. Mitchell DJ, Kim DT, Steinman L, Fathman CG and Rothbard JB. Polyarginine enters cells more efficiently than other polycationic homopolymers. The journal of peptide research : official journal of the American Peptide Society. 2000; 56(5):318-325.

146. Drin G, Cottin S, Blanc E, Rees AR and Temsamani J. Studies on the internalization mechanism of cationic cell-penetrating peptides. The Journal of biological chemistry. 2003; 278(33):31192-31201.

147. Kauffman WB, Fuselier T, He J and Wimley WC. Mechanism Matters: A Taxonomy of Cell Penetrating Peptides. Trends in biochemical sciences. 2015; 40(12):749-764.

148. Thoren PE, Persson D, Esbjorner EK, Goksor M, Lincoln P and Norden B. Membrane binding and translocation of cell-penetrating peptides. Biochemistry. 2004; 43(12):3471-3489.

149. Rothbard JB, Jessop TC, Lewis RS, Murray BA and Wender PA. Role of membrane potential and hydrogen bonding in the mechanism of translocation of guanidinium-rich peptides into cells. Journal of the American Chemical Society. 2004; 126(31):9506-9507.

150. Mishra A, Lai GH, Schmidt NW, Sun VZ, Rodriguez AR, Tong R, Tang L, Cheng J, Deming TJ, Kamei DT and Wong GCL. Translocation of HIV TAT peptide and analogues induced by multiplexed membrane and cytoskeletal interactions. Proceedings of the National Academy of Sciences. 2011; 108(41):16883-16888.

151. Killian JA, Burger KNJ and de Kruijff B. Phase separation and hexagonal HII phase formation by gramicidins A, B and C in dioleoylphosphatidylcholine model membranes. A study on the role of the tryptophan residues. Biochimica et Biophysica Acta (BBA) - Biomembranes. 1987; 897(2):269-284.

152. Bechara C, Pallerla M, Zaltsman Y, Burlina F, Alves ID, Lequin O and Sagan S. Tryptophan within basic peptide sequences triggers glycosaminoglycan-dependent endocytosis. FASEB journal : official publication of the Federation of American Societies for Experimental Biology. 2013; 27(2):738-749.

153. Maiolo JR, Ferrer M and Ottinger EA. Effects of cargo molecules on the cellular uptake of arginine-rich cell-penetrating peptides. Biochimica et biophysica acta. 2005; 1712(2):161-172.

154. Rydberg HA, Matson M, Amand HL, Esbjorner EK and Norden B. Effects of tryptophan content and backbone spacing on the uptake efficiency of cell-penetrating peptides. Biochemistry. 2012; 51(27):5531-5539.

155. Bechara C and Sagan S. Cell-penetrating peptides: 20 years later, where do we stand? FEBS letters. 2013; 587(12):1693-1702.

156. Durzynska J, Przysiecka L, Nawrot R, Barylski J, Nowicki G, Warowicka A, Musidlak O and Gozdzicka-Jozefiak A. Viral and other cell-penetrating peptides as vectors of therapeutic agents in medicine. The Journal of pharmacology and experimental therapeutics. 2015; 354(1):32-42.

157. Di Pisa M, Chassaing G and Swiecicki JM. Translocation mechanism(s) of cell-penetrating peptides: biophysical studies using artificial membrane bilayers. Biochemistry. 2015; 54(2):194-207.

158. Mudhakir D and Harashima H. Learning from the viral journey: how to enter cells and how to overcome intracellular barriers to reach the nucleus. The AAPS journal. 2009; 11(1):65-77.

159. Ruczynski J, Wierzbicki PM, Kogut-Wierzbicka M, Mucha P, Siedlecka-Kroplewska K and Rekowski P. Cell-penetrating peptides as a promising tool for delivery of various molecules into the cells. Folia histochemica et cytobiologica. 2014; 52(4):257-269.

160. Mukherjee S, Ghosh RN and Maxfield FR. Endocytosis. Physiological reviews. 1997; 77(3):759-803.

161. Doherty GJ and McMahon HT. Mechanisms of endocytosis. Annual review of biochemistry. 2009; 78:857-902.

162. Lim JP and Gleeson PA. Macropinocytosis: an endocytic pathway for internalising large gulps. Immunology and cell biology. 2011; 89(8):836-843.

163. Spiering D and Hodgson L. Dynamics of the Rho-family small GTPases in actin regulation and motility. Cell Adhesion & Migration. 2011; 5(2):170-180.

164. Robinson MS. Forty Years of Clathrin-coated Vesicles. Traffic (Copenhagen, Denmark). 2015; 16(12):1210-1238.

165. Carpentier JL, Gorden P, Anderson RG, Goldstein JL, Brown MS, Cohen S and Orci L. Co-localization of 125I-epidermal growth factor and ferritin-low density lipoprotein in coated pits: a quantitative electron microscopic study in normal and mutant human fibroblasts. The Journal of cell biology. 1982; 95(1):73-77.

166. Neutra MR, Ciechanover A, Owen LS and Lodish HF. Intracellular transport of transferrin- and asialoorosomucoid-colloidal gold conjugates to lysosomes after receptor-mediated endocytosis. The journal of histochemistry and cytochemistry : official journal of the Histochemistry Society. 1985; 33(11):1134-1144.

167. Schmid SL and Frolov VA. Dynamin: functional design of a membrane fission catalyst. Annual review of cell and developmental biology. 2011; 27:79-105.

168. Rothman JE and Schmid SL. Enzymatic recycling of clathrin from coated vesicles. Cell. 1986; 46(1):5-9.

169. Pelkmans L and Helenius A. Endocytosis via caveolae. Traffic (Copenhagen, Denmark). 2002; 3(5):311-320.

170. Podar K, Tai YT, Cole CE, Hideshima T, Sattler M, Hamblin A, Mitsiades N, Schlossman RL, Davies FE, Morgan GJ, Munshi NC, Chauhan D and Anderson KC. Essential role of caveolae in interleukin-6- and insulin-like growth factor I-triggered Akt-1-mediated survival of multiple myeloma cells. The Journal of biological chemistry. 2003; 278(8):5794-5801.

171. Kiss AL. Caveolae and the regulation of endocytosis. Advances in experimental medicine and biology. 2012; 729:14-28.

172. Pelkmans L, Fava E, Grabner H, Hannus M, Habermann B, Krausz E and Zerial M. Genome-wide analysis of human kinases in clathrin- and caveolae/raft-mediated endocytosis. Nature. 2005; 436(7047):78-86.

173. Nabi IR and Le PU. Caveolae/raft-dependent endocytosis. The Journal of cell biology. 2003; 161(4):673-677.

174. Lamaze C, Dujeancourt A, Baba T, Lo CG, Benmerah A and Dautry-Varsat A. Interleukin 2 receptors and detergent-resistant membrane domains define a clathrin-independent endocytic pathway. Mol Cell. 2001; 7(3):661-671.

175. Sabharanjak S, Sharma P, Parton RG and Mayor S. GPI-Anchored Proteins Are Delivered to Recycling Endosomes via a Distinct cdc42-Regulated, Clathrin-Independent Pinocytic Pathway. Developmental Cell. 2002; 2(4):411-423.

176. Naslavsky N, Weigert R and Donaldson JG. Convergence of non-clathrin- and clathrin-derived endosomes involves Arf6 inactivation and changes in phosphoinositides. Mol Biol Cell. 2003; 14(2):417-431.

177. Glebov OO, Bright NA and Nichols BJ. Flotillin-1 defines a clathrin-independent endocytic pathway in mammalian cells. Nature cell biology. 2006; 8(1):46-54.

178. Mayor S and Pagano RE. Pathways of clathrin-independent endocytosis. Nat Rev Mol Cell Biol. 2007; 8(8):603-612.

179. Soldati T and Schliwa M. Powering membrane traffic in endocytosis and recycling. Nat Rev Mol Cell Biol. 2006; 7(12):897-908.

180. Elkin SR, Lakoduk AM and Schmid SL. Endocytic pathways and endosomal trafficking: a primer. Wiener medizinische Wochenschrift (1946). 2016; 166(7-8):196-204.

181. Madani F, Abdo R, Lindberg S, Hirose H, Futaki S, Langel U and Graslund A. Modeling the endosomal escape of cell-penetrating peptides using a transmembrane pH gradient. Biochimica et biophysica acta. 2013; 1828(4):1198-1204.

182. Yang ST, Zaitseva E, Chernomordik LV and Melikov K. Cell-penetrating peptide induces leaky fusion of liposomes containing late endosome-specific anionic lipid. Biophys J. 2010; 99(8):2525-2533.

183. Coriat R, Faivre S, Dreyer C, Mir O, Bouattour M, Goldwasser F and Raymond E. First-in-human phase I and pharmacokinetic study of DTS-108 in patients with advanced carcinomas. J Clin Oncol. 2012; 30:2557.

184. Cousins MJ, Pickthorn K, Huang S, Critchley L and Bell G. The safety and efficacy of KAI-1678- an inhibitor of epsilon protein kinase C (epsilonPKC)-versus lidocaine and placebo for the treatment of postherpetic neuralgia: a crossover study design. Pain medicine (Malden, Mass). 2013; 14(4):533-540.

185. Copolovici DM, Langel K, Eriste E and Langel U. Cell-penetrating peptides: design, synthesis, and applications. ACS nano. 2014; 8(3):1972-1994.

186. Shin MC, Zhang J, Min KA, Lee K, Byun Y, David AE, He H and Yang VC. Cell-penetrating peptides: achievements and challenges in application for cancer treatment. Journal of biomedical materials research Part A. 2014; 102(2):575-587.

187. Stewart KM, Horton KL and Kelley SO. Cell-penetrating peptides as delivery vehicles for biology and medicine. Organic & biomolecular chemistry. 2008; 6(13):2242-2255.

188. Wadia JS, Stan RV and Dowdy SF. Transducible TAT-HA fusogenic peptide enhances escape of TAT-fusion proteins after lipid raft macropinocytosis. Nature medicine. 2004; 10(3):310-315.

189. Kaplan IM, Wadia JS and Dowdy SF. Cationic TAT peptide transduction domain enters cells by macropinocytosis. Journal of Controlled Release. 2005; 102(1):247-253.

190. Fittipaldi A, Ferrari A, Zoppe M, Arcangeli C, Pellegrini V, Beltram F and Giacca M. Cell membrane lipid rafts mediate caveolar endocytosis of HIV-1 Tat fusion proteins. The Journal of biological chemistry. 2003; 278(36):34141-34149.

191. Duchardt F, Fotin-Mleczek M, Schwarz H, Fischer R and Brock R. A comprehensive model for the cellular uptake of cationic cell-penetrating peptides. Traffic (Copenhagen, Denmark). 2007; 8(7):848-866.

192. Maiolo JR, Ferrer M and Ottinger EA. Effects of cargo molecules on the cellular uptake of arginine-rich cell-penetrating peptides. Biochimica et Biophysica Acta (BBA) - Biomembranes. 2005; 1712(2):161-172.

193. Hirose H, Takeuchi T, Osakada H, Pujals S, Katayama S, Nakase I, Kobayashi S, Haraguchi T and Futaki S. Transient focal membrane deformation induced by arginine-rich peptides leads to their direct penetration into cells. Molecular therapy : the journal of the American Society of Gene Therapy. 2012; 20(5):984-993.

194. Gruenberg J and van der Goot FG. Mechanisms of pathogen entry through the endosomal compartments. Nat Rev Mol Cell Biol. 2006; 7(7):495-504.

195. Yamauchi Y and Helenius A. Virus entry at a glance. Journal of cell science. 2013; 126(6):1289-1295.

196. Heulot M, Chevalier N, Puyal J, Margue C, Michel S, Kreis S, Kulms D, Barras D, Nahimana A and Widmann C. The TAT-RasGAP317-326 anti-cancer peptide can kill in a caspase-, apoptosis-, and necroptosis-independent manner. Oncotarget. 2016; 7(39):64342-64359.

197. Storr SJ, Carragher NO, Frame MC, Parr T and Martin SG. The calpain system and cancer. Nat Rev Cancer. 2011; 11(5):364-374.

198. Lakshmikuttyamma A, Selvakumar P, Kanthan R, Kanthan SC and Sharma RK. Overexpression of m-calpain in human colorectal adenocarcinomas. Cancer epidemiology, biomarkers & prevention : a publication of the American Association for Cancer Research, cosponsored by the American Society of Preventive Oncology. 2004; 13(10):1604-1609.

199. Liu L, Xing D, Chen WR, Chen T, Pei Y and Gao X. Calpain-mediated pathway dominates cisplatin-induced apoptosis in human lung adenocarcinoma cells as determined by real-time single cell analysis. Int J Cancer. 2008; 122(10):2210-2222.

200. Ono Y, Saido TC and Sorimachi H. Calpain research for drug discovery: challenges and potential. Nat Rev Drug Discov. 2016; 15(12):854-876.

201. Pamonsinlapatham P, Gril B, Dufour S, Hadj-Slimane R, Gigoux V, Pethe S, L'Hoste S, Camonis J, Garbay C, Raynaud F and Vidal M. Capns1, a new binding partner of RasGAP-SH3 domain in K-Ras(V12) oncogenic cells: modulation of cell survival and migration. Cellular signalling. 2008; 20(11):2119-2126.

202. Barras D, Lorusso G, Lhermitte B, Viertl D, Rüegg C and Widmann C. Fragment N2, a caspase-3-generated RasGAP fragment, inhibits breast cancer metastatic progression. International Journal of Cancer. 2014; 135(1):242-247.

203. Sanjana NE, Shalem O and Zhang F. Improved vectors and genome-wide libraries for CRISPR screening. Nature methods. 2014; 11(8):783-784.

204. Kang SH, Cho MJ and Kole R. Up-regulation of luciferase gene expression with antisense oligonucleotides: implications and applications in functional assay development. Biochemistry. 1998; 37(18):6235-6239.

205. Annibaldi A, Dousse A, Martin S, Tazi J and Widmann C. Revisiting G3BP1 as a RasGAP Binding Protein: Sensitization of Tumor Cells to Chemotherapy by the RasGAP 317-326 Sequence Does Not Involve G3BP1. PloS one. 2011; 6(12).

206. Shalem O, Sanjana NE, Hartenian E, Shi X, Scott DA, Mikkelsen TS, Heckl D, Ebert BL, Root DE, Doench JG and Zhang F. Genome-scale CRISPR-Cas9 knockout screening in human cells. Science. 2014; 343(6166):84-87.

207. Li W, Xu H, Xiao T, Cong L, Love MI, Zhang F, Irizarry RA, Liu JS, Brown M and Liu XS. MAGeCK enables robust identification of essential genes from genome-scale CRISPR/Cas9 knockout screens. Genome biology. 2014; 15(12):554.

208. D'Astolfo DS, Pagliero RJ, Pras A, Karthaus WR, Clevers H, Prasad V, Lebbink RJ, Rehmann H and Geijsen N. Efficient intracellular delivery of native proteins. Cell. 2015; 161(3):674-690.

209. Shalem O, Sanjana NE, Hartenian E, Shi X, Scott DA, Mikkelsen TS, Heckl D, Ebert BL, Root DE, Doench JG and Zhang F. Genome-Scale CRISPR-Cas9 Knockout Screening in Human Cells. Science. 2014; 343(6166):84-87.

210. Wang T, Wei JJ, Sabatini DM and Lander ES. Genetic Screens in Human Cells Using the CRISPR-Cas9 System. Science. 2014; 343(6166):80-84.

211. Wulff H, Miller MJ, Hansel W, Grissmer S, Cahalan MD and Chandy KG. Design of a potent and selective inhibitor of the intermediate-conductance Ca2+-activated K+ channel, IKCa1: a potential immunosuppressant. Proceedings of the National Academy of Sciences of the United States of America. 2000; 97(14):8151-8156.

212. Wulff H, Gutman GA, Cahalan MD and Chandy KG. Delineation of the clotrimazole/TRAM-34 binding site on the intermediate conductance calcium-activated potassium channel, IKCa1. The Journal of biological chemistry. 2001; 276(34):32040-32045.

213. Godfraind T. Mechanism of action of cardiac glycosides. European heart journal. 1984; 5 Suppl F:303-308.

214. Schroeder BC, Hechenberger M, Weinreich F, Kubisch C and Jentsch TJ. KCNQ5, a novel potassium channel broadly expressed in brain, mediates M-type currents. The Journal of biological chemistry. 2000; 275(31):24089-24095.

215. Takeuchi T, Kosuge M, Tadokoro A, Sugiura Y, Nishi M, Kawata M, Sakai N, Matile S and Futaki S. Direct and rapid cytosolic delivery using cell-penetrating peptides mediated by pyrenebutyrate. ACS chemical biology. 2006; 1(5):299-303.

216. Kosuge M, Takeuchi T, Nakase I, Jones AT and Futaki S. Cellular internalization and distribution of arginine-rich peptides as a function of extracellular peptide concentration, serum, and plasma membrane associated proteoglycans. Bioconjugate chemistry. 2008; 19(3):656-664.

217. Kosuge M, Takeuchi T, Nakase I, Jones AT and Futaki S. Cellular internalization and distribution of arginine-rich peptides as a function of extracellular peptide concentration, serum, and plasma membrane associated proteoglycans. Bioconjugate Chem. 2008; 19(3):656-664.

218. Abes S, Turner JJ, Ivanova GD, Owen D, Williams D, Arzumanov A, Clair P, Gait MJ and Lebleu B. Efficient splicing correction by PNA conjugation to an R(6)-Penetratin delivery peptide. Nucleic Acids Research. 2007; 35(13):4495-4502.

219. Rothbard JB, Jessop TC and Wender PA. Adaptive translocation: the role of hydrogen bonding and membrane potential in the uptake of guanidinium-rich transporters into cells. Advanced drug delivery reviews. 2005; 57(4):495-504.

220. Ben-Dov N and Korenstein R. Proton-induced endocytosis is dependent on cell membrane fluidity, lipid-phase order and the membrane resting potential. Biochimica et biophysica acta. 2013; 1828(11):2672-2681.

221. Klapperstuck T, Glanz D, Klapperstuck M and Wohlrab J. Methodological aspects of measuring absolute values of membrane potential in human cells by flow cytometry. Cytometry Part A : the journal of the International Society for Analytical Cytology. 2009; 75(7):593-608.

222. Krasznai Z, Marian T, Balkay L, Emri M and Tron L. Flow cytometric determination of absolute membrane potential of cells. Journal of photochemistry and photobiology B, Biology. 1995; 28(1):93-99.

223. Eisenman G, Sandblom J and Neher E. Interactions in cation permeation through the gramicidin channel. Cs, Rb, K, Na, Li, Tl, H, and effects of anion binding. Biophysical Journal. 1978; 22(2):307-340.

224. Superti F, Seganti L, Ruggeri FM, Tinari A, Donelli G and Orsi N. Entry pathway of vesicular stomatitis virus into different host cells. The Journal of general virology. 1987; 68 (Pt 2):387-399.

225. Sun X, Yau VK, Briggs BJ and Whittaker GR. Role of clathrin-mediated endocytosis during vesicular stomatitis virus entry into host cells. Virology. 2005; 338(1):53-60.

226. Cureton DK, Massol RH, Saffarian S, Kirchhausen TL and Whelan SP. Vesicular stomatitis virus enters cells through vesicles incompletely coated with clathrin that depend upon actin for internalization. PLoS pathogens. 2009; 5(4):e1000394.

227. Radoshitzky SR, Abraham J, Spiropoulou CF, Kuhn JH, Nguyen D, Li WH, Nagel J, Schmidt PJ, Nunberg JH, Andrews NC, Farzan M and Choe H. Transferrin receptor 1 is a cellular receptor for New World haemorrhagic fever arenaviruses. Nature. 2007; 446(7131):92-96.

228. Radoshitzky SR, Kuhn JH, Spiropoulou CF, Albarino CG, Nguyen DP, Salazar-Bravo J, Dorfman T, Lee AS, Wang E, Ross SR, Choe H and Farzan M. Receptor determinants of zoonotic transmission of New World hemorrhagic fever arenaviruses. Proceedings of the National Academy of Sciences of the United States of America. 2008; 105(7):2664-2669.

229. Abraham J, Kwong JA, Albarino CG, Lu JG, Radoshitzky SR, Salazar-Bravo J, Farzan M, Spiropoulou CF and Choe H. Host-species transferrin receptor 1 orthologs are cellular receptors for nonpathogenic new world clade B arenaviruses. PLoS pathogens. 2009; 5(4):e1000358.

230. Smelt SC, Borrow P, Kunz S, Cao W, Tishon A, Lewicki H, Campbell KP and Oldstone MB. Differences in affinity of binding of lymphocytic choriomeningitis virus strains to the cellular receptor alpha-dystroglycan correlate with viral tropism and disease kinetics. Journal of virology. 2001; 75(1):448-457.

231. Oppliger J, Torriani G, Herrador A and Kunz S. Lassa Virus Cell Entry via Dystroglycan Involves an Unusual Pathway of Macropinocytosis. Journal of virology. 2016; 90(14):6412-6429.

232. Iwasaki M, Ngo N and de la Torre JC. Sodium hydrogen exchangers contribute to arenavirus cell entry. Journal of virology. 2014; 88(1):643-654.

233. Quirin K, Eschli B, Scheu I, Poort L, Kartenbeck J and Helenius A. Lymphocytic choriomeningitis virus uses a novel endocytic pathway for infectious entry via late endosomes. Virology. 2008; 378(1):21-33.

234. Jae LT, Raaben M, Herbert AS, Kuehne AI, Wirchnianski AS, Soh TK, Stubbs SH, Janssen H, Damme M, Saftig P, Whelan SP, Dye JM and Brummelkamp TR. Virus entry. Lassa virus entry requires a trigger-induced receptor switch. Science. 2014; 344(6191):1506-1510.

235. Tani H, Iha K, Shimojima M, Fukushi S, Taniguchi S, Yoshikawa T, Kawaoka Y, Nakasone N, Ninomiya H, Saijo M and Morikawa S. Analysis of Lujo virus cell entry using pseudotype vesicular stomatitis virus. Journal of virology. 2014; 88(13):7317-7330.

236. Zaydman MA and Cui J. PIP2 regulation of KCNQ channels: biophysical and molecular mechanisms for lipid modulation of voltage-dependent gating. Frontiers in physiology. 2014; 5:195.

237. Zhang H, Craciun LC, Mirshahi T, Rohacs T, Lopes CM, Jin T and Logothetis DE. PIP(2) activates KCNQ channels, and its hydrolysis underlies receptor-mediated inhibition of M currents. Neuron. 2003; 37(6):963-975.

238. Vives E. Cellular uptake [correction of utake] of the Tat peptide: an endocytosis mechanism following ionic interactions. Journal of molecular recognition : JMR. 2003; 16(5):265-271.

239. Caron NJ, Quenneville SP and Tremblay JP. Endosome disruption enhances the functional nuclear delivery of Tat-fusion proteins. Biochem Biophys Res Commun. 2004; 319(1):12-20.

240. Illien F, Rodriguez N, Amoura M, Joliot A, Pallerla M, Cribier S, Burlina F and Sagan S. Quantitative fluorescence spectroscopy and flow cytometry analyses of cell-penetrating peptides internalization pathways: optimization, pitfalls, comparison with mass spectrometry quantification. Sci Rep. 2016; 6:36938.

241. Busetto S, Trevisan E, Patriarca P and Menegazzi R. A single-step, sensitive flow cytofluorometric assay for the simultaneous assessment of membrane-bound and ingested Candida albicans in phagocytosing neutrophils. Cytometry Part A : the journal of the International Society for Analytical Cytology. 2004; 58(2):201-206.

242. Tunnemann G, Martin RM, Haupt S, Patsch C, Edenhofer F and Cardoso MC. Cargo-dependent mode of uptake and bioavailability of TAT-containing proteins and peptides in living cells. FASEB journal : official publication of the Federation of American Societies for Experimental Biology. 2006; 20(11):1775-1784.

243. Li L, Wan T, Wan M, Liu B, Cheng R and Zhang R. The effect of the size of fluorescent dextran on its endocytic pathway. Cell biology international. 2015; 39(5):531-539.

244. Hopkins CR, Miller K and Beardmore JM. Receptor-mediated endocytosis of transferrin and epidermal growth factor receptors: a comparison of constitutive and ligand-induced uptake. Journal of cell science Supplement. 1985; 3:173-186.

245. Liu AP, Aguet F, Danuser G and Schmid SL. Local clustering of transferrin receptors promotes clathrin-coated pit initiation. The Journal of cell biology. 2010; 191(7):1381-1393.

246. Bechara C, Pallerla M, Burlina F, Illien F, Cribier S and Sagan S. Massive glycosaminoglycan-dependent entry of Trp-containing cell-penetrating peptides induced by exogenous sphingomyelinase or cholesterol depletion. Cellular and molecular life sciences : CMLS. 2015; 72(4):809-820.

247. Trimmer James S. Subcellular Localization of K+ Channels in Mammalian Brain Neurons: Remarkable Precision in the Midst of Extraordinary Complexity. Neuron. 2015; 85(2):238-256.

248. van den Bout I and Divecha N. PIP5K-driven PtdIns(4,5)P2 synthesis: regulation and cellular functions. Journal of cell science. 2009; 122(Pt 21):3837-3850.

249. Duan Y, Weinstein AM, Weinbaum S and Wang T. Shear stress-induced changes of membrane transporter localization and expression in mouse proximal tubule cells. Proceedings of the National Academy of Sciences of the United States of America. 2010; 107(50):21860-21865.

250. Alvarez-Baron CP, Jonsson P, Thomas C, Dryer SE and Williams C. The two-pore domain potassium channel KCNK5: induction by estrogen receptor alpha and role in proliferation of breast cancer cells. Molecular endocrinology (Baltimore, Md). 2011; 25(8):1326-1336.

251. Dom G, Shaw-Jackson C, Matis C, Bouffioux O, Picard JJ, Prochiantz A, Mingeot-Leclercq MP, Brasseur R and Rezsohazy R. Cellular uptake of Antennapedia Penetratin peptides is a two-step process in which phase transfer precedes a tryptophan-dependent translocation. Nucleic Acids Res. 2003; 31(2):556-561.

252. Schwab A, Schuricht B, Seeger P, Reinhardt J and Dartsch PC. Migration of transformed renal epithelial cells is regulated by K+ channel modulation of actin cytoskeleton and cell volume. Pflugers Archiv : European journal of physiology. 1999; 438(3):330-337.

253. Lee K, Jung J, Kim M and Guidotti G. Interaction of the alpha subunit of Na,K-ATPase with cofilin. The Biochemical journal. 2001; 353(Pt 2):377-385.

254. Paessler S and Walker DH. Pathogenesis of the viral hemorrhagic fevers. Annual review of pathology. 2013; 8:411-440.

255. Geisbert TW and Jahrling PB. Exotic emerging viral diseases: progress and challenges. Nature medicine. 2004; 10(12 Suppl):S110-121.

256. de la Torre JC. Molecular and cell biology of the prototypic arenavirus LCMV: implications for understanding and combating hemorrhagic fever arenaviruses. Annals of the New York Academy of Sciences. 2009; 1171 Suppl 1:E57-64.

257. Moraz ML and Kunz S. Pathogenesis of arenavirus hemorrhagic fevers. Expert review of anti-infective therapy. 2011; 9(1):49-59.

258. Pasqual G, Rojek JM, Masin M, Chatton JY and Kunz S. Old World Arenaviruses Enter the Host Cell via the Multivesicular Body and Depend on the Endosomal Sorting Complex Required for Transport. PLoS pathogens. 2011; 7(9).

259. Brandenburg B and Zhuang X. Virus trafficking – learning from single-virus tracking. Nature reviews Microbiology. 2007; 5(3):197-208.

260. Agarwal JJ, Zhu Y, Zhang Q-Y, Mongin AA and Hough LB. TRAM-34, a Putatively Selective Blocker of Intermediate-Conductance, Calcium-Activated Potassium Channels, Inhibits Cytochrome P450 Activity. PloS one. 2013; 8(5):e63028.

261. El-Andaloussi S, Johansson HJ, Lundberg P and Langel U. Induction of splice correction by cell-penetrating peptide nucleic acids. The journal of gene medicine. 2006; 8(10):1262-1273.

262. Urata S and Yasuda J. Molecular mechanism of arenavirus assembly and budding. Viruses. 2012; 4(10):2049-2079.

263. Morth JP, Poulsen H, Toustrup-Jensen MS, Schack VR, Egebjerg J, Andersen JP, Vilsen B and Nissen P. The structure of the Na+,K+-ATPase and mapping of isoform differences and disease-related mutations. Philosophical transactions of the Royal Society of London Series B, Biological sciences. 2009; 364(1514):217-227.

264. Lingrel JB, Williams MT, Vorhees CV and Moseley AE. Na,K-ATPase and the role of α isoforms in behavior. Journal of Bioenergetics and Biomembranes. 2007; 39(5):385-389.

265. Geering K. The functional role of beta subunits in oligomeric P-type ATPases. J Bioenerg Biomembr. 2001; 33(5):425-438.

266. Eil R, Vodnala SK, Clever D, Klebanoff CA, Sukumar M, Pan JH, Palmer DC, Gros A, Yamamoto TN, Patel SJ, Guittard GC, Yu Z, Carbonaro V, Okkenhaug K, Schrump DS, Linehan WM, et al. Ionic immune suppression within the tumour microenvironment limits T cell effector function. Nature. 2016; 537(7621):539-543.

267. Kuo YC, Huang KY, Yang CH, Yang YS, Lee WY and Chiang CW. Regulation of phosphorylation of Thr-308 of Akt, cell proliferation, and survival by the B55alpha regulatory subunit targeting of the protein phosphatase 2A holoenzyme to Akt. The Journal of biological chemistry. 2008; 283(4):1882-1892.

268. Yokoyama N and Miller WT. Inhibition of Src by direct interaction with protein phosphatase 2A. FEBS letters. 2001; 505(3):460-464.

269. Shajahan AN, Tiruppathi C, Smrcka AV, Malik AB and Minshall RD. Gbetagamma activation of Src induces caveolae-mediated endocytosis in endothelial cells. The Journal of biological chemistry. 2004; 279(46):48055-48062.

270. Reis CR, Chen PH, Srinivasan S, Aguet F, Mettlen M and Schmid SL. Crosstalk between Akt/GSK3beta signaling and dynamin-1 regulates clathrin-mediated endocytosis. The EMBO journal. 2015; 34(16):2132-2146.

271. Garay C, Judge G, Lucarelli S, Bautista S, Pandey R, Singh T and Antonescu CN. Epidermal growth factor-stimulated Akt phosphorylation requires clathrin or ErbB2 but not receptor endocytosis. Mol Biol Cell. 2015; 26(19):3504-3519.

272. Seshacharyulu P, Pandey P, Datta K and Batra SK. Phosphatase: PP2A structural importance, regulation and its aberrant expression in cancer. Cancer letters. 2013; 335(1):9-18.

273. Sarbassov DD, Guertin DA, Ali SM and Sabatini DM. Phosphorylation and regulation of Akt/PKB by the rictor-mTOR complex. Science. 2005; 307(5712):1098-1101.

274. Feng J, Park J, Cron P, Hess D and Hemmings BA. Identification of a PKB/Akt hydrophobic motif Ser-473 kinase as DNA-dependent protein kinase. The Journal of biological chemistry. 2004; 279(39):41189-41196.

275. Orrenius S, Zhivotovsky B and Nicotera P. Regulation of cell death: the calcium-apoptosis link. Nat Rev Mol Cell Biol. 2003; 4(7):552-565.

276. Paredes RM, Etzler JC, Watts LT and Lechleiter JD. Chemical Calcium Indicators. Methods (San Diego, Calif). 2008; 46(3):143-151.

277. Morgan AJ and Jacob R. Ionomycin enhances Ca2+ influx by stimulating store-regulated cation entry and not by a direct action at the plasma membrane. Biochemical Journal. 1994; 300(Pt 3):665-672.

278. Wie MB, Koh JY, Won MH, Lee JC, Shin TK, Moon CJ, Ha HJ, Park SM and Kim HC. BAPTA/AM, an intracellular calcium chelator, induces delayed necrosis by lipoxygenase-mediated free radicals in mouse cortical cultures. Progress in neuro-psychopharmacology & biological psychiatry. 2001; 25(8):1641-1659.

279. Babic Z, Crkvencic M, Rajic Z, Mikecin AM, Kralj M, Balzarini J, Petrova M, Vanderleyden J and Zorc B. New sorafenib derivatives: synthesis, antiproliferative activity against tumour cell lines and antimetabolic evaluation. Molecules (Basel, Switzerland). 2012; 17(1):1124-1137.

280. Homma S, Ishii Y, Morishima Y, Yamadori T, Matsuno Y, Haraguchi N, Kikuchi N, Satoh H, Sakamoto T, Hizawa N, Itoh K and Yamamoto M. Nrf2 enhances cell proliferation and resistance to anticancer drugs in human lung cancer. Clinical cancer research : an official journal of the American Association for Cancer Research. 2009; 15(10):3423-3432.

281. Wang XJ, Hayes JD and Wolf CR. Generation of a stable antioxidant response element-driven reporter gene cell line and its use to show redox-dependent activation of nrf2 by cancer chemotherapeutic agents. Cancer Res. 2006; 66(22):10983-10994.

282. DePristo MA, Banks E, Poplin R, Garimella KV, Maguire JR, Hartl C, Philippakis AA, del Angel G, Rivas MA, Hanna M, McKenna A, Fennell TJ, Kernytsky AM, Sivachenko AY, Cibulskis K, Gabriel SB, et al. A framework for variation discovery and genotyping using next-generation DNA sequencing data. Nature genetics. 2011; 43(5):491-498.

283. Cibulskis K, Lawrence MS, Carter SL, Sivachenko A, Jaffe D, Sougnez C, Gabriel S, Meyerson M, Lander ES and Getz G. Sensitive detection of somatic point mutations in impure and heterogeneous cancer samples. Nature biotechnology. 2013; 31(3):213-219.

284. Koboldt DC, Zhang Q, Larson DE, Shen D, McLellan MD, Lin L, Miller CA, Mardis ER, Ding L and Wilson RK. VarScan 2: somatic mutation and copy number alteration discovery in cancer by exome sequencing. Genome research. 2012; 22(3):568-576.

285. Wang K, Li M and Hakonarson H. ANNOVAR: functional annotation of genetic variants from high-throughput sequencing data. Nucleic acids research. 2010; 38(16):e164.

286. Anjum S, Morganella S, D'Angelo F, Iavarone A and Ceccarelli M. VEGAWES: variational segmentation on whole exome sequencing for copy number detection. BMC bioinformatics. 2015; 16:315.

287. Krzywinski M, Schein J, Birol I, Connors J, Gascoyne R, Horsman D, Jones SJ and Marra MA. Circos: an information aesthetic for comparative genomics. Genome research. 2009; 19(9):1639-1645.

288. Rubio-Perez C, Tamborero D, Schroeder MP, Antolin AA, Deu-Pons J, Perez-Llamas C, Mestres J, Gonzalez-Perez A and Lopez-Bigas N. In silico prescription of anticancer drugs to cohorts of 28 tumor types reveals targeting opportunities. Cancer cell. 2015; 27(3):382-396.

289. Parrales A and Iwakuma T. Targeting Oncogenic Mutant p53 for Cancer Therapy. Frontiers in oncology. 2015; 5:288.

290. Keshelava N, Zuo JJ, Waidyaratne NS, Triche TJ and Reynolds CP. p53 mutations and loss of p53 function confer multidrug resistance in neuroblastoma. Medical and pediatric oncology. 2000; 35(6):563-568.

291. Brachova P, Thiel KW and Leslie KK. The consequence of oncomorphic TP53 mutations in ovarian cancer. International journal of molecular sciences. 2013; 14(9):19257-19275.

292. Yu JL, Rak JW, Coomber BL, Hicklin DJ and Kerbel RS. Effect of p53 status on tumor response to antiangiogenic therapy. Science. 2002; 295(5559):1526-1528.

293. Owatari S, Akune S, Komatsu M, Ikeda R, Firth SD, Che XF, Yamamoto M, Tsujikawa K, Kitazono M, Ishizawa T, Takeuchi T, Aikou T, Mercer JF, Akiyama S and Furukawa T. Copper-transporting P-type ATPase, ATP7A, confers multidrug resistance and its expression is related to resistance to SN-38 in clinical colon cancer. Cancer Res. 2007; 67(10):4860-4868.

294. Furukawa T, Komatsu M, Ikeda R, Tsujikawa K and Akiyama S. Copper transport systems are involved in multidrug resistance and drug transport. Current medicinal chemistry. 2008; 15(30):3268-3278.

295. Li Z-h, Zheng R, Chen J-t, Jia J and Qiu M. The role of copper transporter ATP7A in platinum-resistance of esophageal squamous cell cancer (ESCC). Journal of Cancer. 2016; 7(14):2085-2092.

296. Li Z-h, Qiu M-z, Zeng Z-l, Luo H-y, Wu W-j, Wang F, Wang Z-q, Zhang D-s, Li Y-h and Xu R-h. Copper-transporting P-type adenosine triphosphatase (ATP7A) is associated with platinum-resistance in non-small cell lung cancer (NSCLC). Journal of Translational Medicine. 2012; 10:21-21.

297. Ezzoukhry Z, Louandre C, Trecherel E, Godin C, Chauffert B, Dupont S, Diouf M, Barbare JC, Maziere JC and Galmiche A. EGFR activation is a potential determinant of primary resistance of hepatocellular carcinoma cells to sorafenib. Int J Cancer. 2012; 131(12):2961-2969.

298. Morgillo F, Martinelli E, Troiani T, Orditura M, De Vita F and Ciardiello F. Antitumor activity of sorafenib in human cancer cell lines with acquired resistance to EGFR and VEGFR tyrosine kinase inhibitors. PloS one. 2011; 6(12):e28841.

299. Goel Hira L, Pursell B, Shultz Leonard D, Greiner Dale L, Brekken Rolf A, Vander Kooi Craig W and Mercurio Arthur M. P-Rex1 Promotes Resistance to VEGF/VEGFR-Targeted Therapy in Prostate Cancer. Cell Reports. 14(9):2193-2208.

300. Brognard J, Zhang Y-W, Puto LA and Hunter T. Cancer-Associated Loss-of-Function Mutations Implicate DAPK3 as a Tumor Suppressing Kinase. Cancer research. 2011; 71(8):3152-3161.

301. Yu L, Su YS, Zhao J, Wang H and Li W. Repression of NR4A1 by a chromatin modifier promotes docetaxel resistance in PC-3 human prostate cancer cells. FEBS letters. 2013; 587(16):2542-2551.

302. Correa S, Binato R, Du Rocher B, Ferreira G, Cappelletti P, Soares-Lima S, Pinto LF, Mencalha A and Abdelhay E. ABCB1 regulation through LRPPRC is influenced by the methylation status of the GC -100 box in its promoter. Epigenetics. 2014; 9(8):1172-1183.

303. Zhang L, Sun S, Zhou J, Liu J, Lv J-H, Yu X-Q, Li C, Gong L, Yan Q, Deng M, Xiao L, Ma H, Liu J-P, Peng Y-L, Wang D, Liao G-P, et al. Knockdown of Akt1 Promotes Akt2 Upregulation and Resistance to Oxidative-Stress-Induced Apoptosis Through Control of Multiple Signaling Pathways. Antioxidants & redox signaling. 2011; 15(1):1-17.

304. Han J, Jun Y, Kim SH, Hoang H-H, Jung Y, Kim S, Kim J, Austin RH, Lee S and Park S. Rapid emergence and mechanisms of resistance by U87 glioblastoma cells to doxorubicin in an in vitro tumor microfluidic ecology. Proceedings of the National Academy of Sciences of the United States of America. 2016; 113(50):14283-14288.

305. Marcucci F, Stassi G and De Maria R. Epithelial-mesenchymal transition: a new target in anticancer drug discovery. Nat Rev Drug Discov. 2016; 15(5):311-325.

306. Perl AK, Wilgenbus P, Dahl U, Semb H and Christofori G. A causal role for E-cadherin in the transition from adenoma to carcinoma. Nature. 1998; 392(6672):190-193.

307. Deryugina EI and Quigley JP. Matrix metalloproteinases and tumor metastasis. Cancer metastasis reviews. 2006; 25(1):9-34.

308. Scanlon CS, Van Tubergen EA, Inglehart RC and D'Silva NJ. Biomarkers of epithelial-mesenchymal transition in squamous cell carcinoma. Journal of dental research. 2013; 92(2):114-121.

309. Fischer KR, Durrans A, Lee S, Sheng J, Li F, Wong ST, Choi H, El Rayes T, Ryu S, Troeger J, Schwabe RF, Vahdat LT, Altorki NK, Mittal V and Gao D. Epithelial-to-mesenchymal transition is not required for lung metastasis but contributes to chemoresistance. Nature. 2015; 527(7579):472-476.

310. Zheng X, Carstens JL, Kim J, Scheible M, Kaye J, Sugimoto H, Wu CC, LeBleu VS and Kalluri R. Epithelial-to-mesenchymal transition is dispensable for metastasis but induces chemoresistance in pancreatic cancer. Nature. 2015; 527(7579):525-530.

311. Housman G, Byler S, Heerboth S, Lapinska K, Longacre M, Snyder N and Sarkar S. Drug resistance in cancer: an overview. Cancers. 2014; 6(3):1769-1792.

312. Li L, Hu Y, Ylivinkka I, Li H, Chen P, Keski-Oja J and Hyytiäinen M. NETRIN-4 Protects Glioblastoma Cells FROM Temozolomide Induced Senescence. PloS one. 2013; 8(11):e80363.

313. Januchowski R, Swierczewska M, Sterzynska K, Wojtowicz K, Nowicki M and Zabel M. Increased Expression of Several Collagen Genes is Associated with Drug Resistance in Ovarian Cancer Cell Lines. J Cancer. 2016; 7(10):1295-1310.

314. Davies KD, Mahale S, Astling DP, Aisner DL, Le AT, Hinz TK, Vaishnavi A, Bunn PA, Jr., Heasley LE, Tan A-C, Camidge DR, Varella-Garcia M and Doebele RC. Resistance to ROS1 Inhibition Mediated by EGFR Pathway Activation in Non-Small Cell Lung Cancer. PloS one. 2013; 8(12):e82236.

315. Ho TT, He X, Mo YY and Beck WT. Transient resistance to DNA damaging agents is associated with expression of microRNAs-135b and -196b in human leukemia cell lines. International journal of biochemistry and molecular biology. 2016; 7(2):27-47.

316. Wang T, Wei JJ, Sabatini DM and Lander ES. Genetic screens in human cells using the CRISPR/Cas9 system. Science (New York, NY). 2014; 343(6166):80-84.

317. Wu XM, Fu JG, Ge WZ, Zhu JY, Wang JY, Zhang W, Qian W and Huo KK. Screen p53 mutations in hepatocellular carcinoma by FASAY: a novel splicing mutation. Journal of Zhejiang University Science B. 2007; 8(2):81-87.

318. Levine AJ and Oren M. The first 30 years of p53: growing ever more complex. Nat Rev Cancer. 2009; 9(10):749-758.

319. Gao J, Aksoy BA, Dogrusoz U, Dresdner G, Gross B, Sumer SO, Sun Y, Jacobsen A, Sinha R, Larsson E, Cerami E, Sander C and Schultz N. Integrative analysis of complex cancer genomics and clinical profiles using the cBioPortal. Science signaling. 2013; 6(269):pl1.

320. Cerami E, Gao J, Dogrusoz U, Gross BE, Sumer SO, Aksoy BA, Jacobsen A, Byrne CJ, Heuer ML, Larsson E, Antipin Y, Reva B, Goldberg AP, Sander C and Schultz N. The cBio cancer genomics portal: an open platform for exploring multidimensional cancer genomics data. Cancer discovery. 2012; 2(5):401-404.

321. Kaspar JW, Niture SK and Jaiswal AK. Nrf2:INrf2 (Keap1) signaling in oxidative stress. Free radical biology & medicine. 2009; 47(9):1304-1309.

322. Ishii T, Itoh K, Takahashi S, Sato H, Yanagawa T, Katoh Y, Bannai S and Yamamoto M. Transcription factor Nrf2 coordinately regulates a group of oxidative stress-inducible genes in macrophages. The Journal of biological chemistry. 2000; 275(21):16023-16029.

323. Kim YC, Masutani H, Yamaguchi Y, Itoh K, Yamamoto M and Yodoi J. Hemin-induced activation of the thioredoxin gene by Nrf2. A differential regulation of the antioxidant responsive element by a switch of its binding factors. The Journal of biological chemistry. 2001; 276(21):18399-18406.

324. Zhang DD. Mechanistic studies of the Nrf2-Keap1 signaling pathway. Drug metabolism reviews. 2006; 38(4):769-789.

325. Kobayashi A, Kang MI, Okawa H, Ohtsuji M, Zenke Y, Chiba T, Igarashi K and Yamamoto M. Oxidative stress sensor Keap1 functions as an adaptor for Cul3-based E3 ligase to regulate proteasomal degradation of Nrf2. Mol Cell Biol. 2004; 24(16):7130-7139.

326. Zhang DD, Lo SC, Cross JV, Templeton DJ and Hannink M. Keap1 is a redox-regulated substrate adaptor protein for a Cul3-dependent ubiquitin ligase complex. Mol Cell Biol. 2004; 24(24):10941-10953.

327. Yoo NJ, Kim HR, Kim YR, An CH and Lee SH. Somatic mutations of the KEAP1 gene in common solid cancers. Histopathology. 2012; 60(6):943-952.

328. Singh A, Misra V, Thimmulappa RK, Lee H, Ames S, Hoque MO, Herman JG, Baylin SB, Sidransky D, Gabrielson E, Brock MV and Biswal S. Dysfunctional KEAP1-NRF2 interaction in non-small-cell lung cancer. PLoS medicine. 2006; 3(10):e420.

329. Shibata T, Kokubu A, Gotoh M, Ojima H, Ohta T, Yamamoto M and Hirohashi S. Genetic alteration of Keap1 confers constitutive Nrf2 activation and resistance to chemotherapy in gallbladder cancer. Gastroenterology. 2008; 135(4):1358-1368, 1368 e1351-1354.

330. Takahashi T, Sonobe M, Menju T, Nakayama E, Mino N, Iwakiri S, Nagai S, Sato K, Miyahara R, Okubo K, Hirata T, Date H and Wada H. Mutations in Keap1 are a potential prognostic factor in resected non-small cell lung cancer. Journal of surgical oncology. 2010; 101(6):500-506.

331. Zhang M, Zhang C, Zhang L, Yang Q, Zhou S, Wen Q and Wang J. Nrf2 is a potential prognostic marker and promotes proliferation and invasion in human hepatocellular carcinoma. BMC Cancer. 2015; 15(1):531.

332. Adamson PC, Houghton PJ, Perilongo G and Pritchard-Jones K. Drug discovery in paediatric oncology: roadblocks to progress. Nat Rev Clin Oncol. 2014; 11(12):732-739.

333. Poon I, Baxter AA, Lay FT, Mills GD, Adda CG, Payne JA, Phan TK, Ryan GF, White JA, Veneer PK, van der Weerden NL, Anderson MA, Kvansakul M and Hulett MD. Phosphoinositide-mediated oligomerization of a defensin induces cell lysis. eLife. 2014; 3:e01808.

334. Azordegan N, Fraser V, Le K, Hillyer LM, Ma DW, Fischer G and Moghadasian MH. Carcinogenesis alters fatty acid profile in breast tissue. Molecular and cellular biochemistry. 2013; 374(1-2):223-232.

335. Riboni L, Campanella R, Bassi R, Villani R, Gaini SM, Martinelli-Boneschi F, Viani P and Tettamanti G. Ceramide levels are inversely associated with malignant progression of human glial tumors. Glia. 2002; 39(2):105-113.

336. Llado V, Lopez DJ, Ibarguren M, Alonso M, Soriano JB, Escriba PV and Busquets X. Regulation of the cancer cell membrane lipid composition by NaCHOleate: effects on cell signaling and therapeutical relevance in glioma. Biochimica et biophysica acta. 2014; 1838(6):1619-1627.

337. Litan A and Langhans SA. Cancer as a channelopathy: ion channels and pumps in tumor development and progression. Frontiers in cellular neuroscience. 2015; 9:86.

338. Sontheimer H. An unexpected role for ion channels in brain tumor metastasis. Experimental biology and medicine (Maywood, NJ). 2008; 233(7):779-791.

339. Hatten ME and Roussel MF. Development and cancer of the cerebellum. Trends in neurosciences. 2011; 34(3):134-142.

340. Pedersen SF and Stock C. Ion channels and transporters in cancer: pathophysiology, regulation, and clinical potential. Cancer Res. 2013; 73(6):1658-1661.

341. Djamgoz MB, Coombes RC and Schwab A. Ion transport and cancer: from initiation to metastasis. Philosophical transactions of the Royal Society of London Series B, Biological sciences. 2014; 369(1638):20130092.

342. Werle M and Bernkop-Schnurch A. Strategies to improve plasma half life time of peptide and protein drugs. Amino acids. 2006; 30(4):351-367.

343. Michod D, Annibaldi A, Schaefer S, Dapples C, Rochat B and Widmann C. Effect of RasGAP N2 fragment-derived peptide on tumor growth in mice. Journal of the National Cancer Institute. 2009; 101(11):828-832.

344. Mengelbier LH, Karlsson J, Lindgren D, Valind A, Lilljebjorn H, Jansson C, Bexell D, Braekeveldt N, Ameur A, Jonson T, Kultima HG, Isaksson A, Asmundsson J, Versteeg R, Rissler M, Fioretos T, et al. Intratumoral genome diversity parallels progression and predicts outcome in pediatric cancer. Nature communications. 2015; 6:6125.

345. Somasundaram R, Villanueva J and Herlyn M. Intratumoral Heterogeneity as a Therapy Resistance Mechanism: Role of Melanoma Subpopulations. Advances in pharmacology (San Diego, Calif). 2012; 65:335-359.

346. Rauf SM, Endou A, Takaba H and Miyamoto A. Effect of Y220C mutation on p53 and its rescue mechanism: a computer chemistry approach. The protein journal. 2013; 32(1):68-74.

347. Liu X, Wilcken R, Joerger AC, Chuckowree IS, Amin J, Spencer J and Fersht AR. Small molecule induced reactivation of mutant p53 in cancer cells. Nucleic Acids Res. 2013; 41(12):6034-6044.

348. Boeckler FM, Joerger AC, Jaggi G, Rutherford TJ, Veprintsev DB and Fersht AR. Targeted rescue of a destabilized mutant of p53 by an in silico screened drug. Proceedings of the National Academy of Sciences of the United States of America. 2008; 105(30):10360-10365.

349. Wiman KG. Pharmacological reactivation of mutant p53: from protein structure to the cancer patient. Oncogene. 2010; 29(30):4245-4252.

350. Zhu AX, Rosmorduc O, Evans TR, Ross PJ, Santoro A, Carrilho FJ, Bruix J, Qin S, Thuluvath PJ, Llovet JM, Leberre MA, Jensen M, Meinhardt G and Kang YK. SEARCH: a phase III, randomized, double-blind, placebo-controlled trial of sorafenib plus erlotinib in patients with advanced hepatocellular carcinoma. Journal of clinical oncology : official journal of the American Society of Clinical Oncology. 2015; 33(6):559-566.

351. Konermann S, Brigham MD, Trevino AE, Joung J, Abudayyeh OO, Barcena C, Hsu PD, Habib N, Gootenberg JS, Nishimasu H, Nureki O and Zhang F. Genome-scale transcriptional activation by an engineered CRISPR-Cas9 complex. Nature. 2015; 517(7536):583-588.

352. Solimando DA, Jr. and Waddell JA. Lenvatinib and Palbociclib. Hospital pharmacy. 2015; 50(7):578-582.

353. Yamamoto Y, Matsui J, Matsushima T, Obaishi H, Miyazaki K, Nakamura K, Tohyama O, Semba T, Yamaguchi A, Hoshi SS, Mimura F, Haneda T, Fukuda Y, Kamata J, Takahashi K, Matsukura M, et al. Lenvatinib, an angiogenesis inhibitor targeting VEGFR/FGFR, shows broad antitumor activity in human tumor xenograft models associated with microvessel density and pericyte coverage. Vascular cell. 2014; 6:18.

354. Taketomi A. Clinical trials of antiangiogenic therapy for hepatocellular carcinoma. International journal of clinical oncology. 2016; 21(2):213-218.

355. Erazo-Oliveras A, Muthukrishnan N, Baker R, Wang TY and Pellois JP. Improving the endosomal escape of cell-penetrating peptides and their cargos: strategies and challenges. Pharmaceuticals (Basel, Switzerland). 2012; 5(11):1177-1209.

356. Rizzuti M, Nizzardo M, Zanetta C, Ramirez A and Corti S. Therapeutic applications of the cell-penetrating HIV-1 Tat peptide. Drug Discov Today. 2015; 20(1):76-85.

ANNEX I

A WxW MOTIF IS REQUIRED FOR THE ANTICANCER ACTIVITY OF THE TAT-RasGAP$_{317-326}$ PEPTIDE.

Contribution:

This work has been published in the Journal of Biological Chemistry in 2014. I performed all the revisions of the paper.

THE JOURNAL OF BIOLOGICAL CHEMISTRY VOL. 289, NO. 34, pp. 23701–23711, August 22, 2014

A *WXW* Motif Is Required for the Anticancer Activity of the TAT-RasGAP$_{317–326}$ Peptide*

Received for publication, April 24, 2014, and in revised form, July 4, 2014 Published, JBC Papers in Press, July 9, 2014, DOI 10.1074/jbc.M114.576272

David Barras[‡], Nadja Chevalier[‡], Vincent Zoete[§], Rosemary Dempsey[‡], Karine Lapouge[¶], Monilola A. Olayioye[‖], Olivier Michielin[§], and Christian Widmann[‡1]

From the [‡]Department of Physiology, University of Lausanne, 1005 Lausanne, Switzerland, the [§]Molecular Modeling Group, Swiss Institute of Bioinformatics (SIB), Quartier Sorge, Bâtiment Génopode, 1015 Lausanne, Switzerland, the [¶]Department of Fundamental Microbiology, University of Lausanne, 1015 Lausanne, Switzerland, and the [‖]Institute of Cell Biology and Immunology, University of Stuttgart, 70569 Stuttgart, Germany

Background: TAT-RasGAP$_{317–326}$ is a Ras GTPase-activating protein (RasGAP)-derived peptide that requires deleted in liver cancer-1 (DLC1) for its antimetastatic activities.
Results: A *WXW* motif within TAT-RasGAP$_{317–326}$ mediates RasGAP-DLC1 interaction.
Conclusion: The tryptophan residues of TAT-RasGAP$_{317–326}$ are crucial for its activity
Significance: The *WXW* motif could be used to design anticancer small molecules bearing TAT-RasGAP$_{317–326}$ activities.

TAT-RasGAP$_{317–326}$, a cell-permeable 10-amino acid-long peptide derived from the N2 fragment of p120 Ras GTPase-activating protein (RasGAP), sensitizes tumor cells to apoptosis induced by various anticancer therapies. This RasGAP-derived peptide, by targeting the deleted in liver cancer-1 (DLC1) tumor suppressor, also hampers cell migration and invasion by promoting cell adherence and by inhibiting cell movement. Here, we systematically investigated the role of each amino acid within the RasGAP$_{317–326}$ sequence for the anticancer activities of TAT-RasGAP$_{317–326}$. We report here that the first three amino acids of this sequence, tryptophan, methionine, and tryptophan (WMW), are necessary and sufficient to sensitize cancer cells to cisplatin-induced apoptosis and to reduce cell migration. The WMW motif was found to be critical for the binding of fragment N2 to DLC1. These results define the interaction mode between the active anticancer sequence of RasGAP and DLC1. This knowledge will facilitate the design of small molecules bearing the tumor-sensitizing and antimetastatic activities of TAT-RasGAP$_{317–326}$.

Cancer is the second leading cause of death worldwide (1). Ninety percent of cancer-related death is attributed to metastases (1). Surgery, chemotherapy, and radiotherapy remain at present the main clinical therapeutic tools to treat cancer. These treatments are very efficacious against some cancers but are of limited long term efficacy against others. Besides developing new anticancer modalities, increasing the efficacy of current therapies is of clear and timely interest.

p120 Ras GTPase-activating protein (from now on referred to as RasGAP)[2] is a multidomain protein. It was first reported as a negative modulator of the Ras signaling pathway (2). This activity requires the GAP domain of the protein (2). It was found later that other domains of the protein had signaling activities that were not related to its function as a GAP. For example, the N-terminal moiety of RasGAP can positively regulate MAP kinase kinases such as Ras and Mos (3). RasGAP is also a specific caspase-3 substrate (4). Because of the presence of two sites within RasGAP that have differential sensitivities toward caspase-3-mediated cleavage, the RasGAP/caspase-3 module acts as a stress sensor in cells (5). In the presence of low stresses, caspase-3 is mildly activated, and this leads to the partial cleavage of RasGAP into an N-terminal fragment that exerts potent, Akt-dependent, antiapoptotic activities (4, 6, 7). When cells are subjected to strong stresses, RasGAP is fully processed by caspase-3, further cleaving the N-terminal fragment and henceforth destroying its ability to protect cells.

One of the fragments generated by the full cleavage of RasGAP by caspase-3, fragment N2 (RasGAP$_{158–455}$), has the capacity to increase the sensitivity to anticancer treatments of various tumor cell lines, both *in vitro* and *in vivo* (6, 8). Similarly to fragment N2, a cell-permeable 10-amino acid peptide contained within the SH3 domain of fragment N2, called TAT-RasGAP$_{317–326}$, was found to efficiently sensitize cancer cells to anticancer agent-induced apoptosis (9) and to inhibit tumor growth when combined with chemotherapy (8). We recently reported that fragment N2 was an efficient inhibitor of the metastatic cascade (10). TAT-RasGAP$_{317–326}$ also inhibited cell migration and invasion into basement membrane matrix by strengthening adhesiveness of the cells to their substratum (11). However, in an attempt to use TAT-RasGAP$_{317–326}$ as an antimetastatic tool, we found, using mouse models, that this peptide was not always delivered efficiently to tumors (10). This delivery issue would call for the development of small molecules bearing the activity of RasGAP$_{317–326}$. However, such

* This work was supported by a grant from Oncosuisse (KFS-02543-02-2010). C. W. is a co-inventor of the TAT-RasGAP$_{317–326}$ compound as an antitumor agent (patent owned by the University of Lausanne) and may receive royalties from patent licensing if the compound is commercialized.
[1] To whom correspondence should be addressed: Dept. of Physiology, Bugnon 7, 1005 Lausanne, Switzerland, Tel.: 41-21-692-5123; Fax: 41-21-692-5505, E-mail: Christian.Widmann@unil.ch.
[2] The abbreviations used are: RasGAP, Ras GTPase-activating protein; DLC, deleted in liver cancer protein; ANOVA, analysis of variance; ITC, isothermal titration calorimetry; oligo, oligonucleotide; h, human; TAT, transactivator of transcription.

development would greatly benefit from a better understanding of the mode of action of TAT-RasGAP$_{317–326}$.

Actin cytoskeleton dynamics controls adhesion, migration, and invasion and is mainly regulated by the small GTPases of the Rho family (*e.g.* Rho itself, Rac, and Cdc42 (12, 13)). We found that the TAT-RasGAP$_{317–326}$ molecular properties by which it induces adhesion and inhibits migration rely on modulation of the actin cytoskeleton and requires deleted in liver cancer-1 (DLC1), a RhoGAP that functions as a tumor and metastasis suppressor (11, 14). Therefore, understanding whether and how TAT-RasGAP$_{317–326}$ engages DLC1 is of crucial interest.

Although peptide therapeutics are gathering increasing interest for the treatment of tumors (15), classical issues associated with peptide-based therapy are impeding their development. These issues consist of the rapid clearance from the body, the lack of targetable ability, their short half-lives, and their expensive production costs. Consistent with this, the Lipinski's rule-of-five, a model that predicts the likeliness of a compound to be translated into an orally active drug, is of bad prognosis for peptide development (16).

The goal of the present study was to characterize the importance of each of the RasGAP$_{317–326}$ amino acids for its sensitizing activity and its ability to increase cell adhesiveness. This was performed to better understand the mode of action of the peptide and to gather structure-function information that could be used for pharmacological development to facilitate the development of a small molecule that mimics TAT-RasGAP$_{317–326}$. Our recent finding that fragment N2 requires DLC1 for its antimetastatic activities prompted us to dissect how these two molecules interact. Here, we report the exact binding mode between DLC1 and TAT-RasGAP$_{317–326}$ and we identify a short W*X*W motif located at the N-terminal end of the peptide that carries its anticancer activities.

EXPERIMENTAL PROCEDURES

Cell Lines and Cell Culture—The osteosarcoma cell line used in this study is U2OS (ATCC; HTB-96). HEK-293T cells were used for protein interaction studies as reported previously (11). The cells were cultured at 37 °C and 5% CO_2 and were maintained in Dulbecco's modified Eagle's medium (DMEM) (Gibco; 61965) supplemented with 10% fetal bovine serum (FBS) (Gibco; 10270) for not more than 2 months and were constantly checked for their morphology.

Peptide Synthesis—The peptides used in this study were made of D-amino acids, which provide resistance to proteases and therefore increase their stability. In order for the side chains to be similarly exposed as in L-form peptides (8), the D-form peptides were synthesized starting with the last C-terminal residue (retro-inverso peptides). The TAT-RasGAP$_{317–326}$ (GRKKRRQRRRGGWMWVTNLRTD), the TAT (HIV-TAT$_{48–57}$) (GRKKRRQRRR), and all the peptides mentioned in the figures were synthesized at the Department of Biochemistry, University of Lausanne, Switzerland using the Fmoc (*N*-(9-fluorenyl)methoxycarbonyl) technology, purified by HPLC, and tested by mass spectrometry as reported earlier (9). Two glycine residues were inserted as a linker between TAT and the peptides of interest.

Trypsin-mediated Detachment Assays, Transfection, Immunoprecipitation, and Western Blotting—Trypsin-mediated detachment assays, Giemsa staining, calcium-phosphate transfection, immunoprecipitation, and Western blotting were performed as reported previously (11). The primary antibodies used were anti-HA (Covance; MMS-101r), anti-V5 (Invitrogen; 46-1157) and anti-GFP (Clontech; 632380).

Wound-healing Scratch Assay—Five hundred thousand U2OS were grown in 3.5-cm plates. The day after, the cells were pretreated as indicated in the figures for 3 h. A wound in the cell layer was made with a tip (0.4-mm diameter at its extremity). Five pictures per wound were taken just after wounding (0 h), and then 24 and 48 h after wounding (the same five fields per wound were photographed at each time point). Wound areas were measured using the ImageJ software. The migration area was calculated by subtracting the 48 h value by the 0 h value, and the data were normalized against the untreated condition. For time-course experiments, the data obtained after 24 h were treated similarly than for 48 h.

Apoptosis Measurements—One hundred and fifty thousand U2OS cells were grown in 3.5-cm plates. The day after, the cells were treated for 22 h with 20 μM TAT-coupled peptides in the presence or in the absence of 30 μM cisplatin (Sigma-Aldrich; P4394) as indicated in the figures. The cells were then fixed, and the nuclei were stained in 2% paraformaldehyde containing 10 μg/ml Hoechst 33342 (Molecular Probes; H1399) for 15 min. The pyknotic nuclei were visualized using the Nikon Eclipse TS100 microscope equipped with fluorescence; they were then scored and reported in percentage over total number of cells.

Greyscale Heat Map—Heat map was performed by semi-quantitative evaluation of the effects of the alanine-substituted peptides as compared with wild-type 317–326 peptide. The results on which the heat map is based appear in Fig. 1*B* (adherence; 20 μM values), Fig. 2*A* (migration), and Fig. 2*B* (apoptosis). This heat map is a greyscaled representation of whether the alanine-substituted peptides recapitulate the effects of 317–326. Specifically for apoptosis, the minimal effect (in *black*) was set to the "cisplatin alone" condition, and the maximal effect (in *white*) was set to the "cisplatin + 317–326" condition; for adherence, the minimal effect (in *black*) was set to the "untreated + trypsin" condition, and the maximal effect (in *white*) was set to the "317–326 + trypsin" condition; for migration, the minimal effect (in *white*) was set to the "317–326" condition, and the maximal effect (in *black*) was set to the "untreated" condition.

Plasmids—The extension .dn3 indicates that the backbone plasmid is pcDNA3 (plasmid 1) from Invitrogen. The Stag-HA-hRasGAP[158–455].dn3 (plasmid 644) (here called HA-N2), Stag-HA-hRasGAP[158–455](W317A).dn3 (plasmid 793) (here called HA-N2 (W317A)), and V5-mDLC1[1–1092].dn3 (plasmid 791) (here called V5-DLC1) plasmids were described earlier (11). The Stag-HA-hRasGAP[158–455](W319A).dn3 (plasmid 803) (here called HA-N2 (W319A)) plasmid encodes a Stag- and HA-tagged form of fragment N2 bearing a mutation of tryptophan 319 into an alanine residue (W319A). The template vector used for starting the mutagenesis is the HA-N2 plasmid. Mutagenesis was performed using the mega-primer procedure (17) as follows. (i) The W319A mutation was gener-

ated by PCR amplification of HA-N2 using oligonucleotide (oligo) 1019 (human RasGAP nucleotides 1052–1097 (NCBI entry M23379) except for nucleotides (underlined) that create a W319A mutation and a silent mutation generating a Bsu36I restriction site: (GAA TTA GAA GAT GGA TGG ATG GCG (W319A) GTT ACA AACC (N1-N2 of Bsu36I) TA AGG (N7 of Bsu36I) ACAGATG)) and oligo 62 (TACCTAGCATGAACA-GATTG (random sequence) AGGGGCAAACAACAGATG (pcDNA3 nucleotides 1080–1063)). (ii) The PCR product obtained in (i) was purified and elongated on the HA-N2 template. (iii) The PCR reaction was resumed after the addition of oligo 28 and oligo 70. The PCR in (iii) was digested with BsiWI and NotI and ligated into plasmid HA-N2 digested with the same enzymes. The DLC1 mutant plasmids were generated using the same methodology. The V5-mDLC1[1–1092] (R677A).dn3 (plasmid 804) (here called V5-DLC1 (R677A)) plasmid encodes a V5-tagged form of the *Mus musculus* DLC1 transcript variant 2 (NM_015802.3) bearing a mutation of arginine 677 into an alanine residue (R677A). The template vector used for starting the mutagenesis is the V5-DLC1 plasmid. Mutagenesis was performed as follows. (i) The R677A mutation was generated by PCR amplification of V5-DLC1 using oligo 1016 (mouse *Dlc1* nucleotides 2368–2411 (NCBI entry NM_015802.3) except for nucleotides (underlined) that create a R677A mutation and a silent mutation generating an EcoRI restriction site: (GTC GGG CTC TTC GCG (R677A) AAG TCA GGT GTC AAA TCC CG A (N2 of EcoRI) AT T (N5 of EcoRI) CAGGCT) and oligo 62. (ii) The PCR product obtained in (i) was purified and elongated on the V5-DLC1 template. (iii) The PCR reaction was resumed after the addition of oligo 28 (TAATACGACTCACTATAGGGAGA (pcDNA3 sequence 863–885)) and oligo 70 (TACCTAGCATGAACAGATTG (same random sequence as in nucleotide oligo 62)). The PCR in (iii) was digested with EcoRV and XhoI and ligated into plasmid V5-DLC1 digested with the same enzymes. The V5-mDLC1[1–1092](N829A,L830A).dn3 (plasmid 805) (here called V5-DLC1 (N829A,L830A)) plasmid encodes a V5-tagged form of the *M. musculus* DLC1 transcript variant 2 (NM_015802.3) bearing a mutation of asparagine 829 and leucine 830 into alanine residues (N829A,L830A). The template vector used for starting the mutagenesis is the V5-DLC1. Mutagenesis was performed as follows. (i) The N829A and L830A mutations were generated by PCR amplification of V5-DLC1 using oligo 1017 (mouse *Dlc1* nucleotides 2821–2859 (NCBI entry NM_015802.3) except for nucleotides (underlined) that create the N829A and L830A mutations and a new NotI restriction site: (AAA GAC CTG AAT GAA GCGGCC (N829A,L830A and (N1–6) of NotI) GCG GCG ACT CAA GGG CTG) and oligo 62). (ii) The PCR product obtained in (i) was purified and elongated on the V5-DLC1 template. (iii) The PCR reaction was resumed after the addition of oligo 28 and oligo 70. The PCR in (iii) was digested with EcoRI and XhoI and ligated into plasmid V5-DLC1 digested with the same enzymes. The extension .gfp indicates that the backbone plasmid is pEGFP-C1 (plasmid 6) from Clontech and encodes the green fluorescent protein. The pEGFP-hDLC1.gfp (plasmid 811) (here called GFP-DLC1), pEGFP-hDLC2.gfp (plasmid 812) (here called GFP-DLC2) and pEGFP-hDLC3.gfp (plasmid 813) (here called GFP-DLC3) plasmids encode GFP-tagged versions of human DLC1, DLC2α, and DLC3α, respectively, and were described earlier (18, 19).

The extension .pgx indicates that the backbone plasmid is pGEX-4T-1 from GE Healthcare. GST-hDLC1[625–878].pgx (plasmid 816) (here called GST-DLC1-GAP) is an expression vector encoding the GST fusion human DLC1 GAP domain corresponding to nucleotide 1873–2634 of the human *DLC1* gene (GenBank: AAK97501.1).

In Silico Prediction of Protein Interaction—The rigid docking of p120 RasGAP to DLC1 was performed using the PatchDock web server (20, 21), version beta 1.3, with the default complex type and a 4.0 Å clustering root mean square deviation. The DLC1 GAP domain (Protein Data Bank (PDB) ID: 3KUQ (22, 23)) was used as the receptor and the RasGAP SH3 domain (PDB ID: 2J05 (24)) as the ligand. The receptor and ligand binding sites were not imposed, and no additional constraint was applied during the docking. The best-scored calculated binding mode was retained for structural analysis.

Recombinant Protein Production and Isothermal Titration Calorimetry—Recombinant GST-DLC1-GAP domain was produced as reported previously using BL21 transformed with the GST-GAP-DLC1.pgx construct (25). Elution of the GST-DLC1-GAP domain in 30 mM reduced L-glutathione (Sigma-Aldrich, G4251, in 50 mM Tris (pH:7.4), 100 mM NaCl) was followed by 2 h of dialysis in 4 liters of PBS. The dialysis buffer was then used as titration buffer and to resuspend TAT-$RasGAP_{317–326}$ and the corresponding tryptophan mutants. Isothermal titration calorimetry was performed as reported previously using the ITC200 system (GE Healthcare Life Sciences) unless otherwise mentioned (26). The sample cell (200 μl) was loaded with 50 μM GST-DLC1-GAP, whereas the TAT-$RasGAP_{317–326}$ and the tryptophan mutant concentrations in the syringe were 500 μM. The titration experiment started with an injection of 0.5 μl followed by 15 injections of 2.49 μl, each lasting 5 s, with a 3-min interval between each injection. Controls and measurements were performed as reported earlier (26).

Statistical Analysis—All experiments were performed independently. The results were expressed as mean $\pm$ 95% confidence intervals. One-way ANOVAs and repeated measurement ANOVAs were performed using the R software (version 2.11.0) and were followed by a Tukey test for multiple comparisons. Asterisks denote statistically significant differences (p value < 0.05).

RESULTS

The individual contribution of each amino acid of the RasGAP 317–326 sequence was evaluated through an alanine-scanning approach. This approach has been successfully used to identify several protein-protein interactions (27). For example, it has been employed to map the binding between the human immunodeficiency virus (HIV) GP120 glycoprotein and the human CD4 receptor (28). This methodology consists of substituting amino acids of interest into alanine residues (27). Alanine that has a methyl side chain is considered as neutral and, in contrast to glycine that is also a small amino acid with only a hydrogen side chain, prevents introduction of conformational flexibility. Alanine substitutions therefore tend to keep

intact the overall secondary structure of the investigated protein (27).

We first evaluated the consequence of these mutations on adhesion induced by TAT-RasGAP$_{317–326}$ (from now on referred to as 317–326). Alanine substitutions of the tryptophan residues at positions 317 and 319 abrogated the capacity of the peptide to increase cell adherence (Fig. 1, *A* and *B*). Substitutions at positions 318, 320, 323, 324, and 325 strongly reduced the pro-adherence activity of 317–326, but some residual adherence was nevertheless observed. Replacement of amino acids 321, 322, and 326 had no or only limited effect on the ability of the peptide to increase cell adherence. These results indicate that the tryptophan and leucine residues of 317–326 are critically required for the pro-adhesion activity of the peptide. Residues 318, 320, and 324–325 are also important for this activity but do not appear as indispensable as the tryptophan residues because their replacement does not totally abolish the activity of 317–326. One could therefore generate a consensus sequence for RasGAP$_{317–326}$-mediated adhesion increase, **W**M**W**V*XX*LRT*X*, where the *X* represents residues that are not required for this activity and where the bold residues are those that seem the most important for the pro-adhesive activity of the peptide. Interestingly, this consensus sequence is almost identical to the amino acids that are conserved between vertebrates and insects in the RasGAP 317–326 sequence (W*X*WVT*XX*RT*X*) (Fig. 1*C*). Hence the data presented in Fig. 1 indicate that most evolutionary conserved amino acids are important for the increase cell adherence mediated by the 317–326 sequence of RasGAP.

We next assessed whether the amino acids identified to be required for the pro-adhesion activity of 317–326 were also playing a role in the capacity of the peptide to inhibit migration and to sensitize tumor cells to genotoxins. Similarly to the adhesion increase, alanine substitutions of the Trp-317, Trp-319, Leu-323, Arg-324, and Thr-325 amino acids completely or partially abrogated the capacity of 317–326 to inhibit cell migration (Fig. 2*A*) or to favor cell death induced by cisplatin, a commonly used chemotherapeutic agent (Fig. 2*B*). The Met-318 and Val-320 residues seem, however, to be differentially required for 317–326-mediated effects on apoptosis, adhesion, and migration (Fig. 2*C*). This differential requirement of Met-318 and Val-320 could be the consequence of 317–326 mediating its effects on apoptosis, adhesion, and migration via different signaling pathways. Alternatively, this could be explained by a difference in the sensitivity of the assays used to measure apoptosis, adhesion, and migration and/or a difference in the sensitivity of these biological processes themselves. We therefore performed a dose response with 317–326 and measured apoptosis sensitization, adhesion increase, and migration inhibition. Fig. 2*D* shows that these three assays or biological processes do not display similar sensitivities to the RasGAP-derived peptide. Indeed, the EC_{50} for apoptosis sensitization (5 μM) was lower than the EC_{50} for adhesion promotion (11.5 μM), which was lower than the EC_{50} for migration (16.5 μM). In other words, less 317–326 is required to render tumor cells more sensitive to cisplatin-induced apoptosis than is required to mediate increased adhesiveness and even less so to inhibit cell migration. This indicates that a decrease in the activity of the peptide will first impact on its capacity to inhibit migration, then on its ability to increase cell adherence, and lastly on its capacity to sensitize cells to anticancer treatments. Hence a mutation that partially affects the activity of 317–326 should have a stronger impact on migration inhibition than on cell adherence promotion and tumor sensitization. This is particularly obvious with the V320A mutation. This can also be seen somewhat with the M318A and L323A mutations. Therefore, these results are not contradictory with the possibility that modulation of apoptosis, adhesion, and migration by 317–326 is the consequence of one protein or molecule being targeted by the peptide.

If the two N-terminal tryptophan residues of 317–326 are the only crucial residues for the activity of the peptide, it should be possible to shorten the 317–326 sequence without losing its activity. Hence, truncated versions of 317–326 were analyzed for their effects on adhesion, migration, and sensitization to apoptosis. Fig. 3, *A* and *B*, show that 317–323 and 317–321 still induce increased adherence, although to a lower extent than the parental 317–326 peptide. In contrast, 322–326 failed to augment cell adhesiveness. This indicates that the 317–321 sequence is sufficient to increase cell adherence. Although the 322–326 sequence lacked activity, it still may be required for optimal 317–326 activity as revealed by the point mutations within this sequence (Figs. 1 and 2). It was reported that the 322–326 sequence participates in the formation of a β-sheet required for dimerization of the RasGAP SH3 domains. One could therefore hypothesize that the 322–326 fulfills structural functions to constrain the 317–321 stretch in a conformation that is optimal for its activity. Co-incubation of 317–321 and 322–326 failed to potentiate 317–321-induced adhesion, indicating that both domains have to be carried by the same entity to be physiologically fully active. When the active peptides are narrowed down to four (317–320) and three (317–319) amino acids, their pro-adhesive property is even more decreased (Fig. 3*B*). We also tested the ability of the truncated peptides to inhibit migration (Fig. 3*C*) and to sensitize to cisplatin-induced apoptosis (Fig. 3*D*). The slight 317–323-mediated increase of adherence was translated into a weak but statistically significant inhibition of migration, whereas smaller peptides did not affect migration or affected it to a much lesser extent (Fig. 3*C*). On the other hand, the apoptosis-sensitizing effect of the truncated versions, including the 317–319 tripeptide, was similar to the one induced by the full-length peptide (Fig. 3*D*). Of note, the *Drosophila* peptide that carries a leucine residue at position 318 was highly efficient in recapitulating the effects of the human version (Fig. 3, *A–D*). Altogether, these results indicate that the W*X*W motif within the 317–326 sequence carries the anticancer activities of the peptide.

To better understand why the 317–319 tripeptide sensitizes tumor cells to apoptosis but does not recapitulate the effects on adhesion and more importantly on migration, we evaluated the effects of increased dose of 317–319 on migration. Wound closure was measured over a 48-h period to have a longer window for the evaluation of migration dynamics. At a 40 μM concentration, the 317–319 tripeptide significantly inhibited migration (Fig. 4*A*). When the 317–319 concentration increased to 60 μM, the effect on migra-

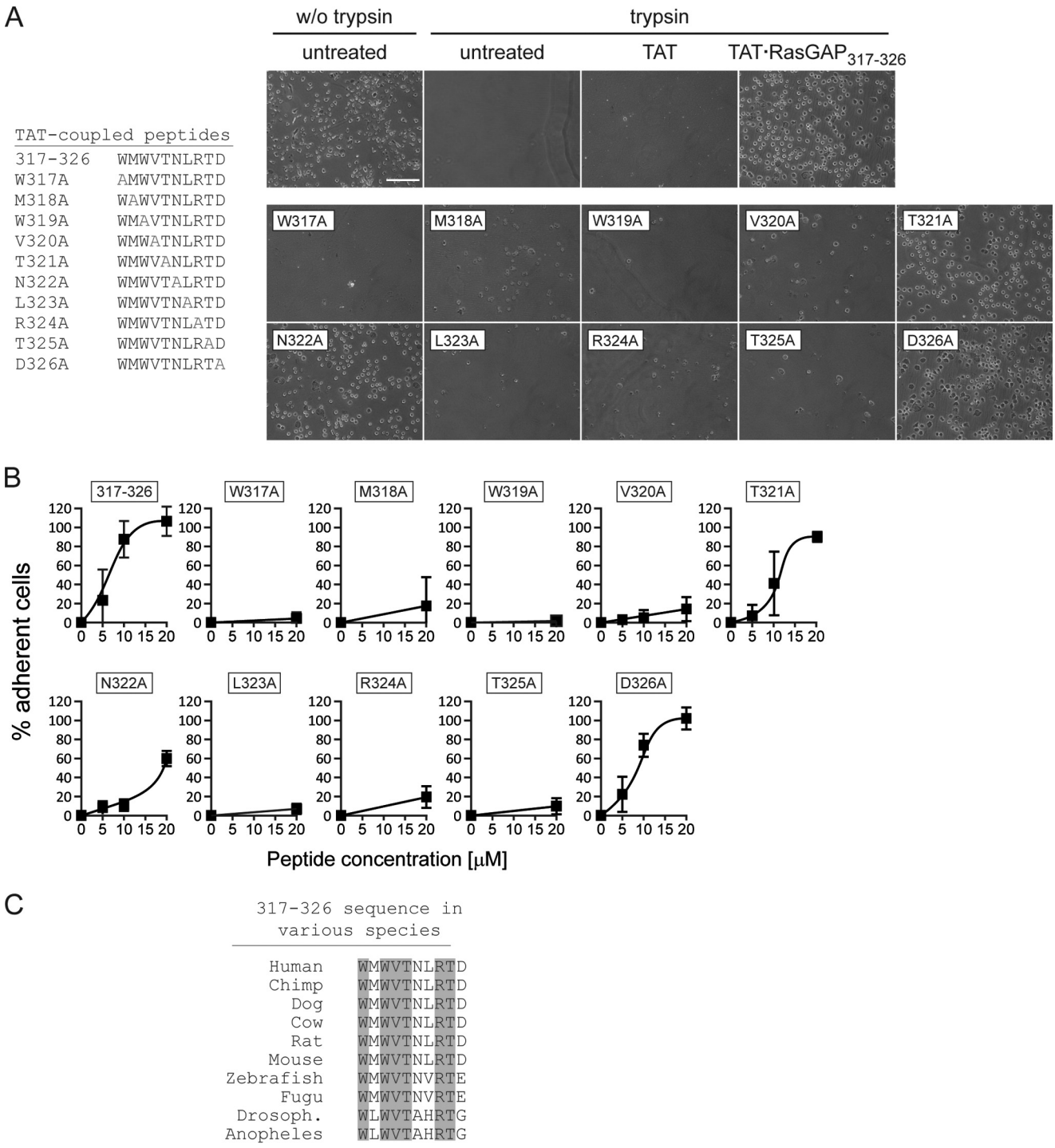

FIGURE 1. **Cell adherence induced by alanine-substituted RasGAP$_{317–326}$ peptides.** *A* and *B*, U2OS cells were cultured overnight and then treated for 8 h with 20 μM TAT or 20 μM of the indicated TAT-coupled peptides or left untreated. The cells were then subjected to trypsin-mediated detachment assays. The images shown in *panel A* correspond to 20 μM peptide-treated cells ($n = 4$ independent experiments). *Scale bar*: 200 μM for all images. *w/o trypsin*, without trypsin. *B*, dose-response quantitation ($n = 4$ independent experiments). *C*, alignment of the p120 RasGAP$_{317–326}$ sequences from different species. The amino acids conserved during evolution are shaded in *gray*. *Drosoph.*, Drosophila.

tion was not stronger than with 40 μM, indicating that 40 μM is already a saturating dose and that 317–319 cannot reach the inhibitory effect obtained with the full-length peptide. In contrast, the dose-response experiment depicted in Fig. 4*B* shows that 317–319 is as efficient as 317–326 in sensitizing tumor cells to cisplatin-induced apoptosis. This finding may indicate that two different molecules are targeted by 317–326 to mediate inhibition of migration and to sensitize tumor cells to death.

The DLC family consists of three isoforms (DLC1, DLC2, and DLC3) with nonredundant activity (14). DLC1 regulates cell migration (29). DLC2 could modulate apoptosis as it can be localized at the mitochondria level (30). Fragment N2, the parental polypeptide from which 317–326 is derived, can bind

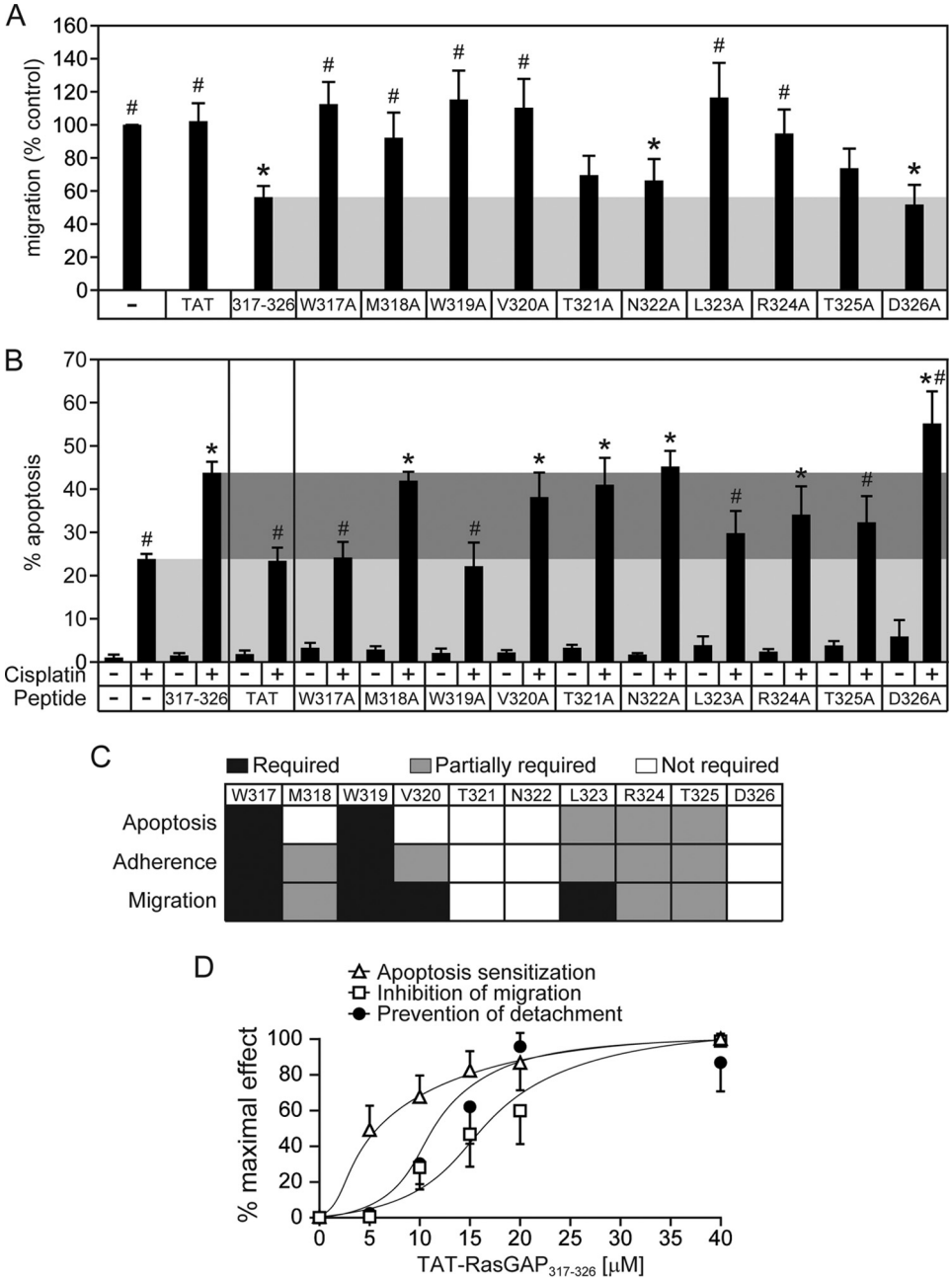

FIGURE 2. **Ability of alanine-substituted RasGAP$_{317–326}$ peptides to inhibit cell migration and sensitize cancer cells against cisplatin-induced apoptosis.** *A*, U2OS cells were grown to confluence and were pretreated for 3 h with 20 μM of the indicated TAT-coupled peptides. The cells were then subjected to wound healing scratch assays. The graph displays the percentage of migration over untreated cells. *Asterisks* and *number signs* denote statistical significant differences after one-way ANOVA (*asterisk*: different from untreated condition; *number sign*: different from 317–326 treatment; $n = 7$ independent experiments). *Error bars* indicate mean ± 95% confidence intervals. *B*, U2OS cells were cultured overnight and were subsequently treated for 22 h with 20 μM of the indicated TAT-coupled peptides in the presence or in the absence of 30 μM cisplatin. The number of pyknotic nuclei was then scored and reported as the percentage of apoptosis. The *light gray region* displays the level of apoptosis induced by cisplatin alone, and the *dark gray region* shows the apoptosis sensitization zone. *Asterisks* and *number signs* denote statistical significant differences after one-way ANOVA with the cisplatin-only treatment and with the cisplatin + 317–326 treatment, respectively ($n = 6$ independent experiments). *Error bars* indicate mean ± 95% confidence intervals, *C*, schematic representation of the importance of each amino acid within the wild-type sequence for the apoptosis sensitization, adhesion promotion, and migration inhibition processes. *D*, comparison of the dose-dependent effect of 317–326 on apoptosis sensitization, adhesion (prevention of detachment), and inhibition of migration. Each experiment was performed as described in earlier figures and panels except that here all the responses are reported as the percentage of the maximum observed effect. *Error bars* indicate mean ± 95% confidence intervals.

DLC1 (11) but whether fragment N2 also binds the other DLC isoforms was not investigated. Fig. 4*C* shows that DLC2, but not DLC3, interacts with fragment N2. As fragment N2 binds both DLC1 and DLC2, this raises the possibility that 317–326 modulates adhesion/migration through DLC1 and apoptosis through DLC2 (model 1 in Fig. 4*D*). Another possibility would be that DLC1 and DLC2 are both required for the effects on adhesion/migration and that a still unidentified protein mediates the apoptotic response (model 2 in Fig. 4*D*). Jaiswal *et al.* (31) have shown that the SH3 domain of RasGAP binds to the DLC1 GAP domain using isothermal titration calorimetry (ITC). However, whether 317–326 directly binds DLC proteins

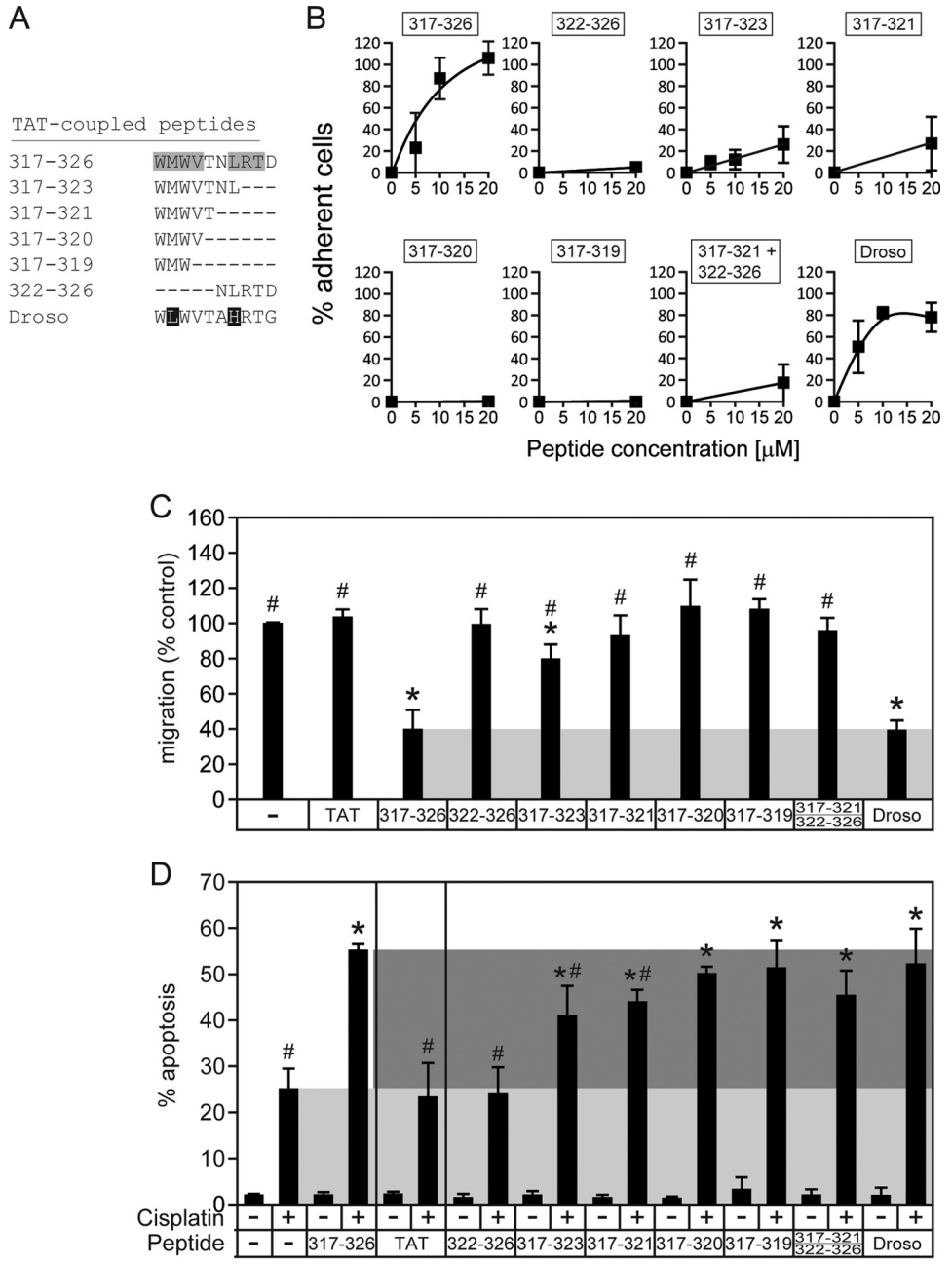

FIGURE 3. **Ability of truncated and variant RasGAP$_{317–326}$ peptides to increase adherence, inhibit cell migration, and sensitize cancer cells to cisplatin-induced apoptosis.** *A*, sequences of the peptides tested. Residues shaded in *gray* are those that are found required for adhesion based on the alanine-scanning performed in Fig. 1. The residues in *white* on a *black background* are those that differ from the residues shaded in *gray*. *Droso*, *Drosophila*. *B*, U2OS cells were cultured overnight and were subsequently treated for 8 h with 20 μM TAT or 20 μM of the indicated TAT-coupled peptides or left untreated. The cells were then subjected to trypsin-mediated detachment assays. *Error bars* indicate mean ± 95% confidence intervals, *C*, U2OS cells were subjected to wound-healing scratch assays in the presence of 20 μM of the indicated TAT-coupled peptides. *Asterisks* and *number signs* denote statistical significant differences after one-way ANOVA from the untreated condition and from the 317–326 treatment, respectively ($n = 7$ independent experiments). *Error bars* indicate mean ± 95% confidence intervals, *D*, U2OS cells were cultured overnight and were subsequently treated for 22 h with 20 μM of the indicated TAT-coupled peptides in the presence or in the absence of 30 μM cisplatin. The number of pyknotic nuclei was then scored and reported as the percentage of apoptosis. The *light gray region* displays the level of apoptosis induced by cisplatin alone, and the *dark gray region* shows the zone where sensitization occurs. *Asterisks* and *number signs* denote statistical significant differences after one-way ANOVA with the cisplatin-only treatment and with the cisplatin + 317–326 treatment, respectively ($n = 6$ independent experiments). *Error bars* indicate mean ± 95% confidence intervals.

has not been reported. We used ITC to assess this point. ITC records temperature changes generated when two molecules interact (32). Repeated injection of 317–326 into the cell containing the DLC1 GAP domain led to a marked variation in temperature (endergonic reaction) that was progressively reduced with subsequent 317–326 injections (indicative of binding site saturation and hence the specificity of the interaction) (Fig. 4*E*, *upper panel*). In contrast, injections of the two tryptophan peptide mutants (W317A and W319A) in the incubation cell of the ITC device containing the DLC1 GAP domain induced minimal temperature changes (these changes are caused by the injection of a given volume in the cell) (Fig. 4*F*).

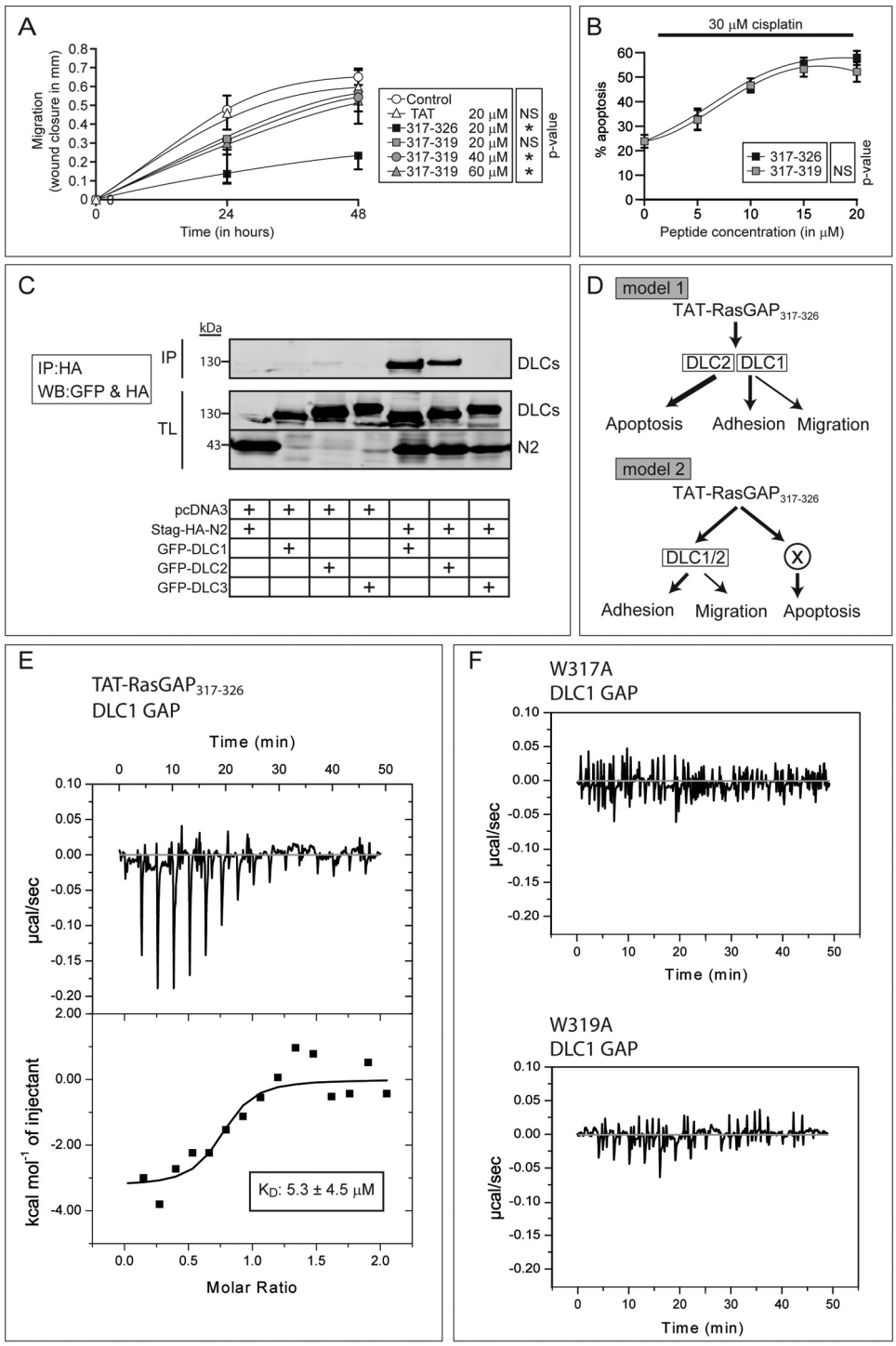

FIGURE 4. **Direct interaction of 317–326 with DLC1 requires a *WXW* motif that is sufficient to mediate the tumor sensitization effect of 317–326.** *A* and *B*, effect of increasing doses of 317–319 on U2OS cell migration over time (*A*) and on sensitization to apoptosis induced by 30 μM cisplatin (*B*) ($n = 3$ independent experiments). *Asterisks* denote statistical significance after repeated measurement ANOVAs (*A*). *Error bars* indicate mean ± 95% confidence intervals, *C*, HEK-293T cells were transfected with the indicated combinations of plasmids. Two milligrams of cell lysates were immunoprecipitated (*IP*) using an anti-HA antibody. Forty μg of total lysates (*TL*) were also loaded. Western blotting (*WB*) against the HA tag (*N2*) and GFP (DLC1–3) was performed. The cropped blot is representative of three independent experiments. *D*, working models. Model 1 suggests that DLC1 and DLC2 mediate every 317–326 anticancer effects, whereas model 2 includes a third player that would mediate the effects of 317–326 on apoptosis. *E*, isothermal titration calorimetry was used to investigate the binding between 317–326 and the GAP domain of DLC1. This panel displays the raw data of the heat pulses resulting from titration of the recombinant GST-DLC1-GAP domain (50 μM) in the calorimetric cell with serial injections of 317–326 at a 500 μM concentration. The *lower panel* displays the integrated heat pulses (in kcal), normalized per mole of 317–326, as a function of the molar ratio (317–326 concentration/DLC1-GAP concentration). The resulting curve was fitted to a model equation allowing the determination of the K_D. The dissociation constant and the molar ratio displayed here are the mean of three experiments. *F*, as controls, the recombinant GST-DLC1-GAP domain was titrated with the RasGAP W317A mutant peptide (*upper right*) and the RasGAP W319A mutant peptide (*lower right*) ($n = 3$ independent experiments).

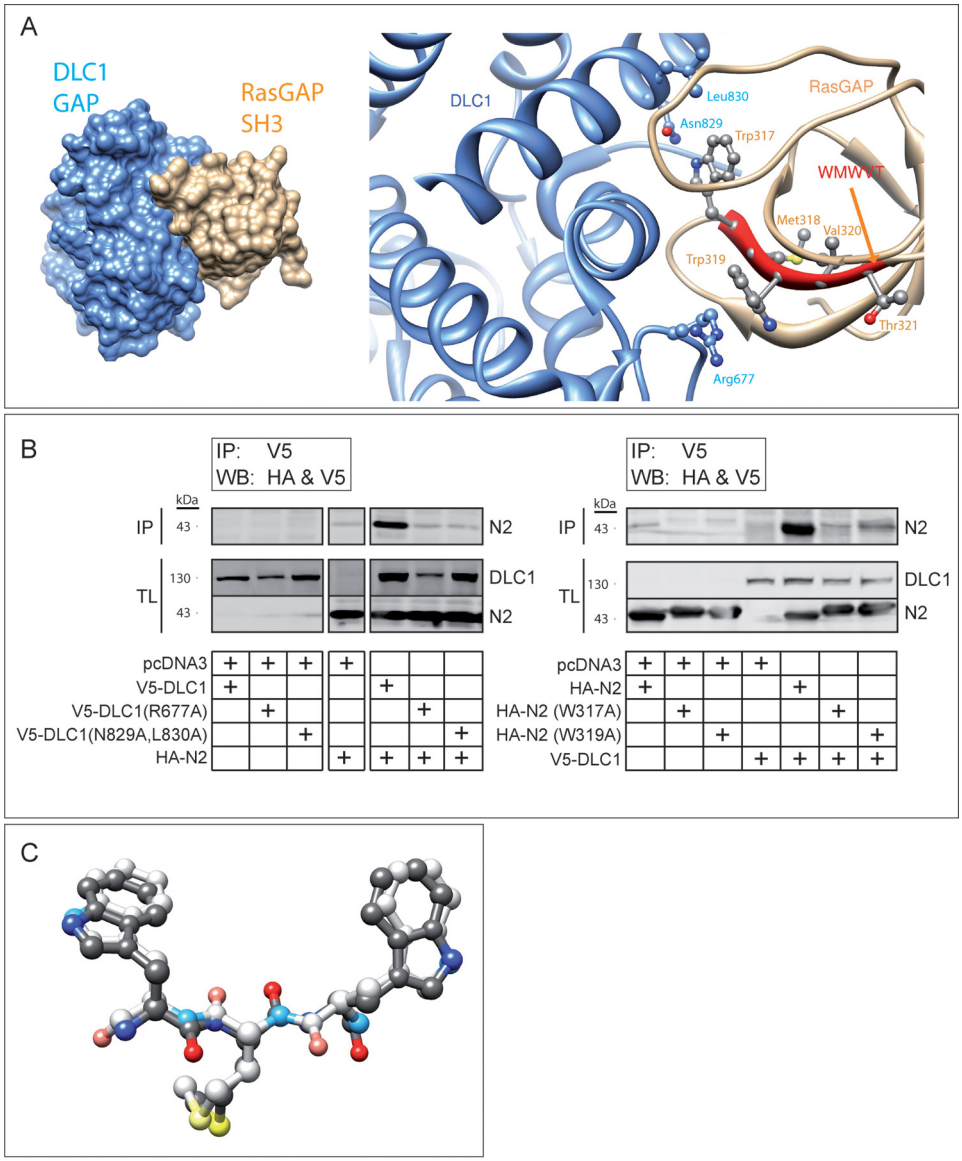

FIGURE 5. **Structural model of RasGAP binding to DLC1.** *A*, *in silico* docking of DLC1 GAP domain (PDB ID: 3KUQ; in *blue*) and RasGAP SH3 domain (PDB ID: 2JO5; in *orange*) interaction. The *right panel* displays the interaction between the SH3 domain of RasGAP and the GAP domain of DLC1. This interaction involves the Trp-317 and Trp-319 residues of RasGAP and the Arg-677, Asn-829, and Leu-830 residues of DLC1. The *left panel* shows a lower magnification image of this interaction. This binding mode had a geometric shape complementarity score of 10024. See Refs. 20 and 21 for score interpretation. The next best binding mode (not shown) had a score of 9804. The spatially nearest calculated pose (not shown) had a root mean square deviation of 15.1 Å as compared with the binding mode displayed in the figure and had a geometric shape complementarity score of 9488. *B*, immunoprecipitation assays displaying the interaction between wild-type fragment N2 and mutants of DLC1 (*left blot*) and between wild-type DLC1 and mutants of fragment N2 (*right blot*). HEK 293T cells were transfected with the indicated combinations of plasmids. Two milligrams of cell lysates were immunoprecipitated (*IP*) using an anti-V5 antibody. Forty μg of total lysates (*TL*) were also loaded. Western blotting (*WB*) against the HA tag (*N2*) and the V5 tag (DLC1) was performed. The left blot was cropped, but all the lanes originate from the same exposure of one given blot. Cropped blots are representative of three independent experiments. *C*, retro-inverso WMW peptide (D-amino acids) superimposed on the conformation of the WMW residues of RasGAP (L-amino acids). The two peptides are colored according to the atom types. *Lighter colors* have been applied to the retro-inverso peptide.

The dissociation constant (K_D) of the interaction between the RasGAP 317–326 sequence and the DLC1 GAP domain was calculated to be ~5 μM (Fig. 4*E*, *lower panel*). This K_D is in agreement with the functional TAT-RasGAP$_{317-326}$ EC_{50} values obtained for apoptosis (5 μM), adhesion (11.5 μM) and migration (16.5 μM) (Fig. 2*D*).

We next wanted to determine the binding mode of 317–326 to DLC1. *In silico* docking experiments of the RasGAP SH3 domain (PDB: 2JO5) to the DLC1 GAP domain (PDB: 3KUQ) revealed a preferred binding mode involving polar and nonpolar interactions of RasGAP Trp-317 to DLC1 Leu-830 and Asn-829, as well as a cation-π interaction between RasGAP Trp-319 and DLC1 Arg-677 (Fig. 5*A*). This *in silico* prediction was in agreement with the immunoprecipitation assays using DLC1 mutants bearing point mutations at position 677 and at positions 829 and 830. Fig. 5*B* (*left blot*) shows that these mutated DLC1 proteins have impaired fragment N2 binding abilities. Conversely, alanine substitutions of Trp-317 and Trp-319 in fragment N2 greatly reduced its capacity to bind wild-type DLC1 (Fig. 5*B*, *right blot*).

Fig. 5*A* was derived from the structure of the RasGAP sequence in its natural L-form. One could question whether the

TAT-RasGAP$_{317–326}$ peptide, synthesized with D-amino acids, adopts a similar configuration. To assess this point, we performed an *in silico* superimposition between the WMW sequences in D-amino acids and the one derived from the SH3 domain of RasGAP (L-form, PDB ID: 2J05). Fig. 5*C* shows a virtual identical structure for both conformations, indicating that the D-amino acid version of 317–326 is likely to engage DLC1 as the corresponding natural L-form does.

DISCUSSION

Increasing the rate of death induced by chemotherapy specifically in cancer cells and impairing their invasiveness are prime strategies to fight cancer. We previously reported that a cell-permeable peptide derived from RasGAP, 317–326, had the ability to act as a dual anticancer peptide by sensitizing tumor cells to anticancer therapy-induced cell death and by hampering invasiveness (8, 9, 11). The mode of action of this peptide is still imprecisely defined. However, recent data demonstrated that the DLC1 tumor suppressor binds to the parental molecule (fragment N2) that contains 317–326 and that DLC1 is required for some of the anticancer activities of 317–326 (11). This new information allowed us to evaluate whether 317–326 is able to bind the DLC1 GAP domain using ITC and their mode of binding using site-directed mutagenesis and *in silico* modeling approaches. The K_D of this interaction is about 10-fold higher than the K_D calculated for the interaction between the SH3 domain of RasGAP with the DLC1 GAP domain (0.6 μM) (31). The weaker binding affinity of 317–326 with the DLC1 GAP domain could be explained by the number of amino acids involved in the interaction. Indeed, it appears that only two amino acids are necessary for this binding, whereas it has been reported that three amino acids are involved in the interaction between the RasGAP SH3 domain and the DLC1 GAP domain (31).

In this study, we show that sensitization to apoptosis, migration, and adhesion was differentially modulated by 317–326 (Fig. 2*D*) but that this globally required the same crucial amino acids (Fig. 2*C*). The full-length RasGAP peptide could be narrowed down to a three-amino acid peptide, 317–319, that still bears most of the anticancer activities of the longer construct (Fig. 4, *A* and *B*). However, in contrast to its effect on apoptosis sensitization, the ability of 317–319 to inhibit migration was reduced as compared with that of the 10 amino acid 317–326 sequence. This suggests that two targets are involved in transducing the RasGAP peptide anticancer properties. Here, we show that another DLC isoform, DLC2, is also engaged by fragment N2 (Fig. 4*E*), raising the possibility that the second target is DLC2. However, this remains to be demonstrated. It has been previously reported that the SH3 of RasGAP inhibits the GAP activity of DLC1 (33). These results have been confirmed very recently by the observation that RasGAP SH3 domain inhibits the GAP activity of DLC1 *in vitro* (31). Therefore, a reasonable assumption is that 317–319, by engaging the Arg-677 finger of DLC1, also inhibits the GAP activity of DLC1. However, DLC1 exerts some of its functions in a GAP-independent manner (29), and it remains possible that 317–326 mediates its effects by modulating the GAP-independent activities of DLC1. In favor of this second possibility is our recent observation that Rho inhibition using the C3 exoenzyme does not prevent 317–326 from increasing adhesion (11).

We have demonstrated here that the Trp-317 and Trp-319 residues are required for 317–326 to mediate its anticancer effects. The importance of these residues for protein-protein interaction is consistent with previously published structural data showing that Trp-317 and Trp-319 establish a hydrophobic pocket allowing the dimerization of the SH3 domain of RasGAP (24). Data collected in the present study suggest that other amino acids, although not strictly required for the biological activity of the RasGAP-derived peptide, are nevertheless of importance, in particular as structural scaffolding residues (amino acids 323–325). Interestingly, the hydrophilic residues of 317–326 (Thr-321, Asn-322, and Asp-326), known to be exposed at the surface of the RasGAP SH3 crystal (24), are dispensable for 317–326-mediated anticancer effects. This suggests that hydrophobicity is a key chemical property through which 317–326 (and likely the endogenous p120 RasGAP SH3 domain) functions. Met-318, a residue that is not strictly conserved during evolution but whose hydrophobicity is however evolutionary conserved (leucine in insects), could be indeed replaced by a hydrophobic leucine residue without any loss in activity of 317–326. Another important question is whether a WaW motif (where a represents an aliphatic residue) can be found elsewhere within the human proteome and be a putative target of DLC1/2. Not surprisingly, hundreds of proteins bear such a motif, but none of them correspond to known DLC-interacting proteins or are predicted to be involved in biological functions potentially modulated by the DLC proteins (data not shown) (29).

The discovery that a very short peptidic motif, consisting of only two tryptophan amino acids separated by a spacer residue (W*X*W), still bears, at least to some extent, the anticancer activities of the parental molecule provides the basis to undertake the rational design of small molecules with similar activities. Such drugs, by potentiating chemotherapy and impinging on metastatic progression, may be of considerable benefit to cancer patients.

REFERENCES

1. Jemal, A., Bray, F., Center, M. M., Ferlay, J., Ward, E., and Forman, D. (2011) Global cancer statistics. *CA Cancer J. Clin.* **61,** 69–90
2. Trahey, M., and McCormick, F. (1987) A cytoplasmic protein stimulates normal N-ras p21 GTPase, but does not affect oncogenic mutants. *Science* **238,** 542–545
3. Pomerance, M., Thang, M. N., Tocque, B., and Pierre, M. (1996) The Ras-GTPase-activating protein SH3 domain is required for Cdc2 activation and Mos induction by oncogenic Ras in *Xenopus* oocytes independently of mitogen-activated protein kinase activation. *Mol. Cell. Biol.* **16,** 3179–3186
4. Yang, J. Y., Michod, D., Walicki, J., Murphy, B. M., Kasibhatla, S., Martin, S. J., and Widmann, C. (2004) Partial cleavage of RasGAP by caspases is required for cell survival in mild stress conditions. *Mol. Cell. Biol.* **24,** 10425–10436
5. Khalil, H., Bertrand, M. J., Vandenabeele, P., and Widmann, C. (2014) Caspase-3 and RasGAP: a stress-sensing survival/demise switch. *Trends Cell Biol.* **24,** 83–89
6. Yang, J. Y., and Widmann, C. (2001) Antiapoptotic signaling generated by caspase-induced cleavage of RasGAP. *Mol. Cell. Biol.* **21,** 5346–5358
7. Yang, J. Y., and Widmann, C. (2002) The RasGAP N-terminal fragment generated by caspase cleavage protects cells in a Ras/PI3K/Akt-dependent

manner that does not rely on NF-κB activation. *J. Biol. Chem.* **277,** 14641–14646
8. Michod, D., Annibaldi, A., Schaefer, S., Dapples, C., Rochat, B., and Widmann, C. (2009) Effect of RasGAP N2 fragment-derived peptide on tumor growth in mice. *J. Natl. Cancer Inst.* **101,** 828–832
9. Michod, D., Yang, J. Y., Chen, J., Bonny, C., and Widmann, C. (2004) A RasGAP-derived cell permeable peptide potently enhances genotoxin-induced cytotoxicity in tumor cells. *Oncogene* **23,** 8971–8978
10. Barras, D., Lorusso, G., Lhermitte, B., Viertl, D., Rüegg, C., and Widmann, C. (2014) Fragment N2, a caspase-3 generated RasGAP fragment, inhibits breast cancer metastatic progression. *Int. J. Cancer* **135,** 242–247
11. Barras, D., Lorusso, G., Ruegg, C., and Widmann, C. (2014) Inhibition of cell migration and invasion mediated by the TAT-RasGAP$_{317–326}$ peptide requires the DLC1 tumor suppressor. *Oncogene* 10.1038/onc.2013.465
12. Raftopoulou, M., and Hall, A. (2004) Cell migration: Rho GTPases lead the way. *Dev. Biol.* **265,** 23–32
13. Nürnberg, A., Kitzing, T., and Grosse, R. (2011) Nucleating actin for invasion. *Nat. Rev. Cancer* **11,** 177–187
14. Durkin, M. E., Yuan, B. Z., Zhou, X., Zimonjic, D. B., Lowy, D. R., Thorgeirsson, S. S., and Popescu, N. C. (2007) DLC-1:a Rho GTPase-activating protein and tumour suppressor. *J. Cell Mol. Med.* **11,** 1185–1207
15. Saladin, P. M., Zhang, B. D., and Reichert, J. M. (2009) Current trends in the clinical development of peptide therapeutics. *IDrugs.* **12,** 779–784
16. Lipinski, C. A., Lombardo, F., Dominy, B. W., and Feeney, P. J. (2001) Experimental and computational approaches to estimate solubility and permeability in drug discovery and development settings. *Adv. Drug Deliv. Rev.* **46,** 3–26
17. Nelson, R. M., and Long, G. L. (1989) A general method of site-specific mutagenesis using a modification of the *Thermus aquaticus* polymerase chain reaction. *Anal. Biochem.* **180,** 147–151
18. Holeiter, G., Heering, J., Erlmann, P., Schmid, S., Jähne, R., and Olayioye, M. A. (2008) Deleted in liver cancer 1 controls cell migration through a Dia1-dependent signaling pathway. *Cancer Res.* **68,** 8743–8751
19. Holeiter, G., Bischoff, A., Braun, A. C., Huck, B., Erlmann, P., Schmid, S., Herr, R., Brummer, T., and Olayioye, M. A. (2012) The RhoGAP protein Deleted in Liver Cancer 3 (DLC3) is essential for adherens junctions integrity. *Oncogenesis.* **1,** e13
20. Schneidman-Duhovny, D., Inbar, Y., Nussinov, R., and Wolfson, H. J. (2005) PatchDock and SymmDock: servers for rigid and symmetric docking. *Nucleic Acids Res.* **33,** W363–WW367
21. Duhovny, D., Nussinov, R., and Wolfson, H. J. (2002) Efficient unbound docking of rigid molecules. in *Algorithms in Bioinformatics, Lecture Notes in Computer Science*, Vol. 2452, pp. 185–200, Springer-Verlag, Berlin Heidelberg
22. Rose, P. W., Beran, B., Bi, C., Bluhm, W. F., Dimitropoulos, D., Goodsell, D. S., Prlic, A., Quesada, M., Quinn, G. B., Westbrook, J. D., Young, J., Yukich, B., Zardecki, C., Berman, H. M., and Bourne, P. E. (2011) The RCSB Protein Data Bank: redesigned web site and web services. *Nucleic Acids Res.* **39,** D392–D401
23. Rose, P. W., Bi, C., Bluhm, W. F., Christie, C. H., Dimitropoulos, D., Dutta, S., Green, R. K., Goodsell, D. S., Prlic, A., Quesada, M., Quinn, G. B., Ramos, A. G., Westbrook, J. D., Young, J., Zardecki, C., Berman, H. M., and Bourne, P. E. (2013) The RCSB Protein Data Bank: new resources for research and education. *Nucleic Acids Res.* **41,** D475–D482
24. Ross, B., Kristensen, O., Favre, D., Walicki, J., Kastrup, J. S., Widmann, C., and Gajhede, M. (2007) High resolution crystal structures of the p120 RasGAP SH3 domain. *Biochem. Biophys. Res. Commun.* **353,** 463–468
25. Erlmann, P., Schmid, S., Horenkamp, F. A., Geyer, M., Pomorski, T. G., and Olayioye, M. A. (2009) DLC1 activation requires lipid interaction through a polybasic region preceding the RhoGAP domain. *Mol. Biol. Cell* **20,** 4400–4411
26. Lapouge, K., Perozzo, R., Iwaszkiewicz, J., Bertelli, C., Zoete, V., Michielin, O., Scapozza, L., and Haas, D. (2013) RNA pentaloop structures as effective targets of regulators belonging to the RsmA/CsrA protein family. *RNA. Biol.* **10,** 1031–1041
27. Morrison, K. L., and Weiss, G. A. (2001) Combinatorial alanine-scanning. *Curr. Opin. Chem. Biol.* **5,** 302–307
28. Ashkenazi, A., Presta, L. G., Marsters, S. A., Camerato, T. R., Rosenthal, K. A., Fendly, B. M., and Capon, D. J. (1990) Mapping the CD4 binding site for human immunodeficiency virus by alanine-scanning mutagenesis. *Proc. Natl. Acad. Sci. U.S.A.* **87,** 7150–7154
29. Barras, D., and Widmann, C. (2014) GAP-independent functions of DLC1 in metastasis. *Cancer Metastasis Rev.* **33,** 87–100
30. Ng, D. C., Chan, S. F., Kok, K. H., Yam, J. W., Ching, Y. P., Ng, I. O., and Jin, D. Y. (2006) Mitochondrial targeting of growth suppressor protein DLC2 through the START domain. *FEBS Lett.* **580,** 191–198
31. Jaiswal, M., Dvorsky, R., Amin, E., Risse, S. L., Fansa, E. K., Zhang, S. C., Taha, M. S., Gauhar, A. R., Nakhaei-Rad, S., Kordes, C., Koessmeier, K. T., Cirstea, I. C., Olayioye, M. A., Häussinger, D., and Ahmadian, M. R. (2014) Functional cross-talk between Ras and Rho pathways: a Ras-specific GTPase-activating protein (p120RasGAP) competitively inhibits the RhoGAP activity of deleted in liver cancer (DLC) tumor suppressor by masking the catalytic arginine finger. *J. Biol. Chem.* **289,** 6839–6849
32. O'Neill, M. A., and Gaisford, S. (2011) Application and use of isothermal calorimetry in pharmaceutical development. *Int. J. Pharm.* **417,** 83–93
33. Yang, X. Y., Guan, M., Vigil, D., Der, C. J., Lowy, D. R., and Popescu, N. C. (2009) p120Ras-GAP binds the DLC1 Rho-GAP tumor suppressor protein and inhibits its RhoA GTPase and growth-suppressing activities. *Oncogene* **28,** 1401–1409

ANNEX II

ALDEHYDE DEHYDROGENASE ACTIVITY PLAYS A KEY ROLE IN THE AGGRESSIVE PHENOTYPE OF NEUROBLASTOMA.

Contribution:

This work has been published in BMC Cancer in 2016. I generated the knockout cells used in the paper.

Flahaut et al. BMC Cancer (2016) 16:781
DOI 10.1186/s12885-016-2820-1

BMC Cancer

RESEARCH ARTICLE Open Access

Aldehyde dehydrogenase activity plays a Key role in the aggressive phenotype of neuroblastoma

Marjorie Flahaut[1], Nicolas Jauquier[2], Nadja Chevalier[1,3], Katya Nardou[1], Katia Balmas Bourloud[1], Jean-Marc Joseph[2], David Barras[4], Christian Widmann[3], Nicole Gross[1], Raffaele Renella[1] and Annick Mühlethaler-Mottet[1*]

Abstract

Background: The successful targeting of neuroblastoma (NB) by associating tumor-initiating cells (TICs) is a major challenge in the development of new therapeutic strategies. The subfamily of aldehyde dehydrogenases 1 (ALDH1) isoenzymes, which comprises ALDH1A1, ALDH1A2, and ALDH1A3, is involved in the synthesis of retinoic acid, and has been identified as functional stem cell markers in diverse cancers. By combining serial neurosphere passages with gene expression profiling, we have previously identified ALDH1A2 and ALDH1A3 as potential NB TICs markers in patient-derived xenograft tumors. In this study, we explored the involvement of ALDH1 isoenzymes and the related ALDH activity in NB aggressive properties.

Methods: ALDH activity and ALDH1A1/A2/A3 expression levels were measured using the ALDEFLUOR™ kit, and by real-time PCR, respectively. ALDH activity was inhibited using the specific ALDH inhibitor diethylaminobenzaldehyde (DEAB), and ALDH1A3 gene knock-out was generated through the CRISPR/Cas9 technology.

Results: We first confirmed the enrichment of ALDH1A2 and ALDH1A3 mRNA expression in NB cell lines and patient-derived xenograft tumors during neurosphere passages. We found that high ALDH1A1 expression was associated with less aggressive NB tumors and cell lines, and correlated with favorable prognostic factors. In contrast, we observed that ALDH1A3 was more widely expressed in NB cell lines and was associated with poor survival and high-risk prognostic factors. We also identified an important ALDH activity in various NB cell lines and patient-derived xenograft tumors. Specific inhibition of ALDH activity with diethylaminobenzaldehyde (DEAB) resulted in a strong reduction of NB cell clonogenicity, and TIC self-renewal potential, and partially enhanced NB cells sensitivity to 4-hydroxycyclophosphamide. Finally, the specific knock-out of *ALDH1A3* via CRISPR/Cas9 gene editing reduced NB cell clonogenicity, and mediated a cell type-dependent inhibition of TIC self-renewal properties.

Conclusions: Together our data uncover the participation of ALDH enzymatic activity in the aggressive properties and 4-hydroxycyclophosphamide resistance of NB, and show that the specific ALDH1A3 isoenzyme increases the aggressive capacities of a subset of NB cells.

Background

Neuroblastoma (NB), which arises from neural crest-derived sympatho-adrenal progenitors, is one of the most life-threatening solid tumors of childhood [1–3]. The hallmark of NB is its extreme biological, genetic, and clinical heterogeneity. This leads to a broad spectrum of clinical outcomes, ranging from spontaneous regression to an aggressive life-threatening disease for high-risk NB, with only 40% long-term survival despite intensive multi-modal therapy [1–3]. While only few recurrent gene mutations have been found in NB tumors, a large number of recurrent somatic genetic alterations have been described, which includes numerical or segmental chromosomal alterations [1, 2, 4–6].

Like their tumor of origin, NB cell lines display important biological heterogeneity. Three cell subtypes arise spontaneously in NB cell line cultures: a) neuro-blastic (N-type), displaying properties of embryonic

* Correspondence: Annick.Muhlethaler@chuv.ch
[1]Pediatric Hematology-Oncology Research Laboratory, Pediatric Division, University Hospital CHUV, Lausanne, Switzerland
Full list of author information is available at the end of the article

sympathoblasts, b) substrate-adherent (S-type), resembling Schwannian, glial or melanocytic progenitor cells, and c) intermediate (I-type) subtype [7]. I-type cells express markers of both N and S subtypes and display bidirectional differentiation potential when treated with specific agents [8–10]. Moreover, I-type cells are significantly more aggressive than N- or S-type cells, and were proposed to represent NB stem cells (SCs) or malignant neural crest SCs [9, 11].

In recent years, emerging evidence has suggested that tumor progression, metastasis, and chemotherapeutic drug resistance are driven by a minor cell subpopulation, designed as cancer stem cells (CSCs) or tumor-initiating cells (TICs) [12–14]. These are capable of self-renewal and differentiation into heterogeneous phenotypic and functional lineages, and are characterized by plasticity [14–16]. In a previous study aiming to identify NB TIC markers, we combined serial neurosphere (NS) passage assays, which allow the enrichment of TICs, with gene expression profiling. This allowed the identification of a gene expression signature associated to NB TICs [17]. Among this gene profile, ALDH1A2 and ALDH1A3 were selected for further investigations of their role in maintaining NB TIC properties. The rationale behind this selection is based on the demonstration of the implication of ALDH activity in the biology of normal SCs and CSCs in other settings [18–21].

ALDHs belong to a superfamily of 19 genes coding for $NAD(P)^+$-dependent enzymes involved in the detoxification of a large number of endogenous and exogenous aldehydes [22, 23]. The ALDH1 subfamily, which includes A1, A2 and A3 isoforms, is involved in the synthesis of retinoic acid, playing therefore an important role in developing tissues [22]. Elevated ALDH activity was first demonstrated in normal hematopoietic progenitor/stem cells and is now commonly used for the isolation of CSCs in multiple tumor settings [24, 25]. Moreover, several ALDH isoenzymes were associated to TICs properties, such as ALDH1A1 in melanoma and lung adenocarcinoma [20, 26], ALDH1B1 in colon cancer [27], ALDH1A3 in breast cancer and NSCLC [28, 29], and ALDH7A1 in prostate cancer [30]. ALDH1 expression was also correlates with cyclophosphamide resistance [23, 31, 32], a chemotherapeutic drug widely used for the treatment of many cancers, including NB. So far, ALDH activity has not been linked to NB tumor initiation or progression. However, a recent paper described the involvement of ALDH1A2 in the regulation of CSC properties in NB [33].

In this study, we aimed at exploring the expression pattern of the three ALDH1 isoforms in NB cell lines and patient-derived xenograft (PDX) tumors. ALDH activity was found to play a role in NB cell aggressive properties, such as clonogenicity, TIC proliferation, and cyclophosphamide resistance. In addition, we revealed that ALDH1A3 is associated with poor prognosis, and *ALDH1A3* gene disruption negatively impacted the aggressiveness of a subset of NB cell lines, suggesting that it can enhance NB tumorigenic properties.

Methods

Ethics statement

All in vivo procedures were performed under the guidelines of the Swiss Animal Protection Ordinance and the Animal Experimentation Ordinance of the Swiss Federal Veterinary Office (FVO). Animal experimentation protocols were approved by the Swiss FVO (authorization number: 1564.6). All reasonable efforts were made to ameliorate suffering, including anesthesia for painful procedures.

Patient-derived xenograft

Tumor material was collected from NB patients, diagnosed in the Hemato-Oncology Unit of the University Hospital of Lausanne (Switzerland), after informed consent and in agreement with local institutional ethical regulations (Protocol 26/05, 07/02/2005). Patient-derived xenografts (PDX) NB1, NB2 and NB4 were produced by in vivo serial subcutaneous transplantations of bone-marrow derived tumor cells in athymic Swiss nude mice (Crl:NU(Ico)-Foxn1nu) from Charles River Laboratory (France) [17]. PDX tumors were dissociated as previously described [17].

Cell culture

All well-characterized NB cell lines [34–36] were grown in Dulbecco's modified Eagle's medium (DMEM) (Gibco, Paisley, UK) supplemented with 10% Fetal Bovine Serum (FBS) (Sigma-Aldrich, St Louis, USA) and 1% penicillin/streptomycin (Gibco). The NB1-C cell line [17] was established from the dissociated NB1 PDX tumor derived from bone marrow metastatic cells (stage 4, NMYC not amplified). NB1-C cells were maintained in Neural Basic Medium (NBM) [DMEM/F12 supplemented with 1% penicillin/streptomycin, 2% B27 (Invitrogen, Carlsbad, USA), 20 ng/ml human recombinant bFGF (Peprotech, Rocky Hill, USA), and 20 ng/ml EGF (Peprotech)].

RNA extraction, reverse transcription, and PCR

Total RNAs from NB cells (1×10^6 cells) was obtained using the RNeasy Mini kit (Qiagen, Hilden, Germany) according to the manufacturer's instructions. RNAs (0.2-1 μg) were reverse transcribed with the PrimeScript™ RT reagent Kit (TAKARA Bio, St.Germain-en-Laye, France) using random primers and oligo dT primers according to the manufacturer's instructions.

The expression levels of ALDH1A1, ALDH1A2, ALDH1A3, and MYC mRNAs were measured by real-

time PCR using specific primers (QuantiTect primer assay, Qiagen), QuantiFast SYBRgreen assay (Qiagen), and the Corbett Rotor-Gene 6000 real-time cycler (Qiagen), as previously described [37]. The cycling conditions comprised 3 min polymerase activation at 95°C, followed by 40 cycles of 3 s at 95°C, 20s at 60°C and 1 s at 72°C for fluorescence acquisition. The ratio of each gene of interest to *HPRT1* gene expression and the relative gene expression were evaluated using the ΔCt and ΔΔCt methods, respectively.

NANOG, SOX2, and MYC expression levels were analyzed by PCR using GoTaq Hot Start Kit (Promega, Madison, USA) with the following primers: NANOG-for 5'-CAGCCCCGATTCTTCCACCAGTCCC-3', NANOG-rev 5'-CGGAAGATTCCCAGTCGGGTTCACC-3', SOX 2-for 5'GGGAAATGGGAGGGGTGCAAAAGAGG-3, SOX2-rev 5'-TTGCGTGAGTGTGGATGGGATTGGT G-3', MYC-for 5'-GCGTCCTGGGAAGGGAGATCCGG AGC-3', MYC-rev 5'-TTGAGGGGCATCGTCGCGGG AGGCTG-3'. Cycling reactions were 2 min at 95°C followed by 35 cycles of 30s at 95°C, 30s at 60°C and 30s at 72°C, and 5 min at 72°C.

ALDEFLUOR assay

ALDH activity was analyzed using the ALDEFLUOR™ kit according to manufacturer's instructions (Stem Cell Technologies, Grenoble, France). Briefly, 1×10^6 NB cells or PDX-dissociated cells were resuspended in 1 ml ALDEFLUOR assay buffer. The ALDH substrate BODIPY™-aminoacetaldehyde (BAAA) was added to the cells. Immediately after mixing, half of the suspension was used as the negative control, by adding 5 μl of the ALDH inhibitor diethylaminobenzaldehyde (DEAB, 3 μM). Cells were incubated for 30–45 minutes at 37°C, then washed twice, and suspended in ALDEFLUOR™ assay buffer containing 1 μg/ml of DAPI (Life Technologies, Switzerland) for viable cells selection. The brightly fluorescent $ALDH^+$ cells were detected in the FL1-channel of a Gallios^{TM} Flow Cytometer (Beckman Coulter, Inc., USA) and data were analyzed using KALUZA™ software (Beckman Coulter, Inc., USA).

ALDH activity inhibition

Cells were pre-treated with DEAB (Sigma-Aldrich) at 50 or 100 μM according to the cell line tested, or for control cells with Dimethyl sulfoxide (DMSO, Sigma-Aldrich) for 3 days prior functional assays, while maintaining the same amount of DEAB or DMSO during the assay.

Proliferation assay

Cell proliferation was assessed using the MTS/PMS cell proliferation kit (Promega). Briefly, 10^4 SK-N-Be2c cells and $2*10^4$ NB1-C cells per well were seeded in a 96-wells plate in DMEM/FCS or in NBM, respectively. Proliferation was monitored by measuring the OD at 405 nm immediately after seeding and after 24, 48, 72 and 96 h in presence of DEAB or DMSO for ALDH inhibition experiments, or without treatment.

Methylcellulose clonogenic assay

Clonogenic assays in semi-solid conditions were performed as described [38]. Briefly, NB cells ($1*10^3$) were grown in 500 μl semi-solid medium containing 53% methylcellulose (Fluka), and 47% DMEM/FCS (for SK-N-Be2c) or 47% NBM (for NB1-C) in poly-Hema (poly2-hydroxyethyl methylacrylate, 16 mg/ml in EtOH; Sigma-Aldrich) -coated 24-wells plates. For ALDH activity inhibition assay, DEAB or DMSO was added in the semi-solid medium, and supplemented every 4 days in 100 μl of medium. After 2 weeks, colonies were counted using an optic microscope (Olympus, Volketswil, Switzerland).

NB neurosphere culture and self-renewal assay

NS culture was performed as described in neural crest stem cell medium (NCSCm) in poly-Hema-coated six wells plates to prevent cell adhesion [17, 39]. For the production of serial NS passages, NB cells (1×10^5 cells/ml) were plated, and spheres were dissociated every 7 days in 0.05% trypsin-EDTA (Invitrogen), subsequently inhibited with Trypsin inhibitor (v/v) (Sigma-Aldrich). At each sphere passage, a part of the dissociated cells were tested for ALDH activity and for ALDH1A1/2/3 mRNA expression. For self-renewal assay, 1×10^4 cells were plated in 500 μl NCSCm in triplicates without treatment, or in presence of DEAB or DMSO for ALDH inhibition experiments.

Cell viability assays

Cells (2×10^4 for SK-N-Be2c, IGR-N91 and IGR-N91R, or $4*10^4$ for NB1-C) were plated in 96-wells plates 24 h before treatment with 4-hydroxycyclophosphamide (4-HCPA, Niomech, Bielefeld, Germany) for 48 h. Cell viability was measured in quadruplicates using the MTS/PMS cell proliferation kit from Promega according to manufacturer's instructions as described [40].

ALDH1A3 knock out through CRISPR/Cas9 technology

Two sgRNAs targeting the early exon of the *ALDH1A3* gene were chosen in the published sgRNA library [41]. Oligos were designed as follow: sgALDH1A3.1: forward 5'-CACCGCTACATGTAACCCTTCAACT-3', reverse 5'-AAACAGTTGAAGGGTTACATGTAGC-3', sgALDH1A3.2: forward 5'- CACCGCGCTCAGCCCG ACGTGGACA-3', reverse 5'- AAACTGTCCACGTCG GGCTGAGCGC-3'. The lentiviral vector lentiCRISPR v2 [42] was obtained from Adgene (Cambridge, USA). LentiCRISPR v2-sgALDH1A3 plasmids were constructed

according to the manufacturer's instructions (Adgene). Virus production and lentiviral infections were performed as previously described [43] with the following modification: pCMVDR8.91 was replaced by psPAX2 (Adgene). Transduced SK-N-Be2c and NB1-C cells were selected 24 h post-infection with 5 μg/ml or 1 μg/ml of puromycin (Sigma-Aldrich), respectively. Control cells were transduced with virus containing the empty lentiCRIPR v2 vector. Clone isolation was performed by limiting dilution in 96-wells plate.

Validation of the ALDH1A3 KO by immunoblotting could not be performed due to the detection (using 3 different anti-ALDH1A3 antibodies) of a non-specific band migrating with a similar velocity as ALDH1A3 in the negative control SH-EP cell line lacking ALDH1A3 mRNA expression. Thus, genome editing in clones was verified by NGS sequencing. PCR amplicons were designed across the *ALDH1A3* genomic regions targeted by the sgRNAs to examine generation of indels. A second PCR was performed to attach Illumina adaptors and barcodes to samples according to manufacturer's instructions. Primers for the second PCR include both a variable length sequence to increase library complexity and an 8 bp barcode for multiplexing of different biological samples. Amplicons were gel extracted, quantified, mixed and sequenced with a MiSeq SR300 (Illumina Inc., San Diego, USA). Sequencing reads were then processed with the following bioinformatic tools to quantify the occurrence of indels in the selected clones. Universal Illumina adapter and quality trimming of the sequencing reads was achieved using *Cutadapt* [44]. The trimmed reads were then aligned to the human reference genome (build GRCh37) using *bwa* [45] and then visualized using Integrative Genomics Viewer (IGV, Broad Institute). In parallel, to quantify the exact number of genetic variants for each CRISPR clone, we developed an R script that quantifies the percentage of each detected variant.

Statistical analysis

Statistical analyses were performed using GraphPad Prism 5.04 (GraphPad Software, Inc., La Jolla, USA). Unpaired two-tailed parametric *t*-test or non parametric Mann Whitney test were carried out to compare two different conditions, as specified in the Figure Legends.

Results

ALDH1A2 and ALDH1A3 expression are enhanced in NB TICs

We have previously identified *ALDH1A2* and *ALDH1A3* genes as potential NB TIC markers as their expression was upregulated during NS selection of NB TICs derived from NB PDX tumors (181x and 9x baseline, respectively by Affymetrix microarray analysis) [17]. To confirm the enrichment in stem-like cells by serial NS passages of NB cell lines, the expression levels of various SC-associated markers were analyzed by RT-PCR and real-time PCR at different sphere passages in the SK-N-Be2c and NB1-C cell lines. NANOG, SOX2, and MYC mRNA expression levels were already increased at the second sphere passage (Additional file 1: Figure S1), confirming the rapid enrichment of NB TICs through serial NS culture.

To validate the prior microarray data and to provide a closer insight into ALDH1 isoenzyme expression status along the NB TIC selection, we analyzed the mRNA expression levels of the three ALDH1 isoforms in four successive NS passages and in parental cells (T0) growing in adherent conditions (Fig. 1). ALDH1A1 mRNA expression levels during TIC selection varied depending on the cell type and NS passages analyzed. In contrast, ALDH1A2 mRNA expression was strongly increased, in early steps of the TIC selection process (s1-s2) and remained elevated in later NS passages (s3-s4) in the I-type SK-N-Be2c cell line, as well as in the NB1 PDX tumor and the related NB1-C cell line (Fig. 1). Moreover, ALDH1A3 mRNA expression was also highly upregulated in the NB1 PDX tumor and in the SK-N-Be2c cell line during TIC selection, while it remained stable in the NB1-C cell line (Fig. 1). Altogether, these results confirm the enrichment of ALDH1A2 and ALDH1A3 mRNA expression observed in the NS microarray profiling derived from the NB PDX tumors [17].

ALDH activity was also measured during successive NS passages from T0 to NS passage 4 (s4) in the SK-N-Be2c and NB1-C cell lines, and in cells derived from the NB1 PDX. The percentage of $ALDH^+$ cells remained stable during TIC selection in all cells analyzed; similarly, the relative fluorescence intensity remained more or less constant during NS passages except for a slight increase in the NB1-C cell line (Fig. 2a and b). These results indicate a lack of correlation between ALDH activity (as measured using the ALDEFLUOR kit) and ALDH1 isoform expression in NB TICs (see Discussion).

NB cell lines and PDX tumors display cell-specific ALDH1 isoenzyme expression profiles and elevated ALDH activity

Next, the expression profile of each ALDH1 isoform was evaluated by real-time PCR in a large panel of NB cell lines and NB PDX tumors. Most NB cell lines analyzed expressed ALDH1A1 and/or ALDH1A3, but rarely ALDH1A2 (Fig. 3a). The less aggressive S-type cell lines expressed significantly higher levels of ALDH1A1 mRNA relative to N/I-type NB cells (Fig. 3a and b). Interestingly, the NB1-C cell line and the related NB1-PDX tumor displayed a similar expression pattern of ALDH1 isoenzymes, with elevated expression levels of ALDH1A1 and A3. Furthermore, the expression level of

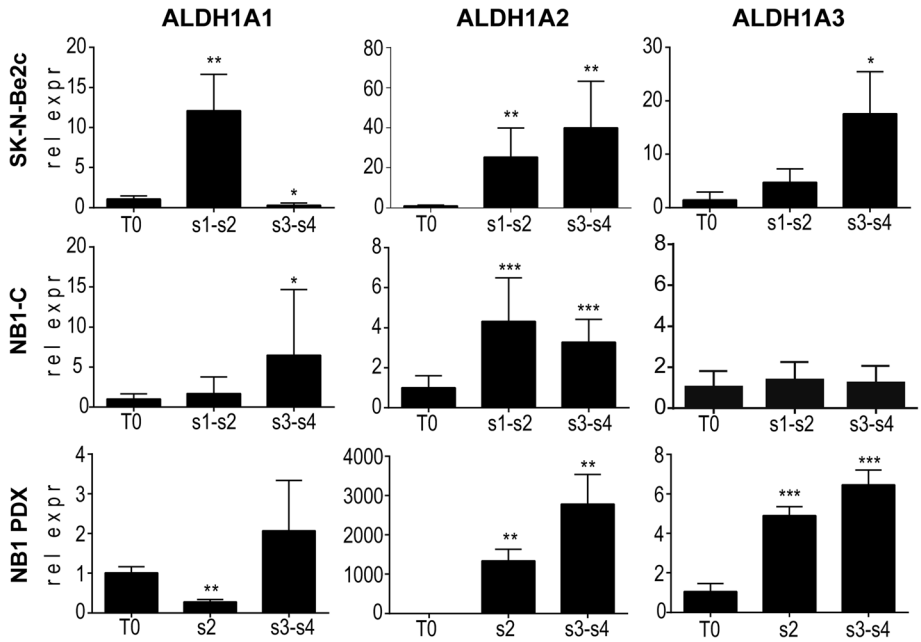

Fig. 1 ALDH1A2 and A3 isoform expression are enhanced during NB self-renewal process. The mRNA expression levels of the three ALDH1 isoforms (ALDH1A1, ALDH1A2 and ALDH1A3) were analyzed by real-time PCR in parental cells (T0) and four sphere passages (s1 to s4) of SK-N-Be2c, NB1-C, and NB1 PDX-derived cells. Data are plotted as ALDH1 mRNA expression relative to the T0 parental cells in pooled s1-s2 and s3-s4 ± SD (unpaired *t*-test: * correspond to $p < 0.05$, ** $p < 0.01$, *** $p < 0.0001$)

ALDH1A3 was significantly enhanced in the three PDX tumors as compared to NB cell lines, suggesting a role of this isoenzyme in in vivo grown tumors (Fig. 3a and b).

Further analysis of ALDH activity revealed elevated, yet heterogeneous, percentages of $ALDH^+$ cells in NB cell lines and PDX tumors, ranging from 1.2 to 69% (Fig. 4a and b).

High ALDH1A3 expression in NB tumors correlates with poor outcome and high-risk prognostic markers

To identify the link between ALDH1 expression and NB aggressiveness, the ALDH1A1/A2/A3 expression patterns were analyzed in NB tumors using the R2: Genomics Analysis and Visualization Platform (http://r2.amc.nl). Analysis of the published dataset of Versteeg and colleagues [5] revealed that high ALDH1A1 expression is significantly associated with good prognosis, while elevated expression of ALDH1A3 is strongly correlated with poor survival (Fig. 5a). The expression level of ALDH1A2 is globally reduced in NB tumors compared to ALDH1A1 and A3 isoforms, but the rare tumors with high ALDH1A2 expression level displayed a very poor survival rate (Fig. 5a). Moreover, low expression levels of ALDH1A1 (Fig. 5b) or high expression levels of ALDH1A3 (Fig. 5c) are associated with unfavorable prognostic factors in NB (i.e., age at diagnosis >18 months, and stage 4 disease).

Inhibition of ALDH activity affects NB aggressive properties

We next investigated whether the inhibition of ALDH activity in NB cell lines affects the NB cell properties associated with aggressiveness, such as proliferation, anchorage-independent growth, and TIC self-renewal. First, we confirmed that subtoxic doses of DEAB, a well-known specific inhibitor of ALDH activity [21], fully inhibit ALDH activity, which can be recovered by DEAB removal (Additional file 1: Figure S2). Treatment with DEAB had no impact on the 2D-proliferation capacities of SK-N-Be2c and NB1-C cell lines (Fig. 6a). However, ALDH activity inhibition strongly affected NB cell clonogenic properties (Fig. 6b), and negatively impacted on TIC self-renewal capacities of SK-N-Be2c and NB1-C cell lines by 43 and 88%, respectively (Fig. 6c).

As ALDH activity was shown to mediate resistance to 4-hydroxycyclophosphamide (4-HCPA), NB cell sensitivity to this chemotherapeutic agent was also measured in presence or absence of DEAB. We observed that ALDH inhibition partly sensitized SK-N-Be2c and NB1-C cell lines to 4-HPCA (Fig. 6d). In addition, we analyzed two cell lines, the drug-sensitive IGR-N91, and the multidrug resistant IGR-N91R, previously established in our lab [35]. Interestingly, ALDH enzymatic inhibition was able to almost completely sensitize the IGR-N91 cells to 4-HCPA and had a strong sensitizing impact on the multidrug resistant IGR-N91R cells (Fig. 6e). Altogether

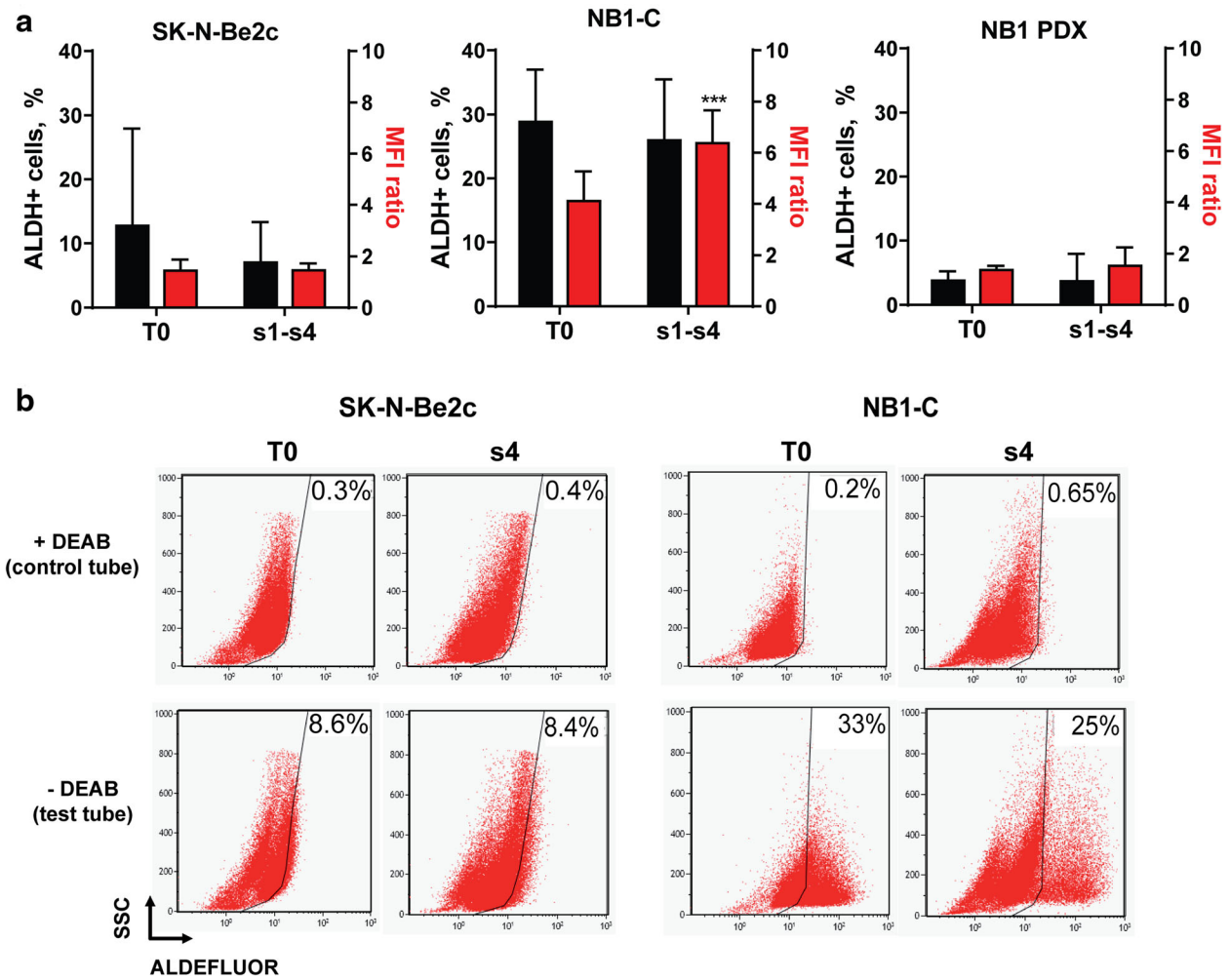

Fig. 2 ALDH activity remains stable during NB TICs selection. ALDH activity was measured using the ALDEFLUOR kit in parental cells (T0) and successive sphere passages (s1 to s4) in SK-N-Be2c, NB1-C, and NB1 PDX-derived cells. **a** The percentage of ALDH$^+$ cells (*black bars*) and the mean fluorescence intensity (MFI) ratio (MFI of the test tube/control tube, red bars) are plotted as mean ± SD of more than 3 experiments according to cell availability at each sphere passage (unpaired t-tests: ***$p < 0.0005$). **b** Representative dot plots showing the ALDH activity in SK-N-Be2c and NB1-C parental cells (T0) and in sphere passages 4 (s4) in presence (control tube) or absence (test tube) of DEAB. The percentage of ALDH$^+$ cells are indicated in the dot plots

these results demonstrate that endogenous ALDH activity plays a role in NB cell aggressive properties and mediates NB cell resistance to the chemotherapeutic drug 4-HCPA.

ALDH1A3 knock out affects NB clonogenic properties

Although ALDH activity measured by the ALDEFLUOR assay was initially mainly attributed to the ALDH1A1 isoform, other ALDH isoenzymes, such as ALDH1A2, ALDH1A3, ALDH2, ALDH3A1, and ALDH9A1, could be involved in the measured ALDH activity [21, 25, 28, 29]. As the ALDH1A3 isoform is associated with poor survival in NB and is the most widely expressed ALDH1 isoform in our panel of NB cell lines and PDX tumors (Figs. 5a and 3a, respectively), we asked whether ALDH1A3 activity plays a functional role in NB aggressive phenotype. To answer this question, ALDH1A3 knock-out (KO) SK-N-Be2c and NB1-C cell lines were generated by CRISPR/Cas9 gene editing (Additional file 1: Figure S3). Similarly, as for the observations after DEAB-mediated ALDH inhibition, ALDH1A3 KO did not affect the 2D-cell proliferation properties, but decreased the 3D-anchorage-independent growth of both NB cell lines (Fig. 7a and b). While, ALDH1A3 KO only impaired the TIC self-renewal properties of the SK-N-Be2c cell line, but had no effect on NB1-C cells (Fig. 7c).

Discussion

In this study, we first confirmed the enrichment of ALDH1A2 and ALDH1A3 expression during NB TICs

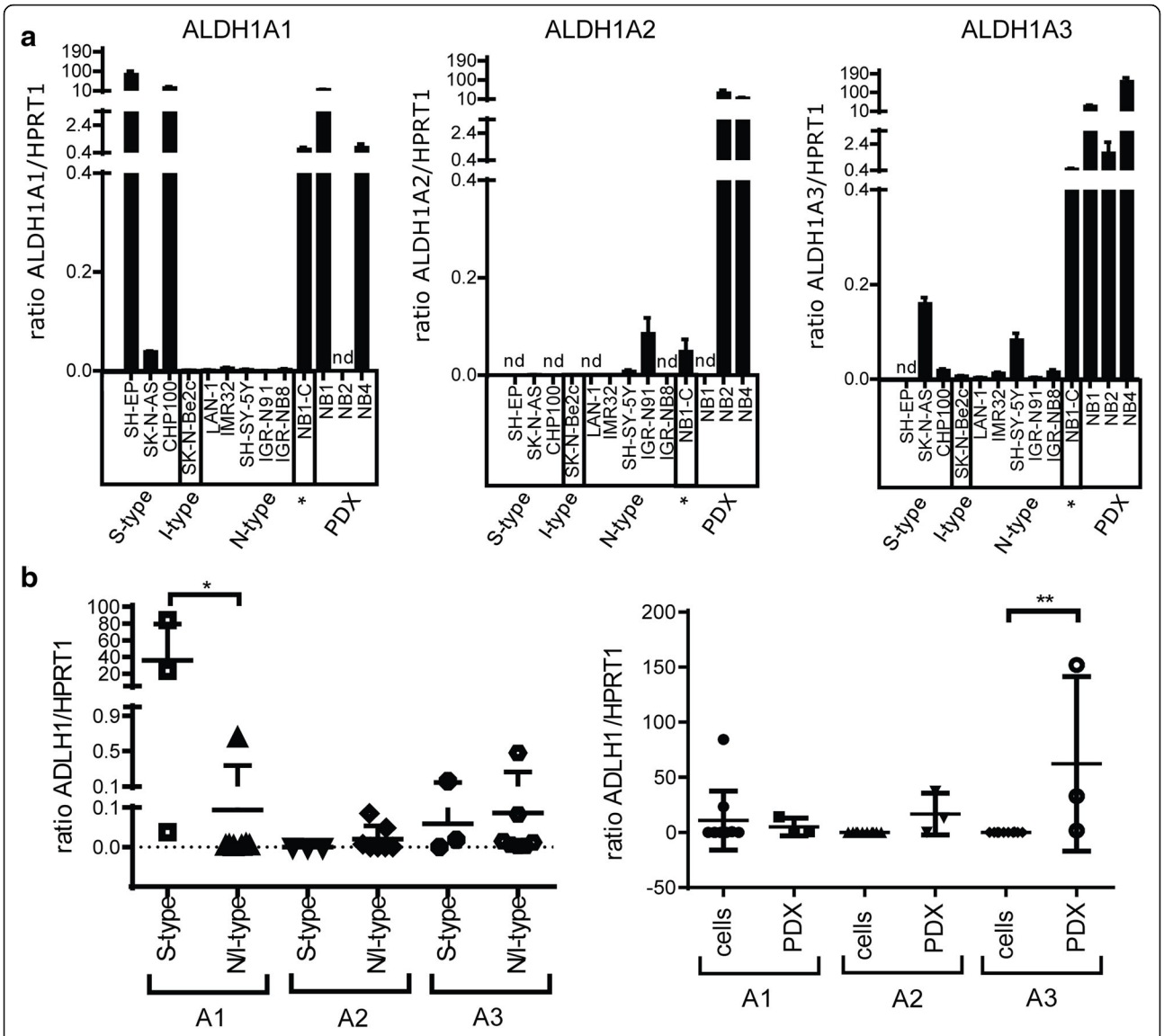

Fig. 3 NB cell lines and PDX tumors display various ALDH isoenzyme expression patterns. **a** Basal endogenous mRNA expression levels of each ALDH1 isoform were measured in 10 NB cell lines (* = serum-free medium) and 3 NB PDX tumors by real-time PCR. Mean ratio of ALDH1 isoform/HPRT1 ± SD are plotted in the bar graphs. Experiments were performed in tri- or quadruplicates (nd: not detected). **b** Comparison of ALDH1A1/A2/A3 mRNA expression levels between S-type versus N/I-type cell lines (*left panel*) and NB cell lines versus PDX tumors (*right panel*). Individual values and mean values ± SD of ALDH1 isoform/HPRT1 ratio are plotted in the dot plots (Mann Whitney test $*p = 0.033$, $**p = 0.007$)

selection in one PDX tumor (NB1), as well as in two distinct cell lines, the NB1-C cells derived from the NB1 PDX tumor, and/or the I-type SK-N-Be2c cell line. The enhancement of ALDH1A2 and ALDH1A3 mRNA expression levels during TIC selection of NB1-PDX derived cells was in accordance with the fold increase (181x and 9x, respectively) as observed in our previous microarray analysis [17]. Interestingly, the implication of ALDH1A2 in the regulation of CSC properties in NB has recently been reported [33]. Moreover, high ALDH1A2 expression in NB correlates with poor survival, suggesting a role for this ALDH1 isoenzyme in NB tumor aggressiveness.

ALDH activity has been demonstrated to select CSCs in leukemia and breast, lung, liver, prostate, brain, and colon cancer [23–25]. However, despite significant overexpression of ALDH1A2 and ALDH1A3 during TIC selection, no increase in the percentage of $ALDH^+$ cells could be observed during NS-passages by ALDEFLUOR assay measurements. This suggests that ALDH enzymatic activity may not be a valuable functional marker of TICs in NB. Similar findings were previously described in melanoma [46].

Our analysis of ALDH1 isoform expression profiles in NB cell lines and PDX tumors revealed differential

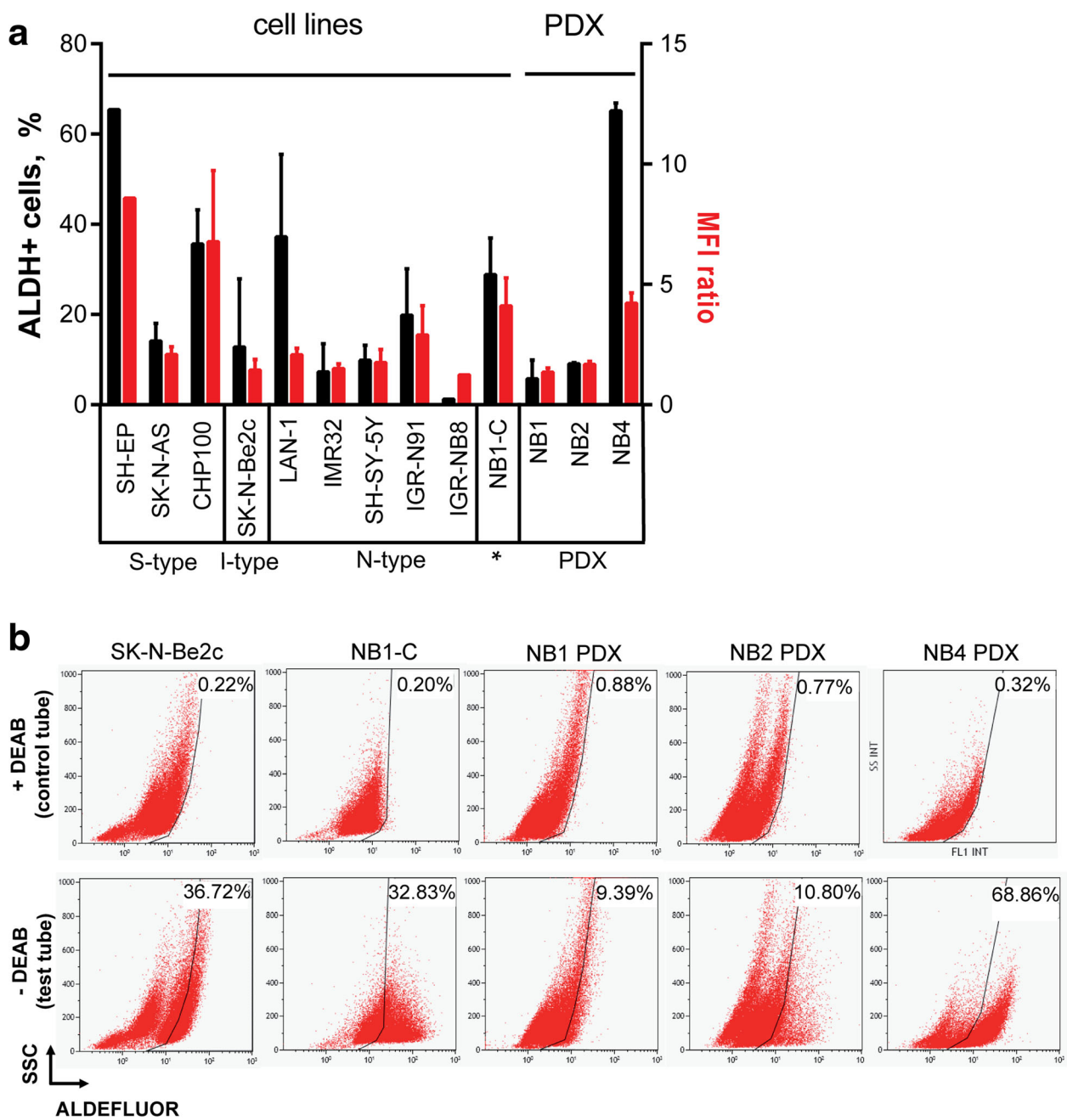

Fig. 4 Heterogeneous ALDH activity is detected in NB cell lines and PDX tumors. **a** The percentage of ALDH$^+$ cells (black bars) and the MFI ratio (MFI of the test tube/control tube, red bars), measured using the ALDEFLUOR kit, are given as mean ± SD of 1 to 8 experiments for the NB cell lines and 3 to 4 experiments for the PDX-dissociated tumor cells. **b** Representative dot plots showing the ALDH activity in SK-N-Be2c, NB1-C cell lines, and cells dissociated from the 3 PDX tumors in presence (control tube) or absence of DEAB (test tube). The percentages of ALDH$^+$ cells are indicated

expression patterns which may rely on the strong heterogeneity of NB tumors and cell lines. The higher expression levels of ALDH1A1 in the less aggressive S-type cell lines is in accordance with the finding that elevated ALDH1A1 expression in NB tumors correlates with a better survival rate and favorable prognostic factors. In other neoplasms, ALDH1A1 has been shown to correlate either with favorable or poor prognosis depending on the tumor setting or on tumor sample sets [23]. Moreover, we observed that ALDH1A3 is strongly expressed in PDX tumors, and that higher ALDH1A3 expression correlates with poor survival and high-risk

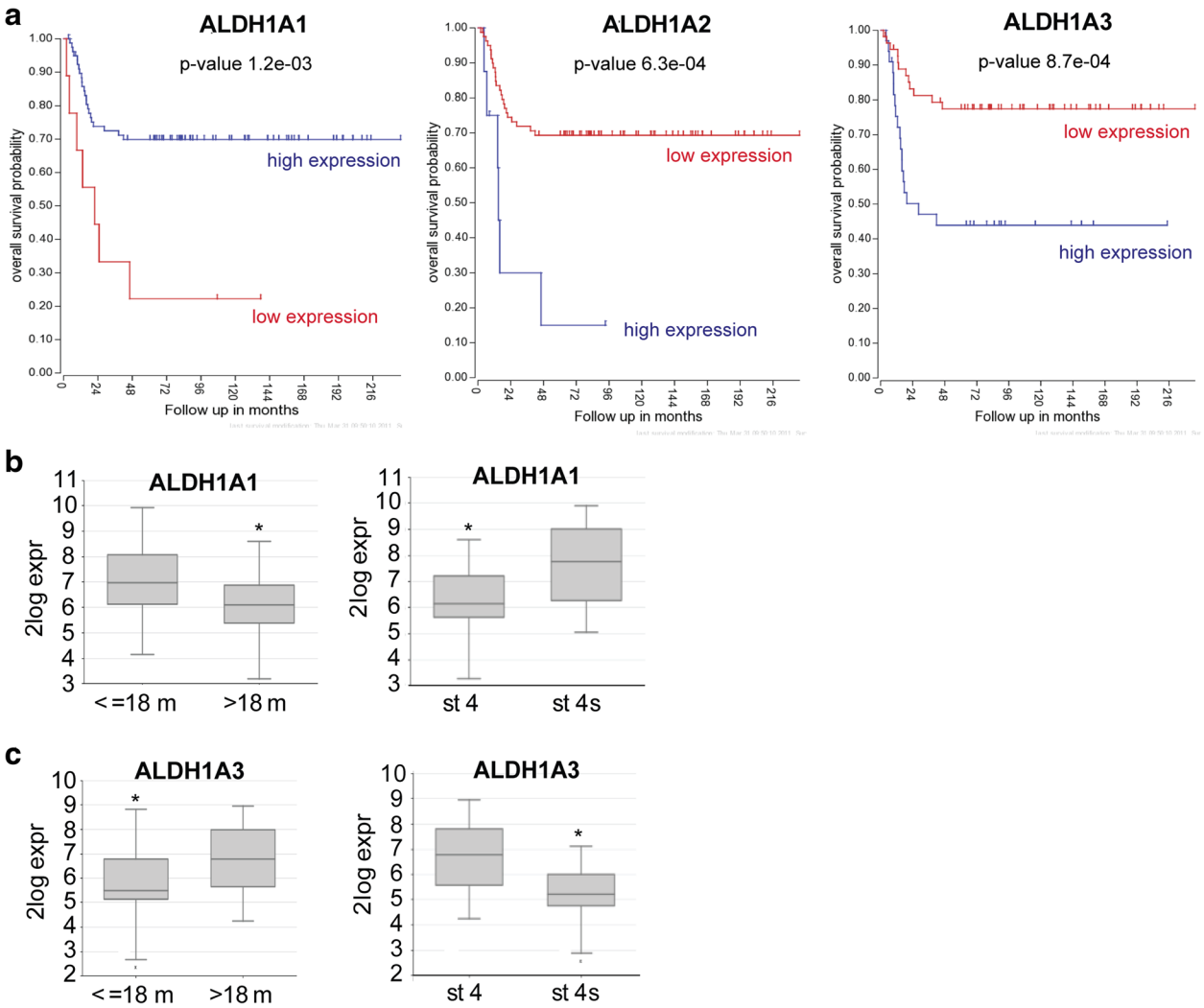

Fig. 5 ALDH1A3 expression is associated with unfavorable prognostic markers and reduced survival, while ALDH1A1 expression correlates with less aggressive NB. **a**-**c** Graphs were generated from the Versteeg database ($n = 88$ NB patients) using the R2: Genomics Analysis and Visualization Platform (http://r2.amc.nl). **a** Kaplan Meier overall survival curves. **b**-**c** ALDH1A1 (**b**) and ALDH1A3 (**c**) mRNA expression levels in NB tumors according to age ≤ or > 18 month at diagnosis (*left panels*) or with stage 4 versus stage 4 s (*right panels*)

prognostic markers. These observations, as well as the ALDH1A3 enrichment in NB TICs, suggest that ALDH1A3 isoenzyme could be linked to NB progression and aggressiveness. This correlates with other studies showing that high ALDH1A3 expression is associated with more aggressive forms of breast, glioblastoma, glioma, and pancreatic cancer [28, 47–49].

NB PDX tumors and cell lines also displayed a strong and heterogeneous ALDH enzymatic activity. However, no correlation between the expression levels of a specific ALDH1 isoform and ALDH activity could be identified in these samples, as well as during NB TIC selection. Although the ALDH enzymatic activity measured by the ALDEFLUOR kit was initially mainly attributed to ALDH1A1, other ALDH isoenzymes were also involved [21, 25, 28, 29]. Further investigations are needed to determine if the ALDH activity detected in NB cells can be associated with a specific ALDH isoenzyme. Yet, we observed that *ALDH1A3* gene disruption had no major impact on the ALDH enzymatic activity in SK-N-Be2c and NB1-C clones (Additional file 1: Figure S4). These data suggest that ALDH1A3 isoenzyme play a negligible role in the conversion of the ALDH substrate, BODIPY-aminoacetaldehyde, to fluorescent BODIPY-aminoacetate reaction products in NB cells, in contrast to breast cancer and non-small cell lung carcinoma [28, 29].

Drug resistance is a hallmark of CSCs or TICs and is considered as a major contributing factor of relapse. Various mechanisms of chemoresistance have been identified in CSCs, including ALDH activity [50]. Indeed, ALDH activity has been associated for a long time with normal SC and CSC resistance to oxazaphosphorines such as

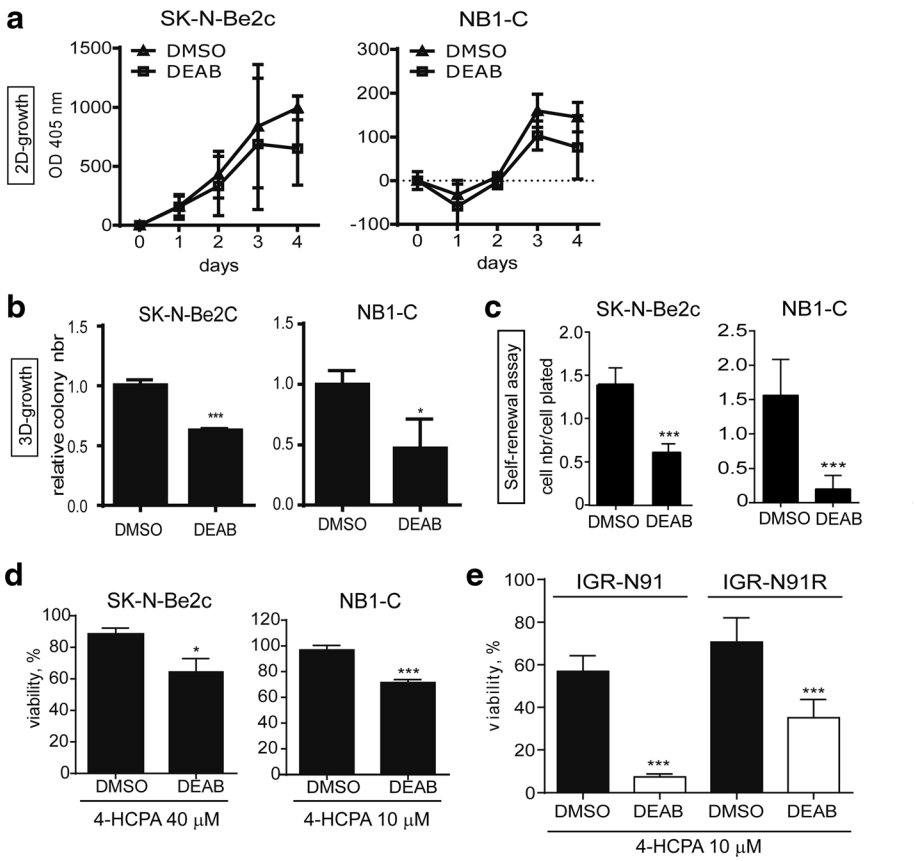

Fig. 6 DEAB-mediated ALDH inhibition affects NB aggressive properties and sensitizes NB cells to 4-hydroxycyclophosphamide. Analyses of the impact of ALDH activity inhibition by DEAB treatment on NB cell proliferation (2D-growth, **a**), clonogenicity (3D-growth, **b**), TICs self renewal (**c**), and sensitivity to 4-HCPA (**a**-**e**). SK-N-Be2c and NB1-C cell lines were pre-treated with 100 or 50 μM of DEAB, respectively, for three days before starting functional assays performed in presence of DEAB or DMSO as control. **a** Mean OD at 405 nm ± SD of 4 (SK-N-Be2c) or 2 (NB1-C) experiments performed in quadruplicates. **b** Mean of relative colony numbers ± SD of 3 experiments performed in duplicates (unpaired *t*-test $*p < 0.05$, $***p \leq 0.0005$). **c** Mean ratio of cell number/cell plated ± SD of 2 experiments performed in triplicates (unpaired *t*-test $***p \leq 0.0001$). **d** Cell viability of SK-N-Be2c and NB1-C cells treated for 48 h with indicated doses of 4-HCPA in presence or absence of DEAB (100 μM and 50 μM, respectively). Mean values ± SD of 3 experiments performed in quadruplicates (unpaired *t*-test $*p < 0.02$, $***p \leq 0.0001$). **e** Cell viability of IGR-N91 and IGR-N91R cells treated for 48 h with indicated doses of 4-HCPA in presence or absence of DEAB (100 μM). Mean values ± SD of 3 experiments performed in quadruplicates (unpaired *t*-test $***p \leq 0.0005$)

cyclophosphamide [23, 25, 51–53], a drug commonly used during NB patient therapy. A cyclophosphamide-resistant phenotype in relation with high ALDH activity has not yet been described in NB. In this study, we demonstrate a significant sensitization of NB cell lines to 4-HCPA, the active metabolite of cyclophosphamide, upon ALDH activity inhibition with DEAB, which represents an original finding. Importantly, the multidrug resistant IGR-N91R cells could be efficiently resensitized to 4-HCPA using DEAB. As DEAB was shown to most potently inhibit ALDH1A1, followed by ALDH2, ALDH1A2, ALDH1B1, ALDH1A3 and ALDH5A1 [54], further studies will be required to determine the specific involvement of individual ALDH isoenzyme in ALDH-mediated resistance to 4-HCPA in NB.

Interestingly, we also demonstrate in this present study that treatments of NB cells with DEAB induced a significant decrease in their anchorage-independent growth and TIC self-renewal properties. *ALDH1A3* gene disruption also impaired the clonogenic properties of both cell lines analyzed. However, *ALDH1A3* KO only affected the TIC self-renewal capacities of the SK-N-Be2c cell line, but not that of NB1-C cells. This observation correlates with the lack of enrichment of the ALDH1A3 isoenzyme in the NB1-C cell line during self-renewal assays, in contrast to ALDH1A3 enrichment in the SK-N-Be2c cells and the NB1 PDX-derived cells (Fig. 1). This suggests that the ALDH1A3 isoenzyme may not play a major role in TIC self-renewal in the NB1-C cell line.

The limitations of the present work are partly due to the difficulty to precisely assess both global ALDH activity and particular isoform inhibition. This is an issue shared by all prior reports on ALDH function. In fact, the ALDEFLUOR kit has been thought to faithfully

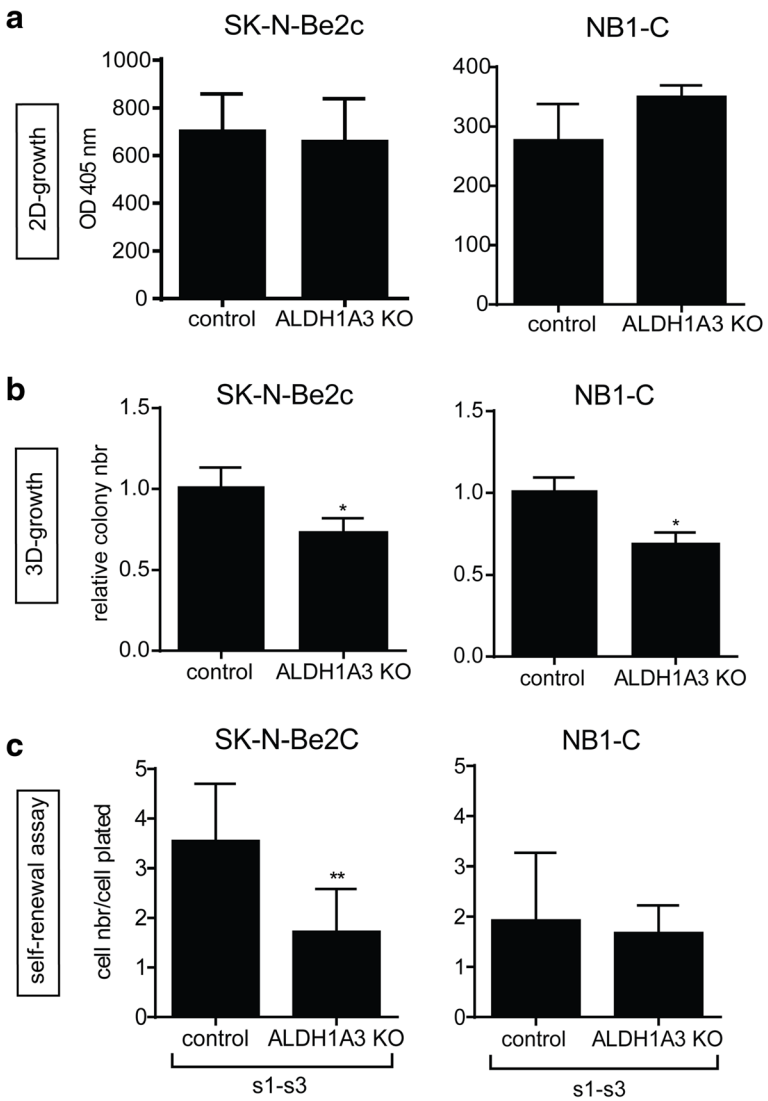

Fig. 7 Specific ALDH1A3 KO impairs NB cell clonogenic properties. **a**-**c** Impact of ALDH1A3 specific KO was analyzed on the proliferation (**a**), clonogenic (**b**), and TIC self-renewal (**c**) capacities. **a** Mean OD at 405 nm ± SD of 3 experiments performed in quadruplicates. **b** Mean of relative colony numbers ± SD of 3 experiments performed in duplicates (unpaired *t*-test $*p < 0.05$). **c** Mean ratio of cell number/cell plated ± SD of 3 experiments performed in duplicates in pooled s1 to s3 passages (s1-s3) (unpaired *t*-test $**p \leq 0.005$)

measure ALDH1A1 isoform activity, a presumption which has subsequently been shown not be entirely correct (see above). Moreover, DEAB selectively inhibits specific ALDH isoenzymes, and this at various levels of efficiency. In this study, we addressed these limitations by performing genetic knock-outs that (from our previous work on TICs) appeared to influence the biology of NB, and investigated their impact. Similarly, as for other metabolic pathways involved in oncogenesis, the functional redundancy of multiple enzymatic isoforms limits the investigation of the mechanistic underpinnings behind the effects we and other observed. Nonetheless, we feel that, while our findings are mostly focused on in vitro assays for oncogenic potential, this study opens new avenues for in vivo investigations. In particular, the ALDH-associated re-sensitization of NB to frequently used chemotherapeutic agents (i.e., cyclophosphamide) will need to be further detailed as it constitutes a potential translational avenue. In addition, the data linking ALDH variation with clinical outcomes in NB patients correlate with our prior work and the current results. We feel they constitute an encouraging step towards further work addressing the role of ALDH isoforms in murine models of NB, in particular PDX.

Conclusions

Our results highlight the impact of ALDH enzymatic activity on the aggressive properties of NB in addition to

its resistance to 4-HCPA. Further work is needed to identify the specific ALDH isoenzyme(s) involved as they may be considered for future therapeutic strategies for high-risk NB.

Additional file

Additional file 1: Figure S1. Stem cell markers are enriched during neurosphere culture. **Figure S2.** DEAB treatment is efficient to transitory inhibit ALDH activity. **Figure S3.** Illustration of the insertions/deletions in the different ALDH1A3 KO clones. **Figure S4.** ALDH1A3 KO has no impact on the percentage of ALDH+ cells. (ZIP 1853 kb)

Abbreviations

4-HCPA: 4-hydroxycyclophosphamide; ALDH: Aldehyde dehydrogenases; CSCs: Cancer stem cells; DEAB: Diethylaminobenzaldehyde; DMSO: Dimethyl sulfoxide; MFI: Mean fluorescence intensity; NB: Neuroblastoma; NBM: Neural basic medium; NCSC: Neural crest stem cell; NS: Neurospheres; PDX: Patient-derived xenograft; TICs: Tumor-initiating cells

Acknowledgements

Not applicable.

Funding

This work was supported by the Swiss National Science Foundation (grant # 310030–13801), FORCE and the KinderKrebsforschung Schweiz Foundation.

Availability of data and materials

The datasets supporting the conclusions of this article are included within the article and its additional files.

Authors' contributions

MF, NJ, KN, KBB, NC, and AMM performed all major experimental work and participated in data analyses; MF, NJ, JMJ, NG, AMM, and RR participated in the design and in the coordination of the study, and in the interpretation of data; MF, AMM, and RR prepared figures and drafted the manuscript. CW and DB provided valuable help on the CRISPR/Cas9 KO and bioinformatic analyses. All authors discussed the results and commented on the manuscript. All authors read and approved the manuscript.

Competing interests

The authors declare that they have no competing interests.

Consent for publication

Not applicable.

Ethics approval and consent to participate

Tumor material was collected from NB patients, diagnosed in the Hemato-Oncology Unit of the University Hospital of Lausanne (Switzerland), after informed consent. This study was approved by the ethics committee for clinical research of the Faculty of Biology and Medicine of the University of Lausanne (Protocol 26/05, 07/02/2005).

Author details

[1]Pediatric Hematology-Oncology Research Laboratory, Pediatric Division, University Hospital CHUV, Lausanne, Switzerland. [2]Pediatric Surgery, Pediatric Division, University Hospital CHUV, Lausanne, Switzerland. [3]Department of Physiology, University of Lausanne, Lausanne, Switzerland. [4]SIB Swiss Institute of Bioinformatics, Bioinformatics Core Facility, Lausanne, Switzerland.

Received: 9 June 2016 Accepted: 26 September 2016
Published online: 10 October 2016

References

1. Maris JM. Recent advances in neuroblastoma. N Engl J Med. 2010;362(23):2202–11.
2. Schleiermacher G, Janoueix-Lerosey I, Delattre O. Recent insights into the biology of neuroblastoma. Int J Cancer. 2014;135(10):2249–61.
3. Pinto NR, Applebaum MA, Volchenboum SL, Matthay KK, London WB, Ambros PF, Nakagawara A, Berthold F, Schleiermacher G, Park JR, et al. Advances in risk classification and treatment strategies for neuroblastoma. J Clin Oncol. 2015;33(27):3008–17.
4. Janoueix-Lerosey I, Schleiermacher G, Delattre O. Molecular pathogenesis of peripheral neuroblastic tumors. Oncogene. 2010;29(11):1566–79.
5. Molenaar JJ, Koster J, Zwijnenburg DA, van Sluis P, Valentijn LJ, van der Ploeg I, Hamdi M, van Nes J, Westerman BA, van Arkel J, et al. Sequencing of neuroblastoma identifies chromothripsis and defects in neuritogenesis genes. Nature. 2012;483(7391):589–93.
6. Pugh TJ, Morozova O, Attiyeh EF, Asgharzadeh S, Wei JS, Auclair D, Carter SL, Cibulskis K, Hanna M, Kiezun A, et al. The genetic landscape of high-risk neuroblastoma. Nat Genet. 2013;45(3):279–84.
7. Biedler JL, Helson L, Spengler BA. Morphology and growth, tumorigenicity, and cytogenetics of human neuroblastoma cells in continuous culture. Cancer Res. 1973;33(11):2643–52.
8. Ciccarone V, Spengler BA, Meyers MB, Biedler JL, Ross RA. Phenotypic diversification in human neuroblastoma cells: expression of distinct neural crest lineages. Cancer Res. 1989;49(1):219–25.
9. Ross RA, Spengler BA, Domenech C, Porubcin M, Rettig WJ, Biedler JL. Human neuroblastoma I-type cells are malignant neural crest stem cells. Cell Growth Differ. 1995;6(4):449–56.
10. Ross RA, Spengler BA, Rettig WJ, Biedler JL. Differentiation-inducing agents stably convert human neuroblastoma I-type cells to neuroblastic (N) or nonneuronal (S) neural crest cells. Prog Clin Biol Res. 1994;385:253–9.
11. Walton JD, Kattan DR, Thomas SK, Spengler BA, Guo HF, Biedler JL, Cheung NK, Ross RA. Characteristics of stem cells from human neuroblastoma cell lines and in tumors. Neoplasia. 2004;6(6):838–45.
12. Dean M, Fojo T, Bates S. Tumour stem cells and drug resistance. NatRevCancer. 2005;5(4):275–84.
13. Clevers H. The cancer stem cell: premises, promises and challenges. Nat Med. 2011;17(3):313–9.
14. Visvader JE, Lindeman GJ. Cancer stem cells: current status and evolving complexities. Cell Stem Cell. 2012;10(6):717–28.
15. Reya T, Morrison SJ, Clarke MF, Weissman IL. Stem cells, cancer, and cancer stem cells. Nature. 2001;414(6859):105–11.
16. Nguyen LV, Vanner R, Dirks P, Eaves CJ. Cancer stem cells: an evolving concept. Nat Rev Cancer. 2012;12(2):133–43.
17. Coulon A, Flahaut M, Muhlethaler-Mottet A, Meier R, Liberman J, Balmas-Bourloud K, Nardou K, Yan P, Tercier S, Joseph JM, et al. Functional sphere profiling reveals the complexity of neuroblastoma tumor-initiating cell model. Neoplasia. 2011;13(10):991–1004.
18. Ginestier C, Hur MH, Charafe-Jauffret E, Monville F, Dutcher J, Brown M, Jacquemier J, Viens P, Kleer CG, Liu S, et al. ALDH1 is a marker of normal and malignant human mammary stem cells and a predictor of poor clinical outcome. Cell Stem Cell. 2007;1(5):555–67.
19. Douville J, Beaulieu R, Balicki D. ALDH1 as a functional marker of cancer stem and progenitor cells. Stem Cells Dev. 2009;18(1):17–25.
20. Luo Y, Dallaglio K, Chen Y, Robinson WA, Robinson SE, McCarter MD, Wang J, Gonzalez R, Thompson DC, Norris DA, et al. ALDH1A isozymes are markers of human melanoma stem cells and potential therapeutic targets. Stem Cells. 2012;30(10):2100–13.
21. Moreb JS, Ucar D, Han S, Amory JK, Goldstein AS, Ostmark B, Chang LJ. The enzymatic activity of human aldehyde dehydrogenases 1A2 and 2 (ALDH1A2 and ALDH2) is detected by Aldefluor, inhibited by diethylaminobenzaldehyde and has significant effects on cell proliferation and drug resistance. Chem Biol Interact. 2012;195(1):52–60.
22. Koppaka V, Thompson DC, Chen Y, Ellermann M, Nicolaou KC, Juvonen RO, Petersen D, Deitrich RA, Hurley TD, Vasiliou V. Aldehyde dehydrogenase inhibitors: a comprehensive review of the pharmacology, mechanism of action, substrate specificity, and clinical application. Pharmacol Rev. 2012;64(3):520–39.
23. Tomita H, Tanaka K, Tanaka T, Hara A. Aldehyde dehydrogenase 1A1 in stem cells and cancer. Oncotarget. 2016;7(10):11018–32.
24. Alison MR, Guppy NJ, Lim SM, Nicholson LJ. Finding cancer stem cells: are aldehyde dehydrogenases fit for purpose? J Pathol. 2010;222(4):335–44.
25. Marcato P, Dean CA, Giacomantonio CA, Lee PW. Aldehyde dehydrogenase: its role as a cancer stem cell marker comes down to the specific isoform. Cell Cycle. 2011;10(9):1378–84.
26. Sullivan JP, Spinola M, Dodge M, Raso MG, Behrens C, Gao B, Schuster K, Shao C, Larsen JE, Sullivan LA, et al. Aldehyde dehydrogenase activity

selects for lung adenocarcinoma stem cells dependent on notch signaling. Cancer Res. 2010;70(23):9937–48.
27. Chen Y, Orlicky DJ, Matsumoto A, Singh S, Thompson DC, Vasiliou V. Aldehyde dehydrogenase 1B1 (ALDH1B1) is a potential biomarker for human colon cancer. Biochem Biophys Res Commun. 2011;405(2):173–9.
28. Marcato P, Dean CA, Pan D, Araslanova R, Gillis M, Joshi M, Helyer L, Pan L, Leidal A, Gujar S, et al. Aldehyde dehydrogenase activity of breast cancer stem cells is primarily due to isoform ALDH1A3 and its expression is predictive of metastasis. Stem Cells. 2011;29(1):32–45.
29. Shao C, Sullivan JP, Girard L, Augustyn A, Yenerall P, Rodriguez-Canales J, Liu H, Behrens C, Shay JW, Wistuba II, et al. Essential role of aldehyde dehydrogenase 1A3 for the maintenance of non-small cell lung cancer stem cells is associated with the STAT3 pathway. Clin Cancer Res. 2014;20(15):4154–66.
30. van den Hoogen C, van der Horst G, Cheung H, Buijs JT, Lippitt JM, Guzman-Ramirez N, Hamdy FC, Eaton CL, Thalmann GN, Cecchini MG, et al. High aldehyde dehydrogenase activity identifies tumor-initiating and metastasis-initiating cells in human prostate cancer. Cancer Res. 2010;70(12):5163–73.
31. Kastan MB, Schlaffer E, Russo JE, Colvin OM, Civin CI, Hilton J. Direct demonstration of elevated aldehyde dehydrogenase in human hematopoietic progenitor cells. Blood. 1990;75(10):1947–50.
32. Moreb J, Schweder M, Suresh A, Zucali JR. Overexpression of the human aldehyde dehydrogenase class I results in increased resistance to 4-hydroperoxycyclophosphamide. Cancer Gene Ther. 1996;3(1):24–30.
33. Hartomo TB, Van Huyen Pham T, Yamamoto N, Hirase S, Hasegawa D, Kosaka Y, Matsuo M, Hayakawa A, Takeshima Y, Iijima K, et al. Involvement of aldehyde dehydrogenase 1A2 in the regulation of cancer stem cell properties in neuroblastoma. Int J Oncol. 2015;46(3):1089–98.
34. Thiele CJ. Neuroblastoma. In: Human Cell Culture. Volume J. R.W. Masters and B. Palsson, edn.; 1999: 21–53.
35. Flahaut M, Muhlethaler-Mottet A, Martinet D, Fattet S, Bourloud KB, Auderset K, Meier R, Schmutz NB, Delattre O, Joseph JM, et al. Molecular cytogenetic characterization of doxorubicin-resistant neuroblastoma cell lines: evidence that acquired multidrug resistance results from a unique large amplification of the 7q21 region. Genes Chromosomes Cancer. 2006;45(5):495–508.
36. Schlesinger HR, Gerson JM, Moorhead PS, Maguire H, Hummeler K. Establishment and characterization of human neuroblastoma cell lines. Cancer Res. 1976;36(9 pt.1):3094–100.
37. Muhlethaler-Mottet A, Flahaut M, Bourloud KB, Nardou K, Coulon A, Liberman J, Thome M, Gross N. Individual caspase-10 isoforms play distinct and opposing roles in the initiation of death receptor-mediated tumour cell apoptosis. Cell Death Dis. 2011;2(1), e125.
38. Montavon G, Jauquier N, Coulon A, Peuchmaur M, Flahaut M, Bourloud KB, Yan P, Delattre O, Sommer L, Joseph JM, et al. Wild-type ALK and activating ALK-R1275Q and ALK-F1174L mutations upregulate Myc and initiate tumor formation in murine neural crest progenitor cells. Oncotarget. 2014;5(12):4452–66.
39. Fuchs S, Herzog D, Sumara G, Buchmann-Moller S, Civenni G, Wu X, Chrostek-Grashoff A, Suter U, Ricci R, Relvas JB, et al. Stage-specific control of neural crest stem cell proliferation by the small rho GTPases Cdc42 and Rac1. Cell Stem Cell. 2009;4(3):236–47.
40. Muhlethaler-Mottet A, Bourloud KB, Auderset K, Joseph JM, Gross N. Drug-mediated sensitization to TRAIL-induced apoptosis in caspase-8-complemented neuroblastoma cells proceeds via activation of intrinsic and extrinsic pathways and caspase-dependent cleavage of XIAP. Bcl-xL RIP Oncogene. 2004;23(32):5415–25.
41. Shalem O, Sanjana NE, Hartenian E, Shi X, Scott DA, Mikkelsen TS, Heckl D, Ebert BL, Root DE, Doench JG, et al. Genome-scale CRISPR-Cas9 knockout screening in human cells. Science. 2014;343(6166):84–7.
42. Sanjana NE, Shalem O, Zhang F. Improved vectors and genome-wide libraries for CRISPR screening. Nat Methods. 2014;11(8):783–4.
43. Flahaut M, Muhlethaler-Mottet A, Auderset K, Bourloud KB, Meier R, Popovic MB, Joseph JM, Gross N. Persistent inhibition of FLIP(L) expression by lentiviral small hairpin RNA delivery restores death-receptor-induced apoptosis in neuroblastoma cells. Apoptosis. 2006;11(2):255–63.
44. Martin M. Cutadapt removes adapter sequences from high-throughput sequencing reads. EMBnetjournal. 2011;17(1):10–2.
45. Li H, Durbin R. Fast and accurate short read alignment with Burrows-Wheeler transform. Bioinformatics. 2009;25(14):1754–60.
46. Prasmickaite L, Engesaeter BO, Skrbo N, Hellenes T, Kristian A, Oliver NK, Suo Z, Maelandsmo GM. Aldehyde dehydrogenase (ALDH) activity does not select for cells with enhanced aggressive properties in malignant melanoma. PLoS ONE. 2010;5(5):e10731.
47. Jia J, Parikh H, Xiao W, Hoskins JW, Pflicke H, Liu X, Collins I, Zhou W, Wang Z, Powell J, et al. An integrated transcriptome and epigenome analysis identifies a novel candidate gene for pancreatic cancer. BMC Med Genet. 2013;6:33.
48. Zhang W, Yan W, You G, Bao Z, Wang Y, Liu Y, You Y, Jiang T. Genome-wide DNA methylation profiling identifies ALDH1A3 promoter methylation as a prognostic predictor in G-CIMP- primary glioblastoma. Cancer Lett. 2013;328(1):120–5.
49. Mao P, Joshi K, Li J, Kim SH, Li P, Santana-Santos L, Luthra S, Chandran UR, Benos PV, Smith L, et al. Mesenchymal glioma stem cells are maintained by activated glycolytic metabolism involving aldehyde dehydrogenase 1A3. Proc Natl Acad Sci U S A. 2013;110(21):8644–9.
50. Abdullah LN, Chow EK. Mechanisms of chemoresistance in cancer stem cells. Clin Translational Med. 2013;2(1):3.
51. Hilton J. Role of aldehyde dehydrogenase in cyclophosphamide-resistant L1210 leukemia. Cancer Res. 1984;44(11):5156–60.
52. Kohn FR, Sladek NE. Aldehyde dehydrogenase activity as the basis for the relative insensitivity of murine pluripotent hematopoietic stem cells to oxazaphosphorines. Biochem Pharmacol. 1985;34(19):3465–71.
53. Dylla SJ, Beviglia L, Park IK, Chartier C, Raval J, Ngan L, Pickell K, Aguilar J, Lazetic S, Smith-Berdan S, et al. Colorectal cancer stem cells are enriched in xenogeneic tumors following chemotherapy. PLoS ONE. 2008;3(6), e2428.
54. Morgan CA, Parajuli B, Buchman CD, Dria K, Hurley TD. N, N-diethylaminobenzaldehyde (DEAB) as a substrate and mechanism-based inhibitor for human ALDH isoenzymes. Chem Biol Interact. 2015;234:18–28.

Additional Files

Fig S1. Stem cell markers are enriched during neurosphere culture. (A) The expression levels of the stem cell markers Nanog, Sox2 and Myc were analyzed by RT-PCR in total RNA obtained from SK-N-Be2c and NB1-C parental cells (T0) and the sphere passage s2. The *HPRT1* gene was used as control. (B) MYC mRNA expression was analyzed by real-time PCR in the sphere passages s2, and s5 relative to parental cells (T0). Mean relative expression ± SD of two experiments performed in duplicates were plotted in the bare graph (unpaired t-test, *p<0.05).

Fig S2. DEAB treatment is efficient to transitory inhibit ALDH activity. ALDH activity was analyzed in untreated SK-N-Be2c cells, after prolonged treatment with 100 □M DEAB for 5 days, or after 3 days in presence of DEAB followed by 2 days in absence of DEAB. Representative dot plots are shown.

Fig S3. Illustration of the insertions/deletions in the different ALDH1A3 KO clones. DNA sequences of WT *ALDH1A3* gene and mutated alleles of 2 clones of SK-N-Be2c cells and 2 clones NB1-C cells identified by MiSeq Illumina sequencing. Insertions/deletions are indicated in red. The sgALDH1A3.1 and sgALDH1A3.2 are highlighted in light grey and in dark grey, respectively, and the PAM sequence is labeled in black bold. The number of reads and percentage of each allele/total number of reads are indicated, as well as the total coverage. Note that three alleles were found in the SK-N-Be2c clone 1.9, indicating a triploidy of this genomic region, which was confirmed by the ratio of 2 different indels found in clone 1.18. The alleles 1 and 2 have the same indel. In addition, only one indel could be identified in each NB1-C clone, suggesting LOH in this genomic region. All indels lead to premature stop codons in the N-term end of the ALDH1A3 protein as indicated.

Fig S4. ALDH1A3 KO has no impact on the percentage of ALDH$^+$ cells. ALDH activity was measured using the ALDEFLUOR kit in control and ALDH1A3 KO SK-N-Be2c and NB1-C clones. (A) The percentage of ALDH$^+$ cells are plotted as mean ± SD of 2 experiments.

Fig S1

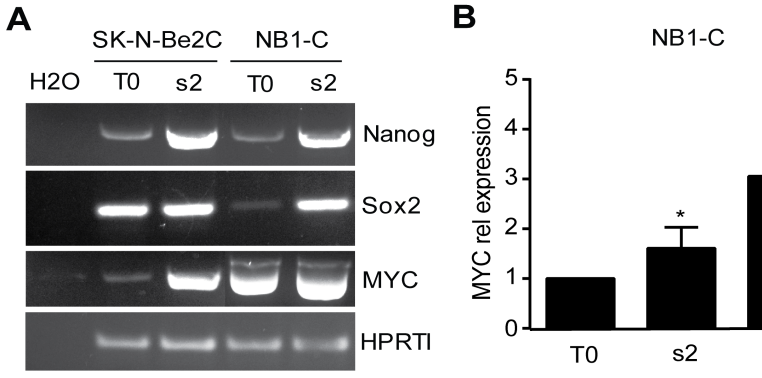

Fig S2

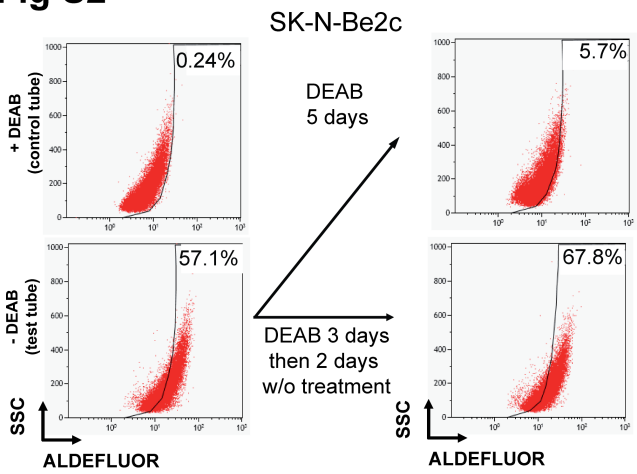

Fig S3

	Nbr of reads/Total read (%)
SK-N-Be2c clone 1.9 (stop codon after 60/93 aa)	Total coverage 79.4%
WT ALDH1A3 AAAAAGTTTGCTACATGTAACCCTT-C----------AACTCGGGAGC	0 (0%)
allele 1 AAAAAGTTTGCTACATGTAACCCTT-CA----------AACTCGGGAGC	295982 (28%)
allele 2 AAAAAGTTTGCTACATGTAACCCTTACTCGTAAGTTACATGTAACTCGGGAGC	348526 (33%)
allele 3 AAAAA----------GAGC	196337 (19%)
SK-N-Be2c clone 1.18 (stop codon after 60/93 aa)	Total coverage 86%
WT ALDH1A3 AAAAAGTTTGCTACATGTAACCCTTCAACTCGGGAGCAAATATGTGAAGTGGA	1307 (0.002%)
allele 1/2 AAAAAGTTTGCTACATGTAACCCTTCA-CTCGGGAGCAAATATGTGAAGTGGA	391707 (61.86%)
allele 3 AAAAAGTTTGCTACATGTAACCCTT--ACTCGGGAGCAAATATGTGAAGTGGA	150518 (23.77%)
NB1-C clone 1.23 (stop after 86 aa)	Total coverage 91%
wt ALDH1A3 AAAAAGTTTGCTACATGTAACCCTTC----------	5 (0%)
allele 1 AAAAAGTTTGCTACATGTAACCCTTCTTCACTTCTGCCTGAGACACCTTACA	45028 (100%)
wt ALDH1A3 ----------	
allele 1 GCTCCGTCCTGCTTCCATGTCATTCTGCTCCTTTTGTAAAATGTGAACCAGG	
wt ALDH1A3 ----------AACTCGGGAGCAAATA	
allele 1 TCTACAGCTCAATGTAGCTTAATGCTATACCTCTATAACTCGGGAGCAAATA	
NB1-C clone 2.2 (stop after 93 aa)	Total coverage 77.3%
wt ALDH1A3 TGTTCTGGTCGCTCAGCCCGACGTGGACAAGGCTGTGGAGGCTGCACAGGTT	0 (0%)
allele 1 TGTTCTGGTCGCTCAGCCCGACGTG-ACAAGGCTGTGGAGGCTGCACAGGTT	87585 (100%)

Fig S4